

US EPA ARCHIVE DOCUMENT

EPA-600/3-80-065
JULY 1980

Ecological Research Series

MATHEMATICAL MODELS OF WATER QUALITY IN LARGE LAKES

Part 2. Lake Erie

Environmental Research Laboratory
Office of Research and Development
U.S. Environmental Protection Agency
Duluth, Minnesota 55804

EPA-600/3-80-065
July 1980

MATHEMATICAL MODELS OF WATER QUALITY LARGE LAKES

PART 2. LAKE ERIE

By

Dominic M. Di Toro
John P. Connolly

Manhattan College
Environmental Engineering and Science Division
Riverdale, New York

Grant No. R803030

Project Officer

William L. Richardson
Large Lakes Research Station
Environmental Research Laboratory-Duluth
Grosse Ile, Michigan 48138

ENVIRONMENTAL RESEARCH LABORATORY
OFFICE OF RESEARCH AND DEVELOPMENT
U.S. ENVIRONMENTAL PROTECTION AGENCY
DULUTH, MINNESOTA 55804

DISCLAIMER

This report has been reviewed by the Large Lakes Research Station, Grosse Ile Laboratory, U.S. Environmental Protection Agency, and approved for publication. Approval does not signify that the contents necessarily reflect the views and policies of the U.S. Environmental Protection Agency, nor does mention of trade names or commercial products constitute endorsement or recommendation for use.

FOREWORD

The Great Lakes represent a vast, complex system of competing water uses including a delicate, and interacting ecosystem. They comprise 80% of the surface freshwater in North America and provide 45 million people in the basin with almost unlimited water for drinking, industrial processing, and recreation. Lucrative sport and commercial fisheries rely on these waters as do the transport of tremendous quantities of raw and refined commercial products and the disposal of residual industrial and municipal materials.

Optimal use of these water resources demands that a balance be maintained between the economic welfare of the region and the health of the ecosystem. To arrive at this balance, a rational and quantitative understanding of the interacting and competing components must be developed.

This report documents the results of a three-year research project to develop a water quality model for Lake Erie. Sufficient detail is presented so that much of the methodology can be applied to other waterbodies. Also, it is intended to present results and background for Great Lakes researchers and managers who have already used this research in the decision-making process. Specifically, these results have been used in renegotiating the U.S.-Canadian Great Lakes Agreement and to decide on the allowable phosphorus load to Lake Erie.

Appreciation is extended to the scientific reviewers at the University of Michigan, National Oceanic and Atmospheric Administration (NOAA)-Great Lakes Environmental Research Laboratory, and the Canadian Centre for Inland Waters. The report has also received extensive review by several state and Canadian agencies.

William L. Richardson, P.E.
Environmental Scientist
ERL-D, Large Lakes Research Station
Grosse Ile, Michigan 48138

ABSTRACT

This research was undertaken to develop and apply a mathematical model of the water quality in large lakes, particularly Lake Huron and Saginaw Bay (Part 1) and Lake Erie (Part 2).

A mathematical model was developed for analysis of the interactions between nutrient discharges to Lake Erie, the response of phytoplankton to these discharges, and the dissolved oxygen depletion that occurs as a consequence. Dissolved oxygen, phytoplankton, chlorophyll for diatoms and non-diatoms, zooplankton biomass, nutrient concentrations in available and unavailable forms and inorganic carbon are considered in the model. Extensive water quality data for Lake Erie was analyzed and statistically reduced. Comparison of data from 1970 and 1973-1974 to model calculations served for calibration of the model. A verification computation was also performed for 1975, a year when no anoxia was observed.

Recent developments in phytoplankton growth and uptake kinetics are included in this analysis. The methods of sedimentary geochemistry are expanded to include an analysis of sediment oxygen demand within the framework of mass balances. Projected effects of varying degrees of phosphorus removal on dissolved oxygen, anoxic area, chlorophyll, transparency and phosphorus concentration are presented.

This report was submitted in fulfillment of Grant No. R803030 by Manhattan College under the sponsorship of the U.S. Environmental Protection Agency. This report covers the project period March 26, 1974 to March 25, 1977.

CONTENTS

Disclaimer	ii
Foreword	iii
Abstract	iv
List of Tables	viii
List of Figures	xi
Acknowledgments	xviii
 1. Introduction	 1
2. Summary	3
2.1 Framework	4
2.2 Calibration - Phytoplankton and Nutrients	5
2.3 Calibration - Dissolved Oxygen	10
2.4 Verification	11
2.5 Projections	14
3. Recommendations	16
4. Description of Study Area, Mass Discharge Rates, Sedimentation	16
4.1 Morphometry	16
4.2 Hydrology	16
4.3 Segmentation	17
4.4 Rates of Mass Discharge	19
4.5 Estimate of Detroit River Mass Discharge	20
4.6 Lake Erie Wastewater Management Study	21
4.7 Atmospheric Loading	28
4.8 Nitrogen Fixation	28
5. Data Compilation and Reduction	29
5.1 Historical Data	29
5.2 Calibration Dataset	29
5.2.1 Canada Centre for Inland Waters Cruise Data	31
5.2.2 Nutrient Control Program Cruise Data	31
5.2.3 Project Hypo Cruise Data	33

6.	Kinetics	48
6.1	Introduction	48
6.2	Phytoplankton Growth and Death	52
6.2.1	Nutrient Dependence of Phytoplankton Growth	52
6.2.2	Nutrient Uptake	56
6.2.3	Validity of Cellular Equilibrium Approximation	58
6.2.4	Dynamic Equations at Cellular Equilibrium	60
6.2.5	Discussion and Conclusions	62
6.3	Multiple Nutrient Limitation	65
6.4	Measure of Biomass	65
6.5	Stoichiometry and Uptake Kinetics	66
6.6	Kinetic Formulations	67
6.7	Dissolved Oxygen Kinetics	71
6.8	Water Column Production and Respiration	71
6.9	Appendix - Mathematical Details	78
6.9.1	Apparent Half-Saturation Constant	78
6.9.2	Growth Rate - Substrate Variations	78
6.9.3	Solution of the Cellular Equilibrium Equations	78
7.	Sediment-Water Interactions: Mass Transport and Kinetics	80
7.1	Nitrogen	80
7.2	Carbon and Oxygen	83
7.3	Phosphorus and Silica	88
8.	Mass Transport Calibration	90
8.1	Hydrodynamic Circulation	90
8.2	Heat Balance	92
9.	Structure and Computational Details	103
9.1	One-Group and Two-Group Phytoplankton Kinetics	103
9.2	Determination of Anoxia	104
9.3	Exogenous Variables	104
9.4	Time Scale	108
9.5	Carbon Dioxide and Alkalinity	108
9.6	Air-Water Interface Exchange	110
9.7	Settling Velocities	111
9.8	Mass Balance Equations	112
10.	Calibration	113
10.1	Dissolved Oxygen	113
10.2	Phytoplankton	118
10.3	Nitrogen	126
10.4	Phosphorus	126
10.5	Silica	135
10.6	Secchi Disk Depth	141

10.7	Zooplankton Carbon	141
10.8	Carbon	141
10.9	Production and Respiration Rates	147
10.10	Sediment Calibration	147
11.	Verification	153
11.1	Analysis of Calibration and Verification Error	164
12.	Estimated Effects of Phosphorus Loading Reductions	166
12.1	Time of Steady-State	166
12.2	Simulation Results	168
12.3	On the Uncertainty of the Predictions	182
	Appendix	184
	References	199

LIST OF TABLES

	<u>Page</u>
1. Sources and Sinks of Dissolved Oxygen, Central Basin Hypolimnion, 1970	10
2. Dissolved Oxygen Calibration - Residual Analysis, 1970	12
3. Lake Erie Flow Budget	17
4. Segment Parameters	19
5. Detroit River Phosphorus Loadings Rate (metric tons/yr)	21
6. Nitrogen Fixation	28
7. Lake Erie Limnological Data Summary - Historical Datasets	30
8. Lake Erie Limnological Data Summary - DataSets Used in Model	32
9. Growth and Nutrient Uptake Parameters	55
10. Comparison of Growth Rates	56
11. Phytoplankton Growth	69
12. Phytoplankton Respiration and Non-Predatory Mortality Reaction Stoichiometric Equation	71
13. Herbivorous Zooplankton Growth Reaction Stoichiometric Equation	73
14. Carnivorous Zooplankton Growth Reaction Stoichiometric Equation	74
15. Zooplankton Respiration Reaction Stoichiometric Equation	75
16. Nitrification Reaction Stoichiometric Equation	76

17. Denitrification Reaction Stoichiometric Equation	77
18. Mineralization Reaction Stoichiometric Equation	78
19. Sediment Reactions	88
20. Heat Flux and Surface Temperatures	96
21. Sources and Sinks of Dissolved Oxygen, Central Basin Hypolimnion, 1970	117
22. Annual Sedimentation Fluxes	151
23. Transport Parameters	152
24. Computed and Observed Sediment Interstitial Water Concentrations, Central Basin	153
25. Calculated Average Central Basin Concentrations and Oxygen Consumption Rates for 1970 and 1975	163
26. Percentage Contribution of Oxygen Sinks to Dissolved Oxygen Deficit at the Time of Minimum Dissolved Oxygen in the Central Basin Hypolimnion	165
27. Calibration and Verification Residual Analysis	166
28. Results of Simulation of Phosphorus Point Source Reduction to 0.1 mg/l	168
29. Loading Condition Versus Annual Total Phosphorus Load	169
30. Simulation Results, Summer Average	181
31. Comparison of Results - This Work and the U.S. Army Corps of Engineers' Phosphorus Model	183
A1. Morphometry and Hydrodynamic Regime for 1970	186
A2. 1975 Resegmentation	187
A3. Water Temperature (°C)	188
A4. Solar Radiation Data	188
A5. Photoperiod Data	189

A6.	Loadings to Lake Erie Western Basin (kg/day) Calibration Year - 1970, Verification Year - 1975	190
A7.	Loadings to Lake Erie Central Basin (kg/day) Calibration Year - 1970, Verification Year - 1975	190
A8.	Loadings to Lake Erie Eastern Basin (kg/day) Calibration Year - 1970, Verification Year - 1975	191
A9.	Mass Loading of Chlorides to Lake Erie (metric tons/day) Calibration Year - 1970, Verification Year - 1975	192
A10.	Phosphorus Loads Used for Projections - Western Basin	193
A11.	Phosphorus Loads Used for Projections - Central Basin	194
A12.	Phosphorus Loads Used for Projections - Eastern Basin	195
A13.	Boundary Conditions	196
A14.	Lake Erie Model Initial Conditions	197
A15.	Settling Velocities	198
A16.	Chemical Thermodynamic Parameters for Aqueous Phase Computations	199
A17.	Equations for Oxygen and Carbon Dioxide Aqueous Saturation	199

LIST OF FIGURES

	<u>Page</u>
1. Lake Erie calibration results, 1970	4
2. Lake Erie calibration results, 1970 epilimnion	5
3. Schematic diagram of the dissolved oxygen mass balance computation	6
4. Lake Erie basin calibration for dissolved oxygen and related variables, 1970	8
5. Lake Erie central basin calibration	9
6. Comparison of 1970 calibration and 1975 verification of dissolved oxygen, chlorophyll a, orthophosphorus, nitrate nitrogen	11
7. Observed hypolimnion mean dissolved oxygen versus minimum observed hypolimnion dissolved oxygen (top). Predicted mean hypolimnion dissolved oxygen just prior to overturn versus lake total phosphorus loading (bottom)	13
8. Lake Erie model segmentation of western, central and eastern basins: Water segments 1-6, epilimnion (top) and hypolimnion (middle); sediment segments 7-10 (bottom)	18
9. Total phosphorus loading (10^3 kg/day) to Lake Erie, 1970-1975	23
10. Orthophosphorus loading (10^3 kg/day) to Lake Erie, 1970-1975	24
11. Organic nitrogen loading (10^3 kg/day) to Lake Erie, 1970-1975	25
12. Inorganic nitrogen loading (10^4 kg/day) to Lake Erie, 1970-1975	26
13. Dissolved silica loading (10^4 kg/day) to Lake Erie, 1970-1975	27

14.	Comparison of chlorophyll <i>a</i> concentrations ($\mu\text{g/l}$) for the western basin and eastern basin epilimnion. Segment averages + standard deviations for each cruise are shown for 1970, 1973-1974 and 1975 datasets	34
15.	Comparison of chlorophyll <i>a</i> concentrations ($\mu\text{g/l}$) for the central basin epilimnion and hypolimnion. No chlorophyll data available for the hypolimnion during 1970	35
16.	Total phosphorus concentrations (mg/l) for the western basin and eastern basin epilimnion	36
17.	Total phosphorus concentrations (mg/l) for the central basin epilimnion and hypolimnion	37
18.	Soluble reactive phosphorus concentrations (mg/l) for the western basin and eastern basin epilimnion. No data available for the eastern basin during 1973-1974	38
19.	Soluble reactive phosphorus concentrations (mg/l) for the central basin epilimnion and hypolimnion	39
20.	Comparison of ammonia concentrations (mg/l as N) for the western basin and eastern basin epilimnion. No data available for the eastern basin during 1975	40
21.	Comparison of ammonia concentrations (mg/l as N) for the central basin epilimnion and hypolimnion	41
22.	Comparison of nitrate concentrations (mg/l as N) for the western basin and eastern basin epilimnion	42
23.	Comparison of nitrate concentrations (mg/l as N) for the central basin epilimnion and hypolimnion	43
24.	Comparison of reactive silica concentrations (mg/l as SiO_2) for the western basin and eastern basin epilimnion	44
25.	Comparison of reactive silica concentrations (mg/l as SiO_2) for the central basin epilimnion and hypolimnion	45
26.	Comparison of dissolved oxygen concentrations (mg/l) for the central basin epilimnion and hypolimnion	46
27.	Lake Erie state variable interactions. Representations of dissolved oxygen and phosphorus nutrient cycles	50

28.	Lake Erie state variable interactions. Representations of nitrogen and silica nutrient cycles	51
29.	The range of possible cell nutrient content and the ratio of the apparent half-saturation constant for growth to the half-saturation constant for uptake as a function of β , the ratio of maximum specific uptake to maximum growth rate and the dimensionless half-saturation constant for the dependence of nutrient uptake on internal nutrient concentration. The observed ranges in β for silica, nitrogen and phosphorus limited growth are shown	58
30.	Normalized growth rate as a function of normalized extent nutrient concentration: a comparison of the Michaelis-Menten expression to that derived from the internal cellular kinetics with uptake as a function of both external and internal nutrient concentration	60
31.	A comparison of the solutions to the dynamic equations (25)-(27) and the cellular equilibrium approximation equations (29)-(32). The parameters are for <i>Scenedesmus</i> sp. and phosphorus-limited growth	64
32.	Percent error between the cellular equilibrium approximation and the dynamic equations for various values of β and $\xi = K_q/q_0$. The curves correspond to the errors in cell concentration, $N(t)$, nutrient concentration, $S(t)$, and cell quota, $q(t)$ as indicated	65
33.	Calculated current patterns across the boundary of the western and central basins based on the prevailing direction and magnitude of Lake Erie winds at a depth of 3 meters and 9.1 meters	92
34.	Calculated heat flux to the central basin using observed temperatures for each cruise	95
35.	Average temperatures in two-meter sections of the central basin for 1970, Project Hypo Cruise 1 and 1975, CCIW Cruise 4	97
36.	Lake Erie model transport calibration, 1970: temperature	98
37.	Lake Erie model transport calibration, 1970: chlorides	99
38.	1970 model transport regime. Horizontal and vertical exchanges (m^2/day) resulting from the calibration	100
39.	Lake Erie model transport calibration, 1975: temperature	102

40.	1975 model transport regime. Horizontal transport are assumed to be the same as for 1970 while vertical exchanges differ as shown	103
41.	Comparison of one-group and two-group phytoplankton calculation for Lake Erie central basin epilimnion and western basin	106
42.	Mean dissolved oxygen ($\mu\text{g/l}$) for the central basin hypolimnion segments versus the minimum dissolved oxygen (mg/l) observed for each cruise	107
43.	Cruise average dissolved oxygen (mg/l) for the central basin hypolimnion segments versus the fraction of stations anoxic for that cruise	108
44.	Average monthly wind velocities (mph) around Lake Erie and variation of non-algal extinction coefficient (m^{-1}) with wind velocity	110
45.	Lake Erie model calibration for dissolved oxygen (mg/L), 1970	115
46.	Lake Erie model calibration for dissolved oxygen (mg/l), 1973-1974	116
47.	Dynamics of central basin hypolimnion dissolved oxygen calibration illustrating the relative importance of the individual oxygen sinks	118
48.	Lake Erie model calibration for phytoplankton chlorophyll ($\mu\text{g/l}$), 1970. The calculated curve is the sum of the diatom chlorophyll and non-diatom chlorophyll	120
49.	Lake Erie model calibration for phytoplankton chlorophyll ($\mu\text{g/l}$), 1973-1974. The calculated curve is the sum of the diatom chlorophyll and non-diatom chlorophyll	121
50.	The distribution of chlorophyll ($\mu\text{g/l}$) between diatoms and non-diatoms and model calibration for % diatom biomass	122
51.	Western basin phytoplankton growth and death dynamics for diatoms and non-diatoms. The curves are the calculated rates from the appropriate kinetic expressions	123
52.	Central basin epilimnion phytoplankton growth and death dynamics for diatoms and non-diatoms	124
53.	Eastern basin epilimnion phytoplankton growth and death dynamics for diatoms and non-diatoms	125

54.	Lake Erie model calibration, nutrient limitation multipliers, 1970. The curves are the growth rate reduction factors due to silica, nitrogen and phosphorus limitation effects	126
55.	Calculated nitrogen species distribution. Non-living organic nitrogen, ammonia nitrogen, nitrate plus nitrite nitrogen, phytoplankton nitrogen and the resultant total nitrogen are shown	128
56.	Lake Erie model calibration for organic nitrogen (mg N/l), 1970. Profiles are the sum of the computed phytoplankton and non-living organic nitrogen	129
57.	Lake Erie model calibration for organic nitrogen (mg N/l), 1973-1974. Profiles are the sum of the computed phytoplankton and non-living organic nitrogen	130
58.	Lake Erie model calibration for ammonia nitrogen (mg N/l), 1970	131
59.	Lake Erie model calibration for ammonia nitrogen (mg N/l), 1973-1974 . . .	132
60.	Lake Erie model calibration for nitrate nitrogen (mg N/l), 1970	133
61.	Lake Erie model calibration for nitrate nitrogen (mg N/l), 1973-1974	134
62.	Calculated phosphorus species distribution. Unavailable phosphorus, orthophosphorus, phytoplankton phosphorus and the resultant total phosphorus are shown	135
63.	Lake Erie model calibration for total phosphorus (mg PO ₄ -P/l), 1970	137
64.	Lake Erie model calibration for total phosphorus (mg PO ₄ -P/l), 1973-1974	138
65.	Lake Erie model calibration for orthophosphorus (mg PO ₄ -P/l), 1970	139
66.	Lake Erie model calibration for orthophosphorus (mg PO ₄ -P/l), 1973-1974	140
67.	Lake Erie model calibration for reactive silica (mg SiO ₂ /l), 1970	141
68.	Lake Erie model calibration for Secchi depth (m), 1970	143
69.	Lake Erie model calibration for zooplankton carbon (mg/l), 1970	144

70.	Dynamics of zooplankton population for western basin and eastern basin epilimnion. The curves are the calculated rates from the appropriate kinetic expressions	145
71.	Lake Erie model calibration for alkalinity, expressed as mg/l, of calcium carbonate equivalents, 1970	146
72.	Lake Erie model calibration for pH, 1970	147
73.	Lake Erie model calibration for the rate of primary production expressed as mg/m ³ /hr of carbon, 1970. Observations are shipboard ¹⁴ C measurements	149
74.	Lake Erie model calibration for biochemical oxygen demand (mg/l O ₂), 1967	150
75.	Lake Erie model verification for phytoplankton chlorophyll (µg/l), 1975	155
76.	Lake Erie model verification for organic nitrogen (mg N/l), 1975	156
77.	Lake Erie model verification for ammonia nitrogen (mg N/l), 1975	157
78.	Lake Erie model verification for nitrate nitrogen (mg N/l), 1975	158
79.	Lake Erie model verification for total phosphorus (mg PO ₄ -P/l), 1975	159
80.	Lake Erie model verification for orthophosphorus (mg PO ₄ -P/l), 1975	160
81.	Lake Erie model verification for reactive silica (mg SiO ₂ /l), 1975	161
82.	Lake Erie model verification for dissolved oxygen (mg/l), 1975	162
83.	Dynamics of central basin hypolimnion dissolved oxygen. The contributions of each of the oxygen sinks for the 1975 oxygen profile are shown	164
84.	Western basin loads (lbs/day) for orthophosphorus and unavailable phosphorus under two reduction schemes: (a) with point sources reduced to 0.5 mg/l and (b) diffuse sources reduced by 25% after point sources are reduced to 1 mg/l	170
85.	Summer average epilimnion chlorophyll (µg/l) versus lake total phosphorus loading (metric tons/yr). There are separate responses for point and diffuse source reductions and for each basin	171

86.	Summer average epilimnion total phosphorus ($\mu\text{g PO}_4\text{-P/l}$), versus lake total phosphorus loading (metric tons/yr). The pattern is similar to the chlorophyll results	173
87.	Summer average Secchi disk depth (m) versus lake total phosphorus loading (metric tons/yr). Load reductions will result in a significant increase in water clarity in the central and eastern basins	174
88.	Total phosphorus discharge to Lake Ontario versus lake total phosphorus loading (metric tons/yr). This loading is calculated based on the eastern basin epilimnion concentration and the existing flow to the Niagara River	175
89.	Area of anoxia (km^2) versus lake total phosphorus loading (metric tons/yr) showing both the short-term and ultimate effects	177
90.	Central basin hypolimnion oxygen consumption rate (mg/l/day) versus lake total phosphorus loading (metric tons/yr). The consumption rate is the sum of all water column and sediment oxygen sinks in the hypolimnion	178
91.	Minimum central basin hypolimnion dissolved oxygen (volume averaged concentration just prior to overturn in mg/l) versus lake total phosphorus loading (metric tons/yr)	179
92.	Summer average central basin hypolimnion dissolved oxygen (mg/l) versus lake total phosphorus loading (metric tons/yr)	180

ACKNOWLEDGMENTS

This work would not have been possible without the assistance and cooperation of many colleagues. The efforts of the members of the U.S. Environmental Protection Agency's Large Lakes Research Station, Grosse Ile, Michigan, were critical. In particular, thanks are due to Nelson Thomas for his guidance, support and knowledge of Lake Erie, William Richardson, as an understanding and helpful project officer, and Victor Bierman, for his insightful and critical comments. The efforts of the staff in transferring data to STORET is greatly appreciated. Without that effort and the STORET system, this analysis would have been much more cumbersome.

The concurrent analysis of the mass discharges of nutrients to Lake Erie by the members of the Lake Erie Wastewater Management Study Group, U.S. Army Corps of Engineers, Buffalo District, was another critical contribution. The timely cooperation and responses to requests by Steven Yaksich is greatly appreciated and this significant contribution is acknowledged.

The datasets used in this analysis were derived from three sources and to each of these groups a special thanks is due:

The Canada Centre for Inland Waters, for their cruise data and to Noel Burns for the numerous discussions of Lake Erie phenomena.

The Center for Lake Erie Area Research (CLEAR) of the Ohio State University and to Charles Herdendorf for its timely cooperation.

The Great Lakes Laboratory at the State University College of Buffalo and to Robert Sweeney for a useful set of sediment data.

Finally, our own colleagues at Manhattan College who contributed in many and important ways: Robert Thomann and Donald O'Connor and the members of the staff: Walter Matystik, William Beach and Joanne Guerriero. The friendly and timely assistance of Kathryn King and Eileen Lutomski who typed this report is greatly appreciated.

CHAPTER 1

INTRODUCTION

This report presents an analysis of the interactions between nutrient discharges to Lake Erie, the response of phytoplankton to these discharges, and the dissolved oxygen depletion that occurs as a consequence. The framework of the analysis is based on the principle of conservation of mass which is applied to the relevant variables. Chapter 2 presents a summary of the results of the analysis and projections of the response of Lake Erie to reduced phosphorus mass discharges. Chapter 3 lists recommendations for improving the utility and reliability of the computations.

Chapter 4 presents the details of the lake morphometry, hydrology, sedimentation, and nutrient mass discharges to the lake. Chapter 5 presents the water column data used for the analysis. Chapter 6 discusses the kinetics which represent the physical, chemical, and biological processes that affect the variables of concern in the water column. Recent developments in phytoplankton growth and uptake kinetics are analyzed and a more tractable version of these equations is presented. The complete kinetic structure is presented in a series of tables which define the stoichiometry of the reaction, the reaction rate expression, and the parameter values used in the computation.

In Chapter 7, the method for analyzing the interaction of the sediment and the overlying water is developed. The methods of sedimentary geochemistry are expanded to include an analysis of sediment oxygen demand within the framework of the mass balances. This novel approach related the sediment oxygen demand to the flux of algae and detritus to the

sediment, the decomposition reactions in the sediment and the mass transport mechanisms that affect the sediment solids and the interstitial water.

The seasonal vertical and horizontal mass transport for Lake Erie is analyzed in Chapter 8. The method relies on the analysis of tracer substances, specifically temperature and chloride. A simplified method for the computation of interbasin transport based on heat balances is developed.

The overall structure of the computation and the rationales which lead to the specific forms of the equations are presented in Chapter 9. The exogenous variables and the method for relating central basin hypolimnion average dissolved oxygen to anoxic area are presented. The computational method employed for the carbon dioxide-alkalinity systems are discussed and the final forms of the mass balance equations are presented and related to the specification of the water column kinetics in Chapter 6, the sediment reactions and mass transport in Chapter 7, and the lake transport in Chapter 8.

Chapter 10 contains a detailed presentation of the results of the calibration to the data presented in Chapter 5. Data from 1970 and 1973-1974 are compared to calculations for all the state variables and the successes and failures of the computation are discussed. Dissolved oxygen, phytoplankton chlorophyll for diatoms and non-diatoms, zooplankton biomass, nutrient concentration in available and unavailable forms, and inorganic carbon are considered. The sediment portion of the

computation is also calibrated to available observations although these are less complete.

Chapter 11 includes the results of a verification computation for 1975, a year when no anoxia was observed. The computations are in reasonable agreement with these observations as well. The principal cause of the abnormal condition was a shallower thermocline but the consequences were quite interesting and reflected the differing balances between areal and volumetric sinks of oxygen. A statistical analysis of the calibration and verification results is included.

Chapter 12 contains the projected effects of varying degrees of phosphorus removal. Considerable uncertainty results from the inability to project long-term deep sediment behavior, and the time scale of these effects. Dissolved oxygen, anoxia area, chlorophyll, transparency, and phosphorus concentrations are all calculated as functions of total phosphorus discharge to the lake. It is estimated that a discharge of 10,000 metric tons/yr will essentially eliminate anoxia in the central basin. A crude estimate of the uncertainty of this projection is 10-20% based on calibration and verification uncertainty.

CHAPTER 2

SUMMARY

This chapter is a summary of the principle results and conclusions of this report as they relate to the relationship between phosphorus discharges and dissolved oxygen depletion in Lake Erie. It summarizes the methods used to analyze the present effects of phosphorus discharges on the algal and dissolved oxygen distribution of Lake Erie and presents the results of calculations which attempt to predict the impact of phosphorus loading reductions. The chapters that follow present, in detail, the conceptual framework, the data employed, the mathematical formulations and their justification, the calibration and the verification calculations, and the complete results of the projection calculations. This presentation is an overview of the methods and results without detailed technical justifications.

2.1 FRAMEWORK

A direct causal chain links phosphorus inputs to the dissolved oxygen concentrations in Lake Erie. Phosphorus entering the lake increases the in-lake phosphorus concentrations. If the other nutrients required for phytoplankton growth are in excess supply and the population is not light limited, the plankton will respond and an increased concentration of biomass will result. The organic carbon synthesized and the dissolved oxygen liberated affect the dissolved oxygen concentration: the latter directly, the former via subsequent oxidation. A quantitative assessment of these phenomena is required if projections of the effects of phosphorus loading reductions are to be attempted.

Two essentially separate phenomena must be understood: the interaction of phytoplankton and nutrients, and the interactions of the sources and sinks for dissolved oxygen. The methods employed for both these calculations are based on mass balance equations.

The kinetics employed are designed to simulate the annual cycle of phytoplankton production, its relation to the supply of nutrients, and the effect on dissolved oxygen. The calculation is based on formulating the kinetics which govern the interactions between the biota and the forms of the nutrients and applying them to the regions of Lake Erie within the context of conservation of mass equations. The fifteen variables for which these calculations are performed are:

Phytoplankton

1. Diatom chlorophyll *a*
2. Non-diatom chlorophyll *a*

Zooplankton

3. Herbivorous zooplankton carbon
4. Carnivorous zooplankton carbon

Nitrogen

5. Organic nitrogen
6. Ammonia nitrogen
7. Nitrate nitrogen

Phosphorus

8. Unavailable phosphorus
9. Soluble reactive phosphorus

Silica

10. Unavailable silica
11. Soluble reactive silica

Carbon, Hydrogen, Oxygen

12. Detrital organic carbon
13. Dissolved inorganic carbon
14. Alkalinity
15. Dissolved oxygen

2.2 CALIBRATION - PHYTOPLANKTON AND NUTRIENTS

A critical requirement for establishing the credibility of the analysis is a complete calibration which compares the computation to the available observations. A summary of these

comparisons is shown in Figure 1. The average concentration of chlorophyll *a* is both computed and observed to decrease from west-to-east. The spring diatom bloom appears to be of comparable magnitude in all basins, whereas the magnitude of the fall non-diatom bloom progressively decreases from west-to-east. Shipboard ^{14}C primary production measurements are compared to the comparable kinetic expression in the calculation. The observed three-fold variation from west-to-east is correctly reproduced. Total phosphorus concentrations are observed and calculated to decrease from west-to-east. The higher observed concentrations in the late fall and early spring are attributed to wind-driven resuspension of sedimentary phosphorus due to high winds during this period. These effects do not appear to persist into the productive period of the year.

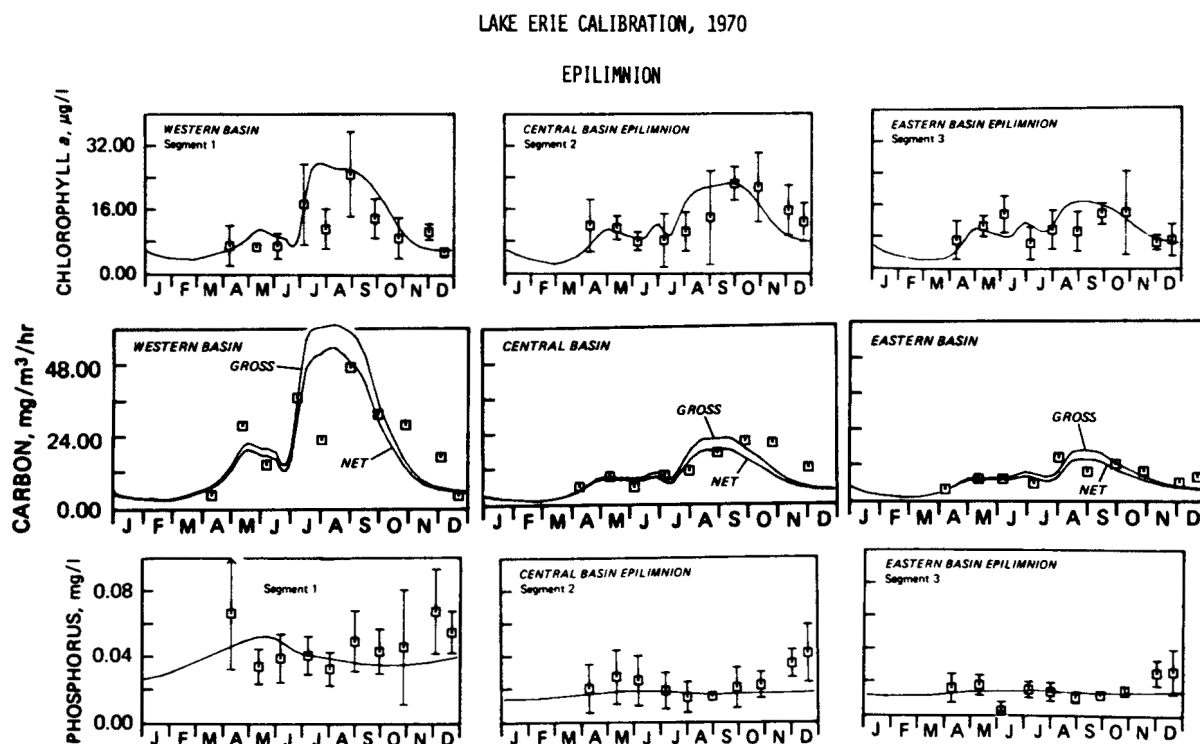


Figure 1. Lake Erie calibration results, 1970. Epilimnion western basin (left-hand side); central basin (center); eastern basin (right-hand side), chlorophyll *a*, µg/l (top), ^{14}C shipboard primary production mg C m³/hr (middle), total phosphorus mg/l (bottom). Symbols: Mean \pm standard deviation, lines are the computations.

The calculated and observed orthophosphorus, nitrate nitrogen (the ammonia concentrations are quite small), and silica concentrations are shown in Figure 2. The depletion of silica terminates the spring diatom bloom, whereas the exhaustion of nitrogen primarily in the western basin and phosphorus in the central and eastern basins terminates the non-diatom bloom. Again, the progressively decreasing concentrations from west-to-east are suggested but not as pronounced as in the previous figure. The somewhat scattered behavior of silica in the western basin is unexplained at present.

One of the principle purposes of calibration is to demonstrate that the calculation can reproduce

the major features of the seasonal distribution of phytoplankton and nutrients over a range of observed concentrations. The fact that the western, central, and eastern basin distributions are all reasonably well reproduced using the same kinetic structure and coefficients suggests that the calculation has a certain generality and can reproduce conditions as distinct as those in the western and eastern basin.

2.3 CALIBRATION - DISSOLVED OXYGEN

The second phenomena of concern are those that influence the dissolved oxygen balance in the basins. Since the comparatively shallow

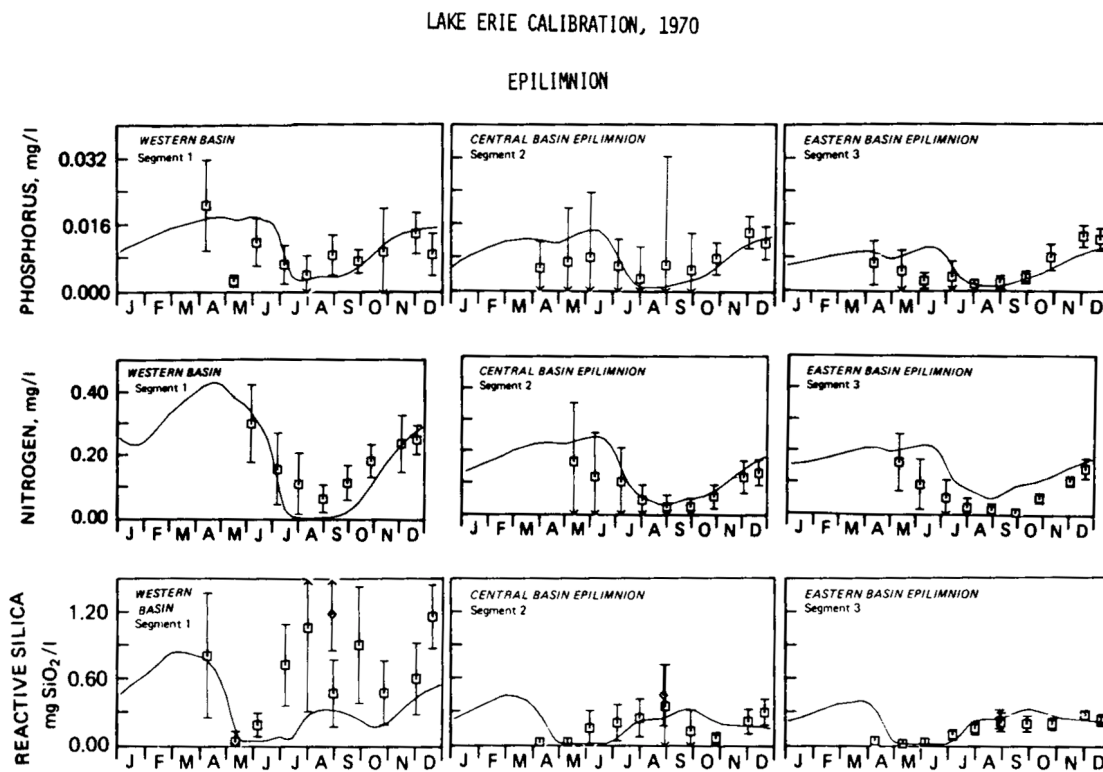


Figure 2. Lake Erie calibration results, 1970 epilimnion. Western basin (left-hand side), central basin (center), eastern basin (right-hand side), orthophosphorus (top), nitrate nitrogen (middle), reactive silica (bottom).

western basin is essentially completely mixed vertically and remains nearly saturated throughout the year, it is not of concern, although it is part of the oxygen balance calculation. Three regions are represented in each basin: the epilimnion, the hypolimnion, and the surface sediment layer. The principle sources and sinks of dissolved oxygen are associated with the phytoplankton and detrital organic carbon in these segments. Although nitrification is included in the calculation, its effect is negligible. The principle aerobic reactions which affect dissolved oxygen are primary production and respiration of phytoplankton, and the oxidation of detrital

organic carbon via bacterial synthesis and respiration. The primary production reaction liberates dissolved oxygen and decreases total carbon dioxide. The aerobic respiration reactions consume dissolved oxygen and liberate carbon dioxide. Thus, both dissolved oxygen and total inorganic carbon mass balances are considered. This provides an additional variable for the calibration, giving a total of four principles state variables of concern as shown in Figure 3. Of these, three are directly observed. As discussed below, biochemical oxygen demand (BOD) measurements provide an indirect requirement of the fourth variable, the detrital organic carbon.

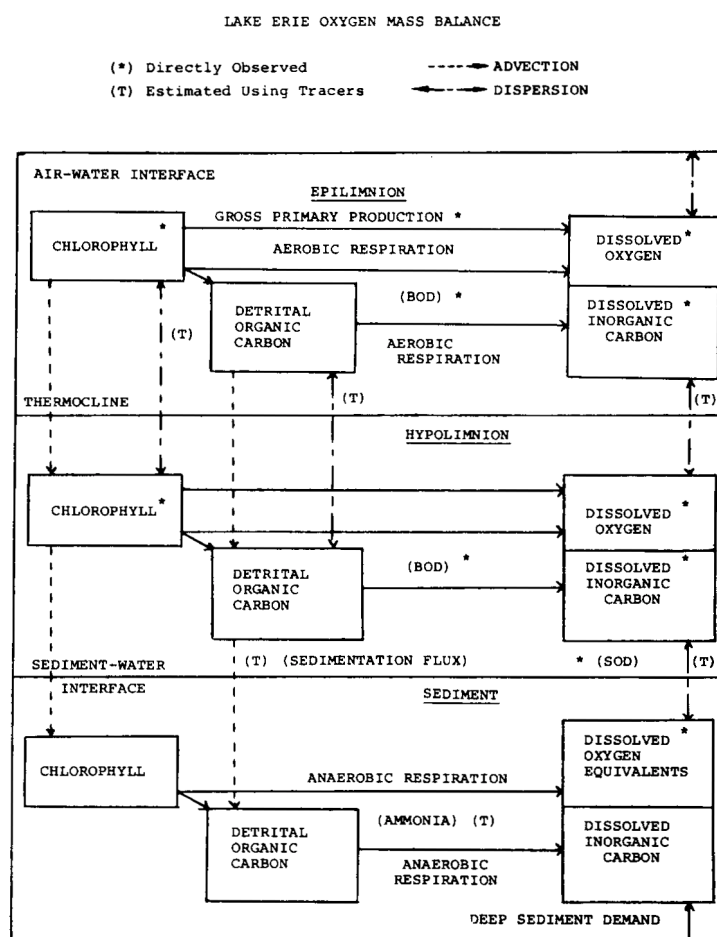


Figure 3. Schematic diagram of the dissolved oxygen mass balance computation. The epilimnion, hypolimnion (for central and eastern basins), and surface sediment segments as indicated. Directly observed concentrations and reaction rates are indicated (*). Transport rates estimated using tracers are indicated (T).

The concentrations of concern are affected by two classes of transport phenomena: dispersion, which exchanges matter across the segment interfaces; and advection, which in the vertical direction, is associated with settling of the particulates. These are shown in Figure 3, together with the principal reactions of concern. If all the transport fluxes and reaction rates were directly observed, then the mass balance calculation could be accomplished by simple summations. These could then be compared to the observed concentrations as a check on the reaction and transport fluxes. Unfortunately, neither all the variables nor all the fluxes are observed, as indicated in Figure 3. These must either be estimated using tracers or from the calibration itself.

Air-water interface exchange is assigned based on wind velocity and empirical relationships. Thermocline exchange is estimated using temperature as a tracer. Hypolimnion-interstitial water exchange is estimated using chloride as a tracer. Settling velocities of phytoplankton and detrital carbon are assigned based on literature values and the calibration. Sedimentation settling velocity is estimated using pollen tracers and sedimentation trap results.

Certain reaction rates are also directly observed; for example, primary production. The aerobic respiration rate of oxygen is directly observed as BOD. Since this rate is the sum of both detrital oxidation and phytoplankton respiration, it provides an indirect measurement of the detrital carbon concentration.

For the sediment segment, direct observations of the dissolved oxygen equivalents in the interstitial water are available. However, due to the complex chemistry associated with the anaerobic respiration, the total carbon dioxide (CO_2) is not easily computed. The interstitial ammonia concentration provides a tracer which is liberated as the anaerobic respirations proceed, so that this reaction rate can be estimated.

As previously discussed, the purpose of the calibration is to estimate the individual kinetic coefficients based on the observed state variable concentrations and composite reaction rates, and to demonstrate their applicability in differing regions of the lake. The results for the central basin are shown in Figure 4. Dissolved oxygen, while remaining essentially saturated in the epilimnion, declines after stratification to a minimum of 1.0 mg/l before overturn. The lack of fit after overturn is due to an inaccurate estimate of the vertical dispersion. The pH comparison is a direct calibration of the total CO_2 computation since the pH is determined by changes in total CO_2 , the alkalinity being essentially constant. There is a dramatic difference between the epilimnion pH reflecting the net total CO_2 loss which is occurring and the hypolimnion pH reflecting the net total CO_2 production.

The chlorophyll concentrations also reflect the production in the surface layer, the settling into the hypolimnion and the respiration and other losses. Figure 5 gives the comparisons to epilimnion primary production and BOD in both layers. The larger quantity of BOD in the epilimnion reflects the larger quantity of phytoplankton and detrital organic carbon. The table presents the observed and computed sediment interstitial water concentrations. The ammonia and oxygen equivalents are within the range of observations. The deep sediment flux of oxygen equivalents is chosen to match both the observed oxygen equivalent concentration and also the observed oxygen equivalent flux which is observed as the sediment oxygen demand at the sediment-water interface. Similar comparisons for the eastern basin have also been made with essentially comparable results.

A summary of the computed sources and sinks of dissolved oxygen in the central basin hypolimnion during the summer stratified conditions is presented in Table 1. The aqueous reactions: phytoplankton respiration and detrital organic carbon oxidation consume a total of 5.08 mg O_2 /l during the period of stratification. The oxygen decrease attributed to sediment

LAKE ERIE CENTRAL BASIN CALIBRATION

1970

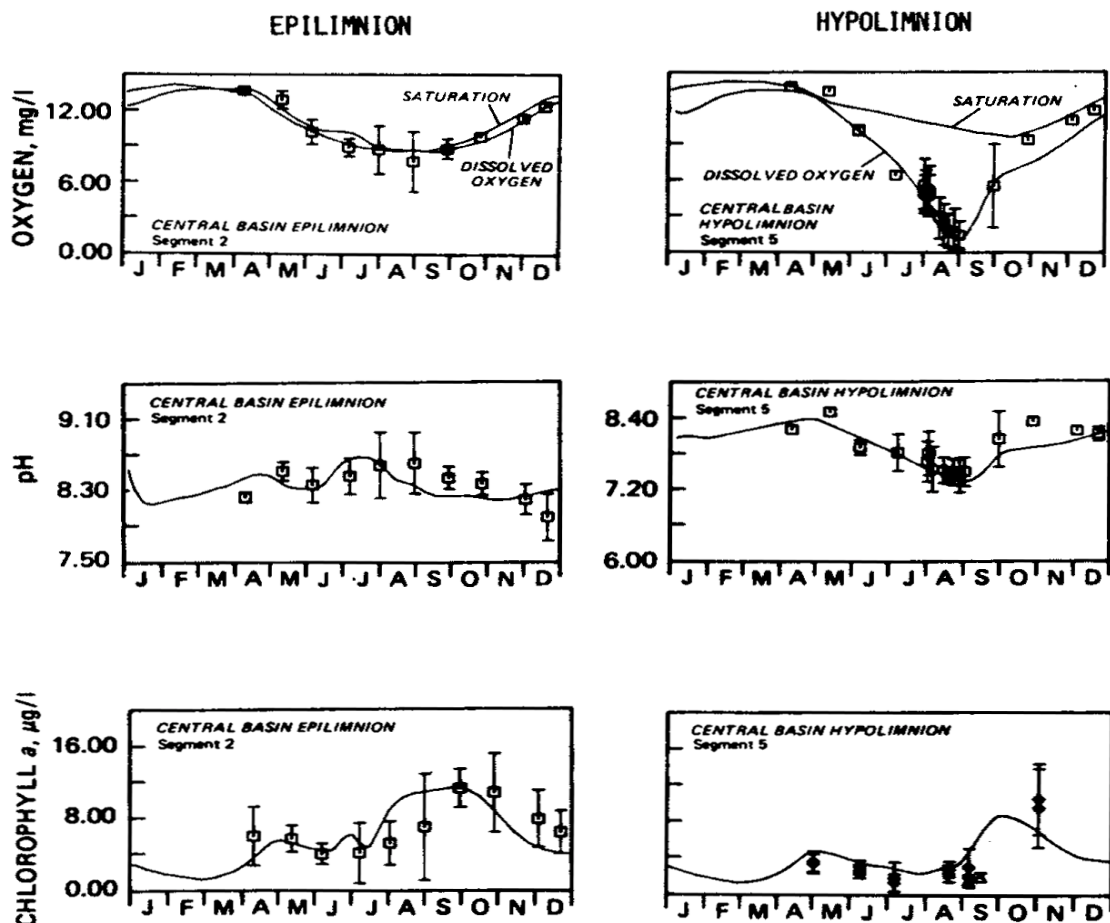


Figure 4. Lake Erie basin calibration for dissolved oxygen and related variables, 1970. Epilimnion (left-hand side), hypolimnion (right-hand side), dissolved oxygen mg/l (top), pH (middle), chlorophyll a µg/l (bottom). The hypolimnion chlorophyll a data is 1973-1974, as no 1970 data are available.

LAKE ERIE CENTRAL BASIN

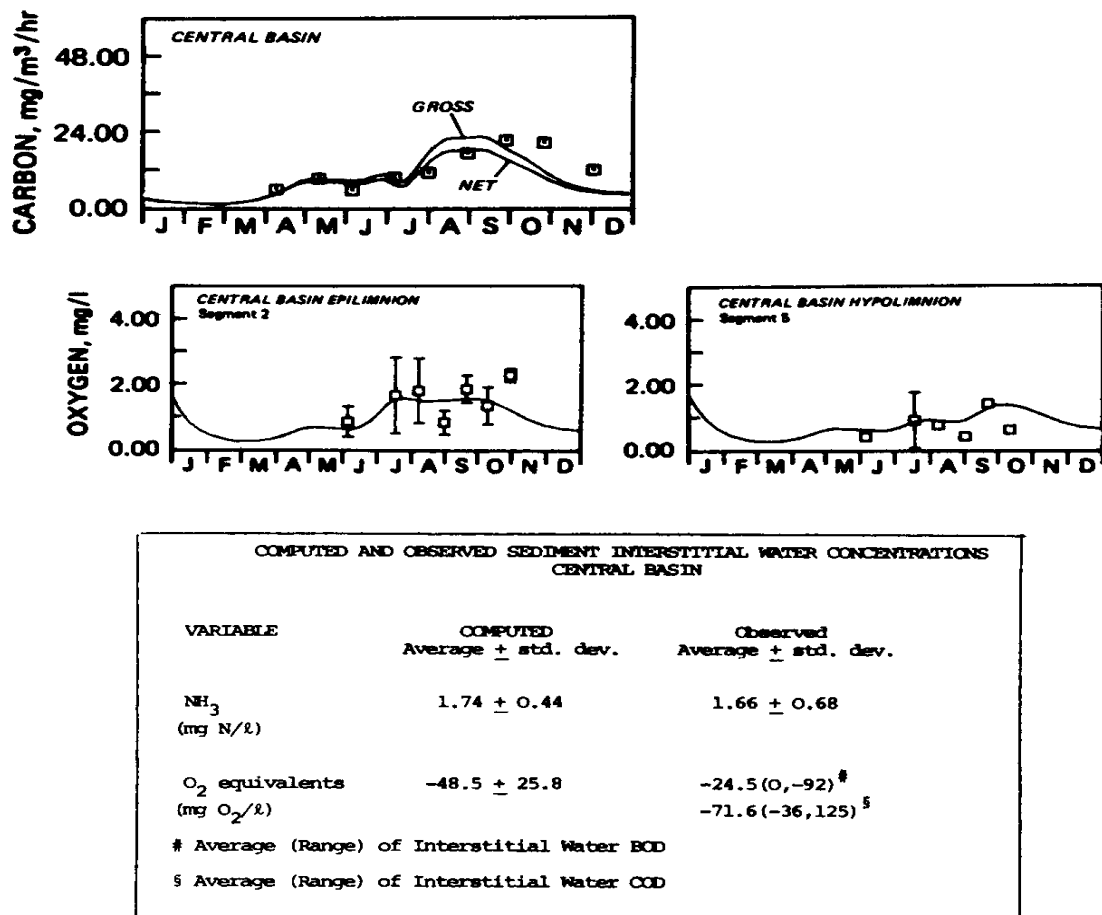


Figure 5. Lake Erie central basin calibration. Epilimnion (left-hand side), hypolimnion (right-hand side), shipboard ¹⁴C primary production (top). No hypolimnion data available, BOD₅ (middle). This is 1967 data as no 1970 data are available.

Table 1. Sources and Sinks of Dissolved Oxygen, Central Basin Hypolimnion, 1970

Reaction	Average-Volumetric Depletion Rate	Dissolved O ₂ Change
Source (+) Sink (-)	(mg O ₂ /l day)	Day 180-240 (mg O ₂ /l)
Phytoplankton Respiration	-0.20	-1.80
Detrital Organic Carbon Oxidation	-0.0646	-3.88
Sediment Oxygen Demand	-0.0597	-3.58
Thermocline Transport	-0.0305	1.83
Total O ₂ Change		-6.83

oxidation is 3.58 mg O₂/l. These sinks are balanced by the only significant source considered in the computation: transport of dissolved oxygen through the thermocline, which increases the concentration by 1.83 mg O₂/l. The net result is a decrease of 6.83 mg O₂/l during the sixty-day period analyzed in this table. These sources and sinks combine to produce the result shown in Figure 4.

2.4 VERIFICATION

The dissolved oxygen distribution in the central basin in 1975 was quite different from that in previous years and this provides an opportunity to verify the computation. The result is shown in Figure 6. The principal difference between 1975 and the previous four years was the abnormally shallow depth at which the thermocline developed. This increased the volume of oxygen trapped below in the hypolimnion. It is interesting to note that if oxygen depletion were due to purely volumetric consumption, this would have no effect on the dissolved oxygen distribution since the extra trapped dissolved oxygen is exactly balanced by the extra trapped

volumetric dissolved oxygen demand assuming the production of phytoplankton and detrital carbon is the same. However, if the oxygen depletion were due only to areal oxygen demand at the sediment-water interface, then the effect of essentially a doubling of the hypolimnetic volume would be to half the dissolved oxygen depletion. In fact, what was observed and calculated is the result of the combination of these two sinks of dissolved oxygen. The fact that the computations are able to verify the 1975 dissolved oxygen distribution implies that the proportion of volumetric and areal oxygen demand in the calculation are correct.

The chlorophyll, orthophosphorus, and nitrate nitrogen are also shown. Note that slightly less chlorophyll is calculated in 1975 than in 1970 due to a relatively small (12%) phosphorus loading reduction achieved between 1970 and 1975. Although the effect is slight in the chlorophyll, it is calculated and observed in the nitrate distribution. Slightly less nitrate uptake was observed and calculated in 1975. Admittedly, this effect is small but encouraging.

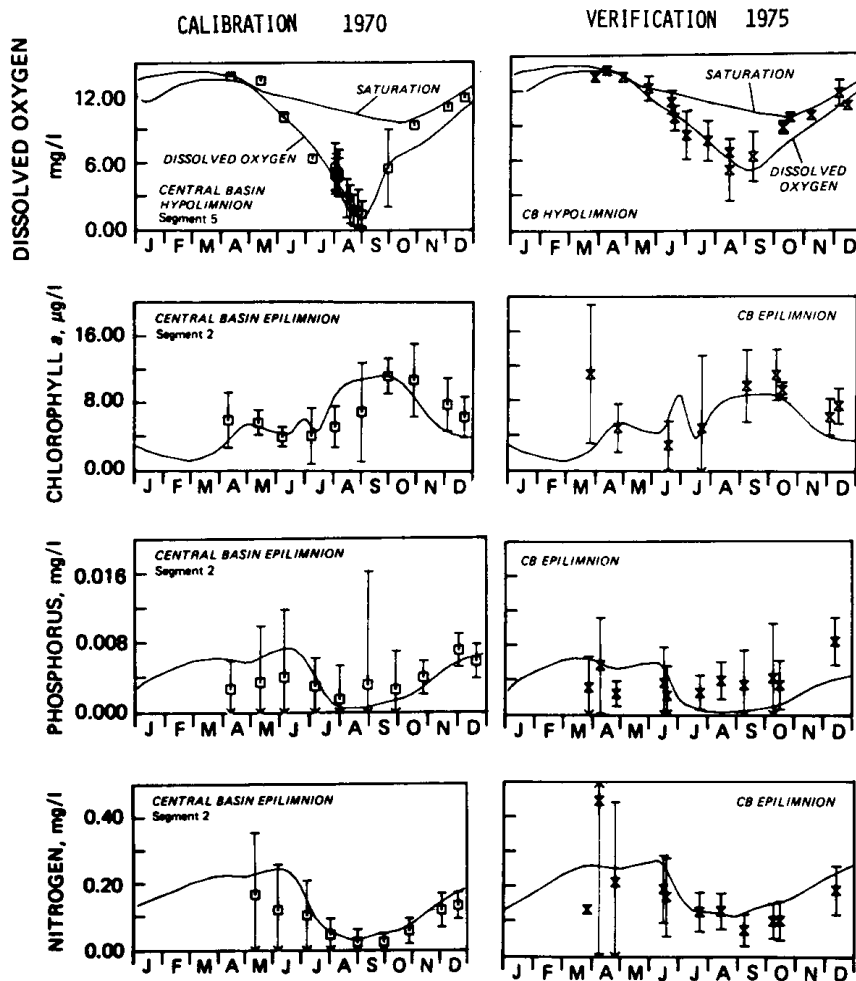


Figure 6. Comparison of 1970 calibration (left-hand side) and 1975 verification (right-hand side) dissolved oxygen (top), chlorophyll *a* (upper middle), orthophosphorus (lower middle), nitrate nitrogen (bottom).

2.5 PROJECTIONS

A comprehensive calculation of this sort can be used to calculate the effects of phosphorus loading reductions on the dissolved oxygen, in particular, in the central basin. An immediate question regarding these calculations is: how accurate are these projections likely to be. Although there is no firm methodology available at present to answer this question, it is certainly the case that the projections are not likely to be any more accurate than the calibration and verification. An analysis of the residuals, the

observed minus calculated dissolved oxygen concentration for the central basin is shown in Table 2.

Residual standard deviations of ~ 0.5 to 1.0 mg/l imply that the prediction error standard deviation is likely to be at least this large for any specific time during the computation. In terms of median relative error (~ 5-15%), the calibration and verification of the central basin is among the more precisely calibrated of dissolved oxygen models (Thomann, 1979).

Table 2. Dissolved Oxygen Calibration - Residual Analysis, 1970

		Mean (mg/l)	Residual* Standard Deviation (mg/l)	Median** Relative Error (%)
Central Basin				
Epilimnion	1970	-0.13	0.60	4
	1973-1974	-0.16	1.26	7
	1975	-0.24	0.95	6
Hypolimnion	1970	0.56	0.77	12
	1973-1974	0.63	1.08	15
	1975	0.29	0.93	8

*Residual = Calculated-Observed.

**Relative Error = |Calculated-Observed|/Observed.

The critical question concerning the central basin is: at what phosphorus mass discharge rate will the anoxia in the central basin be eliminated. For the mass balance calculation, the entire hypolimnion is represented effectively by one segment. However, the anoxic area that develops is confined to a region close to the sediment water interface. Therefore, it is necessary to relate the volume average hypolimnetic dissolved oxygen concentration to the minimum dissolved oxygen in the hypolimnion. The results are shown in Figure 7, which is a plot of both these observations. It is clear from these data that for a hypolimnetic average oxygen concentration of 4.0 mg/l, anoxia begins in the basin.

The projection computations are also shown. The short-term effect is the projected concentration five years after an abrupt reduction in phosphorus loading as specified in the abscissa. The ultimate effect assumes that the deep sediment oxygen demand has responded to the reduction of the influx of organic carbon to the sediment in proportion to the reduction computed in the surface sediment

segment. The solid line corresponds to point source reductions, the dotted line to diffuse source reductions which are less effective. A reduction to between 9500 and 12000 metric tons/yr in the total phosphorus loading is projected to eliminate anoxia in the central basin. This range is due to the uncertainty of the long-term deep sediment response.

A further uncertainty is due to the prediction uncertainty of the calculation. If one assumes that the prediction uncertainty in dissolved oxygen is equal to the calibration, then with a linear relationship between loading and concentration (Figure 7), the standard deviation of the projected loading is linearly related to the prediction standard deviation. For a predicted loading of 10,000 metric tons/yr and using a range of 0.5-1.0 mg/l for the prediction standard deviation, the predicted loading standard deviation is ~ 2000 metric tons/yr so that the prediction uncertainty due to calibration uncertainty is estimated to be in the range of 10-20%.

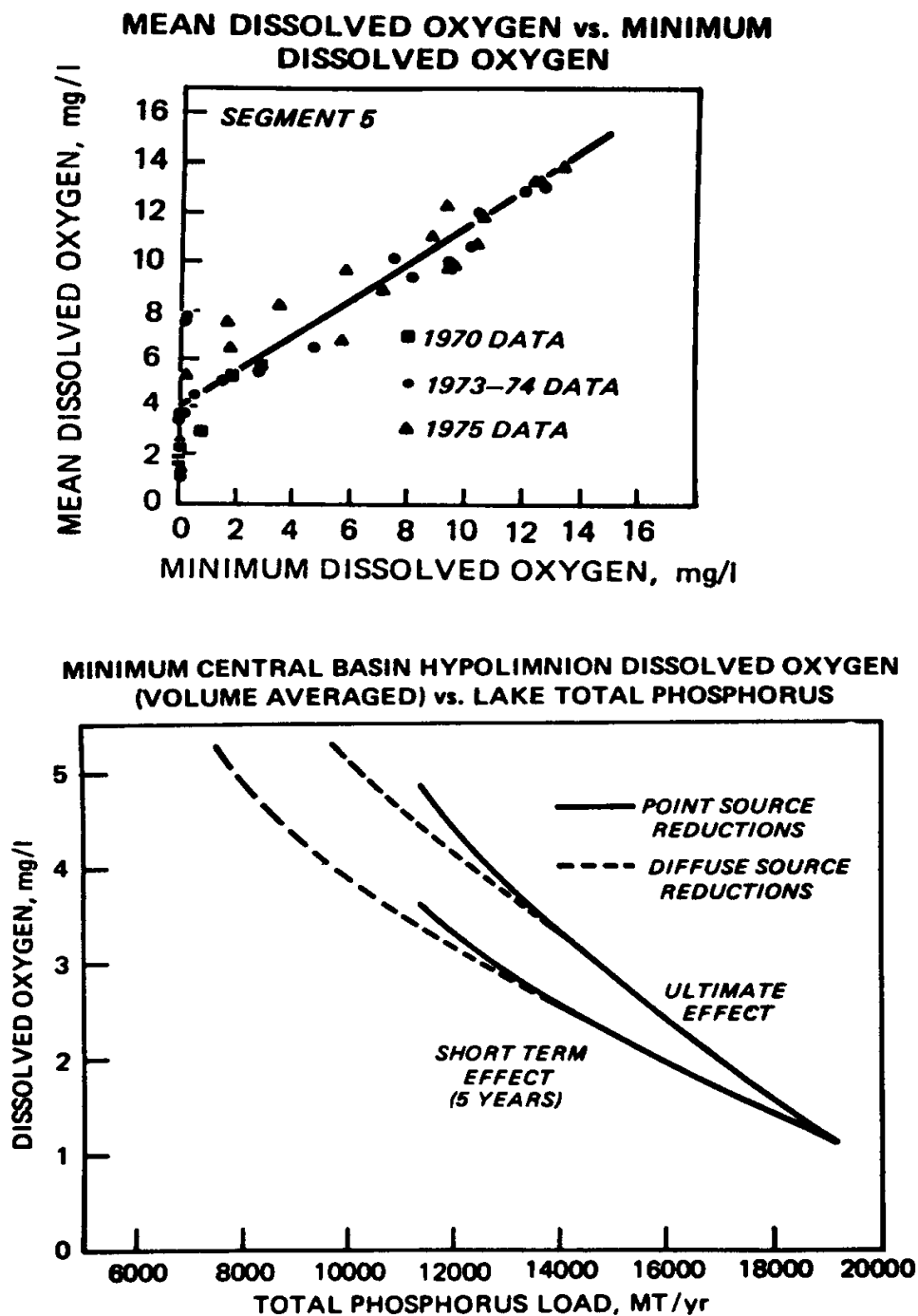


Figure 7. Observed hypolimnion mean dissolved oxygen versus minimum observed hypolimnion dissolved oxygen (top). Predicted mean hypolimnion dissolved oxygen just prior to overturn versus lake total phosphorus loading (bottom).

CHAPTER 3

RECOMMENDATIONS

In the course of this analysis of the relationship between nutrient discharges, phytoplankton growth, and dissolved oxygen depletion, a number of shortcomings in theoretical understanding, observational data, and experimental investigations have been uncovered. These recommendations are based upon these considerations.

The most critical requirement is an assessment of the degree of uncertainty to be associated with the projected response of Lake Erie to reductions in phosphorus loading. A number of different avenues of investigation should be pursued in order to develop a response to this question of uncertainty.

The major source of uncertainty in the present state of the computations is the behavior of the sediment under present and projected conditions. The computations in this report are based on a one-layer sediment segment. This should be expanded to include a multiple layer vertical analysis which can be calibrated in much more detail with both interstitial water and sediment solids concentrations of the relevant variables. The expected time to steady-state under projected conditions should be calculated.

A more detailed vertical segmentation of the central basin is required in order to assess the magnitude of the areal sediment-water fluxes and the volumetric water reactions. Advances in phytoplankton growth and uptake kinetics should be included in the computation. This, when coupled to a detailed sediment computation, should allow a more refined analysis of these

critical oxygen depleting and nutrient regenerating reactions.

Experiments designed to measure directly the flux of oxygen equivalents from the sediments are required in order to confirm the theoretical structure used in the calculations presented in this report.

A comprehensive data collection program should be pursued which is designed to measure directly all the areal and volumetric rates which either produce or consume oxygen in the central basin hypolimnion. The data used in this report are composited from several years and of particular importance is the volumetric depletion rate measurement (BOD) and direct sediment flux measurement.

A comprehensive monitoring program for the measurement of nutrient loading to the lakes should be continued. Methods of sampling and assumptions regarding methods of calculating the loading from the observations should be agreed upon. The U.S. Army Corps of Engineers (USACOE) efforts in this regard are to be commended. The results of their analysis were a critical component of the calculations presented in this report. For future re-evaluations of the response of the lake to changes in inputs, a comparable effort must be expended in order to obtain reliable loading information.

A statistical methodology should be developed which is capable of addressing the question of uncertainty of projections. The crude analysis presented at the conclusion of this report is only

a rough approximation and should be taken only as an indication of the order of magnitude of the uncertainty. Since this question of uncertainty is central to the use of model computations for decision-making, it should be pursued with the same effort as that expended upon the other facets of the analysis.

As phosphorus removal programs are implemented, it is of utmost importance that the actual response of the lake be documented and compared to projected responses. There is no substitute for observations of response after large scale changes in loading are accomplished. However, a casual inspection of routine monitoring data is not sufficient to test the predictions since the lake is a complex and interactive system. Only integrated calculations and complete observations can isolate the relevant effects, check the predictions in detail,

and determine the extent of agreement or disagreement between observation and prediction. The design of the data collection program should be compatible with the methods of analysis and computation that are to be applied. For computations based on mass balance principles of the sort used in this report, the minimum requirements are measurements of all the state variables and observable rates used in the calibration, both in the water column and the sediment. The nutrient loading rates to the lakes are also required as discussed previously.

Such a comprehensive evaluation should contribute to the development of more detailed knowledge and more reliable predictive methods for the Great Lakes in general and Lake Erie in particular.

CHAPTER 4

DESCRIPTION OF STUDY AREA, MASS DISCHARGE RATES, SEGMENTATION

4.1 MORPHOMETRY

Situated between Lake Huron and Lake Ontario, Lake Erie is the fourth in the chain of Great Lakes. Although all the Great Lakes are similar in their origin and history, Lake Erie exhibits distinct properties.

Volumetrically, Lake Erie is the smallest of the Great Lakes, 470 km^3 (Federal Water Pollution Control Administration (FWPCA), 1968). The surface area of Lake Erie, $25,750 \text{ km}^2$, is slightly larger than that of Lake Ontario (FWPCA, 1968). Lake Erie is the shallowest of the Great Lakes with a maximum depth of 64 m, and an average depth of only 18 m (FWPCA, 1968). The drainage area of Lake Erie is $86,762 \text{ km}^2$ excluding Lake St. Clair (Great Lakes Basin Commission, 1976).

Lake Erie is divided naturally into three basins: the western basin, central basin, and eastern basin. The western and central basins are separated by a chain of bedrock islands. The central and eastern basins are separated by a ridge of sand covered glacial clay.

The western basin is shallow and flat with a muddy bottom. It covers approximately $3,100 \text{ km}^2$ and has an average depth of 7.5 m (FWPCA, 1968). Conditions in the basin are greatly influenced by the Detroit River.

The central basin is the largest of the three basins being approximately $16,300 \text{ km}^2$ in area (FWPCA, 1968). The maximum depth is about 25 m and the average depth is 18.3 m (FWPCA,

1968). The bottom is relatively flat with a mud-sand composition.

The eastern basin has a surface area of $6,220 \text{ km}^2$, a maximum depth of 64 m and an average depth of about 40 m. In contrast to the other basins, the bottom is not flat but steeply sloped.

4.2 HYDROLOGY

Water inflow to Lake Erie is dominated by the Detroit River which drains from Lake Huron-Lake St. Clair. The average flow of the Detroit River between 1936 and 1974 is 188,000 cfs (National Atmospheric and Oceanic Administration (NOAA), 1975) which accounts for over 90 percent of the flow discharged via the Niagara River and Welland Canal. However, since 1967 the flows have been consistently higher than the average, reaching a maximum yearly average of 238,000 cfs (NOAA, 1975). The flow from the Detroit River controls the circulation in the western basin penetrating far southward into the basin and then draining, primarily through the northern island channels (FWPCA, 1968).

Only four other tributaries to Lake Erie exceed an average flow of 1,000 cfs. They are, in order of decreasing contribution, the Maumee, the Grand (Ontario), the Thames, and the Sandusky (FWPCA, 1968). There are some twenty other tributaries feeding Lake Erie. The flow in each of these is small sometimes reaching zero in summer.

Lake Erie has the greatest water loss due to evaporation of any of the Great Lakes (Sly, 1976). This loss has been estimated at about 85 cm (33.5 inches) per year (Derecki, 1964). However, the loss is approximately equal to the water surface precipitation and thus neither figure significantly in the water budget for the lake (Sly, 1976; Brunk, 1964).

Table 3 shows the flow budget for the lake used in the subsequent calculations. Based on these flows, the hydraulic detention time of the lake is approximately 2.5 years, the shortest of the Great Lakes, approximately one-fourth the Lake Ontario retention time and approximately one-tenth of that for Lake Huron. The retention time is related to the lake's response time to changes in mass input rates. However, as shown subsequently, the actual response time for certain substances is significantly longer due to the sediment-water interactions.

4.3 SEGMENTATION

For the purposes of the computations presented subsequently, Lake Erie is divided into ten completely mixed segments to represent the significant geophysical, chemical, and biological variations exhibited throughout the lake. Six of the segments are water column segments and four are sediment segments. The lake is logically divided by basin. In the central and eastern basin where a thermocline develops, epilimnion and hypolimnion segments are

considered. The central basin hypolimnion is separated into two segments representing the bulk of the hypolimnion and a thin bottom layer. Sediment segments underlie each of the hypolimnion segments and the western basin segment. Figure 8 shows this segmentation.

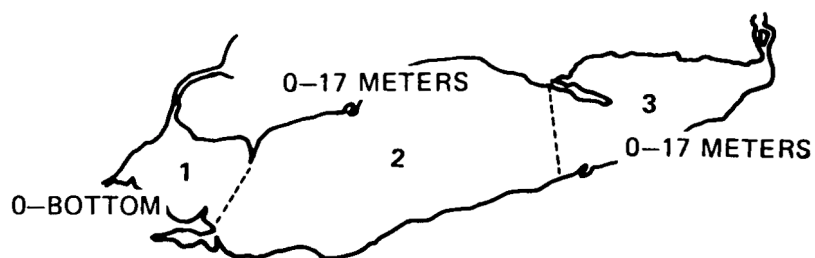
Segment 1 represents the western basin. It extends from the surface to the sediment interface which is assumed to be at the average depth of the basin: 7.5 meters. The eastern boundary of the segment is a straight line from Pelee Point to the edge of Sandusky Bay. Segment 1 receives flow and nutrient loadings from the Detroit and Maumee Rivers which constitute the majority of the mass inputs to the lake.

The central basin epilimnion is represented by segment 2. It is bounded by segment 1 on the west and segment 3 on the east. The eastern boundary extends from just west of Port Ravan, Ontario to a point about fifteen kilometers west of Erie, Pennsylvania. This line follows the natural ridge separating the central and eastern basins. Segment 2 extends from the surface to a depth of 17 meters which is the approximate depth of the thermocline during 1970 and 1974, the years chosen for calibration. For the 1975 verification, the depth of segment 2 is set at 13 meters to reflect the unusually high thermocline in that year, as described subsequently in Chapter 8.

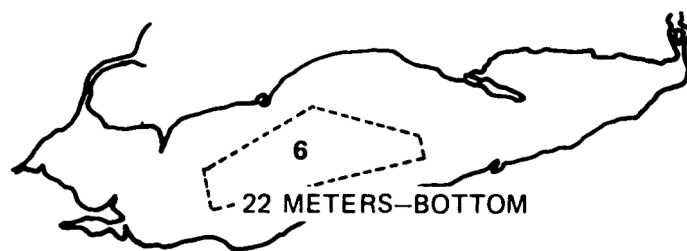
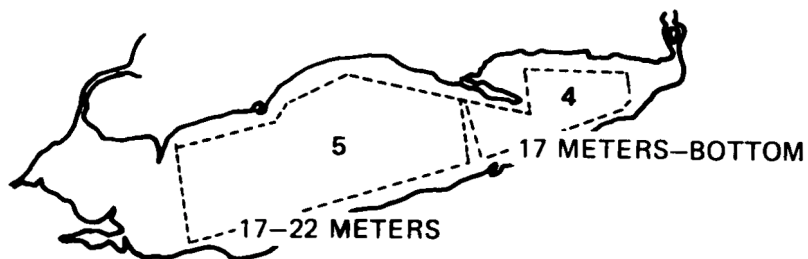
Table 3. Lake Erie Flow Budget

Sources	Flow (cfs)	# of Discharge
Detroit River	209,000	95.0
Maumee River	4,000	1.8
Other Tributaries	7,000	3.2
Discharge		
Niagara Rive and Welland Canal	220,600	

EPILIMNION SEGMENTS



HYPOLIMNION SEGMENTS



SEDIMENT SEGMENTS

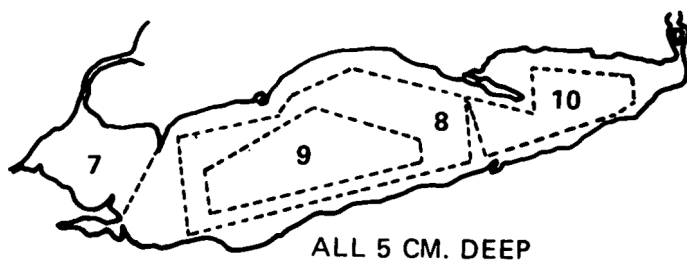


Figure 8. Lake Erie model segmentation of western, central and eastern basins: water segments 1-6, epilimnion (top) and hypolimnion (middle); sediment segments 7-10 (bottom).

Segment 3 corresponds to the eastern basin epilimnion. As with segment 2, the depth is 17 meters. It is the outflow segment of the model discharging to the Niagara River and Welland Canal.

Directly below segment 3 is segment 4, representing the eastern basin hypolimnion. Although the actual maximum depth of the basin is 64 meters, segment 4 extends from 17 meters to the average depth of the basin, 40 meters.

Segments 5 and 6 represent the central basin hypolimnion. The bulk of the hypolimnion makes up segment 5. Segment 6 comprises a thin bottom layer. This differentiation is established in order to reflect the dissolved oxygen gradient in the hypolimnion. Segment 5 extends from 17 meters to 22 meters and segment 6 from 22 meters to the bottom.

The well-mixed surface layer of the sediment which underlies the lake is represented by segments 7 through 10. They are included in order to calculate, dynamically, the nutrient exchange and oxygen demand at the water column-sediment interface. A segment depth

of five centimeters is chosen as the depth of the well-mixed layer in the sediment as discussed subsequently.

The individual segment depths, areas and volumes are listed in Table 4. This information was compiled from bathymetric charts of Lake Erie (NOAA, 1974; Canadian Hydrographic Service, 1971). Basin area versus depth profiles were constructed using a planimeter which were then converted into segment volumes.

4.4 RATES OF MASS DISCHARGE

The first comprehensive documentation of the rates of mass discharge to Lake Erie is reported in the 1969 International Joint Commission (IJC) report (IJC, 1969). Total nitrogen, total phosphorus, chlorides, solids and BOD mass loadings are given for 1967. These are subdivided into major municipal, industrial, and tributary components. The tributary component is further subdivided into the municipal, industrial, and other sources discharging to the tributary load.

Table 4. Segment Parameters

Segment	Depth (meters)	Area (km ²)		Volume (km ³)
		Surface	Bottom	
1	7.5	3010	-	22.6
2	17	15560	9400	234.6
3	17	6150	4177	91.9
4	23	4177	-	82.7
5	5	9400	3750	43.5
6	2	3750	-	7.5
7	0.05	3010	-	0.15
8	0.05	5650	-	0.28
9	0.05	3750	-	0.19
10	0.05	4177	-	0.27

Total lake surface area = 24720 km²

Total lake volume = 482.8 km³

Since the 1969 report, the IJC has published yearly reports, (IJC, 1973, 1974a, 1975, 1976) in which mass loading estimates to Lake Erie are made, separated into industrial, municipal and tributary sources. However, the loadings are not subdivided by basins, which is a requirement for the present calculation. Burns (1976) has reported basin specific mass loadings for 1970. For these estimates, tributary inputs were calculated for mean monthly flow and concentration data. Direct discharges were estimated from the 1969 IJC report. The mass loadings are reported as annual averages for each basin.

The IJC report indicates that the Detroit River is by far the largest contributor of mass loadings to Lake Erie comprising almost 60% of the total phosphorus and 71% of the total nitrogen input. Since the Detroit River discharges into the shallow western basin, the combination of the magnitude of the loadings and the shallowness of the basin result in a strong coupling between Detroit River and western basin conditions. It is necessary, therefore, that the Detroit River contribution be estimated as accurately as possible.

4.5 ESTIMATE OF DETROIT RIVER MASS DISCHARGE

The concentrations of various water quality constituents entering Lake Erie from the Detroit River are monitored separately by two agencies: the Michigan Department of Natural Resources (MDNR) and the Ontario Ministry of the Environment (OME). Because the Detroit River is characterized by lateral concentration gradients (OME, 1972), measurements are taken at several stations along a transect from Michigan to Ontario. The MDNR has eleven stations and OME monitors twelve.

Three different methods are used to determine the mass loading rate to Lake Erie on the transect data. The MDNR divides the river cross-sections into panels each containing ten percent of the total flow and uses the concentration at a station within the panel as the

panel concentration. OME uses the same ten percent panels with the average concentration for the panel. The IJC uses station concentrations in conjunction with the actual percentage of flow for an area of cross-section one-half the distance to the next station. All three agencies use flow distribution measurements made by the U.S. Environmental Protection Agency (USEPA) in 1963 (IJC, 1974b).

The estimates of the mass loadings based on the two datasets and three calculation methods vary widely. Table 5, compiled from the Lake Erie Wastewater Management Preliminary Feasibility Report (USACOE, 1975), shows this variation in the loading estimates for total phosphorus. Differences between the three calculation methods are to be expected. The variation in lateral concentration averaging technique results in different estimates in direct proportion to the steepness of the concentration gradient. Note that using the OME data, the IJC method consistently yields smaller standard deviations than the OME method. Comparing the two datasets using the IJC method, the OME data yields lower loadings than the MDNR data. For 1970, the calibration year for the model, the OME estimate is 62% of the MDNR estimate. The standard deviation of the OME estimate is about one-third that of the MDNR. The estimated difference is even more pronounced in 1972 when the MDNR data yields a loading about twice that of the OME data. These differences demonstrate a lack of concordance between the data from Michigan and the data from Ontario. The larger standard deviations of the MDNR data using the same calculation method imply that there is much more loading variability in the river than that described by the OME data.

The strong influence of the Detroit River on the western basin and all of Lake Erie makes the choice of dataset and calculation method used for the mass loading estimate an important decision. If the estimate is too large, the vertical transport (settling) will be overestimated in order to match observed concentrations. If the loading

Table 5. Detroit River Phosphorus Loading Rates (Metric Tons/Year)

Year	Calculation Method			
	IJC		MDNR	OME
	OME Data	MDNR Data	MDNR Data	OME Data
1967	17380 ± 3645			17836 ± 9456
1968	13997 ± 2020	28308 ± 3980	32790	15583 ± 8727
1969	12340 ± 664	21591 ± 5680	26994	15020 ± 4206
1970	12881 ± 2133	20882 ± 6287	24344	12354 ± 12487
1971	9038 ± 1249	13812 ± 2520	13083	10748 ± 2683
1972	8022 ± 964	15515 ± 6195	16080	9423 ± 2269
1973	8771 ± 868	13884 ± 1299	12321	9572 ± 2004
1974	10963 ± 1455	9547 ± 2338	10950	

Data Source: Lake Erie Wastewater Management Study Preliminary Feasibility Report (USACOE, 1975).

estimate is too small, sediment sources will be overestimated. Therefore, the particular estimate that is chosen has substantial ramifications.

4.6 LAKE ERIE WASTEWATER MANAGEMENT STUDY

The most comprehensive study of mass loadings to Lake Erie has been performed by the USACOE, Buffalo District. As part of their Lake Erie Wastewater Management Study (LEWMS), the USACOE have reviewed previous methods of estimating mass loadings and have proposed and implemented a new method. The USACOE analyzed the three main methods traditionally used in mass loading estimation, comparing them to known loadings based on daily measurements. The three methods are:

A. Average annual flow x average annual concentration;

B. Flow at sampling time x concentration at sampling time, averaged over year;

C. Flow at sampling time x concentration at sampling time x ratio of sampling time flow to yearly average flow.

Loadings were calculated using each method with twelve data points taken from the third, then the ninth, and then the twenty-five day of the month, and then twelve random dates. In addition, estimates were made using all forty-eight measurements. In all cases, the estimates of the actual loads were poor. The USACOE concluded that the reason for the poor estimates was an inadequate accounting of high and low flow events, due to an inappropriate sampling frequency.

The calculation method developed by the USACOE to overcome this difficulty is known as the flow interval method. The flow is divided into equal intervals up to the maximum flow for the

period of record. The average mass loading is calculated for each flow interval based on the concentration data points within that interval. The average mass loading for a period of interest is then the summation of the average for each interval multiplied by the fraction of the period of interest during which the flow is within that interval. When compared with the other loading calculation methods, the flow interval method yielded lower error estimates, although for the conditions used (48 measurements), its estimate was also not very accurate (USACOE, 1975). However, when high flow measurements are included in the dataset, the flow interval method results are very accurate. For this reason, the USACOE recommends the use of the flow interval method in conjunction with a sampling strategy to include high flow measurements.

For streams with very limited databases, the USACOE developed the Regional Phosphorus Load Model (PLM). PLM is basically a correlation between (a) the flow times the difference between the measured phosphorus concentration and the low flow or base phosphorus concentration, divided by the drainage basin area, and (b) the flow divided by the drainage basin area to the 0.85 power. The latter quantity is a modified unit area contribution of flow based on the idea that the most important periods of phosphorus flux are storms and that during peak discharges, only a fraction of the total area near the stream contributes to the observed flow (USACOE, 1975). Data from the Maumee, Portage, Sandusky, Huron, Chagrin, Vermilion, and Cattaraugus Rivers are used in the correlation.

For streams with very little data, if the flow record and low flow phosphorus concentration are known, fluxes may be calculated from the PLM and used in the flow interval method to develop loadings.

Using the IJC method and OME data for the Detroit River, the flow interval method and, where necessary, the PLM for other tributaries, and permit information regarding direct

discharges, the USACOE has calculated total phosphorus loadings of various constituents to each basin of Lake Erie over the period June 1974 to May 1975 (USACOE, 1975).

The calculations to be discussed subsequently required monthly loadings of additional parameters for the period 1970 to 1975. To develop this data, the USACOE used a modification of the flow interval method and daily flow information as well as the above information (Yaksich, 1978). Loadings were calculated for total phosphorus, orthophosphorus, organic nitrogen, ammonia nitrogen, nitrate nitrogen, dissolved silica and chloride, separated into point and non-point sources. Plots are shown in Figures 9-13. Note the peak which consistently appears each spring for all the variables. The effect of this peak is evident in the western basin concentration data for these variables as shown in Chapter 5. Spring basin concentrations especially for ammonia nitrogen, total phosphorus, and orthophosphorus are significantly higher than the rest of the year, reflecting this large winter-spring load and the rapid response of the basin.

These loadings, developed by the USACOE, Buffalo District, are used in the subsequent calculation for both the 1970 calibration year and the 1975 verification year. They are chosen among the available loading estimates for two main reasons:

- (1) They provide monthly values, which is a reasonable time scale for the western basin.
- (2) Based on the information presented regarding the various methods of mass loading estimates and the datasets existing for the Detroit River, it appears that the methods and data used by the USACOE are the most consistent.

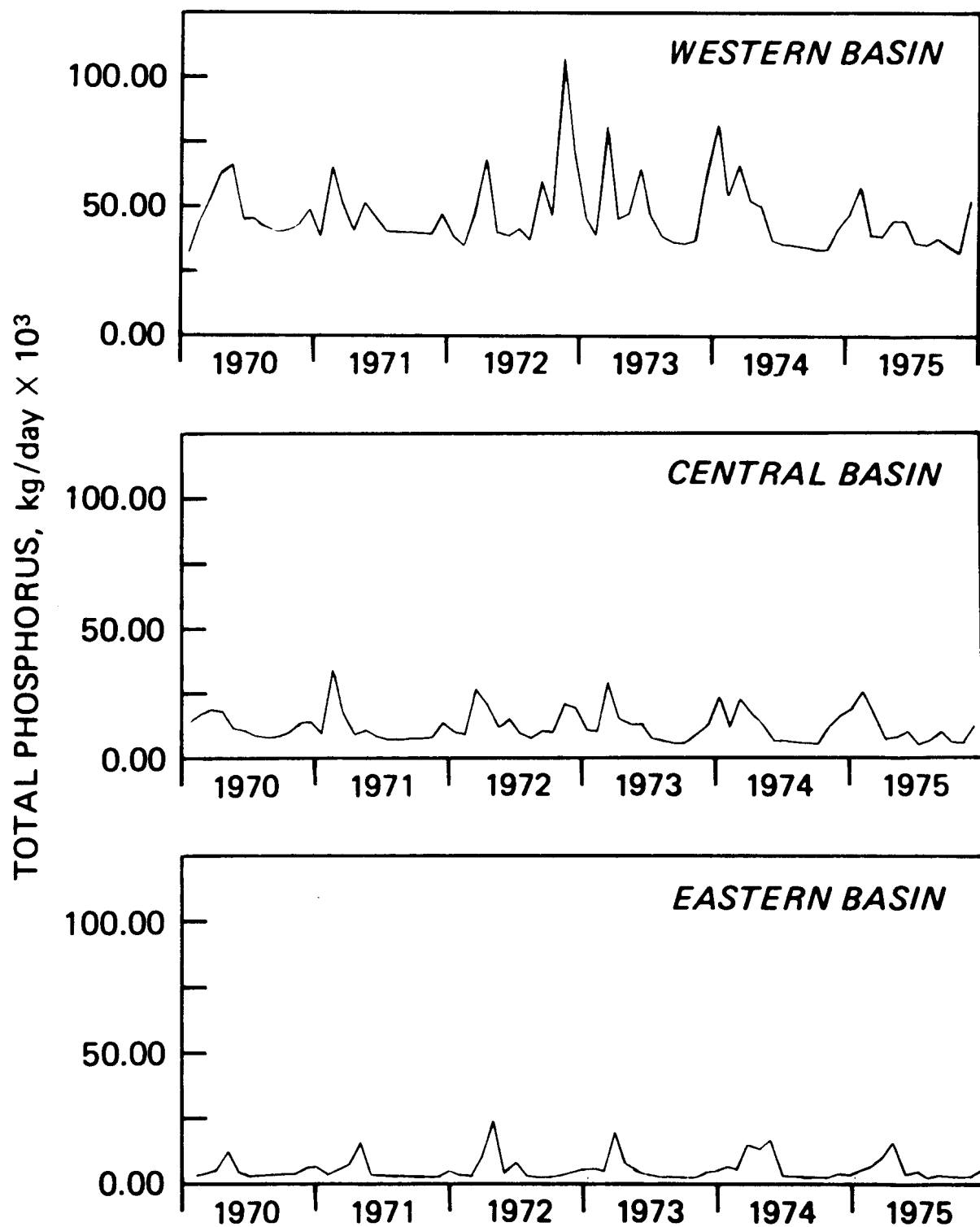


Figure 9. Total phosphorus loading (10^3 kg/day) to Lake Erie, 1970-1975. Western basin (top), central basin (middle), eastern basin (bottom).

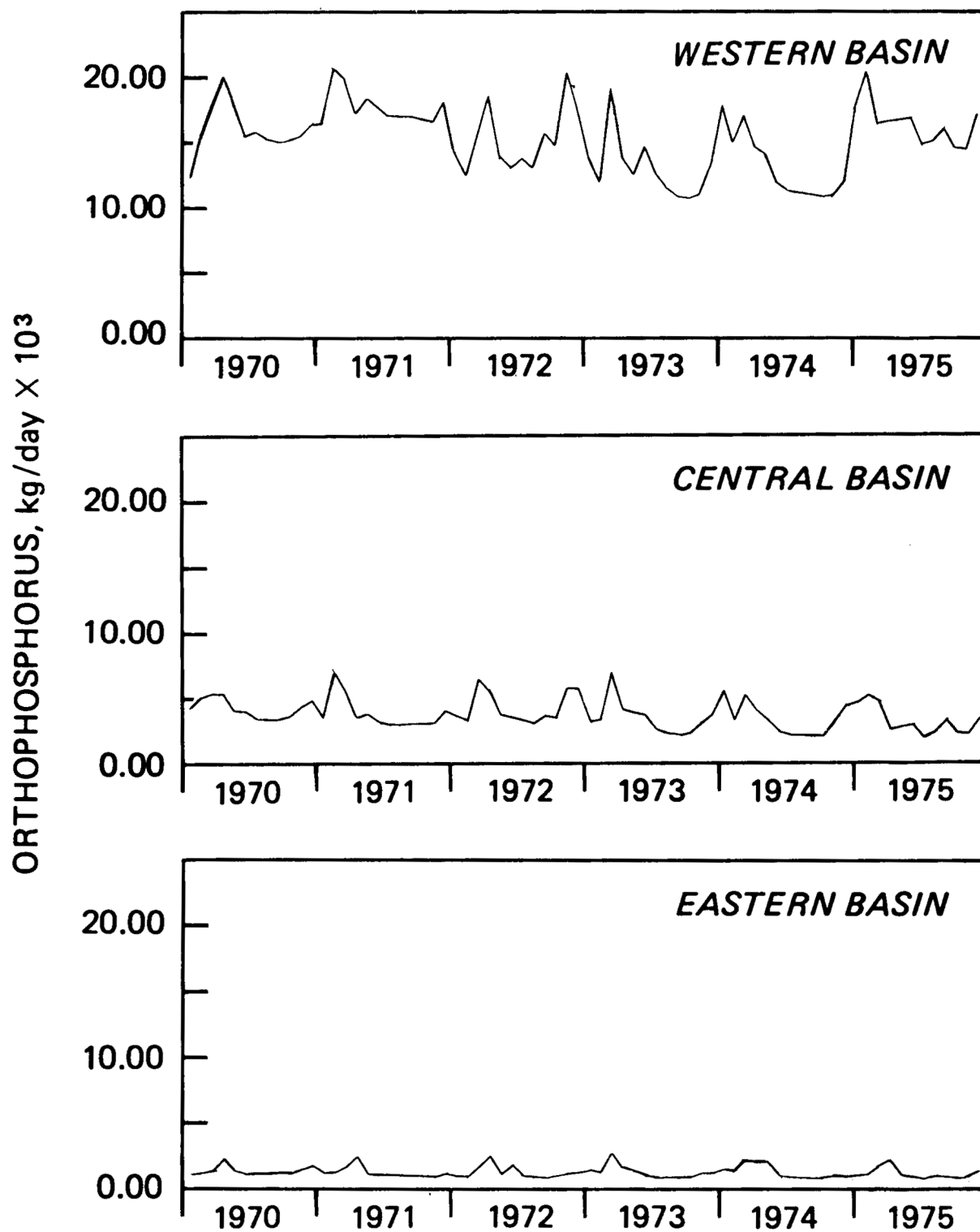


Figure 10. Orthophosphorus loading (10^3 kg/day) to Lake Erie, 1970-1975.

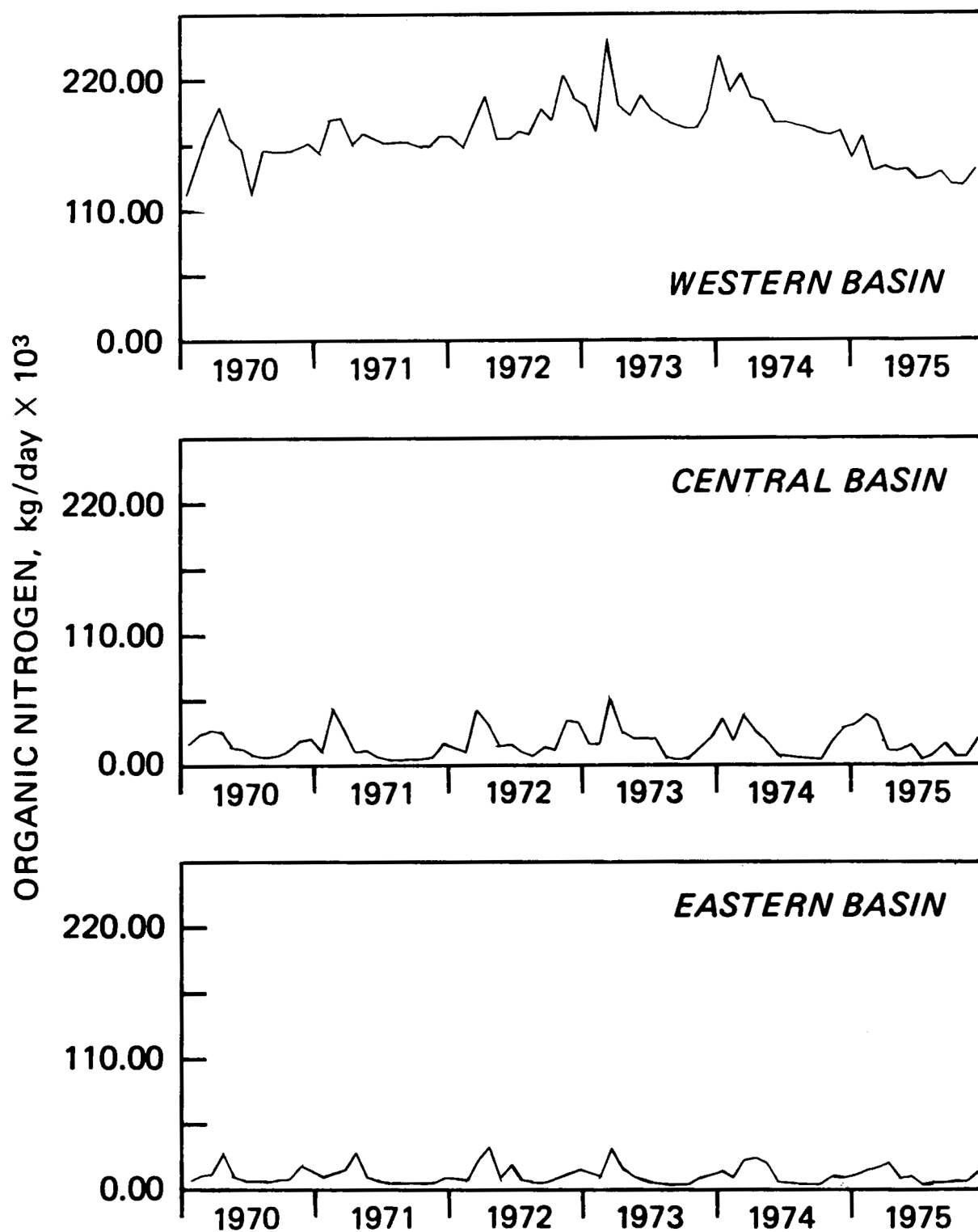


Figure 11. Organic nitrogen loading (10^3 kg/day) to Lake Erie, 1970-1975.

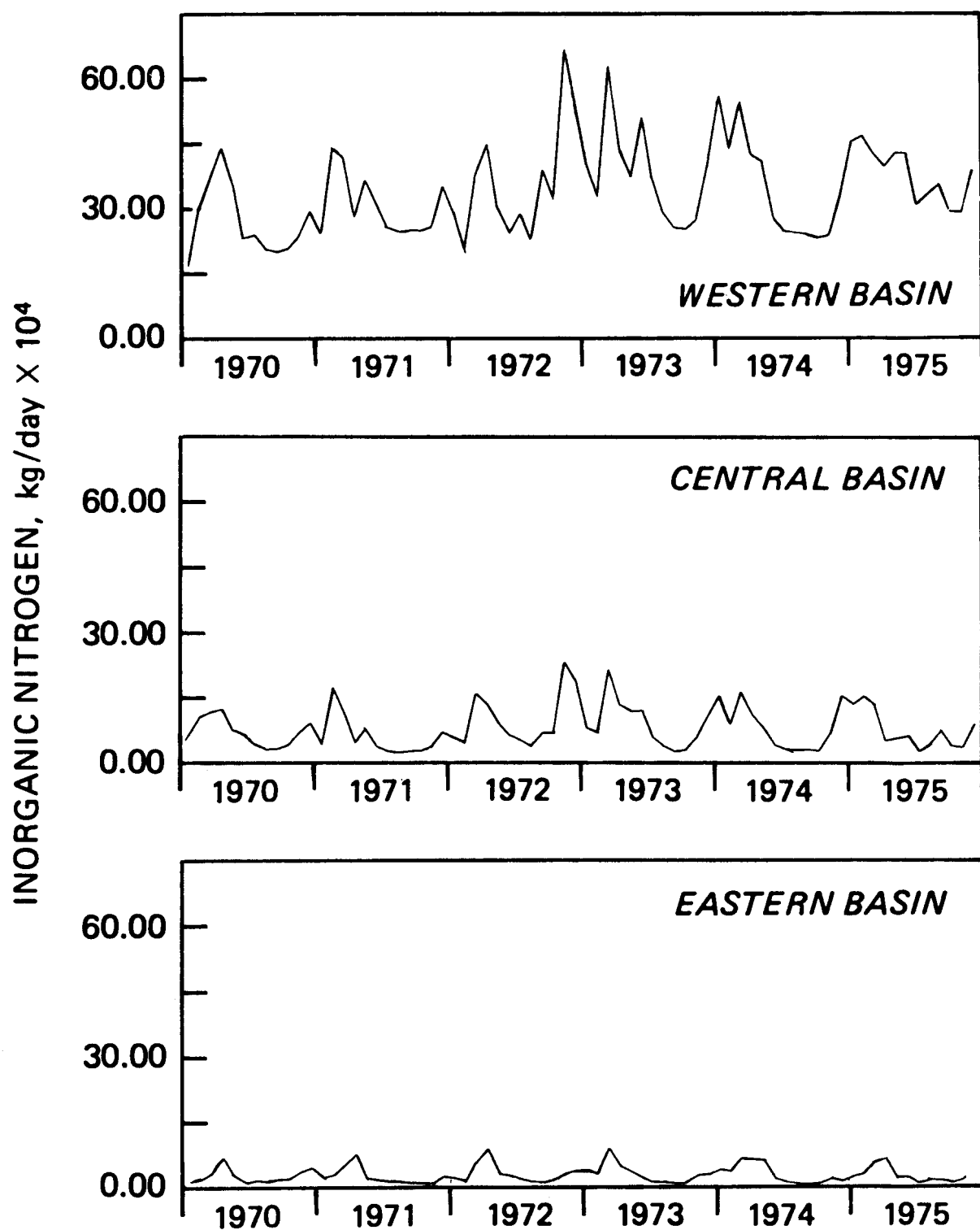


Figure 12. Inorganic nitrogen loading (10^4 kg/day) to Lake Erie, 1970-1975.

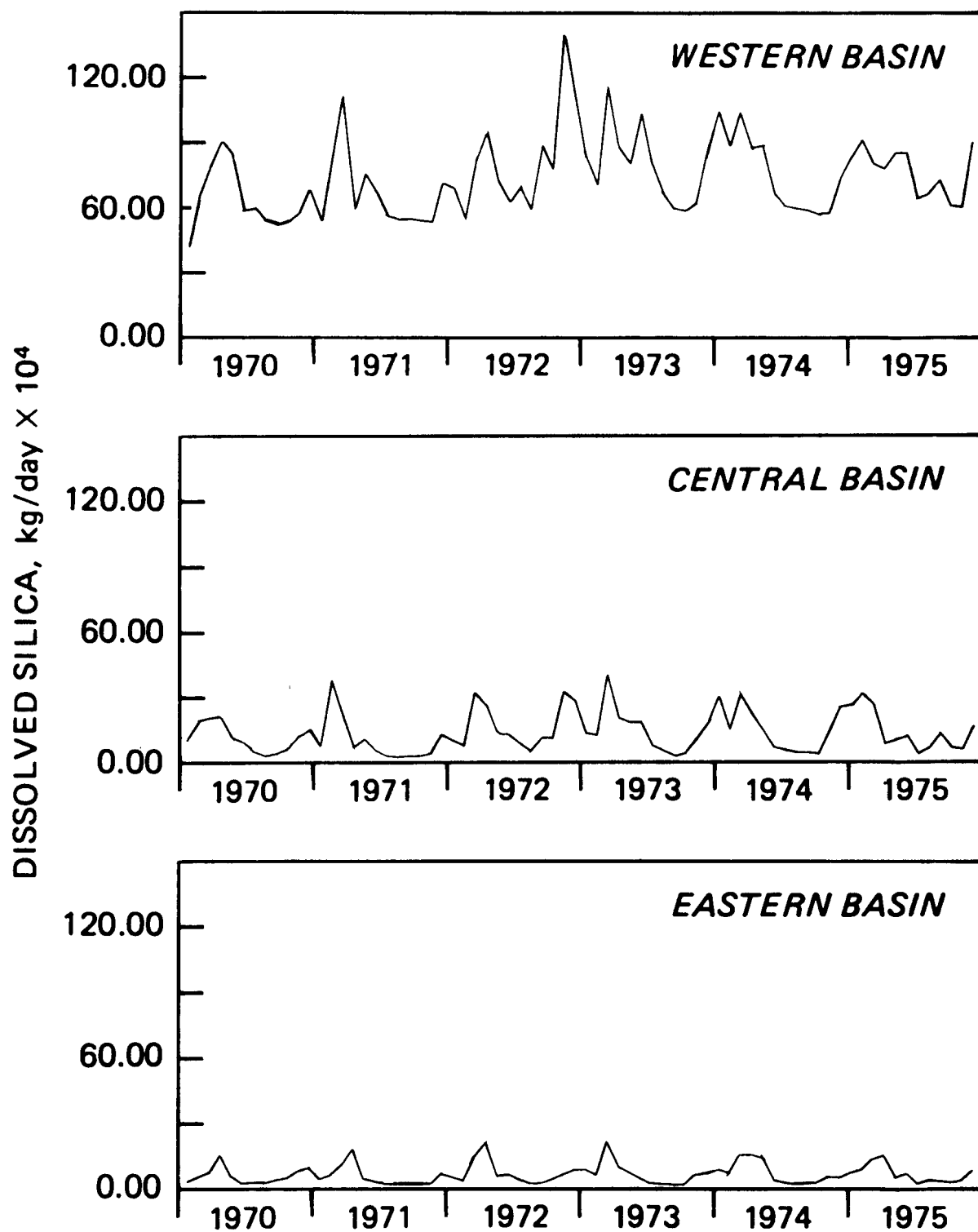


Figure 13. Dissolved silica loading (10^4 kg/day) to Lake Erie, 1970-1975.

4.7 ATMOSPHERIC LOADING

Estimates of the atmospheric loading to Lake Erie are given in the 1970 IJC report (IJC, 1976). The atmospheric phosphorus contribution, 560 metric tons/yr, is insignificant in comparison to other loadings (~ 2%). However, the atmospheric nitrogen load, 37,000 metric tons/yr, comprises about 15.5% of the total nitrogen load to the lake. The atmospheric loadings are assumed to be temporally and spatially constant. The atmospheric phosphorus load is assumed to be in the available form and the atmospheric nitrogen load is assumed to be ammonia nitrogen. A summary of the loadings used in the calculation is given in Tables A6-A9 of the Appendix. They do not include the atmospheric loadings which are inputted separately.

4.8. NITROGEN FIXATION

An additional source of available nitrogen is that fixed by the nitrogen-fixing algae themselves. Measurements of the rate of nitrogen fixation have been made. (Howard *et al.*, 1970). The maximum observed fixation rate is 0.057 mg nitrogen fixed/mg total Kjeldahl nitrogen (TKN)-day for a period of eleven days (day 233-244). For the TKN concentration calculated and observed to be present in the three basins, it is possible to compute the total mass of nitrogen fixed in the three basins at this maximum rate. These are shown in Table 6 below.

The quantities are negligible when compared with the other sources of nitrogen to the lake.

Table 6. Nitrogen Fixation

Segment	Mass of Nitrogen Fixed (Metric Tons/Yr)	Percent of the Lake Total Nitrogen Load
Western Basin	24	0.01
Central Basin Epilimnion	120	0.05
Eastern Basin Epilimnion	39	0.02

CHAPTER 5

DATA COMPILATION AND REDUCTION

5.1 HISTORICAL DATA

Declining fisheries, increasing algal production, and anoxia have motivated significant interest in the water quality of Lake Erie since the late 1920's. As a result, a substantial historical database exists.

The first intensive study of Lake Erie's water quality was conducted by the FWPCA in 1963-1964. Of the data collected prior to this, most are sparse both temporally and spatially. In the FWPCA study, chemical, biological, and bacteriological variables were measured at 158 stations located throughout the lake.

This study was followed in 1966 by the commencement of the Canada Centre for Inland Waters (CCIW) yearly series of cruises. These cruises included the entire lake and were carried out monthly from ice breakup to the end of the year. A comprehensive set of chemical, biological, and bacteriological parameters are measured on each cruise. Table 7 lists the sampling data collected for Lake Erie prior to 1970. Except for BOD, data compiled from 1967 CCIW cruises (CCIW, 1967), no data collected prior to 1970 are used explicitly in this investigation. The 1967 BOD data are important since they are the only available BOD data with extensive temporal and spatial coverage.

5.2 CALIBRATION DATASET

The criteria for selecting an appropriate calibration dataset are adequate temporal and spatial coverage with respect to the time and

space scales of the calculation, and data for all the state variables considered in the calculation. For this investigation, datasets which provide estimates of basin average epilimnion and hypolimnion concentrations of phytoplankton and zooplankton biomass, nutrients and dissolved oxygen at monthly intervals are suitable. All major cruise work done on Lake Erie since 1970 has been concerned with variables associated with eutrophication and consequently comply with most of these requirements.

The majority of the lake data used in this project is obtained from two sources:

1. STORET, USEPA.
2. Limnological Data Reports, Lake Erie, 1970, CCIW.

These data are supplemented with information reported in the literature.

The groups responsible for the collection of the data obtained through STORET and the limnological data reports are:

1. The Ohio State University, Center for Lake Erie Research (CLEAR).
2. The State University College at Buffalo, Great Lake Laboratory (GLL).
3. Canada Centre for Inlands Waters (CCIW).

Table 7. Lake Erie Limnological Data Summary - Historical Datasets*

Year	Agency (Project)	Geographical Extent	No. of Sampling Stations	Variables Measured
1910-1957	GLRI	Water intake at Lorain, OH	1	Temperature, Ts, NO ₃ , Fe, Cl, SO ₄ , HCO ₃ , Na+K, Mg, Ca, Fe, SiO ₂ , Alkalinity (monthly average reported for each year)
1920-1956	GLRI	Water intake at Erie, PA	1	Temp, Ts, NO ₃ , Cl, SO ₄ , HCO ₃ , Na+K, Mg, Ca, Fe, SiO ₂ , Alk (monthly average reported for each year)
1928	USBCF	Eastern Portion	23	Temperature, Alkalinity, N, NH ₃ , NO ₃ , Coliform
1929	USBCF	Eastern and Central Portion	62	DO, CO ₂ , Alk, pH, Cl, Turbidity, Temperature, Transparency, Microplankton, Macroplankton
1929-1930	USBCF	Western Portion		Temperature, Cl, NH ₃ , NO ₂ , NO ₃ , DO, CO ₂ , Alk, pH, Phytoplankton, Zooplankton, Bottom Organisms
1946-1948	IJC	Western Portion	142	Total Coliform, Cl, Phenols, NH ₃ -N, Chlorophyll, Temp, DO, BOD ₅ , Turbidity, Alkalinity, Ts, TVS
1947-1953	GLRI	Central Portion	142	Temperature, DO, CO ₂ , Alkalinity, pH, Secchi (All at four or more depths)
1950-1951	ODNR	Nearshore, OH		Temperature, Total Coliform, DO, Color, pH, Specific Conductivity, SCO ₂ , Fe, Cu, Cr, Ca, Mg, Na+K, HCO ₃ , SO ₄ , Cl, F, NO ₃ , TDS, Hardness, Bottom Fauna
1955	ODLF	Entire Lake	128	Temperature (several depths)
1959	USBCF	Western and Central Basin	50	Temperature, DO (generally three depths), Secchi
1960	ODLF	Entire Lake	60	Temperature, DO, Conductivity (surface and bottom)
1960	USBCF	Entire Lake	168	Temperature, DO, Alkalinity, pH, Specific Conductivity (all for several depths), Secchi, some hourly data
1960	UWO	Entire Lake	60	Temperature, pH, Eh, Alk, Ca, Mg, Na, K, DO, Cl, SO ₄
1961	USBCF	Western Basin	44	Temperature, DO, Alkalinity (several depths)
1961	GLI	Entire Lake	60	Secchi, Color, Temperature, DO, pH, Alk, Conductivity, Phenols, Total Coliform, Solar Radiation
1963	USBCF	Western Basin	24	Temperature, DO (several depths)
1963-1964	FWPCA	Entire Lake	158	Temperature, DO, COD, BOD, Conductivity, DS, TS, Total Alkalinity, pH, Cl, SO ₄ , Ca, Mg, Na, SiO ₂ , Soluble PO ₄ , Total N, NH ₃ -N, Organic N, NO ₃ -N, ABS, Phenols, Zn, Cu, Cd, Ni, Pb, Cr, Bottom Sediment, Chemistry, Benthic Population, Phytoplankton, Total Coliform, Fecal Coliform
1964	GLI	Entire Lake	83 (Max.)	Secchi, Temperature, Conductivity, Turbidity, pH, Eh, Alkalinity, DO
1965	NOAA	Entire Lake	63	Temperature, Color, Radiation, Transparency, pH, Eh, Alkalinity, Chlorophyll, Specific Conductivity, DO

*Compiled from Limnological Systems Analysis of the Great Lakes (Hydroscience, 1973).

Table 7. Lake Erie Limnological Data Summary - Historical Datasets (Continued)

Year	Agency (Project)	Geographical Extent	No. of Sampling Stations	Variables Measured
1966	NWRC	Michigan Shoreline	40	Total Coliform (Michigan beaches)
1966	CCIW		105	Secchi, Temperature, Turbidity, Specific Conductivity, pH, Alkalinity, BOD, DO, PO ₄ , NO ₂ , Cl, Hardness, Phenols, Total Coliform
1967	CCIW	Entire Lake	Max. 192 Min. 77	Secchi, Color, Temp, Turbidity, Specific Conductivity, pH, Alkalinity, BOD, DO, SO ₄ , Cl, SiO ₂ , Hardness, Cd, Ca, Cr, Co, Cu, Fe, Pb, Li, Mg, Mn, Ni, K, Na, Sr, Zn, Total Coliform, Fecal Coliform, TCS, Ortho PO ₄
1967	NOAA	Entire Lake	63	Temperature, Solar Radiation, Transparency, pH, Eh, Alk, Cl, Specific Conductivity, CO, Total Coliform
1967	FWPCA	Western Basin		Temp, Specific Conductivity Cl, Phenol, DO, Total P, Sol P, NO ₃ , NH ₃ , Organic N, Total Coliform, SS, SO ₄
1967-1968	FWPCA	Mid-Lake		Secchi, Temp, Alk, Specific Conductivity, DO, BOD ₅ , COD, pH, Eh, TS, TDS, Cl, NH ₃ , NO ₃ , Organic N, Sol P, Total P, SiO ₂ , Turbidity, Chlorophyll a, Seston, Phytoplankton, Sediment Chemistry, Macroinvertebrates
1968	CCIW	Entire Lake	Max. 87 Min. 33	Secchi, Color, Temperature, Specific Conductivity, pH, Alkalinity, DO Total PO ₄ , Ortho PO ₄ , NH ₃ , NO ₃ , SO ₄ , F, Cl, SiO ₂ , Hardness, Ca, Mg, Na, Chlorophyll a, Total Coliform, Fecal Coliform
1969	CCIW	Entire Lake	85	Secchi, Color, Temperature, Specific Conductivity, Alkalinity, HCO ₃ , DO, SO ₄ , Cl, Hardness, Ca, Mg, K, Na, Total Coliform, Fecal Coliform

5.2.1 Canada Center for Inland Waters Cruise Data

CCIW has been involved in extensive data collection on Lake Erie since 1967. A set of cruises is carried out on the lake each year. These commence following ice breakup and continue until December at approximately monthly intervals. An extensive base of bacteriological, biological, chemical, and physical parameters for the waters of Lake Erie are monitored on each cruise. Spatial grids for these cruises are usually dense, 60 to 100 stations being visited per cruise. At each station, samples are collected at the surface and at three-meter intervals to the bottom. At some of the deep stations in the eastern basin, the

sampling interval is five-meters. A listing of the data available from these cruises is shown in Table 8. The data for 1970 were obtained from the limnological data reports (CCIW, 1970); 1975 data were acquired through STORET.

5.2.2 Nutrient Control Program Cruise Data

The Nutrient Control Program is a three-year study sponsored by the USEPA as part of the Large Lakes Program administered by the USEPA, Grosse Ile Laboratory. It is a comprehensive monitoring program of the chemical and biological parameters of Lake Erie waters designed to determine the effectiveness of nutrient control programs in abating eutrophication. The groups responsible for the

Table 8. Lake Erie Limnological Data Summary - Datasets Used in Model

Year	Agency (Project)	Geographical Extent	No. of Sampling Stations	Variables Measured
1970	CCIW	Whole Lake	59	Secchi, Temperature, Turbidity, Specific Conductivity, pH, Alkalinity, CO ₂ , HCO ₃ , DO, Total PO ₄ , Soluble Reactive PO ₄ , TF PO ₄ , NH ₃ , NO ₃ , Organic Nitrogen, F Organic Nitrogen, TF Nitrogen, SO ₄ , Cl, RS:O ₂ , Cd, Ca, Cr, Co, Cu, Fe, Pb, Li, Mg, Mn, Hg, Mo, Ni, K, Na, Zn, Chlorophyll a, Coliform, Bacterial Biomass, Color
1970	CCIW, USEPA (Project Hypo)	Central Basin	25	Temperature, pH, Eh, Alkalinity, CO ₂ , DO, Ca Hardness, Ca + Mg Hardness, NH ₃ , NO ₂ , NO ₃ , Total Phosphorus, SF Phosphorus, Total Nitrogen, TF Nitrogen, SO ₄ , Fe, Mn, Particulate Organic Carbon, Soluble Organic Carbon, Particulate Organic Nitrogen, Minerals, Phytoplankton, Bacteria, Sediment Oxygen Demand, Wind
1973 to 1975	CLEAR (Nutrient Control Program)	Western and Central Basins	52	Temperature, pH, DO, Conductivity, Secchi, Transmissibility, Alkalinity, NH ₃ , NO ₂ -NO ₃ , Total Phosphorus, Soluble Reactive Phosphorus, Chlorophyll (a,b,c), Particulate Carbon, Particulate Nitrogen, CH ₄ , N ₂ Fixation, Phytoplankton, Zooplankton, Benthos Population
1973 to 1975	GLL (Nutrient Control Program)	Eastern Basin	25	Secchi, Temperature, Specific Conductivity, pH, DO, NH ₃ , NO ₃ , Organic Nitrogen, Total Nitrogen, Total Phosphorus, Dissolved Phosphorus, Particulate Inorganic Carbon, Particulate Organic Carbon, Primary Productivity, Phytoplankton, Zooplankton, Benthos Population
1975	CCIW	Whole Lake	108	Secchi, Temperature, Depth 1% Light, Specific Conductivity, DO, pH, Dissolved Nitrogen, NO ₂ -NO ₃ , Total Particulate Dissolved Phosphorus, Soluble Reactive Phosphorus, Ca, Mg, Na, K, Cl, SO ₄ , Reactive SiO ₂ , Cd, Cu, Zn, Coliform, Fecal Coliform, Fecal Strep, Bacteria, Chlorophyll a, Chlorophyll a-Corrected, Hg

data collection and analysis are CLEAR, the Ohio State University (OSU) (western and central basin) and Great Lakes Laboratory (GLL), State University College at Buffalo (eastern basin). The program began in 1973. Each year a series of cruises are conducted, beginning after ice breakup, and performed at monthly intervals during the spring and fall and bi-monthly during the critical summer period. The parameters available from these cruises are listed in Table 8. All of the Nutrient Control Program data used in this project were obtained through STORET.

5.2.3 Project Hypo Cruise Data

Project Hypo, an ambitious joint undertaking of the CCIW and the USEPA, was an exhaustive study aimed at discovering the degree and causes of the depletion of oxygen during the summer in the central basin of Lake Erie (Burns and Ross, 1972). Sampling work was performed from June through August 1970, although the bulk of the data collected is the result of an intensive phase from July 27 to August 25. Twenty-five stations in the central basin were sampled of which five were termed "major stations". Sampling at these stations was intensive. During the period July 27 to August 25, there were seven major cruises. Table 8 includes a description of the data available from these cruises. At each station, samples were taken one-meter below the surface, one-meter above the thermocline and at one-meter intervals through the hypolimnion to one meter above the bottom. In addition, at the five major stations, mid-thermocline samples were taken where possible. The Project Hypo data were obtained through STORET.

In addition to the cruise data, certain biological parameters have been compiled from published information. The 1970 zooplankton carbon data are from Watson (1974, 1976); 1970 gross primary production data are from Glooschenko *et al.* (1974); phytoplankton species composition data for 1970 are from Munawar and Munawar (1976).

All data are reduced to segment averages for each cruise. In addition, the number of points, maximum value, minimum value, and standard deviation for each average are compiled.

These reduced datasets are:

1. 1970 CCIW
2. Project Hypo, CCIW, and USEPA, 1970
3. 1973 Lake Erie Nutrient Control Program, CLEAR, OSU, and GLL; State University of College at Buffalo
4. 1974 Lake Erie Nutrient Control program, CLEAR and GLL
5. 1975 Lake Erie Nutrient Control Program, CLEAR and GLL
6. 1975 CCIW.

These data are compared in Figures 14-26 which present the segment averages \pm standard deviation for 1970, 1973-1974, and 1975. Chlorophyll concentrations are compared in Figure 14a for the western basin and eastern basin epilimnion. The unimodal distribution of the western basin sharply contrasts with the bimodal distribution in the eastern basin and central basin epilimnion, shown in Figure 15. Also, the similarity in the seasonal patterns for the three years of data is apparent.

Total phosphorus for the western basin, shown in Figure 16, exhibits a spring maxima which then rapidly declines. As the mass loading data indicate, there is a spring loading maxima as well. As shown subsequently, this is insufficient to explain this observed peak and other sources of phosphorus, probably from sediment resuspension, are involved. Eastern basin concentrations appear to be relatively constant, as are central basin epilimnion concentrations with the exception of an early spring peak in 1975. Central basin hypolimnion concentrations,

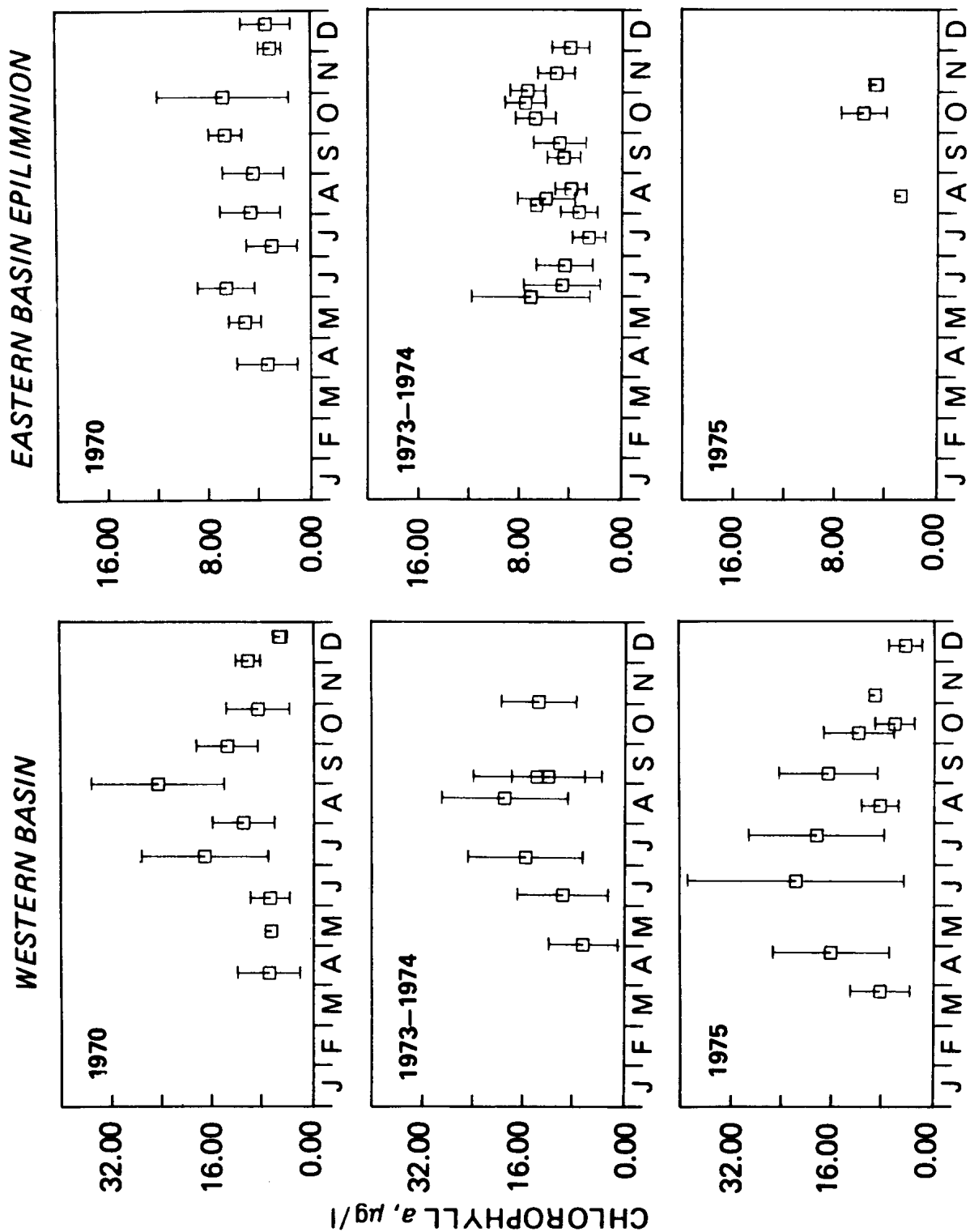


Figure 14. Comparison of chlorophyll *a* concentrations (µg/l) for the western basin and eastern basin epilimnion. Segment averages \pm standard deviations for each cruise are shown for 1970, 1973-1974 and 1975 datasets.

CENTRAL BASIN HYPOLIMNION

CENTRAL BASIN EPILIMNION

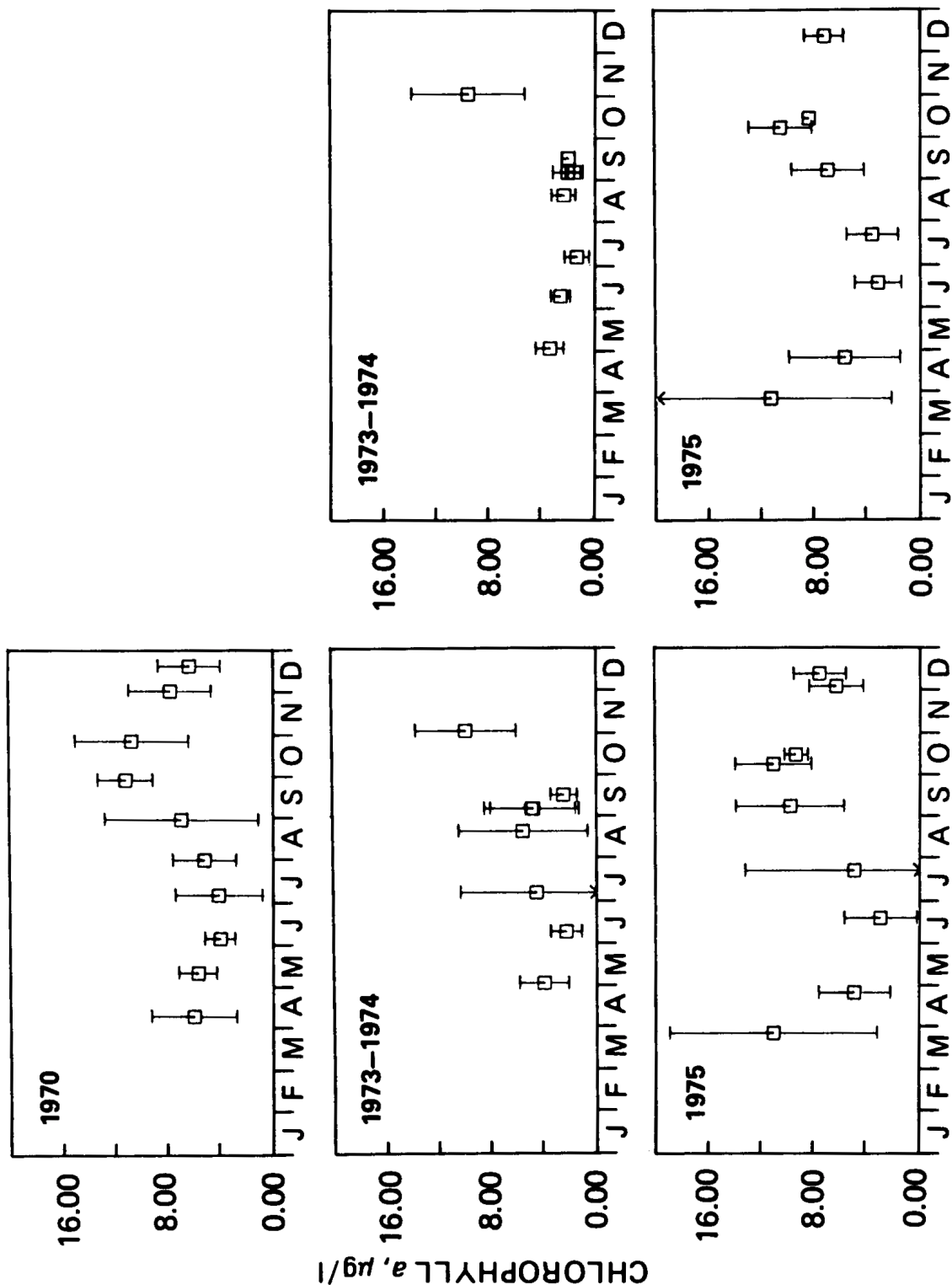


Figure 15. Comparison of chlorophyll *a* concentrations ($\mu\text{g/l}$) for the central basin epilimnion and hypolimnion. No chlorophyll data available for the hypolimnion during 1970.

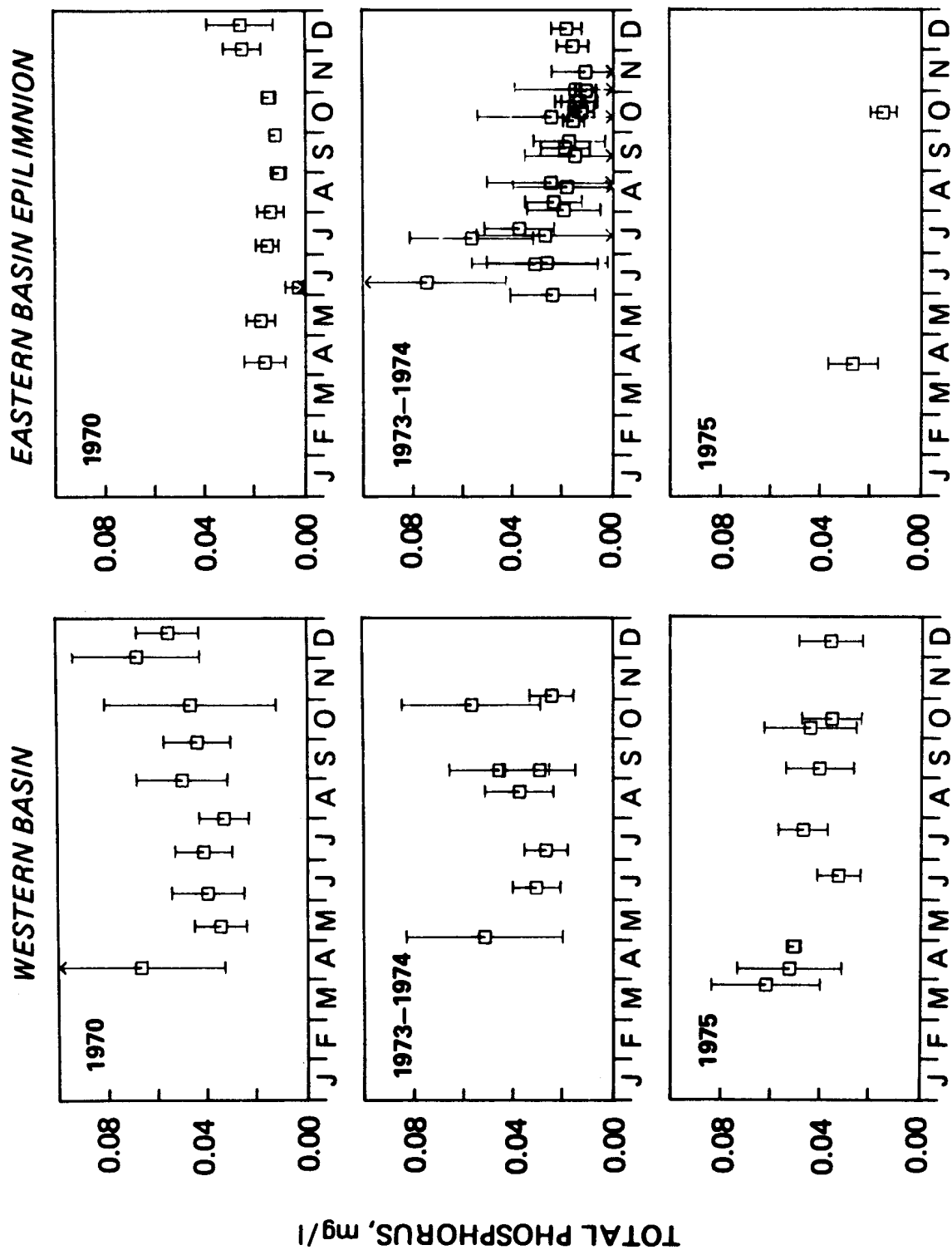


Figure 16. Total phosphorus concentrations (mg/l) for the western basin and eastern basin epilimnion.

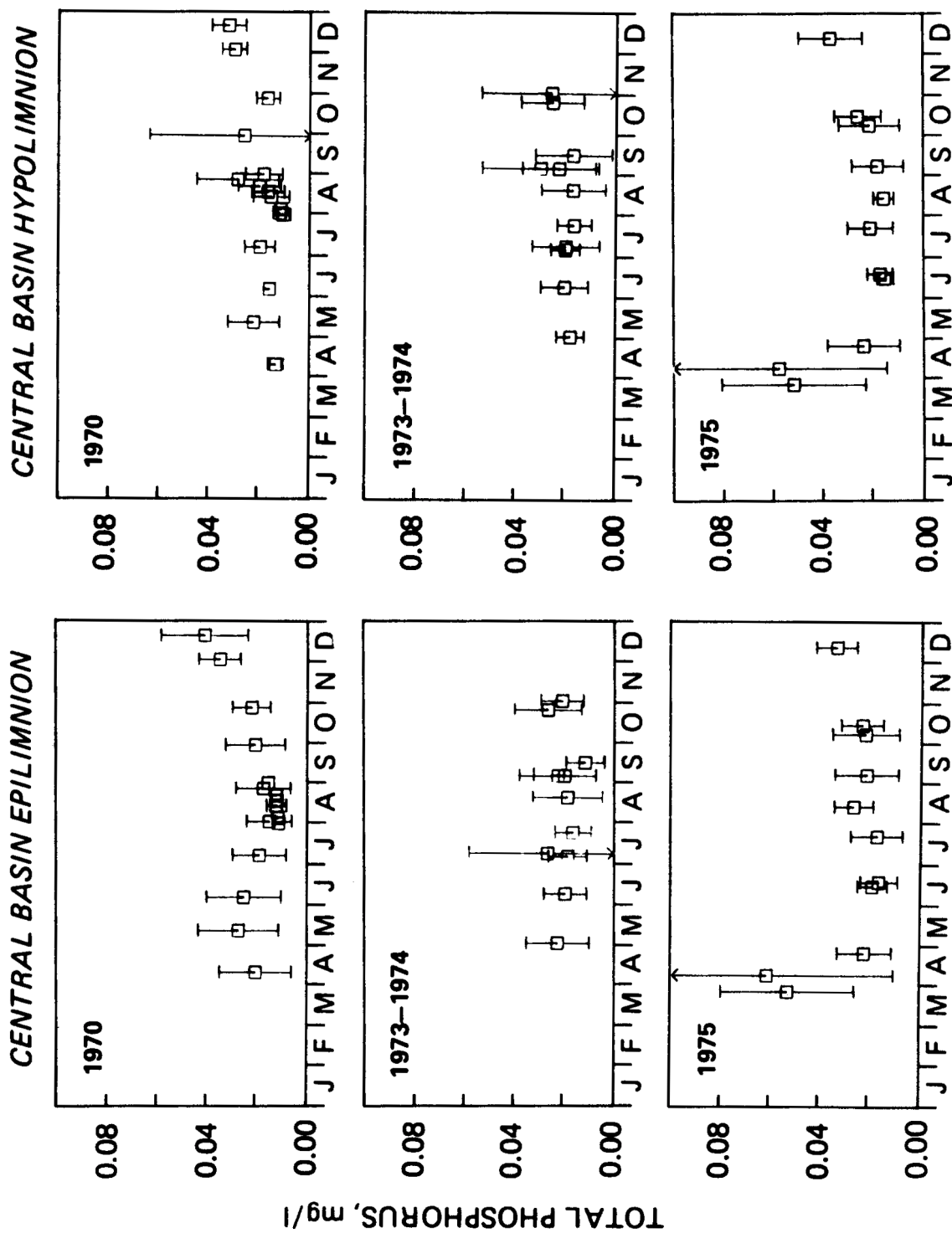


Figure 17. Total phosphorus concentrations (mg/l) for the cental basin epilimnion and hypolimnion.

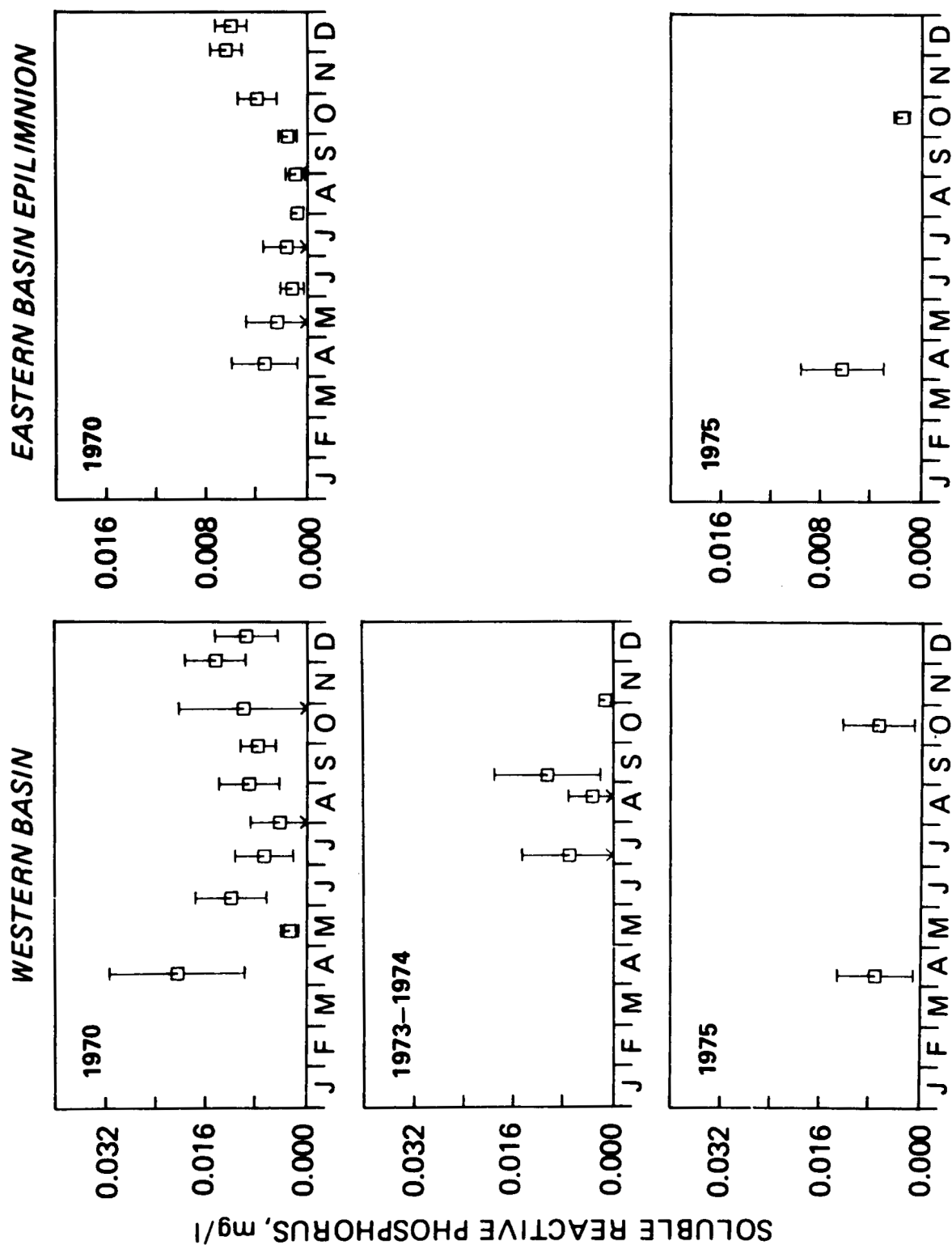


Figure 18. Soluble reactive phosphorus concentrations (mg/l) for the western basin and eastern basin epilimnion. No data available for the eastern basin during 1973-1974.

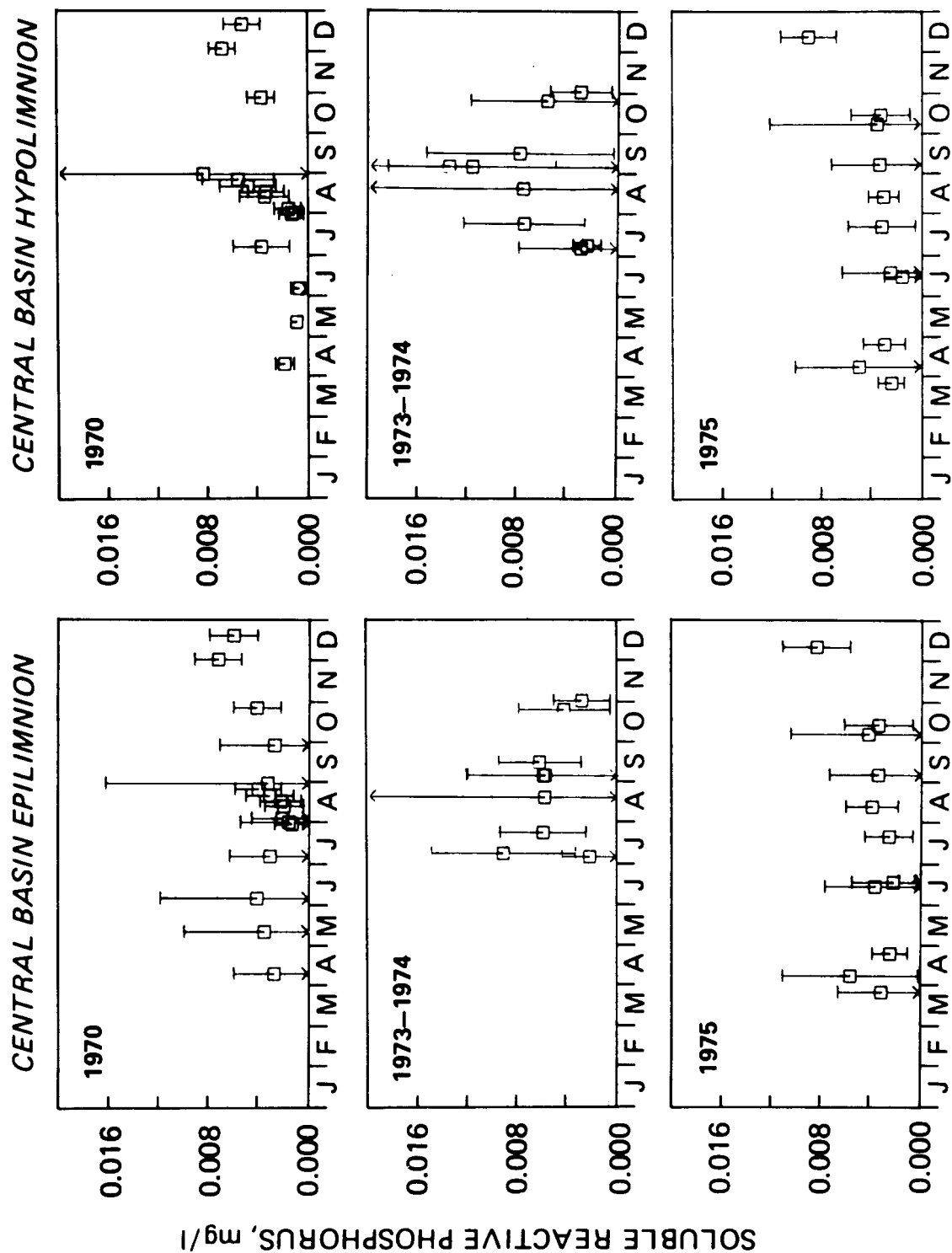


Figure 19. Soluble reactive phosphorus concentrations (mg/l) for the central basin epilimnion and hypolimnion.

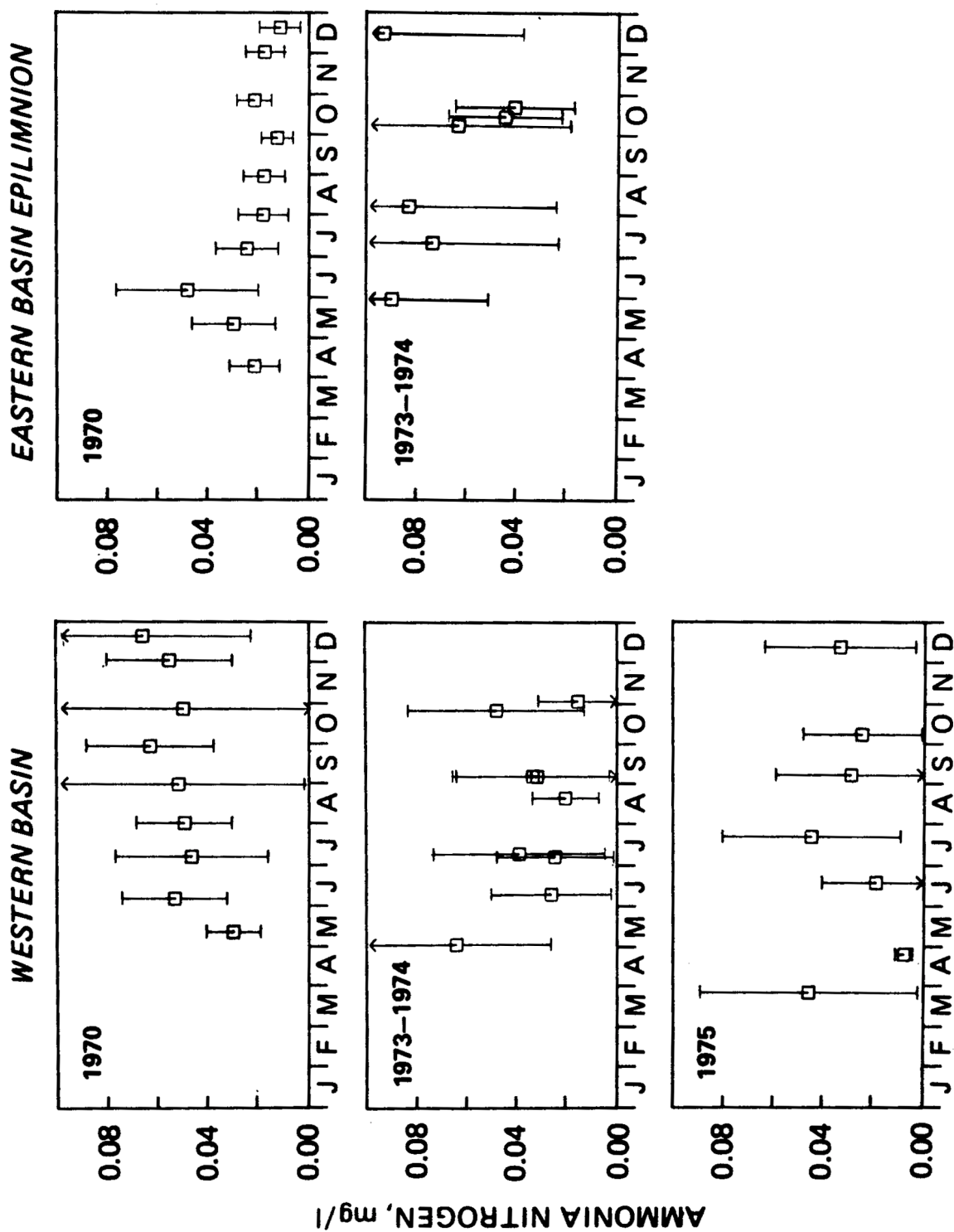


Figure 20. Comparison of ammonia concentrations (mg/l as N) for the western basin and eastern basin epilimnion. No data available for the eastern basin during 1975.

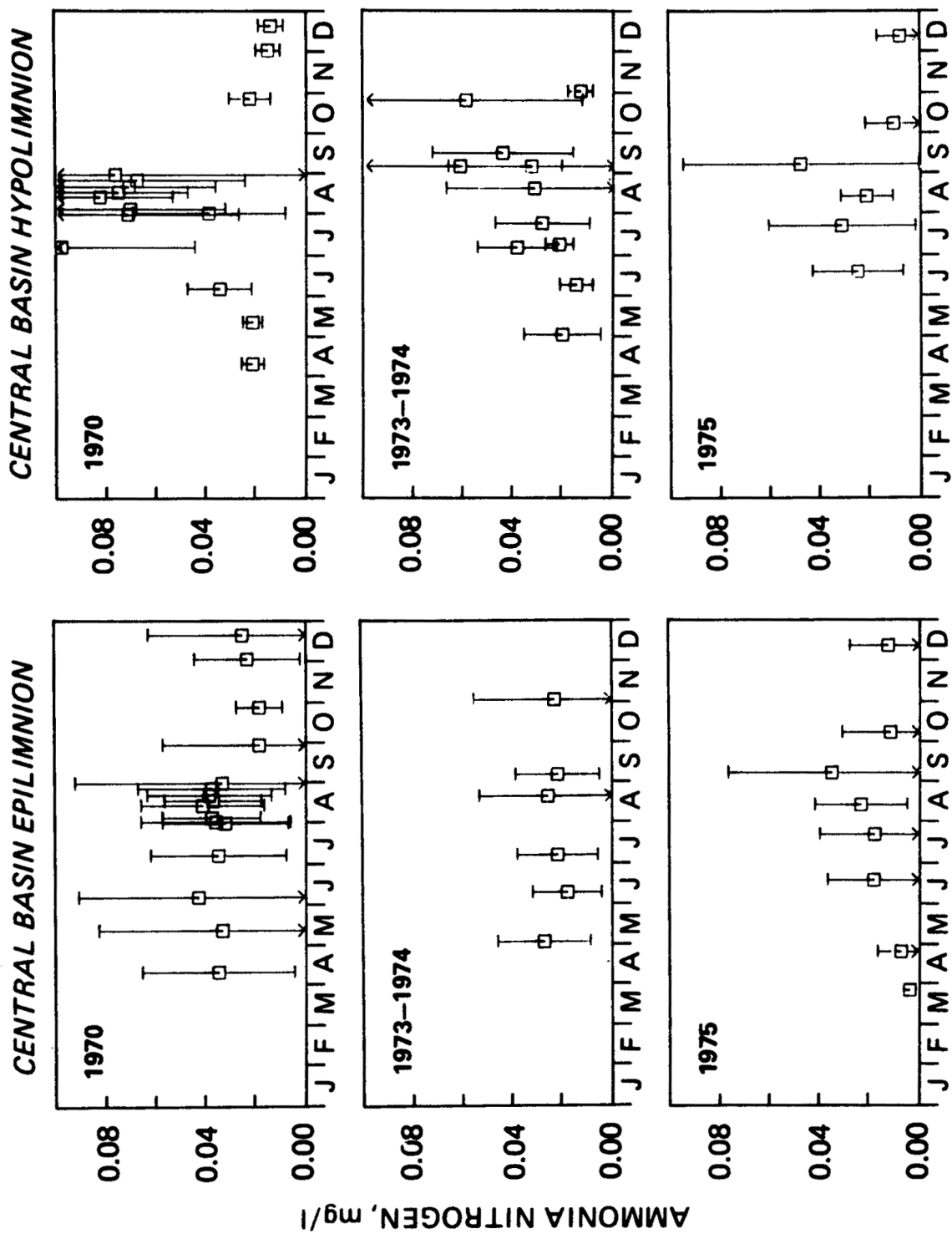


Figure 21. Comparison of ammonia concentrations (mg/l as N) for the central basin epilimnion and hypolimnion.

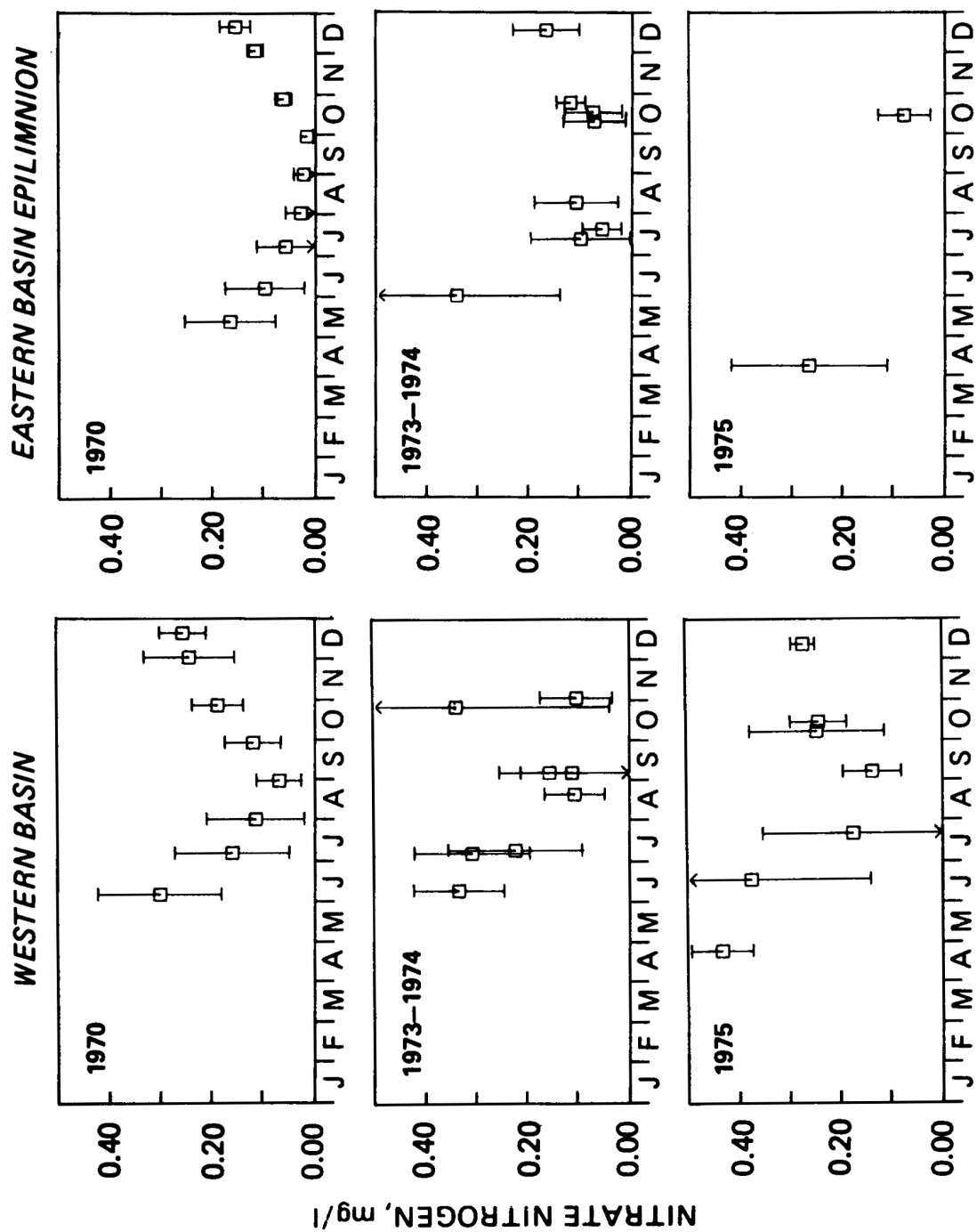


Figure 22. Comparison of nitrate concentrations (mg/l as N) for the western basin and eastern basin epilimnion.

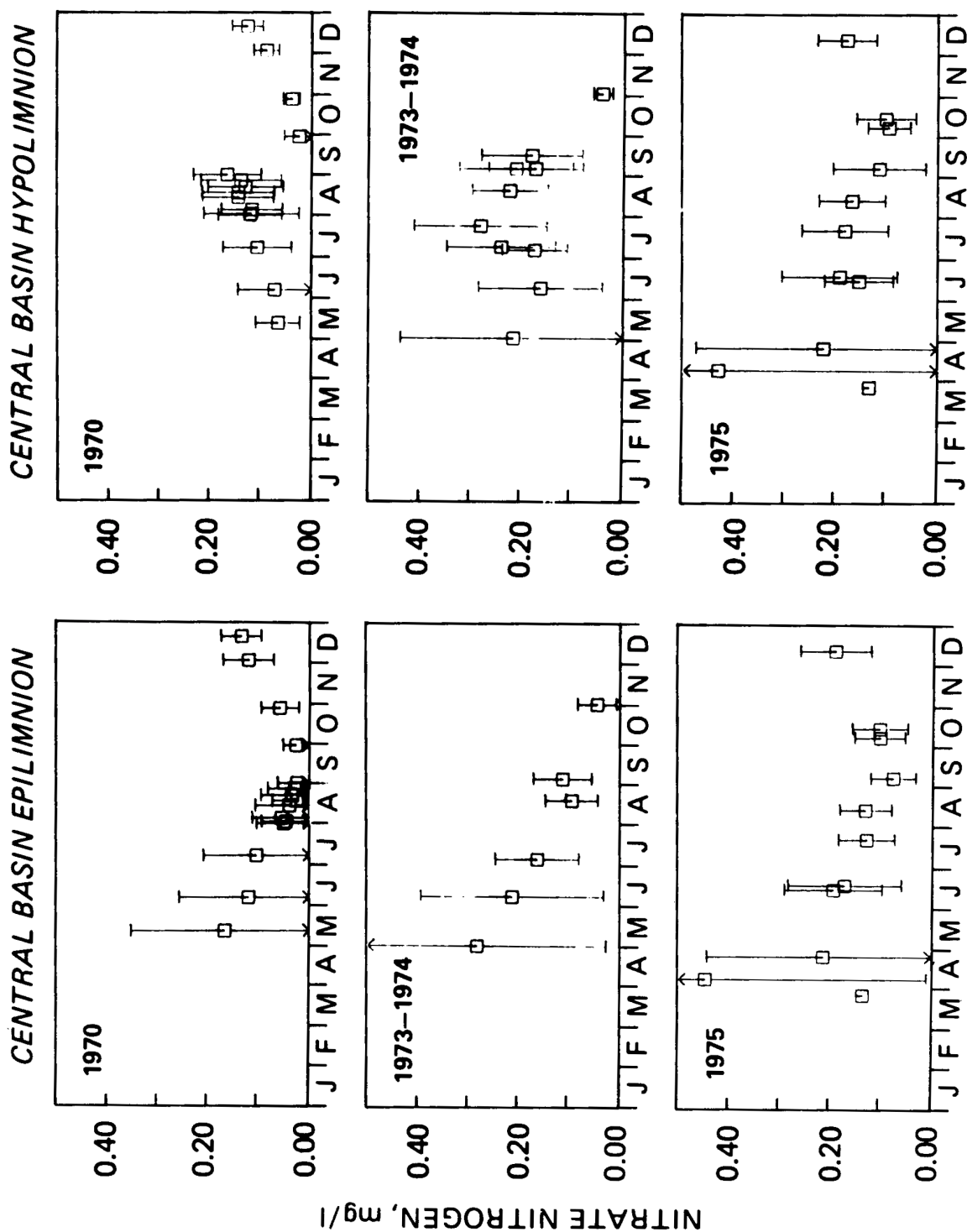


Figure 23. Comparison of nitrate concentrations (mg/l as N) for the central basin epilimnion and hypolimnion.

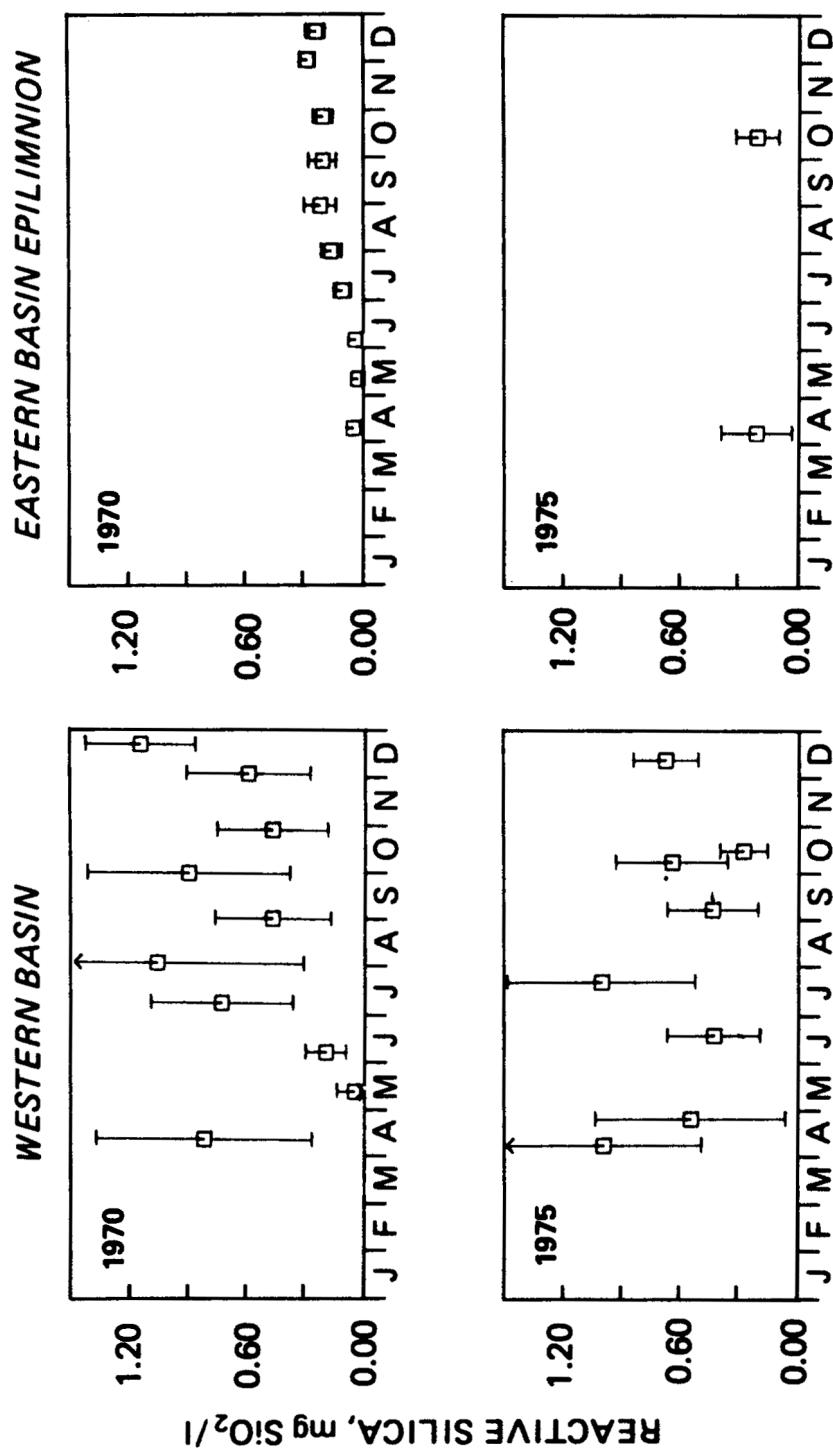


Figure 24. Comparison of reactive silica concentrations (mg/l as SiO₂) for the western basin and eastern basin epilimnion.

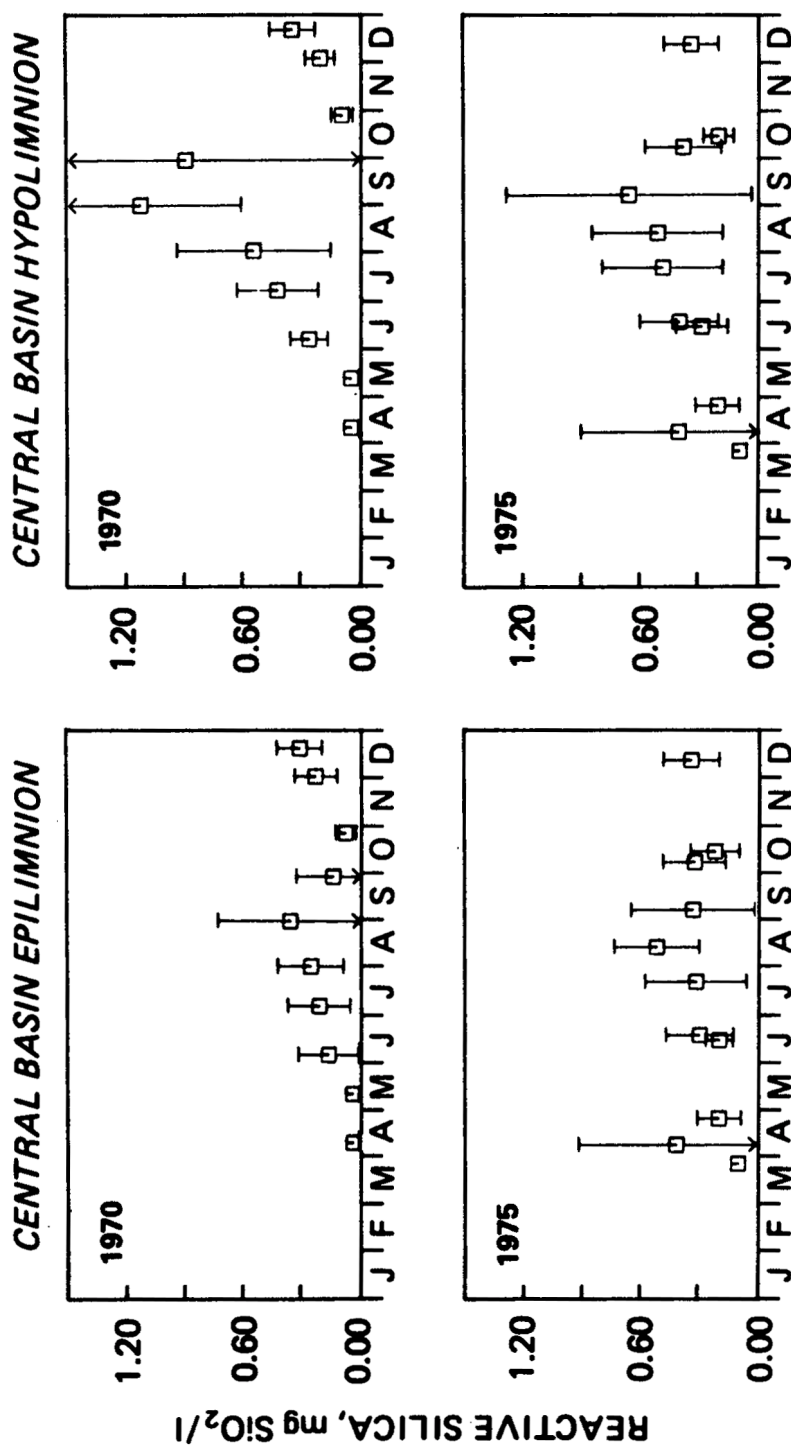


Figure 25. Comparison of reactive silica concentrations (mg/l as SiO₂) for the central epilimnion and hypolimnion.

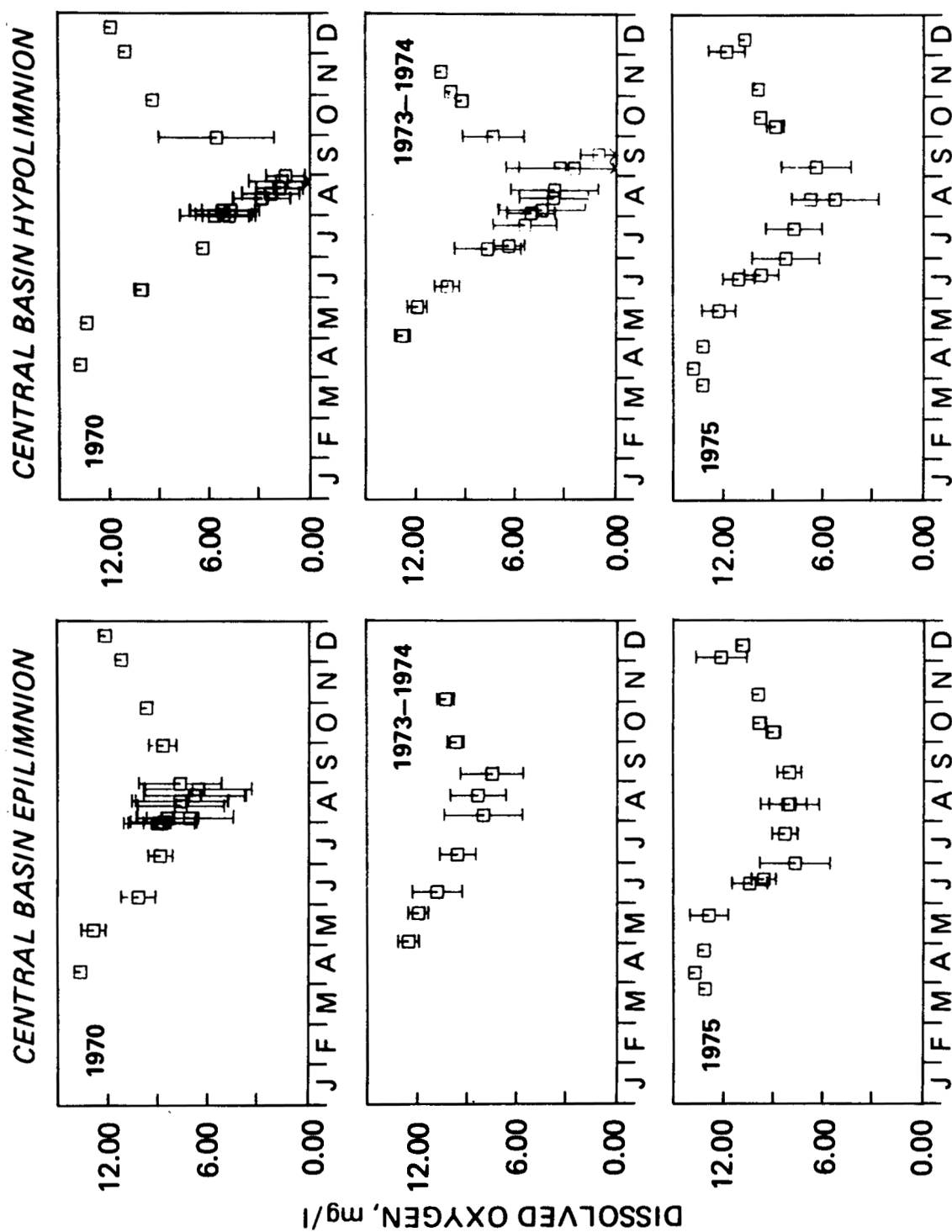


Figure 26. Comparison of dissolved oxygen concentrations (mg/l) for the central basin epilimnion and hypolimnion.

Figure 17, reflect increased phosphorus release during the anoxia in late July and August. This is more clearly seen in the soluble reactive concentrations. The western basin and eastern basin data for 1970, Figure 18, follow the expected pattern with depletion during the periods of phytoplankton growth and the recovery due to overturn and recycle. Central basin hypolimnion data, Figure 19, clearly show the effects of anoxia commencing in late July in both 1970 and 1973-1974. The distinct increase of soluble reactive phosphorus reflects the anaerobic release from the sediments. The absence of this phenomena in 1975 is due to the aerobic conditions that prevailed throughout that year as shown subsequently.

Ammonia concentration, Figure 20 and 21, are small with somewhat erratic in the western basin, eastern basin and central basin epilimnion, whereas the central basin hypolimnion reflects the anaerobic release as did the soluble reactive phosphorus. Nitrate concentrations follow the pattern of seasonal uptake in the surface segments, as shown in Figure 22 and 23, whereas an increasing pattern appears in the central basin hypolimnion as nitrogen is recycled.

Reactive silica concentrations reflect the uptake of silica by diatom growth in the spring in all epilimnion segments as shown in Figures 24 and 25. As diatoms are replaced by non-silica using algae, the concentrations increase due to aerobic regeneration. Anaerobic regeneration in the central basin hypolimnion is also clearly seen in 1970 with less regeneration occurring in 1975 during aerobic conditions.

Dissolved oxygen concentrations for the central basin are shown in Figure 26. The epilimnion is nearly saturated but the average hypolimnion dissolved oxygen concentration decreases to approximately 1.0 mg/l in both 1970 and 1973-1974 just before overturn. 1975 is unique, however, with an average concentration above 4.0 mg/l. This accounts for the lack of anaerobic regeneration of nutrients in 1975, since as shown subsequently, if the average segment five concentration exceeds 4 mg/l, no anoxia is recorded at any of the sampling stations.

The overall impression of similarity between the different years indicates that the total mass loadings of nutrients to the lake have not substantially changed during this period. This is confirmed by the USACOE estimates. However, there is a striking difference in the central basin hypolimnion dissolved oxygen between 1970, 1973-1974, and 1975. The cause for this unusual behavior is discussed in the verification chapter.

The initial calibration of the kinetics is accomplished using the 1970 CCIW data and Project Hypo data. The data for 1973 and 1974 are also included in the calibration because of the similarity of in-lake conditions over the period 1970 to 1974. The 1975 data is used for the independent verification of the model. The fact that the dissolved oxygen data for 1975 differs markedly from the 1970-1974 pattern makes this dataset ideally suited for verification. Both the data collected by CCIW and the data collected by CLEAR and GLL are used in the calibration and verification calculations.

CHAPTER 6

KINETICS

6.1 INTRODUCTION

The calculation employed in this investigation is made up of two, essentially independent components - the kinetics and the transport. This distinction is basic to mass balance calculations. The kinetics control the rates of interconversions among the dependent variables and are independent of location *per se* although they are functions of exogenous variables such as temperature that vary with location. Thus, the rate at which any reaction proceeds is controlled only by the local concentrations of the variables that appear in its reaction rate expression. The same expression is used for each location be it the western basin or the eastern basin hypolimnion.

It is in this sense that the formulation is an attempt to utilize fundamental principles: biological and chemical reactions have no fundamental relation to position, they are only affected by concentrations, light, and temperature. Hence, the kinetic constants which appear in these expressions cannot vary from segment-to-segment.

The kinetics employed are designed to simulate the annual cycle of phytoplankton production, its relation to the supply of nutrients, and the effect on dissolved oxygen. The calculation is based on formulating the kinetics which govern the interactions of the biota and the forms of the nutrients and applying them to the regions of Lake Erie within the context of conservation of mass equations. The fifteen variables for which these calculations are performed are:

Phytoplankton

1. Diatom chlorophyll *a*
2. Non-Diatom chlorophyll *a*

Zooplankton

3. Herbivorous zooplankton carbon
4. Carnivorous zooplankton carbon

Nitrogen

5. Detrital organic nitrogen
6. Ammonia nitrogen
7. Nitrate nitrogen

Phosphorus

8. Unavailable phosphorus
9. Soluble reactive phosphorus

Silica

10. Unavailable silica
11. Soluble reactive silica

Carbon, Hydrogen, Oxygen

12. Detrital organic carbon
13. Dissolved inorganic carbon
14. Alkalinity
15. Dissolved oxygen

An important criteria for the inclusion of variables in the calculation is the existence of adequate field data for the variable, as well as its importance in the processes being considered. For example, it is clear that the recycling

mechanisms are dependent on the bacterial population and, perhaps the microzooplankton, so that a direct calculation of the decomposer population is desirable. However, no comprehensive decomposer biomass data are available and a direct calibration is not possible. Since the reaction kinetic constants are not known *a priori*, their values would be chosen based on only indirect evidence, that is, on how well the calculation as a whole reproduced the data for the other variables being considered. These additional constants and dynamical equations add significantly to the available degrees of freedom in the calculation without an equivalent increase in the data available for their estimation. Thus, one's ability to uniquely specify a consistent set of kinetic constants diminishes rapidly and the calculation becomes more speculative as a consequence. Unfortunately, no adequate statistical theory of estimation is available to guide these choices so that the exact point at which this division is to be made is uncertain at present and is largely a matter of intuitive judgement.

The calculation presented below is based on a strict application of this principle of parsimony, consistent with the objectives of this analysis. The only variables for which no direct or indirect data are available are unavailable silica and the fractions of zooplankton biomass which are herbivorous and carnivorous. Thus, the zooplankton dynamics are necessarily somewhat speculative and cannot be thought of as having a strong foundation in observational fact. The inclusion of unavailable silica is necessary in order that the observed recycling can be calculated in a way consistent with mass balance principles. In this instance that requirement is judged to supercede the requirement of parsimony.

This principle also provides the motivation for the inclusion of inorganic carbon and alkalinity in the calculations. The concern is that the reactions involving oxygen are correctly represented. Since total dissolved carbon dioxide, as well as oxygen, is produced or consumed in these reactions, if this variable is included, it is possible

to check the results against observations of pH if alkalinity is also known. Alkalinity data are available and its production and destruction can be calculated for each reaction based on the appropriate stoichiometric ratio, the only additional constant required. Thus, adding total inorganic carbon and alkalinity to the calculation actually decreases the degree of freedom since more data are available for comparison with no increase in constants that need to be estimated for the inorganic carbon component of the reactions. A computational complication is added since only $\text{CO}_2(\text{aq})$ and not total inorganic carbon is transferred across the air-water interface but methods for accomplishing this calculation are available (Di Toro, 1976).

The interactions of the variables are shown in Figures 27-28 which are representations of the nutrient cycles. Consider phosphorus: the available phosphorus is utilized by both phytoplankton groups for growth. Phosphorus is returned from the biomass pools to the two phosphorus species through several mechanisms. It is returned directly from the phytoplankton through endogenous respiration and non-predatory mortality. Herbivorous zooplankton obtain phosphorus through predation of the phytoplankton and return it through excretion and death. Carnivorous zooplankton preying on herbivorous zooplankton return phosphorus by the same mechanisms. The phosphorus returned from the biomass systems is partly in the available and partly in the unavailable forms. Unavailable phosphorus is converted to available phosphorus at a temperature dependent rate.

The silica species interact in the same manner as the phosphorus species with certain key differences: available silica is utilized only by the diatoms; all silica taken up by herbivorous zooplankton through predation is excreted; and the silica returned from the biomass systems is assumed to be entirely in the unavailable form.

The kinetics of the nitrogen species are fundamentally the same as the other nutrients. Ammonia and nitrate are used by the two

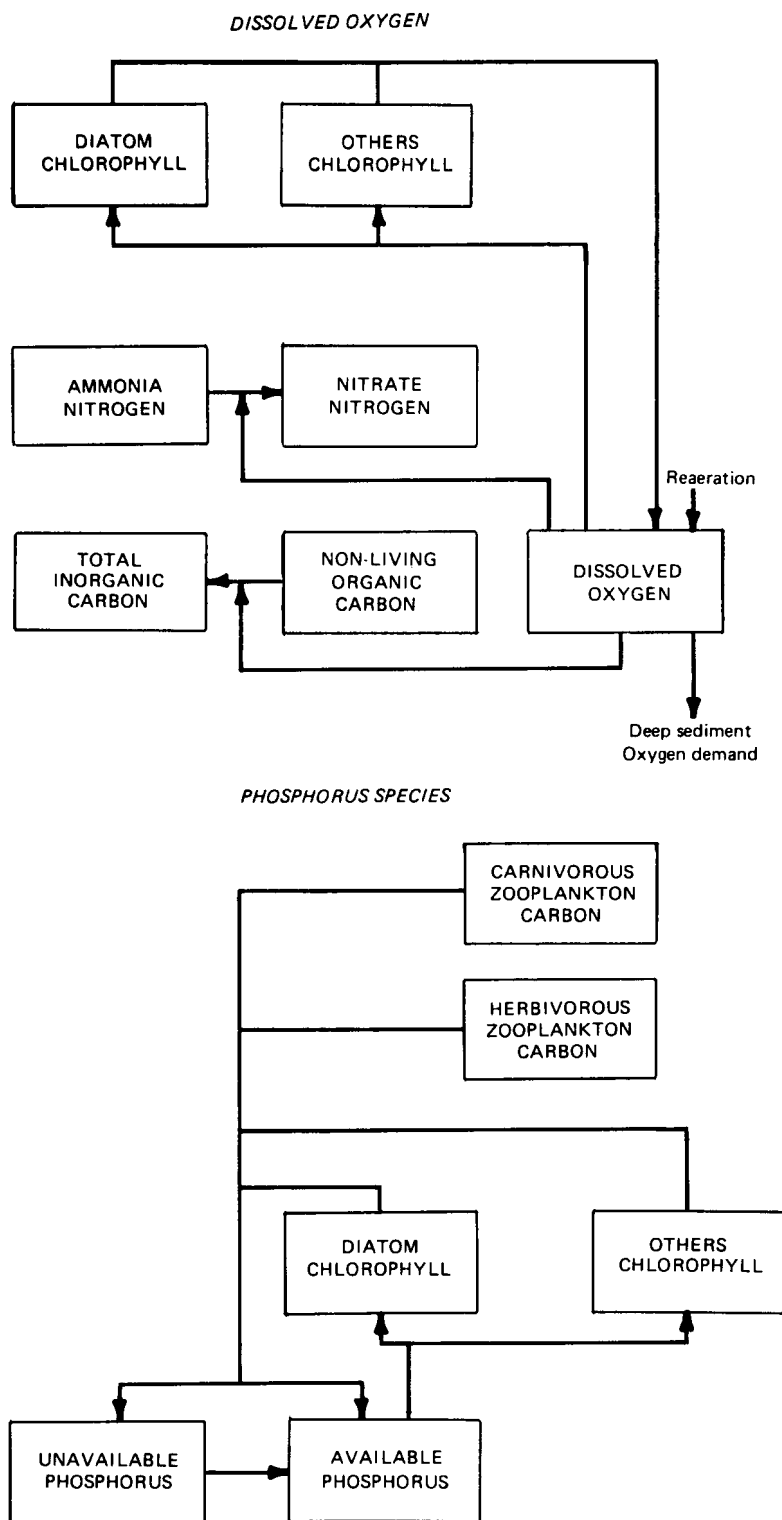


Figure 27. Lake Erie state variable interactions. Representations of dissolved oxygen (top) and phosphorus (bottom) nutrient cycles.

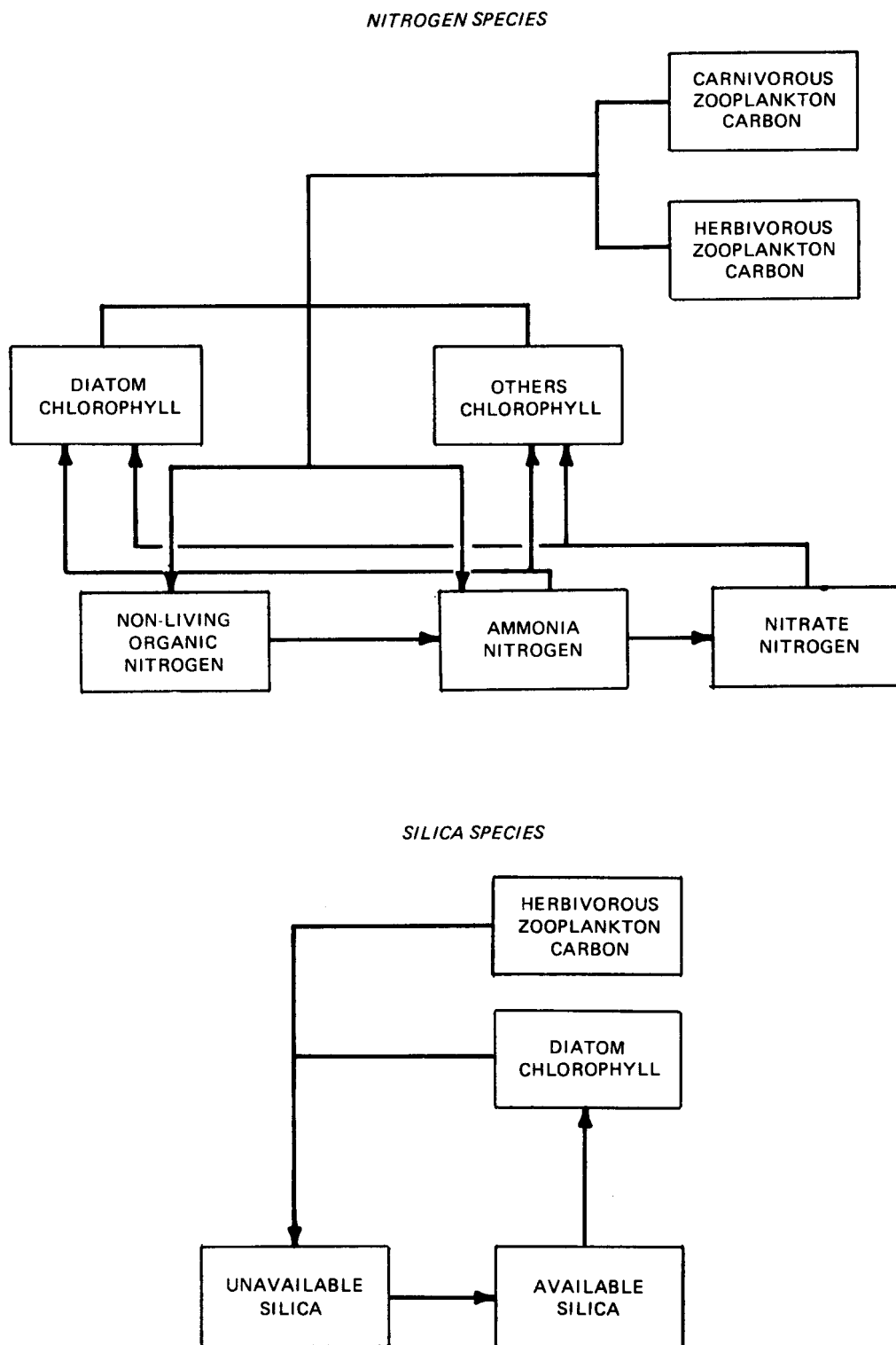


Figure 28. Lake Erie state variable interactions. Representations of nitrogen (top) and silica (bottom) nutrient cycles.

phytoplankton systems for growth. The rate at which each are taken up is proportional to its concentration relative to the total inorganic nitrogen available. The nitrogen returning from the biomass systems follows pathways that are analogous to the phosphorus.

Dissolved oxygen is coupled to the other state variables. The two sources of oxygen considered are reaeration and the evolution by phytoplankton during growth. The sinks of oxygen are oxidation of detrital carbon, nitrification, and respiration by the phytoplankton and zooplankton. The details of these reactions are presented below.

6.2 PHYTOPLANKTON GROWTH AND DEATH

The need to differentiate between diatom and non-diatom chlorophyll arises from a silica depletion that occurs during the spring bloom as is clear from the data presented previously. The formulation of the growth kinetics for each class is identical to that employed in the Lake Huron-Saginaw Bay analysis (Di Toro and Matystik, 1979) with the exception that the silica cycle is explicit in the calculation and a nutrient limitation term for reactive silica is included in the diatom growth rate equation. The Michaelis-Menten expression is used which multiplies the other terms of the rate expression for diatoms. The temperature and light dependencies are identical to those employed previously and have been discussed at length (Di Toro and Matystik, 1979).

The nutrient dependency employed relates the growth rate to the external nutrient concentrations rather than the internal cellular concentration as observed in laboratory chemostat experiments. Since the validity of this approach is a point of some contention, a rather complete analysis of the consequences of this approximation is presented below. The results show that indeed the external nutrient concentration controls the growth rate, albeit indirectly via the internal concentration. The dynamics of the cellular uptake and internal concentration are important only at short time scales which are not significant in seasonal

calculations. The variation of cellular stoichiometry can be important, however, and the constant stoichiometry used in the subsequent calculations must be regarded as an approximation.

6.2.1 Nutrient Dependence of Phytoplankton Growth

The relationships between the growth of phytoplankton and the concentration of the nutrients: carbon, nitrogen, phosphorus and, for diatoms, silica have been extensively investigated (Rhee, 1978). A primary difficulty in presenting a cohort quantitative description of the results is that the nutrient uptake and growth kinetics at the short time scales characteristic of laboratory batch experiments are quite involved and depend on the previous history of the population. In order to circumvent this difficulty to some degree, and to investigate relationships occurring at longer time scales, investigations of growth kinetics in chemostats have been undertaken. The population is subject to an influent of constant composition and a constant dilution rate. At steady-state, the growth rate is reduced to the dilution rate due to a depletion of the nutrient in shortest supply. By operating the chemostat at varying dilution rates, it is possible to observe the state of the population at various growth rates and nutrient concentrations.

For these experiments, the most successful correlation of growth rate, μ , is to the cellular nutrient concentration or cell quota, q , in units of nutrient mass/individual cell, and is expressed by the equation (Droop, 1973a):

$$\frac{\mu}{\mu'_m} = 1 - \frac{q_o}{q} \quad (1)$$

where μ'_m is the theoretical maximum growth rate at infinite cellular nutrient content and q_o is the minimum cell quota at which growth ceases. These two constants are directly estimated from a Droop plot of μq versus q and, therefore, form

a convenient starting point for the analysis. This equation can also be cast in the form:

$$\frac{\mu}{\mu'_m} = \frac{q - q_o}{q_o + (q - q_o)} \quad (2)$$

where the half-saturation constant of the excess nutrient quota, $q - q_o$, is q_o itself. Such behavior has been observed for phosphorus, nitrogen, silica, iron, and vitamin B₁₂ limited chemostats (Rhee, 1978a).

Nutrients are transported across the cell wall at a rate which depends on both the internal and external nutrient concentrations (Rhee, 1978a; Bierman *et al.*, 1973) as well as other physiologically important variables such as temperature and light intensity which, for this analysis, are assumed to be constant and nonlimiting. If S is the external nutrient concentration, then it has been observed, primarily using short-term batch kinetic experiments, that the rate of cellular uptake, v , in units of nutrient mass/cell/unit time, is related to the external nutrient concentration, S , via a Michaelis-Menten equation:

$$v = \frac{V_m S}{K_m + S} \quad (3)$$

where V_m is the maximum uptake rate at a particular cell quota and K_m is the half-saturation constant for uptake.

A simple relationship between growth rate and external nutrient concentration exists if the population is assumed to be independent of the internal cellular concentration and if the population is at steady-state since, for this latter condition, the uptake rate of nutrients must balance the synthesis rate of cells, i.e.:

$$v = \mu q \quad (4)$$

from which it follows that (Droop, 1973a):

$$\mu = \frac{\mu'_m S}{K_s + S} \quad (5)$$

where:

$$\mu'_m = \frac{\mu'_m \beta}{1 + \beta} \quad (6)$$

$$K_s = \frac{K_m}{1 + \beta} \quad (7)$$

and

$$\beta = \frac{V_m}{q_o \mu'_m} \quad (8)$$

For this important special case, the growth rate is related to the external nutrient concentration as in the Monod theory of bacterial growth, with the important modification that the half-saturation constant for growth, K_s , is always less than the half-saturation constant for cellular nutrient uptake K_m , and μ_m is always less than μ'_m . In addition, it has been assumed that the parameters: μ'_m , q_o , K_m , and V_m are constants. The validity of this assumption is examined subsequently. What is important to realize is that for the common case of cellular equilibrium for which Equation (4) applies, the growth rate of the population is indeed related to the external nutrient concentration as shown by Equation (5), which is a direct consequence of the growth Equation (1) and the uptake Equation (3).

The important dimensionless parameter of the theory is β : the ratio of V_m/q_o , the maximum specific uptake rate at $q = q_o$; to μ'_m , the maximum growth rate at $q \rightarrow \infty$. For large β , the apparent half-saturation constant for growth is small relative to the half-saturation constant for uptake: $K_s \approx K_m/\beta$. The reason is that, with β large, the rate of nutrient uptake is large relative

to the growth rate so that a large reduction in uptake rate can be tolerated (i.e., $S \ll K_m$) while still supplying adequate nutrient for growth.

Table 9 presents these experimentally determined parameters for various phytoplankton species. With phosphorus as the limiting nutrient, β is quite large, $\beta \sim 50-200$, indicating that $K_s \ll K_m$. For cases where both these constants have been measured, the estimate of K_s using Equation (7) compares quite well with the observation with a single exception for which the measured $\beta = 18$ also seems small. Thus, the half-saturation constant for growth can be expected to be in the range $K_s \approx 0.01-0.05 \mu\text{M}$ ($0.3-1.5 \mu\text{g PO}_4\text{-P/l}$) whereas the cellular uptake half-saturation constant is much larger: $K_m \approx 0.4-1.9 \mu\text{M}$ ($12-60 \mu\text{g PO}_4\text{-P/l}$).

With nitrogen as the limiting nutrient, β is smaller, $\beta \approx 5-25$, although still large enough for $K_s < K_m$. The half-saturation constant for growth is estimated to be in the range $K_s \approx 0.03-0.3 \mu\text{M}$ ($0.42-4.2 \mu\text{g N/l}$) and K_m has been observed in the range $K_m \approx 0.3-3.0$ ($4.2-42.0 \mu\text{g N/l}$).

For silica limitation, $\beta \approx 1-3$ which indicates that K_s is approximately one-half of K_m . The ranges are $K_s \approx 0.7-4.5 \mu\text{M}$ ($20-130 \mu\text{g Si/l}$) and $K_m \approx 0.5-7.7 \mu\text{M}$ ($14-220 \mu\text{g Si/l}$). For species with both K_s and K_m measured, the application of Equation (7) again yields satisfactory agreement, as shown in Table 9 indicating that the relationship between the cellular parameters and the half-saturation constant for growth are in reasonable accord with the previous analysis.

A similar relationship, Equation (6), exists between the maximum growth rate at infinite cell quota, μ'_m , and the maximum growth rate at infinite external substrate concentration μ_m . An interesting point arises if these parameters are estimated for an algal species using different limiting nutrients. Two examples are presented in Table 7, with μ_m calculated from the appropriate parameters in Table 9 and Equation (6). These experiments were conducted using the same conditions and cell culture so the estimates are directly comparable. It is clear that

the cellular maximum growth rates μ'_m are quite different whereas the maximum growth rate corresponding to the Monod expression μ_m , are much closer.

There is a fundamental reason for this result. While it is possible to increase the external nutrient concentration so that $S \gg K_s$ and $\mu \approx \mu_m$, it is not possible to arbitrarily set $q \gg q_0$ so that $\mu \approx \mu'_m$ since q is controlled by the ratio of substrate uptake rate to growth rate. In fact, it is easy to see that at external concentration S , and steady-state,

$$q = \frac{V_m}{\mu_m} \cdot \frac{K_s + S}{K_m + S} \quad (9)$$

which, for $S \gg K_m$, yields as the maximum cell at large external nutrient concentration:

$$q_\infty = q_0 (1 + \beta) \quad (10)$$

Since β is quite different for phosphorus, nitrogen, and silica, the maximum cell quotas achievable q_∞ , are also different corresponding to different fractions of the μ'_m in the cell quota equation, with the actually achievable maximum growth rate being μ_m . Thus, it is the parameter of significance.

The dimensionless parameter β , the ratio of maximum uptake to maximum growth rate sets the ratio of the extremes of the cell quota, $q_\infty/q_0 = 1 + \beta$, for the possible range of steady-states. For phosphorus, this ratio is calculated to be ~ 100 whereas for nitrogen, it is ~ 10 and for silica, it is ~ 2 . Thus, calculated cell quota for phosphorus is quite variable, for nitrogen less so, and for silica even less. As shown below, however, the observed variation in cell quota for phosphorus is actually less than that predicted by Equation (10), because the uptake rate is a function not only of the external nutrient concentration, S , but also of the internal cell quota q .

Table 9. Growth and Nutrient Uptake Parameters

	μ' m (day ⁻¹)	q _o f- mol/cell*	V _m f- mol/cell/hr*	β	K _m μ -mol/l	K _s μ -mol/l Measured Estimated**		Reference
Phosphorus								
<i>Scenedesmus</i> sp.	1.33	1.6	4.8	54	0.6 ± 0.04	< 0.06	0.011	Rhee (1973)
<i>Asterionella formosa</i>	0.70	1.75	9.9-13.2	9.9-13.2	1.9-2.8	0.02	0.01	Tilman and Kilham (1976)
<i>Cyclotella meneghiniana</i>	0.69	10.7	5.51	18	0.8	0.25	0.04	Tilman and Kilham (1976)
Nitrogen - NH₃								
<i>Thalassiosira pseudonana</i>	~1.3	~4.0	25.3 ± 5.3	~13	0.33 ± 0.27		0.028	Eppley and Renger (1974)
<i>Skeletonema costatum</i> (μ > 1.9/day)	3.6	65	~40	5	~1.0		~0.2	Harrison <i>et al.</i> (1976)
(μ < 1.2/day)	1.2	5 34-67	4.3-8.4	25	0.44		0.018	Conway <i>et al.</i> (1976)
Nitrogen - NO₃								
<i>Thalassiosira pseudonana</i>	~1.3	~4.0	19.8-4.2	~10	0.76 ± 0.2		~0.08	Eppley and Renger (1974)
Silica								
<i>Asterionella formosa</i>	1.21	296	36	2.4	7.7	3.9	3.21	Tilman and Kilham (1976)
<i>Cyclotella meneghiniana</i>	1.16	157	15	2.0	7.5	1.44	3.76	Tilman and Kilham (1976)
<i>Thalassiosira pseudonana</i>	2.75	20	6.9-8.1	3.0-3.6	2.6-5.8	0.83-1.4	0.65-1.4	Paasche (1973)
<i>Skeletonema costatus</i> (μ > 1.44/day)	2.88	25						Harrison <i>et al.</i> (1976)
(μ < 1.2/day)	1.20 2.88	6	2.63-3.68	1.1	1.1-1.8		0.54-0.88	Davis (1976)

* f-mol (femto-mole) = 10⁻¹⁵ mol

**Equation (7)

6.2.2 Nutrient Uptake

The principal assumption underlying the previous analysis is that the growth parameters: u'_m and q_o ; and uptake parameters: K_m and V_m are constant. At constant light and temperature, it appears that u'_m and q_o are reasonably constant indicating that the Droop Equation (1) is a correct representation of growth rate versus cell quota, although some recent data for *Skeletonema costatus* indicates that at high growth rates, $\mu > 1.5 \text{ day}^{-1}$ the correlation changes slope abruptly (see Table 10).

The nutrient uptake rate varies not only within external concentration but also as a function of cell quota. An analysis of this behavior by Rhee (1973) indicates that the uptake rate of phosphorus for *Scenedesmus* is of the form:

$$v = \frac{V_m S}{K_m + S} \frac{K_i}{i + K_i} \quad (11)$$

where i is the cellular concentration of labile polyphosphates. If it is assumed that $i = q - q_o$, then Equation (11) has the form:

$$v = \frac{V_m S}{K_m + S} \frac{K_q}{K_q + (q - q_o)} \quad (12)$$

where $K_q = K_i$. Using Droop's Equation (1) for

the growth rate, it is possible to calculate, at cellular equilibrium, the magnitude of the possible variation in cell quota:

$$\Delta q_\infty = \frac{q_\infty - q_o}{q_o} = \frac{\xi}{2} [-1 + \sqrt{1 + 4\beta/\xi}] \quad (13)$$

where $\xi = K_q/q_o$ and q_∞ is the value of q as $S \rightarrow \infty$ so that Equation (12) reduces to the Michaelis-Menten expression, Equation (3), $\Delta q_\infty = \beta$ which for the large β characteristic of phosphorus uptake, implies an enormous variation. For example, *Scenedesmus* with $\beta = 56$ would be expected to exhibit a $\Delta q_\infty = 56$ with $K_q \rightarrow \infty$. However, with $K_q/q_o = 0.45$ (using $K_q = K_i = 0.73 \text{ f-mol/cell}$ (Rhee, 1973), $\Delta q_\infty = 4.8$ using Equation (13), in comparison to observed $\Delta q_\infty = 6.1$ (Rhee, 1974). Thus, the reduction of v with increasing q is quite significant in reducing the variation in expected cellular composition of phosphorus from a fifty-fold to a five-fold variation.

The variation of cellular stoichiometry based on Equation (13) is shown in Figure 29a for a range of β characteristics of silica, nitrogen, and phosphorus kinetic constants. Large variations in cellular composition occur for large β and large K_q/q_o , whereas if the internal concentration tends to limit the uptake rate, then the range in stoichiometry is less. The effect is expected to be most significant for phosphorus and least significant for silica.

Table 10. Comparison of Growth Rates

	$\mu'_m (\text{day}^{-1})$			$u_m (\text{day}^{-1})$			References
	P	N	Si	P	N	Si	
<i>Asterionella formosa</i>	0.7	-	1.21	0.70	-	0.85	Tilman and Kilham (1976)
<i>Cyclotella meneghiniana</i>	0.69	-	1.16	0.65	-	0.77	Tilman and Kilham (1976)

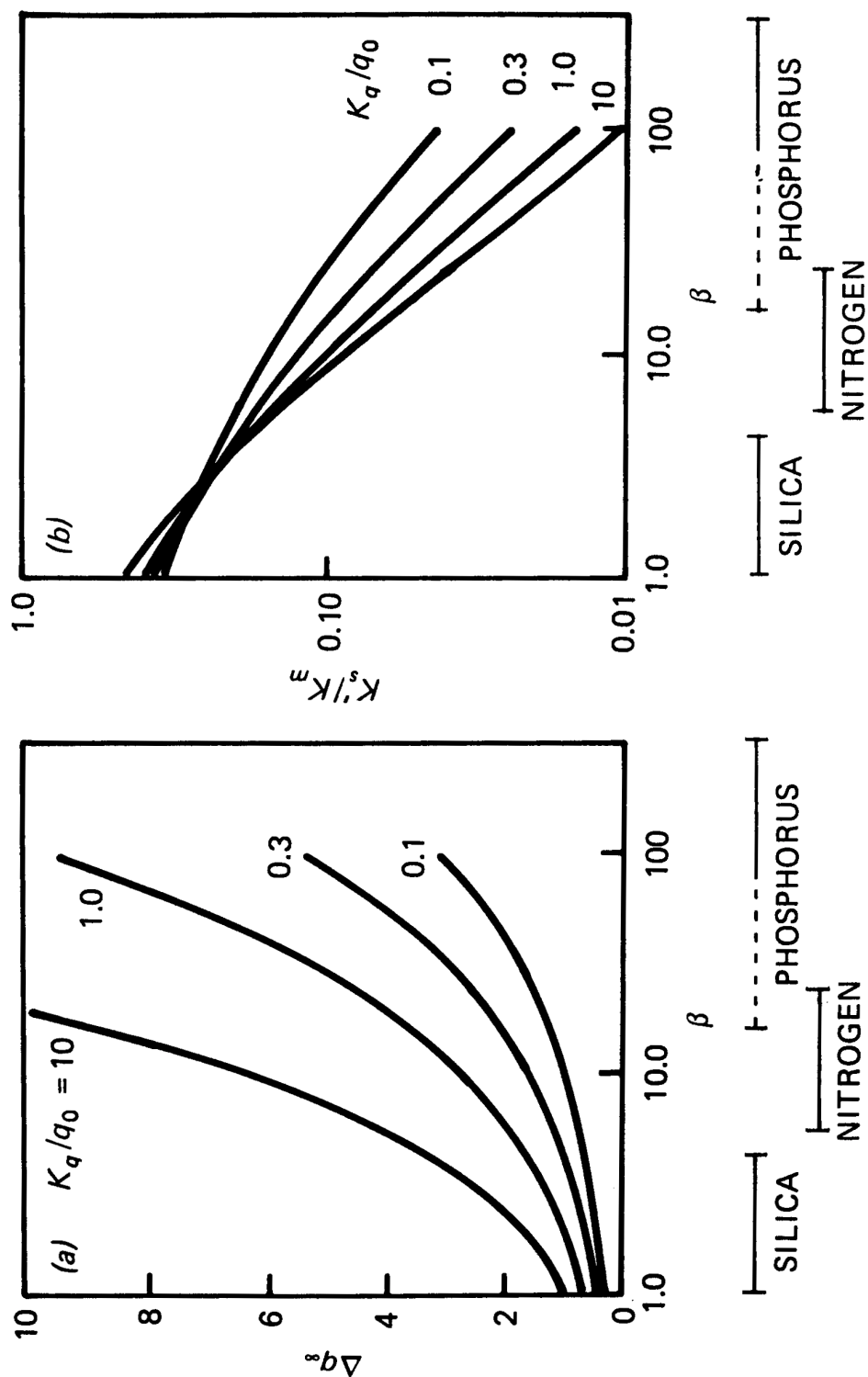


Figure 29. (a) The range of possible cell nutrient content $\Delta q_{\infty} = (q_{\infty} - q)$, and (b) the ratio of the apparent half-saturation constant for growth, K'_s , to the half-saturation constant for uptake K_m , as a function of β , the ratio of maximum specific uptake, V_m/q_0 , to maximum growth rate, μ'_m , and K_q/q_0 the dimensionless half-saturation constant for the dependence of nutrient uptake on internal nutrient concentration. The observed ranges (Table 9) in β for silica, nitrogen, and phosphorus limited growth are shown.

An alternate expression for uptake as a function of external and internal substrate concentration has been incorporated in a species-dependent analysis of phytoplankton growth by Bierman (1976). A similar analysis of the variation of internal stoichiometry yields $\Delta q_{\infty} \approx 4$ for phosphorus uptake of diatoms.

It is pertinent to note that the effect of the modification of the uptake rate incorporated in Equation (12) has only a small effect on the shape of the resulting growth versus external substrate concentration relation. In fact, it is very well approximated by the Michaelis-Menten expression. To see this, define an apparent half-saturation constant for growth, K'_s , and observe that the relationship between q and S can be obtained from the equilibrium $v = \mu q$, yielding:

$$\frac{q - q_o}{q_o} = \frac{\xi}{2} [\sqrt{1 + 4 \rho \beta / \xi} - 1] \quad (14)$$

where $\rho = S/K_m + S$. The cell quota at which the growth rate is one-half the maximum $q_{1/2}$, satisfies the equation:

$$\mu'_m (1 - q_o/q_{1/2}) = 1/2 \mu'_m (1 - q_o/q_{\infty}) \quad (15)$$

where when substituted into Equation (14), yields $S = K'_s$, the apparent half-saturation constant. The relevant formulae are given in the Appendix of this chapter. The result is shown in Figure 29b. For the range of β characteristic of silica limited growth and, to a less extent for nitrogen, the ratio is not sensitive to the magnitude of the internal cellular dependence of uptake. In the region characteristic of phosphorus, the effect is more pronounced. Note that in all cases K'_s is less than K_m .

Since Equation (14) relates q to S , and Equation (1) relates μ to q , it is possible to calculate μ as a function of S implied by these equations. A comparison of these results to the Monod expression:

$$\mu = \frac{\mu_m S}{K'_s + S} \quad (16)$$

is shown in Figure 30. The formulae are given in the Appendix to this chapter. The variation of growth rate is well approximated by the Michaelis-Menten expression regardless of the magnitude of β . The value of K_q/q_o used in this figure produces the largest calculated differences with other values showing even less deviation. Thus, the difference is of no practical importance, indicating that the Monod expression with the proper half-saturation constant is a valid characterization of the growth rate of phytoplankton species at cellular equilibrium.

The difficulty in using the classical Monod theory occurs in the uptake expression, $v = \mu q$, since the cell quota can vary as the external concentrations vary whereas in the conventional Monod theory the cell quota, or the analogous nutrient to biomass stoichiometric ratios, are held constant. The practical import of this phenomena, which is related to the choice of the measure of biomass employed, is discussed below.

6.2.3 Validity of Cellular Equilibrium Approximation

The analysis of the previous section depends on the cellular equilibrium approximation, that is $v = \mu q$. This is certainly true for steady-state chemostat experiments but its applicability to dynamic situations is open to question. The dynamic equation for $q(t)$ follows a mass balance of the cell itself:

$$\frac{dq}{dt} = v - \mu q \quad (17)$$

where $\frac{dq}{dt} = dq/dt$. Consider a perturbation analysis about steady-state values q^* , S^* and let $\varepsilon_q = q - q^*$. Substituting these values and ignoring all higher orders of terms in ε_q yields:

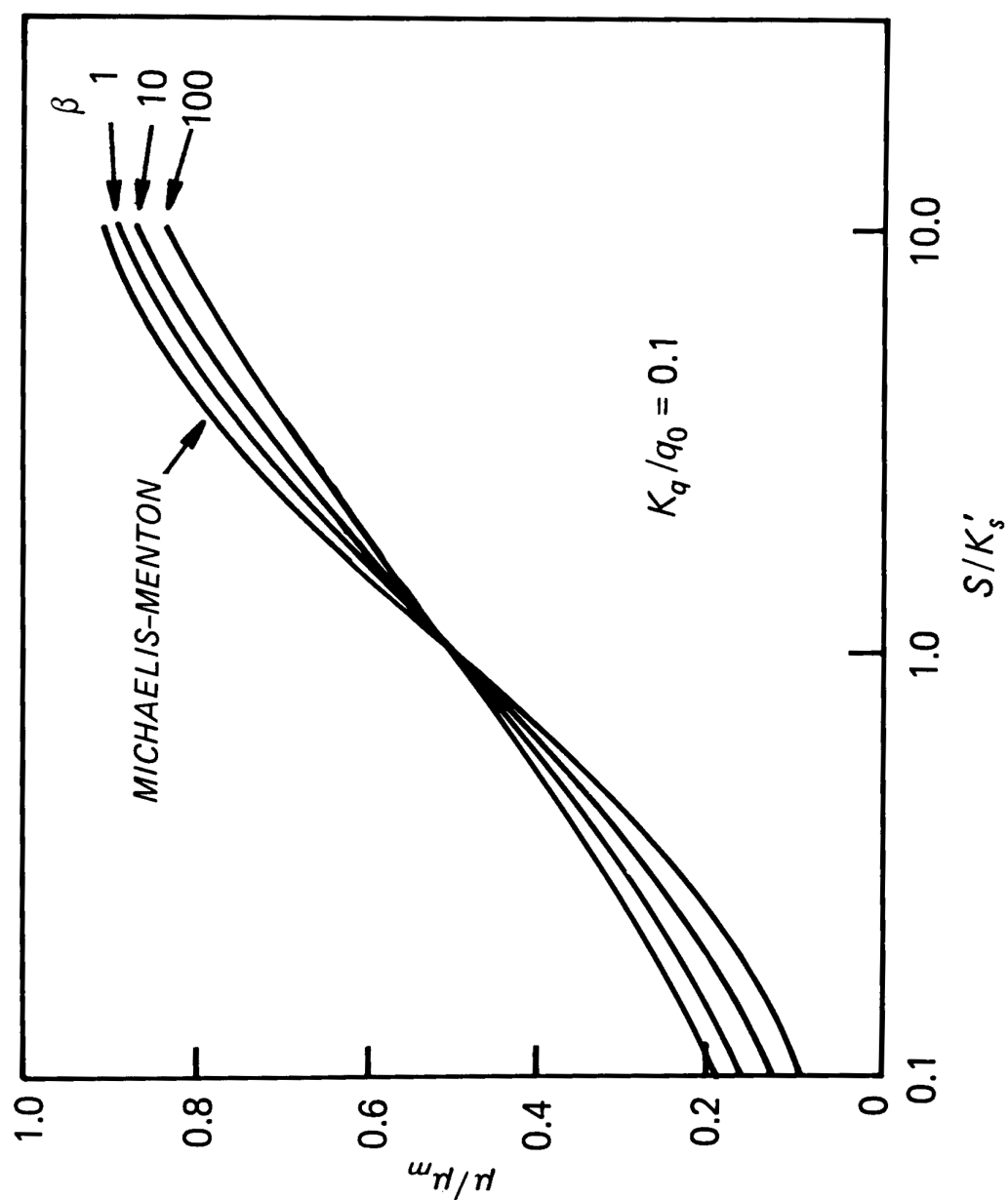


Figure 30. Normalized growth rate as a function of normalized external nutrient concentration: a comparison of the Michaelis-Menten expression to that derived from the internal cellular kinetics with uptake as a function of both external and internal nutrient concentrations.

$$\frac{O}{\varepsilon_q} = - \left(\mu'_m + \frac{v^*}{K_q + q^* - q_0} \right) \varepsilon_q \quad (18)$$

where v^* is the uptake expression, Equation (12), evaluated at q^* and S^* . But from Equation (1), $v^* = \mu'_m (q^* - q_0)$ and Equation 18 becomes:

$$\frac{O}{\varepsilon_q} = - \mu'_m \left(1 + \frac{\Delta q^*}{\xi + \Delta q^*} \right) \varepsilon_q \quad (19)$$

where $\Delta q^* = (q^* - q_0)/q_0$ and $\xi = K_q/q_0$ as before. Thus, ε_q has an exponentially decaying solution:

$$\varepsilon_q = \varepsilon_q(0) e^{-t/T_q} \quad (20)$$

with time constant:

$$T_q = \frac{1}{\mu'_m \left(1 + \frac{\Delta q^*}{\xi + \Delta q^*} \right)} \quad (21)$$

The relationship between μ'_m and the actual growth rate of the population, μ^* , involves two factors: The relationship between μ'_m and the actual maximum growth rate at infinite external substrate concentration, μ_m ; and a factor f , the reduction due to the finite external nutrient concentration: $\mu^* = f\mu_m$. With these reductions, the time constant becomes:

$$T_q = \frac{\Delta q_\infty}{1 + \Delta q_\infty} \frac{1}{1 + \xi + \Delta q_*} f T_\mu \quad (22)$$

where $T_\mu = 1/\mu^*$, the time constant of phytoplankton population growth. The first two fractions in the above expression are both bounded between 1/2 and 1 for all possible values of Δq_∞ and ξ . Thus, it follows that:

$$\frac{1}{4} f T_\mu < T_q < f T_\mu \quad (23)$$

Since growth at less than one-half the maximum is often the case; $f < 1/2$, and:

$$\frac{1}{8} T_\mu < T_q < \frac{1}{2} T_\mu \quad (24)$$

The conclusion drawn from this analysis is that the cells equilibrate with a time constant of approximately one-half to one-eighth the time constant for population changes. It is, therefore, quite reasonable to assume that the cells are at equilibrium even during population growth since the internal concentration can equilibrate as good deal more rapidly than the rate at which population can change.

6.2.4 Dynamic Equations at Cellular Equilibrium

In view of the preceding analysis consider the behavior of the population which is responding to an abrupt increase in external nutrient concentration. Initially, as the concentration of limiting nutrient increases the cells are no longer in equilibrium and begin to assimilate the nutrient thereby increasing their cell quota and, in turn, their growth rate. The population then starts to increase. The results of the previous analysis suggest, however, that the cells reach cellular equilibrium more rapidly than the cells can grow. In other words, the cell uptake occurs over a length of time during which the population size is not changing appreciably. Thus, it is possible that the cells achieve a new cell quota which is in equilibrium, i.e., $v = \mu q$, before the population size has reacted appreciably. Thus, a picture of dynamic equilibrium emerges where the cells are continuously in equilibrium with the slowly changing external substrate concentration. As the population and substrate concentrations change, the cell quota responds and changes also, but always more rapidly so that the cells continuously achieve a condition of cellular equilibrium throughout the response to the

external concentration change. Since this is a considerably simplified picture of how phytoplankton cells respond to substrate variations, it is of interest to formulate the equations which apply to this approximation, which can be called cellular dynamic equilibrium.

The formulation of the growth kinetic equations at cellular equilibrium follow from the general equations for dynamic cell quota by a simple transformation. It is an example if a general technique that can be used to remove fast reactions from general mass balance equations (Di Toro, 1976). Consider the dynamic equations that apply to a chemostat:

$$\dot{N} = \mu'_m (1 - q_o/q) - N/t_o \quad (25)$$

$$\dot{q} = v - \mu q \quad (26)$$

$$\dot{S} = -vN + (S_i - S)/t_o \quad (27)$$

where $N(t)$ is the number of cells/l; t_o is the detention time of the chemostat, the reciprocal of the dilution rate; S_i is the influent substrate concentration; and the dot implies a time derivative. The remaining variables have been defined previously. In order to derive the equations which apply at cellular equilibrium, it is necessary to apply the equation $v = \mu q$. However, it is not true that $\dot{q} = 0$ as would be expected from Equation 26, since this implies a constant cell stoichiometry and as is clear from the description of the expected behavior, the cell stoichiometry is changing in response to the changing conditions. Therefore, although $v = \mu q$ is a good approximation, $\dot{q} = 0$ is not and it is necessary to find equations which are valid regardless of the rate at which cell uptake occurs. The transformation that yields equations which do not involve the dynamic cell uptake reaction requires that a component variable be

identified which is unaffected by that reaction. In this case, a suitable variable is:

$$S_T = S + qN \quad (28)$$

the sum of the substrate concentration in the chemostat and the equivalent cell substrate concentration. The dynamic equation for S_T is obtained directly from the time derivative of Equation (28):

$$\dot{S}_T = \dot{S} + \dot{q}N + q\dot{N}$$

Using Equations (25, 26, 27) and substituting, the result is:

$$\dot{S}_T = (S_i - S_T)/t_o \quad (29)$$

Note that the total substrate concentration is a quantity unaffected by the kinetics of growth and uptake. The growth equation is also unaffected by the uptake reaction so it is applicable:

$$\dot{N} = \mu'_m (1 - q_o/q) N - N/t_o \quad (30)$$

However, in order to apply this equation the cell quota is required. It is obtained by solving the cell equilibrium equation, $v = \mu q$, i.e.:

$$\frac{V_m S}{K_m + S} \cdot \frac{K_q}{K_q + (q - q_o)} = \mu'_m (q - q_o) \quad (31)$$

and the component equation

$$S = qN = S_T \quad (32)$$

simultaneously for the unknown, $S(t)$ and $q(t)$, given the total substrate concentration $S_T(t)$ and the cell number $N(t)$. The solution involves four simultaneous equations: two differential

equations for $N(t)$ and $S_T(t)$ and two algebraic equations for $q(t)$ and $S(t)$. The computational method is discussed in the Appendix to this chapter.

Some typical results are shown in Figure 31 using the parameters characteristic of *Scenedesmus* with phosphate as the limiting nutrient (Table 9). The comparison is between the solution of the dynamic Equations (25-27) and the cellular equilibrium approximations, Equations (29-32). The initial condition is specified as the equilibrium which is reached for an influent of $S_i = 10 \mu\text{g-PO}_4 \text{ P/l}$. At $t = 0$, the influent is abruptly changed to $S_i = 20 \mu\text{g PO}_4 \text{ P/l}$ and the population reacts by increasing in size. The cell equilibrium solution reacts more quickly with an increase in $q(t)$ relative to the dynamic equation. As a consequence, the phosphate concentration at cell equilibrium decreases more rapidly than the dynamic solution. However, the dynamic solution soon catches up and the error in $q(t)$ for the cell equilibrium approximation decreases rapidly as predicted by the perturbation analysis. The residual error in phosphorus concentration takes a somewhat longer time to decay as can be seen.

The effect of β , the ratio of maximum uptake rate to growth rate, can be seen in Figure 32. As β decreases, the error in $q(t)$ tends to increase slightly and the time for the error to decay increases. The largest discrepancies occur for small β and large K_q/q_0 for which $T_q = f T_\mu$ and the cells are not equilibrating very rapidly. In general, however, the approximation appears to be quite satisfactory with errors decreasing to less than 10 in all variables rather rapidly.

6.2.5 Discussion and Conclusions

It is important to note that the cellular equilibrium approximation is essentially a computational simplification. The rapid dynamics of the internal cellular nutrient concentrations are eliminated which in turn removes the possibility of cells having different internal concentrations within a volume segment, since, in this approximation, cells equilibrate immediately as they are

transported to other volume segments. However, these kinetics still allow the cell nutrient content to adjust to changes in external concentrations.

The question of the necessity of even this refinement in practical computation is still unresolved. If algal species are aggregated into functional groups, i.e., diatoms, greens, etc., then the question of an appropriate biomass measure arises since aggregated cell counts are no longer reasonable. However, in one case at least (Rhee, 1973), it has been shown that Droop kinetics do not apply if the species biovolume is used to measure population size. Hence, the fundamental basis of these kinetics for biomass growth comes into question. Further, for aggregated populations, the five kinetic constants that specify the kinetics: μ'_m , K_m , V_m , q_0 , K_q , are known only within ranges and their final values are dependent on a calibration to field data. By contrast, the Monod theory requires three constants: μ'_m , K'_s and a nutrient/biomass ratio. Since the data available for calibration is the same for both kinetic formulations, the two additional constants and additional degrees of freedom which may add uncertainty to the final values obtained from the calibration. At present, it is uncertain whether the increased realism at the expense of an increase in the number of kinetic constants that specify details of this more realistic behavior is an advantageous tradeoff.

It is likely that variable stoichiometry is important in computing the nutrient budget of a lake, particularly for phosphorus. Consider the nutrient flux to the bottom sediment via algal settling. For that fraction of the population which settles during periods of non-nutrient limitation, the cell quota is low in the epilimnion as these cells settle into the hypolimnion if they are exposed to higher external nutrient concentrations then their cell quota will increase. Thus, the nutrient flux to the sediment is larger than what would be calculated if the minimum stoichiometry were employed throughout the calculation.

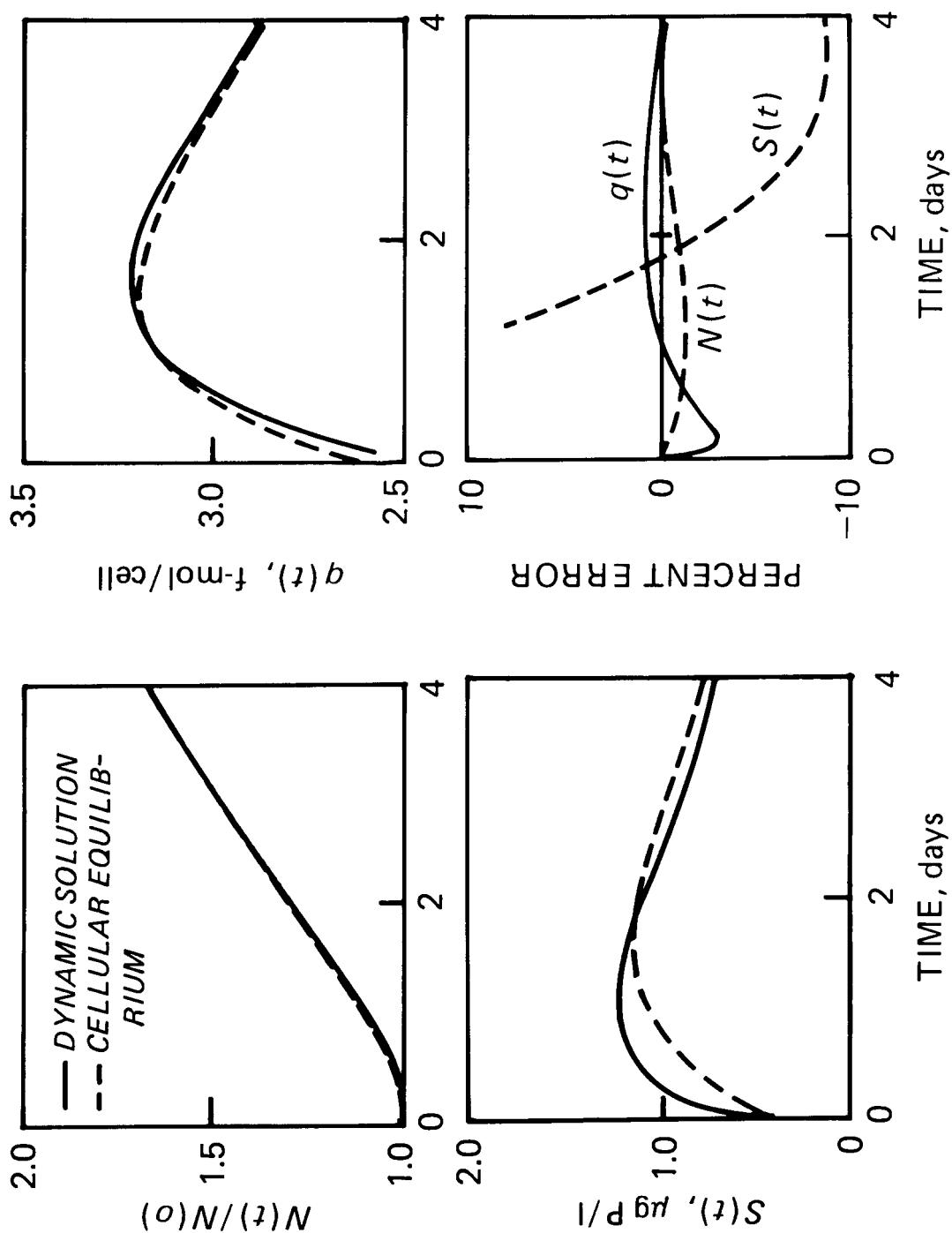


Figure 31. A comparison of the solutions to the dynamic equations (25-27) and the cellular equilibrium approximation equations (29-32). The parameters are for *Scenedesmus* sp. (Table 9) and phosphorus-limited growth. The retention time, $t_0 = 2.0$ days, and $K_q/q_0 = 0.46$. The initial conditions are the equilibrium solution for an influent of $S_i = 10.0 \mu\text{g PO}_4 \text{ P/l}$. The influent is abruptly increased to $S_i = 10.0 \mu\text{g PO}_4 \text{ P/l}$ at $t = 0$.

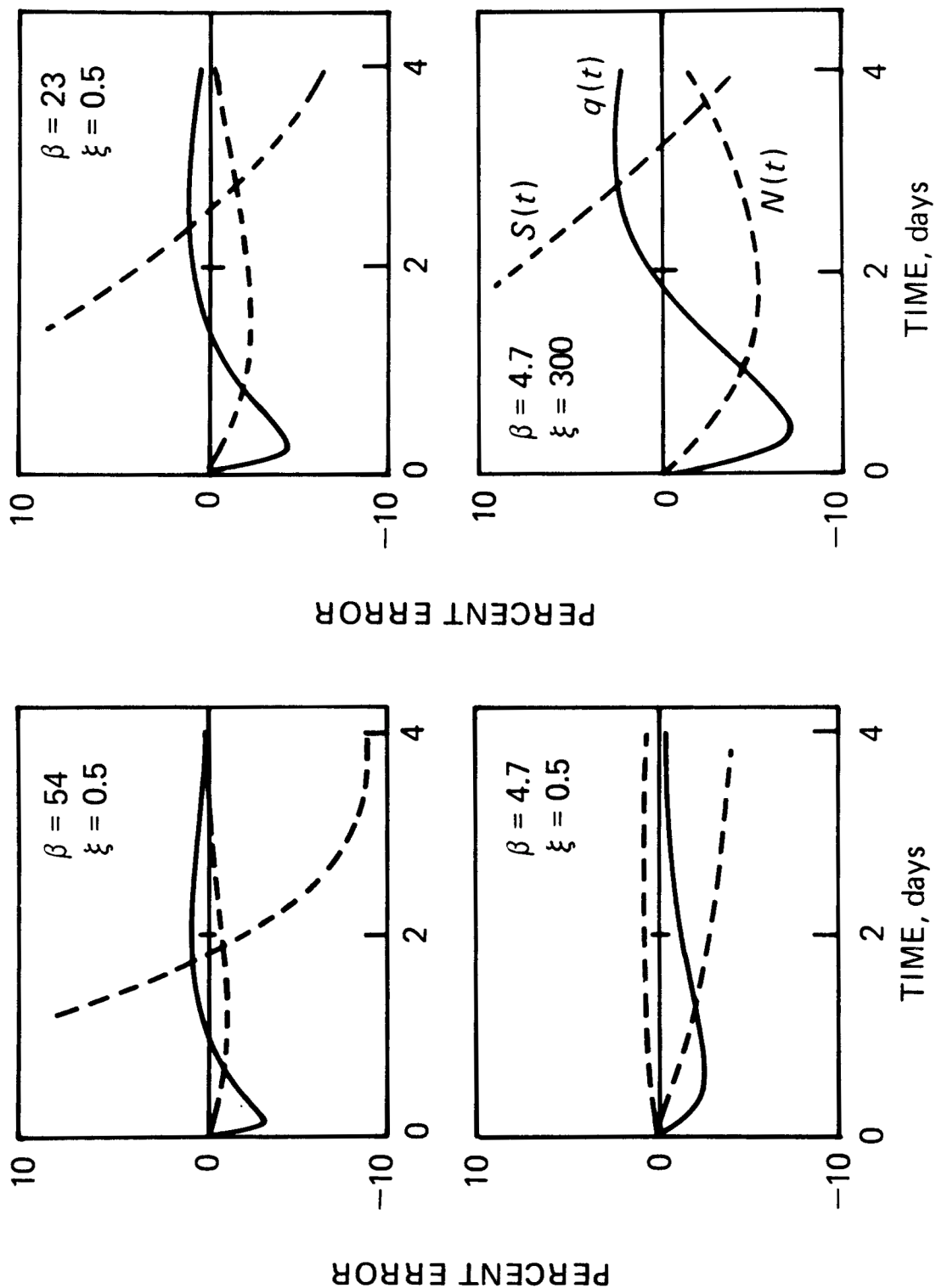


Figure 32. Percent error between the cellular equilibrium approximation and the dynamic equations for various values of β and $\xi = K_q/q_0$. The curves correspond to the errors in cell concentration, $N(t)$, nutrient concentration, $S(t)$, and cell quota, $q(t)$, as indicated.

For constant stoichiometry kinetics, the minimum stoichiometry is, in fact, often chosen since the yield of biomass at nutrient limitation is calculated correctly. Hence, it would appear that nutrient fluxes to the sediment are underestimated for this choice of the nutrient/biomass ratio. If, on the other hand, a stoichiometric ratio is chosen which is more representative on non-nutrient limited conditions, then the computed maximum population will be an underestimate. However, it appears that variable stoichiometry can be important for refined nutrient budgeted calculations. The computational results indicate that the cellular equilibrium approximation is adequate if the rate of change of the substrate concentration is slow relative to phytoplankton growth rate. This is typically the case in natural settings. However, in laboratory experiments, particularly in batch kinetic investigations, these conditions are not met and the fully dynamic equations are necessary.

If this mechanism is judged to be important, then the inclusion of variable cell stoichiometry is necessary.

6.3 MULTIPLE NUTRIENT LIMITATION

The proper formulation of the growth and uptake kinetics for multiple limiting nutrients is an area which is under investigation. The proposals to date make use of the relationships obtained from single limiting nutrient investigations and composite them in various ways. If $\mu_1, \mu_2, \dots, \mu_n$ are the growth rate expressions as functions of nutrient concentrations S_1, S_2, \dots, S_n with maximum rates: $\mu_{1m}, \mu_{2m}, \dots, \mu_{nm}$, then the proposals are:

Multiplicative (Chen, 1970; Di Toro *et al.*, 1971):

$$\mu = \mu_m \cdot \frac{\mu_1}{\mu_{1m}} \cdot \frac{\mu_2}{\mu_{2m}} \dots \frac{\mu_n}{\mu_{nm}} \quad (33)$$

Minimum (Droop, 1974):

$$\mu = \text{Min}(\mu_1, \mu_2, \dots, \mu_n) \quad (34)$$

Reciprocal (Scavia and Park, 1976):

$$\frac{\mu_m}{\mu} = \frac{1}{n} \left(\frac{\mu_{1m}}{\mu_1} + \frac{\mu_{2m}}{\mu_2} + \dots + \frac{\mu_{nm}}{\mu_n} \right) \quad (35)$$

The experimental investigations have been concerned either with growth kinetics or uptake kinetics. For the former, Droop (1973b) proposed the multiplicative expression but found subsequently that experiments using vitamin B₁₂ and phosphorus corresponded to the minimum expression (Droop, 1974). Bierman *et al.* (1973) in an analysis of Rhee's data for nitrogen and phosphorus limitation of *Scenedesmus* (Rhee, 1977) showed that the minimum expression correctly reproduced the experimental data. It is interesting to note that for the latter investigation, the multiplicative expression is satisfactory if μ_m is increased. Thus, in situations for which absolute growth rates are unknown, the difference between the two expressions is in the leading constant. For uptake kinetics, the data of Ketchum (1939) was analyzed using the multiplicative expression (Di Toro *et al.*, 1971) and found to conform.

The majority of evidence to date supports the minimum hypothesis. However, the multiplicative formulation usually fits the variations in experimental data as well, if not their absolute magnitude, as in the case of *Scenedesmus*. Therefore, from an operational point of view, either form is a reasonable representation of limitation, although the minimum is probably preferable.

6.4 MEASURE OF BIOMASS

The kinetics discussed in the previous sections have been shown to be applicable to a single species in well-controlled environments. For application to natural settings, it is necessary to

aggregate the individual species into manageable groupings and to characterize their kinetics as a whole. The initial requirement is an appropriate measure of the aggregated population size. For single species, the direct measure of population size is the number of cells/unit volume. For naturally occurring populations, even this measure may be somewhat ambiguous: it is difficult to distinguish viable and non-viable cells, and colonial species pose a problem since the count usually does not distinguish individual cells and the sizes of the colonies are quite variable.

The sum of the numbers of each species, the total count, is a possibility but since cell sizes vary substantially, the nanoplankton would dominate such an aggregation. To account for this, the total biovolume or wet weight of phytoplankton, assuming unity density, can be calculated using characteristic volumes for each identified species. Unfortunately, volumes can vary appreciably as a function of nutrient status. And, in fact, the growth kinetic equation (1) does not appear to apply, for *Scenedesmus* at least, if cell quota is calculated on a cell volume basis (Rhee, 1973). Conversion to phytoplankton dry weight and carbon involves further species dependent constants which are also nutrient dependent, and therefore, are subject to variation and uncertainty. Thus, although the use of phytoplankton dry weight or carbon concentration is an appealing solution to the issue of aggregation, it suffers from some practical difficulties.

An alternate to this problem is to measure a parameter which is characteristic of all phytoplankton, namely, chlorophyll *a*, and use this as the aggregated variable. The principle advantages are that the measurement is direct; it integrates cell types, age, and it accounts for cell viability. The principle disadvantages are that it is a community measurement with no differentiation of functional groups (e.g., diatoms), and that it is not necessarily a good measurement of standing crop in carbon or dry weight units since the chlorophyll to dry weight and carbon ratios are variable.

As can be seen from the above discussion, no simple aggregate measurement is entirely satisfactory. Further, the use of detailed kinetics which are satisfactory for single species are not necessarily appropriate with biomass or chlorophyll as the population variable. Hence, the analysis of naturally occurring phytoplankton populations as aggregates of species involves a number of simplifications and assumptions, with the result that the actual kinetics employed, although guided by the results discussed in the previous sections, are of necessity empirical.

From a practical point of view, the availability of extensive chlorophyll data for the Great Lakes essentially dictates its use as the aggregate measure of the phytoplankton population. These data, together with somewhat limited species and biomass data, form the basis of the analysis to be discussed subsequently.

6.5 STOICHIOMETRY AND UPTAKE KINETICS

If it is assumed that the growth kinetics discussed in the previous sections are applicable to chlorophyll *a* as the measure of aggregated population, then a Monod expression for growth, with a suitable half-saturation constant, is appropriate. In order to specify the nutrient uptake accompanying this growth, it is necessary to specify the population stoichiometry in units of mass of nutrient uptake/mass of population synthesized. For chlorophyll as the population measure, the relevant ratios are the mass of carbon, nitrogen, phosphorus, and silica per unit mass of chlorophyll *a*. A selection of these ratios has been presented (Di Toro *et al.*, 1971). At first glance, the variability of these ratios is large and the use of constant ratios in the analysis is questionable. However, it is clear that the reason these ratios vary is the varying cellular content of nutrients and chlorophyll which is, in turn, a function of the external nutrient concentration and the past history of the population. Large ratios correspond to excess nutrients and small ratios correspond to that nutrient limiting the growth rate. Thus, the choice of the relevant ratios can be made with

the situation of interest in mind. Since the population to be discussed subsequently are primarily phosphorus and/or silica limited, the stoichiometry chosen can reflect these facts. The operational consequences of this choice is that the population stoichiometry under non-limiting conditions will be underestimated but the maximum chlorophyll concentrations under limiting conditions should be correctly estimated. Hence, the trade-off is a probable lack of realism during a portion of the year versus a correct estimate of population chlorophyll during the period of nutrient limitation. Since this is usually the critical period, and most questions to be answered are usually sensitive to the maximum population size, this choice is a practical expedient.

6.6 KINETIC FORMULATIONS

The kinetics employed for the calculations to be presented subsequently are based on the considerations discussed in the previous sections as well as the experience accumulated during the performance of similar calculations for Lake Ontario (Thomann *et al.*, 1975), Lake Huron and Saginaw Bay (Di Toro and Matystik, 1979) and elsewhere (Di Toro, *et al.*, 1977). The format of the presentation given below is designed to be complete and detailed and yet provide an overview of the reactions.

Table 11 presents the formulation and kinetic constant used for the phytoplankton growth reactions. The left hand side of the reaction stoichiometric equation specifies the quantity of the reactants which are consumed by the reaction and the right hand side specifies the end-products. The square-bracketed species represent concentrations, not necessarily in molar units, but in any convenient set of mass units. The stoichiometric coefficients must, of course, be consistent with these units. The species with a unity stoichiometric coefficient corresponds to the units of the reaction rate. Thus, for phytoplankton growth, the reaction rate has units $\mu\text{g Chl } a/\text{l/day}$ consistent with the stoichiometric equation. The growth kinetics chosen for this investigation incorporate the

temperature and light intensity variations discussed previously (Di Toro and Matystik, 1979). The nutrient dependency follows a Michaelis-Menten expression external substrate concentration with the proper half-saturation constant which, as shown in Figure 30, is an entirely adequate approximation to the results of the kinetics derived from Droop's growth equation, Rhee's uptake equation, and the assumption of cellular equilibrium. Multiple nutrient limitation is incorporated using the product formulation, although the minimum expression would yield comparable results. The stoichiometry of the population is assumed to be constant, and, for the limiting nutrients, at values close to their minimum requirement. As discussed above, this appears to be a practical solution to the problem of fluctuating cellular stoichiometry.

The stoichiometry of the reaction varies in two ways. Inorganic nitrogen uptake is either ammonia or nitrate depending on the ratio of ammonia to total inorganic nitrogen. Nitrite nitrogen is ignored since its concentration is so low. For ammonia and nitrate uptake, alkalinity changes occur consistent with experimental observation (Brewer and Goldman, 1976). Ammonia uptake causes a decrease in alkalinity. For nitrate uptake, the initial step is reduction to ammonia which produces oxygen and alkalinity after which the reaction continues as before.

Gross primary production, as measured in a shipboard incubator, utilizes the same reaction rates except that the light limitation term is not depth averaged since the illumination is uniform for this measurement.

The reaction rate constants are comparable to those used for Lakes Ontario and Huron, although there are some differences due primarily to the division of phytoplankton biomass into diatom and non-diatom fractions.

Phytoplankton endogenous respiration and non-predatory mortality, Table 12, is essentially the reverse of the growth reaction. However, only a portion of the organic carbon is directly oxidized

Table 11. Phytoplankton Growth - I

Reaction Stoichiometric Equation

$$a_{CP}[CO_2] + a_{PP}[PO_4-P] + a_{NP}\{\alpha[NH_4-N] + (1-\alpha)[NO_3-N]\} + a_{SiP}[Si] \xrightarrow{R_1} [Chl\ a] \\ + \{\alpha a_{O_2P} + (1-\alpha)a_{NO_3P}\}[O_2] + \{\alpha a_{NH_4A} + (1-\alpha)a_{NO_3A}\}[Alk]$$

Reaction Rate

$$R_1 = K_1 \theta_1^{T-20} r(I/I_s) \frac{[PO_4-P]}{K_{mP} + [PO_4-P]} \frac{[N]}{K_{mN} + [N]} \frac{[Si]}{K_{mSi} + [Si]} [Chl\ a]$$

Light Reduction

$$r(I/I_s) = \frac{ef}{K_e H} (e^{-\alpha_{1-e}} e^{-\alpha_o})$$

$$\alpha_1 = \alpha_o e^{-K_e H} \quad K_e = \text{extinction coefficient} \quad I_{av} = \text{average daily solar radiation at segment surface}$$

$$\alpha_o = I_{av}/fI_s \quad f = \text{photoperiod} \quad H = \text{segment depth}, \quad T = \text{temperature}$$

Nitrogen Uptake

$$[N] = [NH_4-N] + [NO_3-N] = \text{Total inorganic nitrogen}$$

$$\alpha = [NH_4-N]/[N] = \text{Ammonia fraction}$$

Gross Primary Production

$$G_{PP} = a_{CP} \{R_{1-\text{diatoms}} + R_{1-\text{non-diatoms}}\} \text{ with } r = \frac{I_{Lab}}{I_s} e^{1-I_{Lab}/I_s}$$

$$I_{Lab} = 30.7 \text{ ly/day (Gloosenko et al., 1974)}$$

Table 11. Phytoplankton Growth - I (Continued)**Rate Constants**

Description	Notation	Value		Units
		Diatom	Non-Diatom	
Saturated Growth Rate at 20°C	K_1	2.1	1.6	Day ⁻¹
Temperature Coefficient	θ_1	1.04	1.13	none
Saturating Light Intensity	I_s	225.	350.	ly/day
Half-Saturation Constant for Phosphorus	K_{mP}	1.0	1.0	μg PO ₄ -P/l
Half-Saturation Coefficient for Nitrogen	K_{mP}	25.0	25.0	μg N/l
Half-Saturation Coefficient for Silica	K_{mSi}	30.0	0.00	μg Si/l
Carbon to Chlorophyll Ratio	a_{CP}	100.	100.	μg C/μg Chl <i>a</i>
Phosphorus to Chlorophyll Ratio	a_{pP}	0.5	0.5	μg PO ₄ -P/μg Chl <i>a</i>
Nitrogen to Chlorophyll Ratio	a_{NP}	10.0	10.0	μg N/μg Chl <i>a</i>
Silica to Chlorophyll Ratio	a_{SiP}	40.0	0.00	μg Si/μg Chl <i>a</i>
Oxygen to Chlorophyll Ratio	a_{O2P}	(32/12) a_{CP}	(32/12) a_{CP}	μg O ₂ /μg Chl <i>a</i>
Oxygen to Chlorophyll Ratio (Nitrate Uptake)	a_{NO3P}	(48/14) a_{NP}	(48/14) a_{NP}	μg O ₂ /μg Chl <i>a</i>
Alkalinity to Chlorophyll Ratio (Nitrate Uptake)	a_{NO3A}	$a_{NP}/14.$	$a_{NP}/14.$	Milliequivalents/μg Chl <i>a</i>
Alkalinity to Chlorophyll Ratio (Ammonia Uptake)	a_{NH4A}	$-a_{NP}/14.$	$-a_{NP}/14.$	Milliequivalents/μg Chl <i>a</i>

Table 12. Phytoplankton Respiration and Non-Predatory Mortality Reaction Stoichiometric Equation - II

$$[Chl\ a] = f_{ox} a_{0_2P} [O_2] \xrightarrow{R_2} a_{CP} \{f_{ox} [CO_2] + (1 - f_{ox}) [Org-C]\} + a_{SiP} [Unavailable\ Si] \\ + a_{pP} \{f_A [PO_4-P] + (1 - f_A) [Unavailable\ PO_4]\} + a_{NP} \{f_A [NH_4] + (1 - f_A) [Org-N]\}$$

Reaction Rate

$$R_2 = K_2 \theta_2^{T-20} \frac{[O_2]}{K_{0_2C} + [O_2]} [Chl\ a]$$

Organic Carbon - Inorganic Carbon Liberation

$$f_{ox} = \frac{f_{NR} [O_2]}{K_{O_2C} + [O_2]}$$

Rate Constants

Description	Notation	Value		Units
		Diatom	Non-Diatom	
Endogenous Respiration Rate at 20°C	K_2	0.075	0.075	Day ⁻¹
Temperature Coefficient	θ_2	1.08	1.08	None
Non-Refractory Fraction of Phytoplankton Respiration	f_{NR}	0.7	0.7	None
Half-Saturation Constant for Oxygen Limitation	K_{O_2C}	0.1	0.1	mg O ₂ /l
Available Fraction of Respired Phytoplankton	f_A	0.5	0.5	None

to CO_2 . The remainder is detrital carbon. The estimate used of the fraction of the algal carbon which is refractory is 30%. Similarly, only a fraction of the cellular nitrogen and phosphorus is released in the available form. This is estimated to be 50%. It is assumed that all the silica released is in the unavailable form. The sources for these estimates have been presented (Di Toro and Matystik, 1979).

The rational and experimental data for the zooplankton formulations, presented in Table 13, 14, and 15 have been presented elsewhere (Di Toro and Matystik, 1979). Table 16 presents the formulations for nitrification. The rate is reduced as oxygen concentration approaches the half-saturation constant. Denitrification, which is only effective at the very low or zero oxygen concentration, is only active in the sediment segments as presented in Table 17.

The recycle reaction which transforms the unavailable nutrient to their available forms are listed in Table 18. Their rates are dependent on the chlorophyll concentration as in the Lake Huron calculation (Di Toro and Matystik, 1979).

Since dissolved oxygen is of major concern in Lake Erie, the rationale for these reactions is detailed below.

6.7 DISSOLVED OXYGEN KINETICS

The reduction of dissolved oxygen in the central basin hypolimnion during stratification is a consequence of the aerobic respiratory processes in the water column and the anaerobic respiration in the sediments. Both these processes are significant contributors and, therefore, it is necessary to formulate their kinetics explicitly.

The methodology for the analysis of dissolved oxygen dynamics in natural waters, particularly, in streams, rivers, and estuaries is reasonably well-developed (O'Connor and Thomann, 1972). The long history of applications have focused primarily on the use of BOD as the measure of the quantity of oxygen demanding material and

its rate of oxidation as the controlling kinetic reaction. This has proven to be appropriate for waters receiving a heterogeneous combination of organic wastes of municipal and industrial origin since as aggregate measure of their potential effect is a great simplification that reduces a complex problem to one of tractable dimensions.

The situation in Lake Erie is somewhat similar in this respect since the major source of oxygen demanding material is photosynthetic primary production and the kinetics that control are the aerobic respiration of the phytoplankton, and the bacterial oxidation of detrital organic carbon. The complicating feature is the interplay of the aerobic reactions in the water column and the anaerobic reactions in the sediment.

6.8 WATER COLUMN PRODUCTION AND RESPIRATION

A byproduct of photosynthetic carbon fixation is the production of dissolved oxygen. The reaction stoichiometry is given in Table 11. The rate of nutrient uptake and oxygen production are all proportional to the growth rate of the population since its stoichiometry is fixed.

The reaction describing algal respiration is similar to the growth reaction since it is the reverse process. However, during algal respiration, a fraction of the organic carbon, f_{ox} , is oxidized directly while a portion is not, becoming detrital organic carbon. The reaction is given in Table 12. The detrital organic carbon oxidation reaction proceeds separately and its stoichiometry is given in Table 18. This is the reaction that is analogous to the classical BOD oxidation reaction and it is formulated as first-order with respect to the organic carbon concentration. These three reactions, together with the oxygen consumed during nitrification, are the water column kinetic reactions being considered in this calculation.

It is important to realize that both the rates of oxygen production and community respiration are comparable to direct field observations.

Table 13. Herbivorous Zooplankton Growth Reaction Stoichiometric Equation - III

$$[Chl\ a] \xrightarrow{R_3} \beta\ a_{CP}[Z_H] + (1 - \beta) \{a_{CP}[Org-C] + a_{NP}f_A[NH_4] + (1 - f_A)[Org-N] + a_{pP}f_A[PO_4-P] + (1 - f_A)[Unavailable-PO_4]\} + a_{SIP}[Unavailable-Si]$$

Reaction Rate

$$R_3 = K_3T \frac{K_{mg}}{K_{mg} + [Chl-a]} [Z_H]$$

Assimilation Limitation

$$\beta = \frac{\epsilon_H K_{m\epsilon}}{K_{m\epsilon} + [Chl-a]}$$

Rate Constants

Description	Notation	Value	Units
Filtering Rate	K ₃	0.035	L/mg C/day-°C
Half-Saturation Constant for Filtering Rate Limitation	K _{mg}	15.	µg Chl-a/l
Half-Saturation Constant for Assimilation Rate Limitation	K _{mε}	10.	µg Chl-a/l
Maximum Assimilation Efficiency	ε _H	0.6	None

Table 14. Carnivorous Zooplankton Growth Reaction Stoichiometric Equation - IV

$$\begin{aligned}
 [Z_H] \xrightarrow{R_4} & \epsilon_C [Z_C] + (1 - \epsilon_C) \{ [Org-C] + a_{NC} \{ f_A [NH_4] + (1 - f_A) [Org-N] \} \\
 & + a_{pC} \{ f_A [PO_4-P] + (1 - f_A) [Unavailable-PO_4] \} \}
 \end{aligned}$$

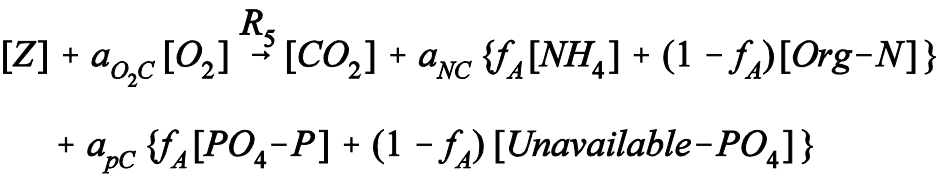
Reaction Rate

$$R_4 = K_4 T [Z_H]$$

Rate Constants

Description	Notation	Value	Units
Filtering Rate	K_4	0.05	l/mg C/day-°C
Assimilation Efficiency	ϵ_C	0.6	None
Nitrogen to Carbon Ratio	a_{NC}	0.1	mg N/mg C
Phosphorus to Carbon Ratio	a_{pC}	0.0005	mg PO ₄ -P/mg C

Table 15. Zooplankton Respiration Reaction Stoichiometric Equation - V



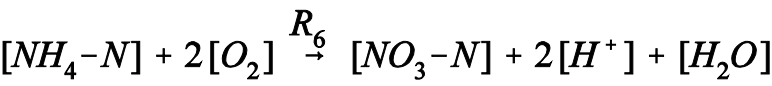
Reaction Rate

$$R_5 = K_5 \theta_5^{T-20} [Z]$$

Rate Constants

Description	Notation	Value		Units
		Herbivorous	Carnivorous	
Respiration Rate at 20°C	K ₅	0.02	0.02	Day ⁻¹
Temperature Coefficient	θ ₅	1.045	1.045	None
Oxygen to Carbon Ratio	a _{O₂C}	2.67	2.67	mg O ₂ /mg C

Table 16. Nitrification Reaction Stoichiometric Equation - VI



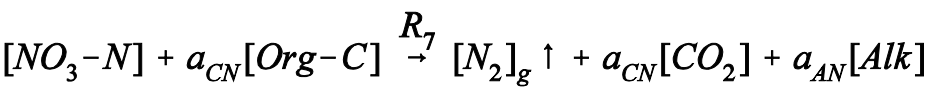
Reaction Rate

$$R_6 = K_6 \theta_6^{T-20} \frac{[O_2]}{K_{nit} + [O_2]} [NH_4-N]$$

Rate Constant

Description	Notation	Value	Units
Nitrification Rate at 20°C	K ₆	0.12	Day ⁻¹
Temperature Coefficient	θ ₆	1.08	None
Half-Saturation Constant for Oxygen Limitation	K _{nit}	2.0	mg O ₂ /l

Table 17. Denitrification Reaction Stoichiometric Equation - VII



Reaction Rate

$$R_7 = K_7 \theta_7^{T-20} \frac{K_{NO_3}}{K_{NO_3} + [O_2]} [NO_3]$$

Rate Constants

Description	Notation	Value	Units
Denitrification Rate	K_7	0.1	Day ⁻¹
Temperate Coefficient	θ_7	1.045	None
Michaelis Constant for Oxygen Limitation	K_{NO_3}	0.1	mg O ₂ /l
Carbon to Nitrogen Ratio	a_{CN}	12/14	mg C/mg N
Alkalinity to Nitrogen Ratio	a_{AN}	1/14	Milliequivalents/mg N

Table 18. Mineralization Reaction Stoichiometric Equation - VIII

Species	Reaction Stoichiometric Equation	Reaction Rate
Organic Carbon	$a_{O_2C}^{-1} [O_2] + [Org-C] \xrightarrow{R_8} [CO_2]$	$R_8 = K_8 \theta_8^{T-20} \frac{[O_2]}{K_{O_2C} + [O_2]} [Org-C]$
Organic Nitrogen	$[Org-N] \xrightarrow{R_9} [NH_4-N]$	$R_9 = K_9 \theta_9^{T-20} \frac{[Chl-a]}{[Chl-a] + K_{mr}} [Unavail-P]$
Unavailable Phosphorus	$[Unavail-P] \xrightarrow{R_{10}} [PO_4-P]$	$R_{10} = K_{10} \theta_{10}^{T-20} \frac{[Chl-a]}{[Chl-a] + K_{mr}} [Unavail-P]$
Unavailable Silica	$[Unavail-Si] \xrightarrow{R_{11}} [Si]$	$R_{11} = K_{11} \theta_{11}^{T-20} [Unavail-Si]$

Rate Constants

Description	Notation	Value	Units
Organic Carbon Mineralization Rate at 20°C	K_8	0.1	Day ⁻¹
Temperature Coefficient	θ_8	1.04	None
Organic Nitrogen Mineralization Rate at 20°C	K_9	0.03	Day ⁻¹
Temperature Coefficient	θ_9	1.08	None
Unavailable Phosphorus Mineralization Rate at 20°C	K_{10}	0.03	Day ⁻¹
Temperature Coefficient	θ_{10}	1.08	None
Unavailable Silica Mineralization Rate at 20°C	K_{11}	0.1	Day ⁻¹
Temperature Coefficient	θ_{11}	1.08	None
Half-Saturation Constant for Chlorophyll Limitation	K_{mr}	5.0	µg Chl-a/l

Gross primary production corresponds to the rate at which reaction 1 proceeds, whereas the classical BOD measurement is, in this formulation, the rate of oxygen consumption due to the respiration reaction, reaction 2, and the organic carbon oxidation, reaction 8. Hence, these measurements provide direct calibration data with which the kinetic constants can be estimated. The formulation for the sediment reactions involves a more detailed explanation of sediment mass transport and kinetics and these are presented in the next chapter.

6.9 APPENDIX - MATHEMATICAL DETAILS

6.9.1 Apparent Half-Saturation Constant

The equation which result from solving Equations 14 and 15 and which are presented in Figure 29b are:

$$\frac{K'_s}{K_m} = \kappa = \frac{\sigma}{1 - \sigma} \quad (A1)$$

with:

$$\sigma = \xi \alpha (1 + \alpha) / \beta \quad (A2)$$

$$\alpha = v / (2 + v \xi) \quad (A3)$$

$$v = \frac{1}{2} [\sqrt{1 + 4\beta/\xi} - 1] \quad (A4)$$

Note that:

$$\Delta q_\infty = \xi v \quad (A5)$$

6.9.2 Growth Rate - Substrate Variations

For the cellular equilibrium theory,

$$\mu = \mu'_m \left(1 - \frac{1}{1 + \Delta q}\right) \quad (A6)$$

and

$$\mu_m = \mu'_m \left(1 - \frac{1}{1 + \Delta q_\infty}\right) \quad (A7)$$

with Δq and Δq_∞ given by Equations 14 and 13.

To obtain $\rho = S/(K_m + S)$ in terms of the dimensionless substrate concentration S/K'_s note that

$$\rho = \frac{S/K_m}{1 + S/K_m} = \frac{\kappa S/K'_s}{1 + \kappa S/K'_s}$$

The ratio of Equation (A6) is compared to

$$\frac{\mu}{\mu_m} = \frac{S/K'_s}{1 + S/K'_s} \quad (A8)$$

in Figure 30.

6.9.3 Solution of the Cellular Equilibrium Equations

The dynamic equations for the cellular equilibrium approximation

$$\frac{d}{dt} S_T = (S_i - S_T) / t_o \quad (A9)$$

$$\frac{d}{dt} N = \mu'_m (1 - q_o/q) N - N / t_o \quad (A10)$$

are solved numerically using a simple ruler one-step method. At each evaluation of the derivatives, the value of $q = q(N, S_T)$ is obtained by solving the nonlinear equations for $y = \Delta q$ and S :

$$y(q_o N) + S = S_T - q_o N \quad (A11)$$

$$y \frac{(\xi + y)}{\beta} - S \left(\frac{\xi}{K_m + S} \right) = 0 \quad (A12)$$

using the Newton-Raphson method. For the solution at $t = \text{zero}$, the initial estimates are $S = S_T$ and $y = \Delta q_\infty$. For subsequent evaluations as the solution of the previous time-step is used as the initial estimate in the Newton-Raphson method.

CHAPTER 7

SEDIMENT-WATER INTERACTIONS: MASS TRANSPORT AND KINETICS

The interactions between sediments and lake waters can have profound effects on the concentrations of oxygen and nutrients in a comparatively shallow lake such as Lake Erie since the areal fluxes from the sediment are substantial sources on a volumetric basis. Additionally, the occurrence of anoxia dramatically increases certain of these fluxes. The details of the mechanisms responsible for this increase are as yet unclear but they are related to a set of complex redox reactions that change the state and concentrations of various nutrients and metals thereby releasing bound nutrients. The anoxia itself is, in part, a result of sedimentary processes which result in the exertion of an oxygen demand at the sediment water interface. The importance of these processes and their interrelation to the processes in the overlying water requires that they be analyzed within a framework that is consistent with that discussed in the previous chapters. The analysis is begun by considering the nitrogen components of the calculation since there already exist reasonably well formulated methods for the description of the ammonia distributions in sediments. The application of analogous methods to oxygen and the mechanism of benthic oxygen demand generation requires additional theory and is presented next. The result is a novel approach to the analysis of benthic oxygen demand. The analysis of the fluxes of phosphorus and silica is basically empirical and concludes the discussion.

7.1 NITROGEN

The methods to be employed in this calculation are based on one-dimensional formulations of mass transport and reaction kinetics in the interstitial waters of the sediment. The simplest of these consider the concentration distribution of substances which are either essentially unreactive or, as in the case of radionuclides, have known decay rate (Goldberg and Koide, 1963; Lerman and Taniguchi, 1972). The basis is the one-dimensional mass transport equation for the concentration of a dissolved substance $c(z,t)$:

$$\frac{\partial c}{\partial t} - D \frac{\partial^2 c}{\partial z^2} + w \frac{\partial c}{\partial z} = S \quad (36)$$

where D is the effective diffusion coefficient of the substance, w is the sedimentation velocity induced by sedimentation, relative to a coordinate system fixed with respect to the sediment surface, and S is the net source or sink of the material. The equation is more complicated if porosity variations and compaction are taken into account (Imboden, 1975), but the principle is the same.

Consider the application of this framework to the nitrogen species in a reducing sediment (Berner, 1974). Particulate organic nitrogen is hydrolyzed to ammonia by bacterial action within the sediment. If this reaction is assumed to be first-order with respect to the organic nitrogen concentration, the equations are:

$$\frac{\partial [\text{Org-N}]}{\partial t} + w \frac{\partial [\text{Org-N}]}{\partial z} = -K[\text{Org-N}] \quad (37)$$

$$\frac{\partial [\text{NH}_3]}{\partial t} - D \frac{\partial^2 [\text{NH}_3]}{\partial z^2} + w \frac{\partial [\text{NH}_3]}{\partial z} = K[\text{Org-N}] \quad (38)$$

where $[\text{Org-N}]$ is the concentration of particulate sedimentary organic nitrogen and $[\text{NH}_3]$ is the concentration of ammonia nitrogen in the interstitial water. Note that the sedimentary organic nitrogen does not diffuse since it is part of the sediment solid. The effects of stirring by benthic organism are neglected in this simple analysis. At steady-state, the solutions are:

$$[\text{Org-N}](z) = [\text{Org-N}]_o e^{-Kz/w} \quad (39)$$

$$[\text{NH}_3](z) = [\text{NH}_3]_o + \frac{[\text{Org-N}]_o}{1 + KD/w^2} (1 - e^{-Kz/w}) \quad (40)$$

where $[\text{Org-N}]_o$ and $[\text{NH}_3]_o$ are the concentrations at the sediment surface, $z = 0$. The result of the conversion is an exponential decrease in sedimentary organic nitrogen and a consequent increase in ammonia. In a reducing sediment, ammonia appears to be conservative so there are no other kinetic sources or sinks.

The importance of this result is that ammonia and organic nitrogen measurements provide a method of estimating the parameter groups K/w and KD/w^2 . If the sedimentation velocity is known from other information, the decay rate and effective diffusion coefficient can be estimated.

The outgoing flux of ammonia through the sediment water interface can be calculated directly from Equation (40):

$$J_{\text{NH}_3} = D \frac{\partial [\text{NH}_3]}{\partial z} \Big|_{z=0} = J_{\text{Org-N}} \frac{\eta}{1 + \eta} \quad (41)$$

where $\eta = KD/w^2$ and $J_{\text{Org-N}}$ is the flux of particulate organic nitrogen into the sediment: $J_{\text{Org-N}} = w [\text{Org-N}]_o$. As the dimensionless parameter η increased, the fraction of this incoming flux of particulate nitrogen that is released to the overlying water as an ammonia flux increases. This result is quite interesting since it relates the fraction of the regenerated nitrogen to three parameters: K , D , and w . As the reaction rate for the conversion of particulate sedimentary nitrogen to ammonia increases, more ammonia is generated which tends to increase its flux. A decreased sedimentation velocity increases the residence time of particulate nitrogen in the sediment which increases the time available for regeneration and, therefore, the fraction of the incoming flux that is returned to the overlying water.

In the application to Lake Erie, one layer of sediment is considered. This simplification is introduced in order that the computations are of manageable proportions, and are consistent with the rather crude vertical segmentation of the water column. The choice of the depth of the sediment layer is based on the depth of sediment mixing induced by the benthic organisms (bioturbation). Although this depth varies considerably, it was judged at the time that a depth of 5 cm approximated this depth in the central basin (Robbins, 1977). It was assumed that a similar depth applied to the other basins. More refined computations would involve multiple sediment layers which included both the organism induced mixing and the interstitial water diffusion. This was judged to be beyond the scope of this initial computation of sediment behavior.

For a one-layer sediment, the mass balance equations are considerably simplified. However, the principle is the same. For one-layer of sediment with thickness H , the mass balance equations are:

$$\frac{d[Orga-N]}{dt} = \frac{J_{Org-N}}{H} - \frac{w}{H} [Org-N] - K[Org-N] \quad (42)$$

$$\frac{d[NH_3]}{dt} = -\frac{E'}{H^2} [NH_3] - \frac{w}{H} [NH_3] + K'[Org-N] \quad (43)$$

where E' is the effective exchange rate. It is assumed in these equations that the ammonia concentration in the overlying water is small relative to the interstitial water concentration. The steady-state solutions are:

$$[Org-N] = \frac{J_{Org-N}}{w(1 + \frac{KH}{w})} \quad (44)$$

$$[NH_3] = \frac{[Org-N]}{(\frac{w}{KH} + \frac{E'}{KH^2})} \quad (45)$$

The outgoing flux of ammonia: $J_{NH_3} = E'[NH_3]/H$, becomes:

$$J_{NH_3} = \frac{J_{Org-N}}{(1 + \frac{wH}{E'}) (1 + \frac{w}{KH})} \quad (46)$$

which is a function of the Peclet number: wH/E' , and a dimensionless reaction rate velocity ratio: w/KH . As shown subsequently in Chapter 9, the appropriate values for Lake Erie are $wH/E' = 0.0044$ and $w/KH = 2.9$ so that ~ 25% of the incoming detrital organic nitrogen flux is returned to the overlying water as ammonia.

In addition to the ammonia produced by the hydrolysis of refractory organic nitrogen in the sediment, ammonia is generated by the anaerobic decomposition of algae. In a study of this reaction (Foree and McCarty, 1970), it has been shown that the anaerobic rate of the decay of algae is substantial ($0.007-0.022 \text{ day}^{-1}$). However, the end-product is not exclusively ammonia. Rather, a fraction of the algal nitrogen, f_r , become refractory organic nitrogen. The equations for this and the hydrolysis reaction are:

$$\frac{dc_1}{dt} = \frac{J_1}{H} - \frac{wc_1}{H} - K_1 c_1 \quad (47)$$

$$\frac{dc_2}{dt} = \frac{J_2}{H} - \frac{wc_2}{H} - K_2 c_2 + K_1 f_r c_1 \quad (48)$$

$$\frac{dc_3}{dt} = -\frac{E'}{H^2} c_3 - \frac{w}{h} c_3 + K_2 c_2 + K_1 (1 - f_r) c_1 \quad (49)$$

where $c_1 = [\text{Algal-N}]$, $c_2 = [\text{Refractory Org-N}]$, $c_3 = [NH_3]$, with the subscripts also denoting the appropriate fluxes and reaction rates. The steady-state solutions for the sediment concentration of algal and refractory nitrogen are straightforward:

$$c_1 = \frac{J_1}{w(\frac{K_1 H}{w} + 1)} \quad (50)$$

$$c_2 = \frac{J_2}{w(\frac{K_2 H}{w} + 1)} + \frac{f_r J_1}{w(\frac{K_1 H}{w} + 1)(\frac{w}{K_1 H} + \frac{K_2}{K_1})} \quad (51)$$

The ammonia flux from both these decomposition reactions is:

$$J_3 = \frac{J_2}{\left(1 + \frac{wH}{E'}\right)\left(1 + \frac{w}{K_2H}\right)} + \frac{J_1}{\left(1 + \frac{wH}{E'}\right)\left(1 + \frac{w}{K_1H}\right)} \left(1 - f_r + \frac{f_r}{1 + \frac{w}{K_2H}}\right) \quad (52)$$

It has three parts: that due to the decay of the refractory organic nitrogen; that due to the direct decay of the labile $(1 - f_r)$ algal nitrogen; and that due to the sequential decay of the remaining refractory algal nitrogen, f_r . With the reaction rate appropriate for the algal decomposition, $w/KH_1 = 0.008$, so that nearly all (99%) of the ammonia produced by direct decomposition of the labile algal nitrogen, which is $(1 - f_r)$ fraction of the total algal nitrogen flux, is returned. However, only 25% of the refractory algal fraction is returned to the overlying water.

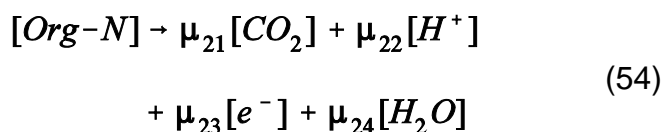
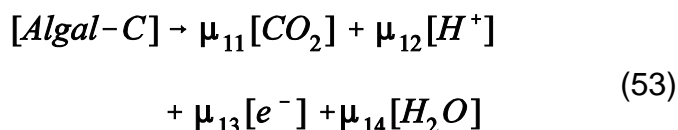
The analysis of the sediment nitrogen concentrations and the resulting flux of ammonia are comparatively straightforward because of the simplicity of the kinetics: hydrolysis and anaerobic algal decay produce a stable end-product, ammonia, which undergoes no further reactions in the anaerobic sediment. This is not the case for the reduced carbon compounds and the other nutrients which are released by the sedimentary decomposition reactions.

7.2 CARBON AND OXYGEN

The reactions which convert algal and refractory carbon to their end-products are more complex. The initial step in which the algal and refractory carbon are converted to reactive intermediates appears to be similar to the refractory organic and algal nitrogen degradation, and in the subsequent calculations, the rates for carbon and nitrogen decomposition are assumed to be equal. However, the reactive intermediates

participate in further reactions: for example, volatile acids react to become methane, and the mechanisms that control these reactions are somewhat uncertain. In addition, few measurements of these intermediate species are available and a calculation which incorporates their concentrations explicitly would of necessity be speculative. Instead, one is led to seek a simplified, yet realistic formulation of these reactions.

The method employed is based on separating the initial reactions that convert sedimentary organic matter into reactive intermediates and the remaining redox reactions that are occurring. The initial decomposition reactions can be expressed as half-reactions in terms of the components chosen for the representation (McCarty, 1971). For example, with CO_2 , H^+ , e^- , and H_2O as the components for carbon, nitrogen, electrons, and water, the half-reactions are:



The half-reaction stoichiometric coefficients μ_{ij} are positive, zero, or negative as appropriate. If the detailed kinetics were being considered, these half-reactions would be combined with the half-reactions of the intermediates to obtain the stoichiometric equation for that reaction.

In the reducing environment of sediments, it is expected that reduced carbon compounds such as volatile acids and methane are the end-products of the reactions. Let $[A_i]$ $i = 1, \dots, N_s$ represent the concentrations of these N_s intermediate and end-product chemical species. Assume that there exists N_r redox reactions

involving these species with stoichiometric coefficients u_{ji} for the i th species in the j th reaction. Let the rate of reaction be R_j . These reactions can be represented as stoichiometric equations:

$$\sum_{i=1}^{N_s} v_{ji} A_i - R_j = 0 \quad j = 1, \dots, N_r \quad (55)$$

occurring at reaction rate R_j . Consider the conservation of mass equations for the interstitial water concentration of these species in a one-dimensional vertical analysis. Let D_i be the diffusion coefficient of species A_i and let w_i be the advective velocity of A_i , as before. For the N_r redox reactions involving the species A_i , the rate at which A_i is produced by reaction j is $u_{ji}R_j$. Let S_i be the net source of A_i due to the sedimentary decomposition reactions, which are not included in the redox reaction set. For this situation, the conservation of mass equations for the concentration of each species, $[A_i]$, is

$$\begin{aligned} \frac{\partial [A_i]}{\partial t} - D_i \frac{\partial^2 [A_i]}{\partial z^2} + w_i \frac{\partial [A_i]}{\partial z} = S_i \\ + \sum_{j=1}^{N_r} v_{ji} R_j \quad j = 1, \dots, N_s \end{aligned} \quad (56)$$

To solve these equations explicitly requires explicit formulations for the sediment kinetics reaction rate expressions, R_j . Since these reactions are quite complex, a complete formulation would be difficult. Instead an alternate method is proposed. The crux of the idea is to eliminate these terms, $\sum_j u_{ji}R_j$, which cause the difficulty and replace Equation (56) with an alternate set of equations. The following fact (Di Toro, 1976) leads to a convenient choice for the transformation: Let B_j , $j = 1, \dots, N_c$ be the names of N_c components and let a_{ij} be the quantity of component B_j in species A_i , i.e., its stoichiometry in terms of the components. The choice of the components of the intermediates is arbitrary but the conventional ones are those

used for the half-reactions of the decomposition reaction, Equations (53) and (54). With the components established, it can be shown (Di Toro, 1976) that, for a set of component conserving reactions, the formula matrix with elements a_{ij} , is orthogonal to the reaction matrix with elements u_{ji} , i.e.:

$$\begin{aligned} \sum_{k=1}^{N_s} v_{jk} a_{ki} = 0 \quad k = 1, \dots, N_c \\ j = 1, \dots, N_r \end{aligned} \quad (57)$$

This fact suggests that the conservative equations be transformed by multiplying Equations (56) by the transpose of the formula matrix yielding:

$$\begin{aligned} \sum_{i=1}^{N_s} \left(\frac{\partial}{\partial t} - D_i \frac{\partial^2}{\partial z^2} + w_i \frac{\partial}{\partial z} \right) a_{ik} [A_i] \\ = \sum_{i=1}^{N_s} a_{ik} S_i + \sum_{j=1}^{N_r} R_j \sum_{i=1}^{N_s} a_{ik} v_{ji} \end{aligned} \quad (58)$$

But the orthogonality relation, Equation (57), implies that the terms involving R_j are zero. This is the fundamental simplification which makes the analysis tractable. The transformed equations are no longer functions of the redox reactions; they are influenced only by the species mass transport coefficients and the decomposition reaction sources, S_i . It is clear from the deviation of the transformed equations that the method is directly applicable to more general equations which consider temporally and spatially variable parameters (Imboden, 1975).

If D_i and w_i are not species dependent, the summations in the left-hand side of the above equation become the component concentrations, $[B_k]$, by the definition of a_{ij} . Therefore, the transformation yields conservation of mass equations for the N_c component concentrations:

$$\frac{\partial [B_k]}{\partial t} - D \frac{\partial^2 [B_k]}{\partial z^2} = w \frac{\partial [B_k]}{\partial z} = \sum_{i=1}^{N_s} a_{ik} S_i \quad (59)$$

$k = 1, \dots, N_c$

The critical and surprising result is that these mass balance equations are independent of the details of the redox reactions and, indeed, of the species concentrations themselves. Rather, they are only functions of the component concentrations. It suffices, however, to compute only the component concentrations which can be treated in exactly the same way as any other variable in the mass transport calculation, without regard to the redox reactions, so long as the mass transport coefficients are independent of the species. This later restriction is admittedly severe since certain species, e.g., methane, can form gas bubbles and would be transported quite differently. Thus, the results using this assumption must be regarded as preliminary.

The convenient choice of components for the calculation are those that parallel the aqueous variables: $[CO_2]$ and $[O_2]$, for the carbon and oxygen components of organic matter. Restricting the calculation to these components eliminated the possibility of explicitly including the effects of other reduced species such as iron, manganese and sulfide which play a role in overall redox reactions and may be involved in the generation of the sediment oxygen demand. In addition, the changes in alkalinity that occur due to component H^+ , are also neglected although marked changes in alkalinity do, in fact, occur. These simplifications appear reasonable in light of the preliminary nature of the sediment calculation.

The decomposition reactions which drive the component mass balance equations are the anaerobic decomposition of the algal carbon, Equation (53), and the anaerobic breakdown of the sedimentary organic carbon, Equation (54), where the stoichiometric equations can now be thought of as being in terms of the components. The substitution for the electron component in

terms of the oxygen component is simply $1/4 O_2 = 1/2 H_2O - H^+ + e^-$. Both reactions are sinks of the component, $[O_2]$, and rapidly drive its concentration negative, indicating that the sediment is reduced rather than oxidized. The negative concentrations achieved can be thought of as the oxygen equivalents of the reduced and products produced by the chains of redox reactions occurring in the sediment. Since the mass balance equation (59) are independent of the actual species concentrations, it is not necessary to calculate the actual distribution among the species. It should be point out that this result is a direct consequence of the species-independent assumption, and a more realistic calculation would require such a determination.

Using the one-layer approximation, the equations for algal and refractory carbon parallel those for nitrogen. The equations for the components are a one-layer version of the mass transport equation (59):

$$\begin{aligned} \frac{d[CO_2]}{dt} = & - \frac{E'}{H^2} [CO_2] - \frac{w}{H} [CO_2] \\ & + \mu_{11} K_1 (1 - f_r) [Algal-C] \\ & + \mu_{21} K_2 [Org-C] \end{aligned} \quad (60)$$

$$\begin{aligned} \frac{d[O_2]}{dt} = & - \frac{E'}{H^2} [O_2] - \frac{w}{H} [O_2] \\ & + \mu_{12} K_1 (1 - f_r) [Algal-C] \\ & + \mu_{22} K_2 [Org-C] \end{aligned} \quad (61)$$

where μ_{11} , μ_{21} are stoichiometric coefficients for $[CO_2]$ in Equations (53) and (54); μ_{12} , μ_{22} are the oxygen stoichiometric coefficients which are one-fourth of the electron stoichiometric coefficients. Again, the steady-state solution is straightforward and the component fluxes are:

$$J_{CO_2} = \frac{\mu_{21} J_{Org-C}}{(1 + \frac{wH}{E'}) (1 + \frac{w}{K_2 H})} + \frac{\mu_{11} J_{Algal-C}}{(1 + \frac{wH}{E'}) (1 + \frac{w}{K_1 H})} (1 - f_r + \frac{f_r}{1 + \frac{w}{K_2 H}}) \quad (62)$$

with exactly the same expression for the flux of the O_2 component with μ_{11} and μ_{21} replaced by μ_{12} and μ_{22} .

The mass balance calculations in the sediment are in terms of the components. Strictly speaking, the mass balance calculations in the water column should also be transformed into component equations, with the species distribution obtained by a separate calculation involving an additional principle such as the requirement that the species be at redox equilibrium. For the carbon and oxygen system, this is exactly what is done. Since the calculated concentration of the oxygen component is positive in the overlying water, it is assumed that the reduced carbon species that are transported across the sediment water interface combine with the available oxygen and are oxidized to CO_2 and H_2O with a consequent reduction of O_2 in the overlying water. No remaining reduced species are assumed to be present so that the resulting O_2 component is equal to the O_2 species concentration if it is positive. If it is negative, the result is interpreted as the oxygen equivalent of the reduced species produced by the redox reactions but no attempt is made to be more specific. In this way, the need for actually calculating the concentrations of the reduced species is eliminated and the carbon and oxygen balance can be calculated in a way that is exactly parallel to the nitrogen balance.

Within this framework the benthic oxygen demand exerted by the sediment is the flux of the O_2 component through the sediment water interface. In terms of the previous equations, the result is:

$$J_{O_2} = a_{O_2C} \left\{ \frac{J_{Orga-C}}{(1 + \frac{wH}{E'}) (1 + \frac{w}{K_2 H})} + \frac{J_{Algal-C}}{(1 + \frac{wH}{e'}) (1 + \frac{w}{K_1 H})} (1 - f_r + \frac{f_r}{1 + \frac{w}{K_2 H}}) \right\} \quad (63)$$

where a_{O_2C} is the oxygen-to-carbon ratio of algal and organic carbon. This expression relates the benthic oxygen demand to the incoming fluxes of algal and detrital carbon. The result is entirely parallel to the ammonia flux and the underlying reason for this parallelism is the assumption that all electron exchanging reactions have species independent transport coefficients. To the extent that this is not the case, e.g., gas bubbles of methane or significant quantities of reduced precipitates forming within the sediment, this equation is in error. It is, however, appealing in its simplicity and utility. A detailed investigation of the applicability of this type of analysis where the assumption of species independent transport is not made is currently underway. For the Lake Erie calculations presented subsequently in this report, the differential equations describing the approximation, Equations (60) and (61), are numerically integrated. As shown subsequently, the results are quite close to the analytical steady-state solutions.

The reaction stoichiometry and rate equations are presented in Table 19. The rate of constant, temperature coefficient, and fraction available for the algal decomposition reaction are obtained from anaerobic decomposition experiments

Table 19. Sediment Reactions

XII. Algal Decomposition

$$[Chl-a] = a_{O_2P} f_A [O_2] \xrightarrow{R_{12}} a_{CP} \{f_A [CO_2] + (1 - f_A) [Org-C]\} a_{NP} \{f_A [NH_4-N] + (1 - f_A) [Org-N]\}$$

XIII. Organic Carbon Decomposition

$$[Org-C] + a_{O_2C} [O_2] \xrightarrow{R_{13}} [CO_2]$$

XIV. Organic Nitrogen Decomposition

$$[Org-N] \xrightarrow{R_{14}} [NH_4-N]$$

XV. Denitrification

$$[NO_3-N] + a_{CN} [Org-C] \xrightarrow{R_{15}} a_{CN} [CO_2] + 1/2 [N_2]$$

Reaction Rate

$$R_{12} = K_{12} \theta_{12}^{T-20} [Chl-a]$$

$$R_{13} = K_{13} \theta_{13}^{T-20} [Org-C]$$

$$R_{14} = K_{14} \theta_{14}^{T-20} [Org-N]$$

$$R_{15} = K_{15} \theta_{15}^{T-20} [NO_3-N]$$

Table 19. Sediment Reactions (Continued)

Reaction Rate Constants

Description	Notation	Value	Units
Anaerobic Algal Decomposition	K_{12}	0.02	Day ⁻¹
Temperature Coefficient	θ_{12}	1.08	-
Fraction Available	f_A	0.7	-
Organic Carbon Decomposition	K_{13}	.00025	Day ⁻¹
Temperature Coefficient	θ_{13}	1.08	-
Organic Nitrogen Decomposition	K_{14}	.00025	Day ⁻¹
Temperature Coefficient	θ_{14}	1.08	-
Denitrification Rate	K_{15}	0.1	Day ⁻¹
Temperature Coefficient	θ_{15}	1.045	-
Deep Sediment O ₂ Flux	J_{O_2} Deep	550	mg O ₂ m ⁻² /day ⁻¹
Temperature Coefficient	θ_{O_2} Deep	1.08	-

(Foree and McCarty, 1970). The organic decomposition rates are obtained from the calibration as discussed in Chapter 9.

The results of the dissolved oxygen and sediment calibrations indicate that the sediment oxygen demand generated by the decomposition in the surface layer is insufficient. This is not unexpected since the active depth in sediments is usually considerably more than 5 cm (Robbins, 1977). To remedy this defect, an additional flux of oxygen equivalent to the deep sediment demand is introduced into the bottom of the sediment segments. It represents the flux of reduced carbon from the deep sediment into

the shallow sediment segments. Its magnitude is estimated from the calibration as described in Chapter 9.

7.3 PHOSPHORUS AND SILICA

The success of the above calculation depends directly on the degree to which species independent transport is a realistic approximation. If the majority of species being considered remain dissolved in the interstitial water of the sediment, then the above analysis is reasonable. For phosphorus and silica, it is well known (Nriagu, 1972, 1976) that the formation of

precipitates affects the interstitial water concentrations and, therefore, the species independent transport assumption is not valid. Further, the dissolved concentrations are also affected by redox reactions which, in turn, affect the nutrient fluxes that occur during aerobic and anaerobic conditions. Hence, a complete analysis of the phosphorus and silica fluxes requires a rather elaborate computation of the solution-precipitate chemistry and its interaction with the mass transport of the dissolved species. Such a calculation was judged to be outside the scope of this project. Instead, an empirical approach is adopted. Observed interstitial water concentrations of phosphorus and silica are used rather than those which are calculated from the integration of the mass balance equations. During aerobic conditions, the diffusive exchange of phosphorus and silica is assumed not to occur and E' for these constituents is set to zero. During anaerobic conditions, the diffusive exchange is set to the same value used for ammonia, carbon, and oxygen. The flux of

phosphorus and silica is due to the exchange between the overlying water and the observed interstitial concentrations of phosphorus and silica. However, since the area of anoxia is not equal to the entire area of the sediment-water interface, the flux is assumed to be proportional to the ratio of the anoxic area to the total area of the interface. The computation of the anoxic area is based on the segment dissolved oxygen concentration and is discussed in Chapter 9.

This approach, while not wholly satisfactory, is at least consistent with the framework within which the fluxes of the other materials are being generated. What is being assumed is that under aerobic conditions, the fluxes of phosphorus and silica are small relative to all other sources, whereas under anaerobic conditions the prevailing concentrations in the sediment interstitial water exchange freely with the overlying water.

CHAPTER 8

MASS TRANSPORT CALIBRATION

A realistic representation of the mass transport mechanisms is a basic requirement for an analysis based on conservation of mass. For a finite difference formulation, the transport between the homogeneous segments is required. The transport mechanisms are of two types: the unidirectional net motion of the water between segments which is termed the advection; and the turbulent mixing and circulations due to velocity and density gradients between segments which is termed the dispersion.

Ideally, the transport regime ought to be the result of a hydrodynamic analysis. However, the relevant calculations have not yet been made and, although models of large lake circulation exist, a number of uncertainties including their level of verification at seasonal time scales preclude a completely hydrodynamic analysis. The results of circulation measurements and calculations are combined with an analysis of inert tracers and temperatures in order to estimate the exchange coefficients between segments. Their values are chosen to be consistent with known details of the circulation patterns and the observed concentrations of the tracers.

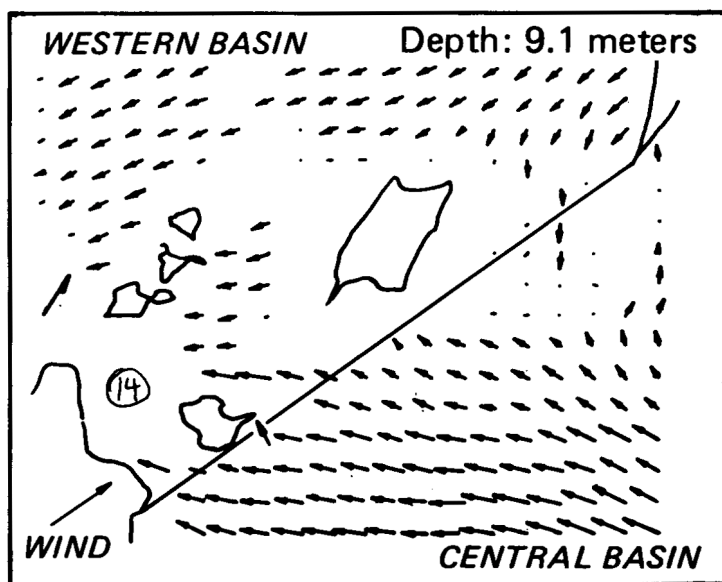
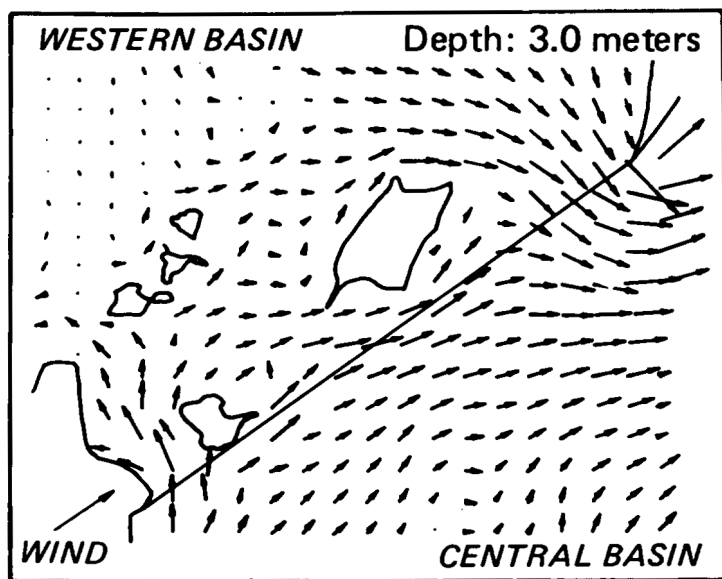
8.1 HYDRODYNAMIC CIRCULATION

A number of studies which include both measurements and calculations of Lake Erie currents are available which set the framework for the specification of transport patterns in Lake Erie (Gedney, 1971; Hamblin, 1971). Unfortunately, the time and space scales of

these results tend to be smaller than the seasonal and basin-wide scales that are appropriate to this analysis. Thus, these results must be supplemented with calibrations based on the seasonal distribution of basin-wide averaged concentrations of tracer constituents. Nevertheless, the hydrodynamic studies can be used to set the order of magnitude of the transport coefficients.

The horizontal wind-driven circulation of the lake dominates the interbasin exchange and an analysis of these velocity fields provides the first estimates of these exchange coefficients. Consider the calculated current patterns (Gedney, 1971) across the boundary of the western and central basins shown in Figure 33 for a wind direction of W67S and a magnitude of 5.2 m/sec based on the prevailing direction and magnitude for Lake Erie winds (Burns and Ross, 1972). Flow is either from the western basin to the central basin or vice-versa. For each direction, the component of the velocity normal to the boundary is estimated at each depth for which current velocities are reported: 0.4, 1.5, 3.0, 4.5, 6.0, 7.6 and 9.1 meters. The velocities are weighted according to the percentage of the total depth they represent and are averaged to produce the average normal velocities which exchange flow across this boundary. The result is a bi-directional velocity of 3.05 cm/sec. The range over the depths is 1.4 to 4.7 cm/sec. For the purpose of comparison, the unidirectional advective component of velocity due to the Detroit River is 3.7 cm/sec. Thus, the circulating and advective velocities are of the same order of magnitude.

Wind direction: W67S Wind magnitude: 5.2 m/sec



Miles 0 5 10

Km 0 7.5 15

Distance

0 1 ft/sec

0 20 cm/sec

Current magnitude

Figure 33. Calculated current patterns across the boundary of the western and central basins based on the prevailing direction and magnitude of Lake Erie winds (direction of W67S and magnitude of 5.2 m/sec) at a depth of 3 meters (top) and 9.1 meters (bottom).

By comparison, the horizontal dispersion to be expected across the boundary is an order of magnitude less. Consider the empirical formula for oceanic diffusion (Okubo, 1971), expressed as an exchanging velocity:

$$V_{ex} = 0.0103 l^{0.15}$$

for $V_{ex} = E/l$ in cm/sec and l in cm. For a length scale on the order of the midpoints of the western and central basins, $l \approx 1.6 \cdot 10^7$ cm and $V_{ex} \approx 0.12$ cm/sec. Thus, the principle mechanisms of mass transport across the western-central basin interface are due to the unidirectional advective velocity and the bi-directional circulating velocities induced by the wind shear and modified by the Coriolis force and lake geometry.

In order to proceed with a purely hydrodynamic analysis, it would be necessary to first verify that the circulation model employed indeed reproduces the observed circulation magnitude and direction. Then, a simulation of the seasonal circulation using observed wind patterns would be undertaken. The exchanging flows could then be extracted from these results. Lacking such a calculation, a more empirical approach has been adopted which employs the observed distribution of tracers.

8.2 HEAT BALANCE

The temperature distribution in Lake Erie is the result of the interaction between the heat fluxes to the lake and the circulation. If the former were known, then the latter could be estimated by fitting the observed temperature distribution to that calculated for a variety of horizontal exchanging velocities and vertical dispersion coefficients. The advantage of such a procedure is that it is at the proper temporal and spatial scales since a seasonal computation using the appropriate segmentation is compared to the appropriately averaged concentrations. Hence, the resulting exchanging velocities and vertical dispersion coefficients are directly applicable to other dissolved constituents.

Heat balance calculations can be attempted from first principles with the exogenous sources specified from other measurements and the within-lake sinks parameterized as a function of air and water temperature, and relative humidity (Edinger and Geyer, 1968). Such a procedure is a reasonably large undertaking. Instead, a more direct estimation method has been developed (Di Toro and Matystik, 1979). The idea is to calculate the net heat flux to the entire lake using the observed temperatures directly. The observed heat change between cruises for each segment is computed from the equation:

$$\Delta H_i = V_i (T_{ik} - T_{ij}) \rho C_p \quad (64)$$

where

- ΔH_i = the change in heat content for segment i (calories)
- V_i = the volume of segment i (cm³)
- T_{ik} = the volume average temperature of segment i for cruise k (°C)
- T_{ij} = the volume average temperature of segment i for cruise j (°C)
- ρ = the density of water (gm/cm³)
- C_p = the specific heat of water (cal/gm-°C)

The segment heat changes are summed to yield the total lake heat change:

$$\Delta H_T = \sum_{i=1}^n \Delta H_i \quad (65)$$

The net average daily flux between cruises is then:

$$J_T = \frac{\Delta H_T}{A_s (t_k - t_j)} \quad (66)$$

where

- J_T = the areal heat flux (cal/cm²-day)
- A_s = the lake surface area (cm²)

t_k = the Julian date of cruise k
 t_j = the Julian date of cruise j

The result of the calculation is shown in Figure 34 for both 1970 and 1975. The net heat flux to the lake in 1975 is lower than 1970 which is reflected in a smaller epilimnion depth for that year, as shown subsequently. The dashed lines represent estimates of the net heat flux during the winter period and are not meant to be definitive.

The lake-wide average net heat flux is not uniformly applicable to the entire lake surface. Although it seems a reasonable assumption that the incoming heat flux is uniform, the outgoing fluxes are not. To see this, consider the simplified expression for total heat flux into segment i , J_i , based on a heat transfer coefficient, K , and an equilibrium temperature, E :

$$J_i = -K(T_{si} - E) \quad (67)$$

where T_{si} is the surface temperature of the i th and segment (Edinger and Geyer, 1968). The heat transfer coefficient and the equilibrium temperature are independent of basin characteristics, depending only on meteorological conditions. Therefore, it appears reasonable to assume that they are constant lake-wide. The surface temperature, however, varies from basin-to-basin. But this variation is known from observations. Hence, it is possible to calculate the net heat flux to each basin. In particular, applying Equation (67) to the entire surface area of the lake yields:

$$J_T = \frac{1}{A_s} \sum_i J_i A_{si} = -K(\bar{T} - E) \quad (68)$$

where:

$$\bar{T} = \frac{1}{A_s} \sum_i T_{si} A_{si} \quad (69)$$

the areal surface average temperature. And substituting Equation (68) into Equation (67) yields:

$$J_i = J_T - K(T_{si} - \bar{T}) \quad (70)$$

so that the surface temperatures can be used to calculate the net heat flux into each basin provided that the heat transfer coefficient is known. It is, in principle, possible to compute the heat transfer coefficient from meteorological data. However, there are substantial uncertainties in such a procedure. In particular, the expression used for evaporation is open to question and the lack of actual over-lake meteorological observations make such a calculation speculative. For these reasons, it was judged that a constant value was sufficient. For Lake Huron, this coefficient is estimated to be 50-65 cal/cm²/day (Rodgers, 1965). A value of $K/\rho C_p = 2$ ft/day (0.67 m/day) corresponding to 61 cal/cm²/day is chosen for the analysis. The results are listed in Table 20. These fluxes provide the forcing functions for the heat balance calculation.

The conservation equation for the segment average temperature T_i is:

$$V_i \frac{dT_i}{dt} = \sum_k E_{ki} (T_k - T_i) + \sum_k Q_{ki} T_k + A_{si} J_i \quad (71)$$

where V_i is the segment volume, E_{ki} is the exchanging flow and Q_{ki} is the advective flow between segment k and i . The integration of this equation for all segment yields the calculated segment temperatures. The method is applied to both 1970 and 1975. The two years differed not only in net heat flux but also in the depth at which the thermocline formed. Since the logical place for the segment boundary between the epilimnion and hypolimnion is within the thermocline, the volume of the central basin

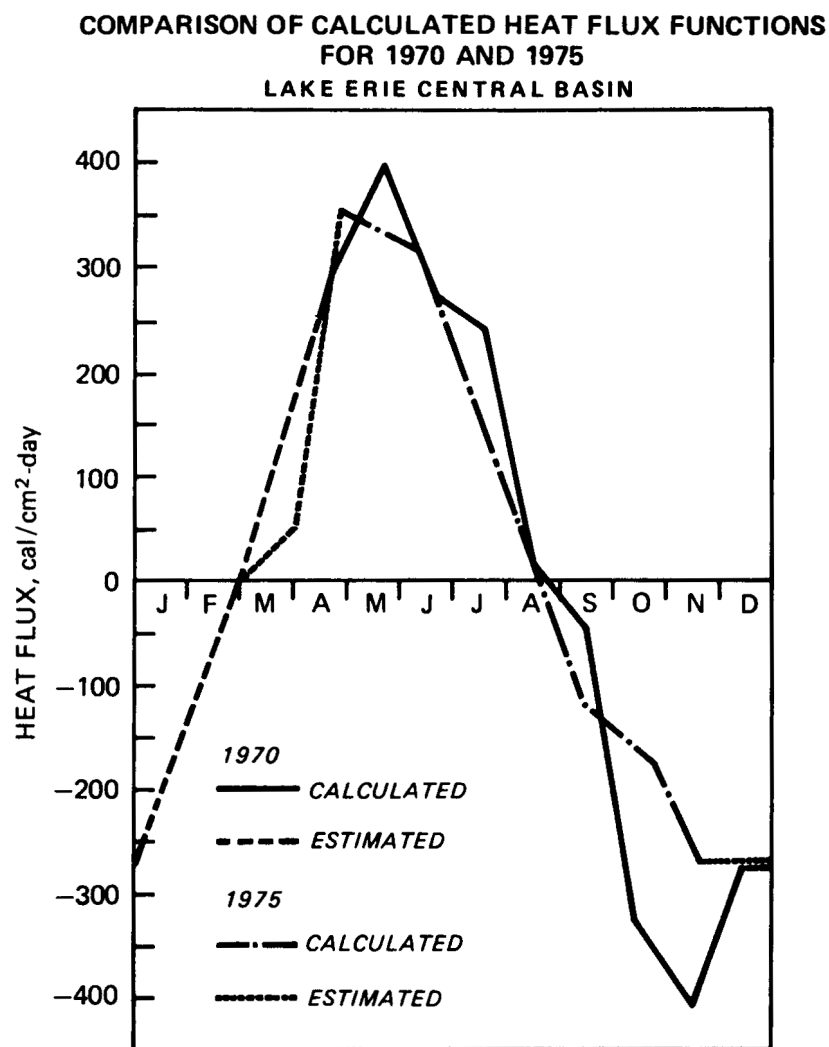


Figure 34. Calculated heat flux (cal/cm²-day) to the central basin using observed temperatures for each cruise. During the winter period, the net heat flux shown is estimated.

Table 20. Heat Flux and Surface Temperatures

Time (Days)	Lakewide Average		Segment 1		Segment 2		Segment 3	
	Surface Temp.	Heat Flux (cm ² -day)	Surface Temp.	Heat Flux (cm ² -day)	Surface Temp.	Heat Flux (cm ² -day)	Surface Temp.	Heat Flux (cm ² -day)
<u>1970</u>								
115	5.05	315.12	8.28	112.12	5.15	302.93	2.88	441.31
143	11.24	409.81	15.06	173.89	11.31	402.49	9.06	539.65
171	17.15	275.03	19.72	118.36	17.17	273.81	15.86	353.67
198	21.71	248.78	22.84	179.90	21.79	243.90	21.02	290.84
225	23.55	17.60	24.37	-32.39	23.61	13.94	23.03	49.30
254	22.07	-36.43	22.65	-71.79	22.23	-46.18	21.44	1.97
282	17.69	-309.07	16.98	-265.79	17.95	-324.92	17.49	-296.88
314	10.78	-393.07	8.59	-259.57	11.07	-410.75	11.22	-419.89
341	5.62	-262.37	2.62	-76.44	5.87	-274.56	6.62	-320.28
<u>1975</u>								
117	6.22	366.16	7.53	286.30	6.34	358.84	5.31	421.64
158	16.16	320.98	17.82	219.48	16.17	320.09	15.33	371.28
199	22.08	122.88	23.11	60.39	21.90	133.88	22.05	124.71
251	19.17	-114.29	19.24	-121.56	19.18	-114.90	19.10	-110.32
292	14.16	-161.21	13.35	-111.86	14.38	-174.62	13.99	-150.54
317	10.83	-259.47	9.34	-168.66	11.00	-269.83	11.12	-277.15

Dates and temperatures are the arithmetic average between consecutive cruises.

segments are adjusted to reflect this fact. The data used to establish these locations are shown in Figure 35. The average temperatures in two-meter sections of the central basin are shown for the cruise dates as indicated. While 17 m is the appropriate depth of the epilimnion in 1970, a shallower thermocline formed at 13 m in 1975.

The comparison between the calculated and observed temperatures for 1970 are shown in Figure 36. Included in the calculation are also the computed and observed chloride distributions as shown in Figure 37. The mass input rates of chloride are based on the USACOE's work discussed previously. They are listed in Table A-9 of the Appendix. The transport coefficients corresponding to this calculation are shown in Figure 38. Between the western basin and central basin epilimnion, the circulating flow is equivalent to a velocity of 2.72 cm/sec. A velocity of 3.46 cm/sec is used between the central and eastern basin

epilimnions. These velocities are comparable to the current magnitudes based on hydrodynamic calculations as indicated previously.

The vertical exchange is based on the unstratified diffusion coefficient range reported by Csanady (1964). Unstratified exchange between the central basin epilimnion and hypolimnion is set at 1 cm²/sec. During stratification, the dispersion is reduced to 0.05 cm²/sec. Between the main body of the hypolimnion and the lower hypolimnion layer (segments 5 and 6), the rate is kept constant at 1 cm²/sec. In the eastern basin, the dispersion reaches a maximum stratification. These parameters are also shown in Figure 38 for 1970.

For the estimate of the 1975 transport, the horizontal exchanges are assumed to be the same as for 1970. However, the vertical exchanges resulting from the calibration differ

CALIBRATION AND VERIFICATION YEAR TEMPERATURE PROFILES USED FOR THERMOCLINE DEPTH SPECIFICATION

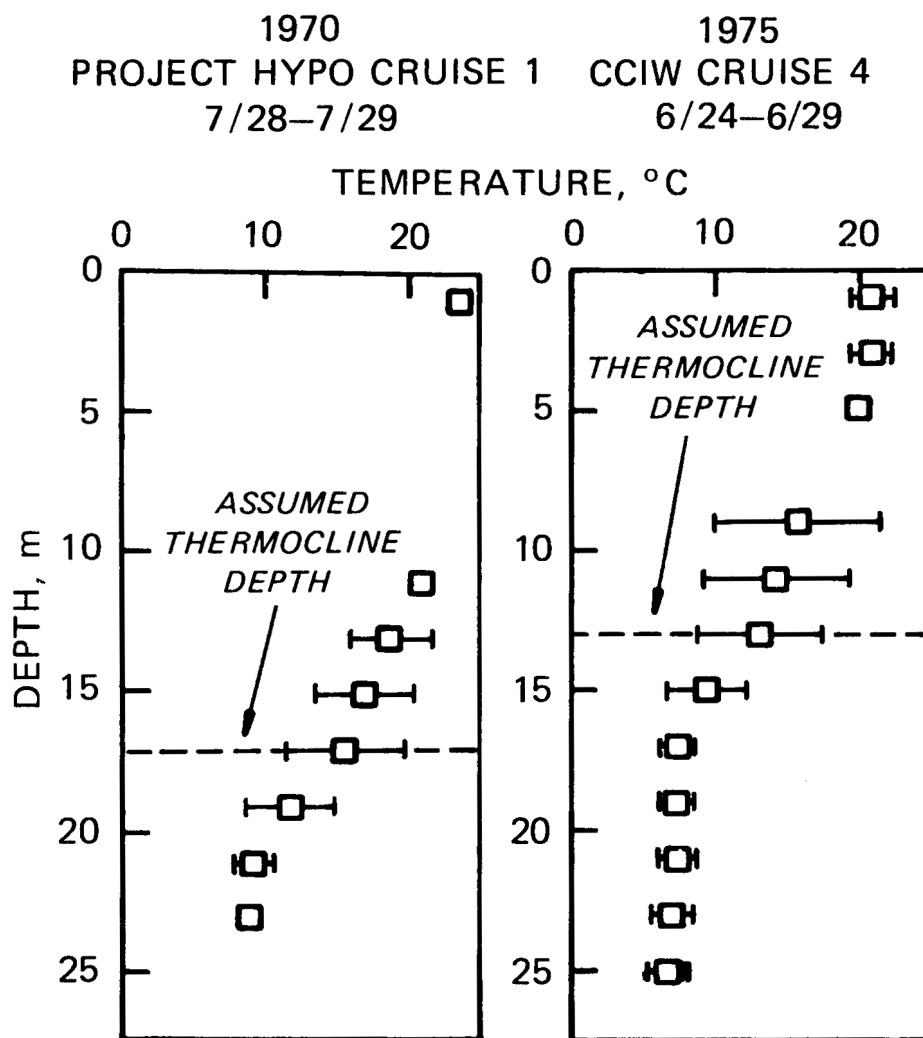


Figure 35. Average temperatures (°C) in two-meter sections of the central basin for 1970, Project Hypo Cruise 1 (left) and 1975, CCIW Cruise 4 (right). This data was used to establish location of the thermocline for each year.

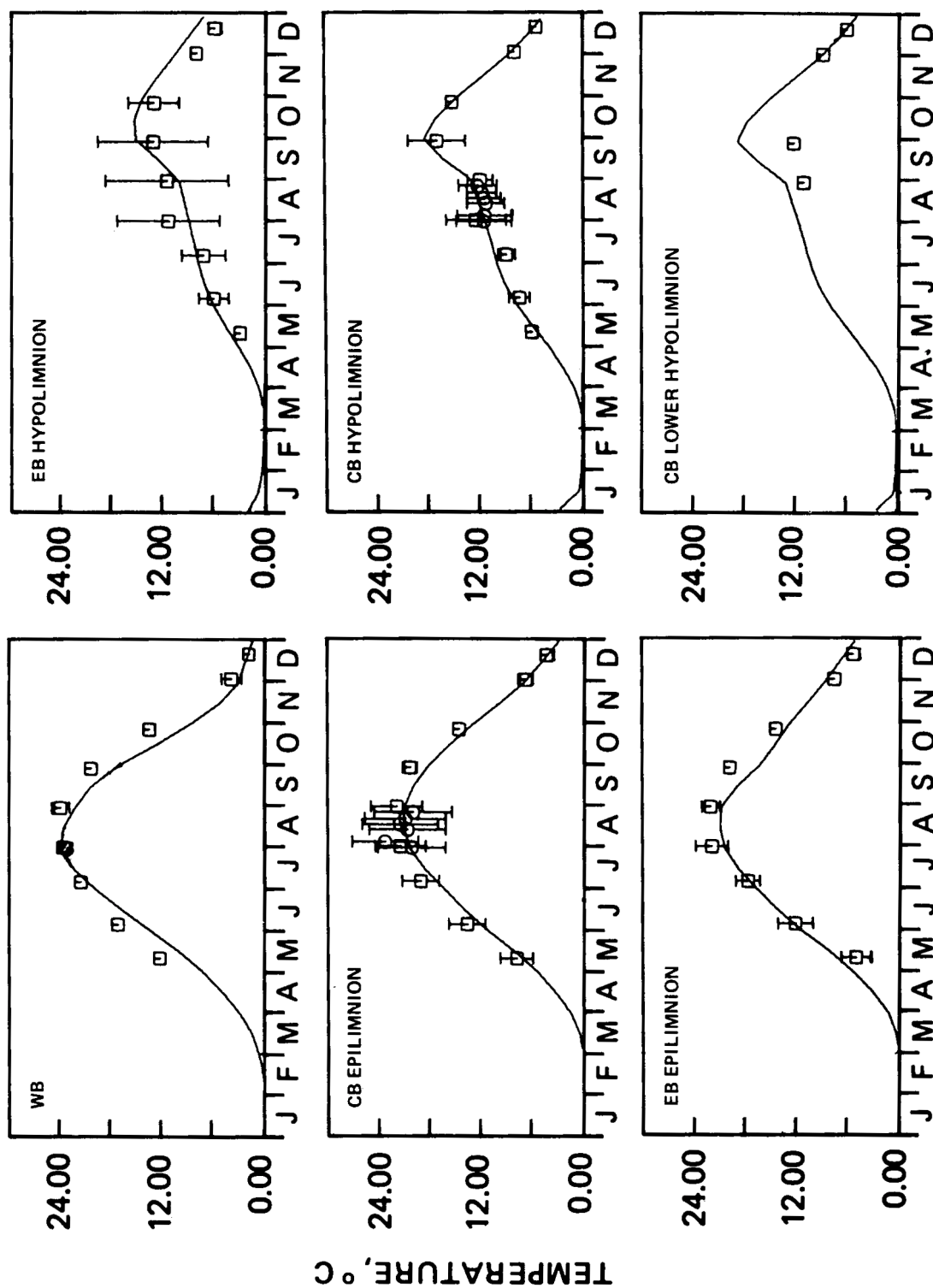


Figure 36. Lake Erie model transport calibration, 1970: Temperature. The calculated profiles are a result of the transport coefficients given in Figure 38. Symbols: Mean \pm standard deviation; lines are the computation.

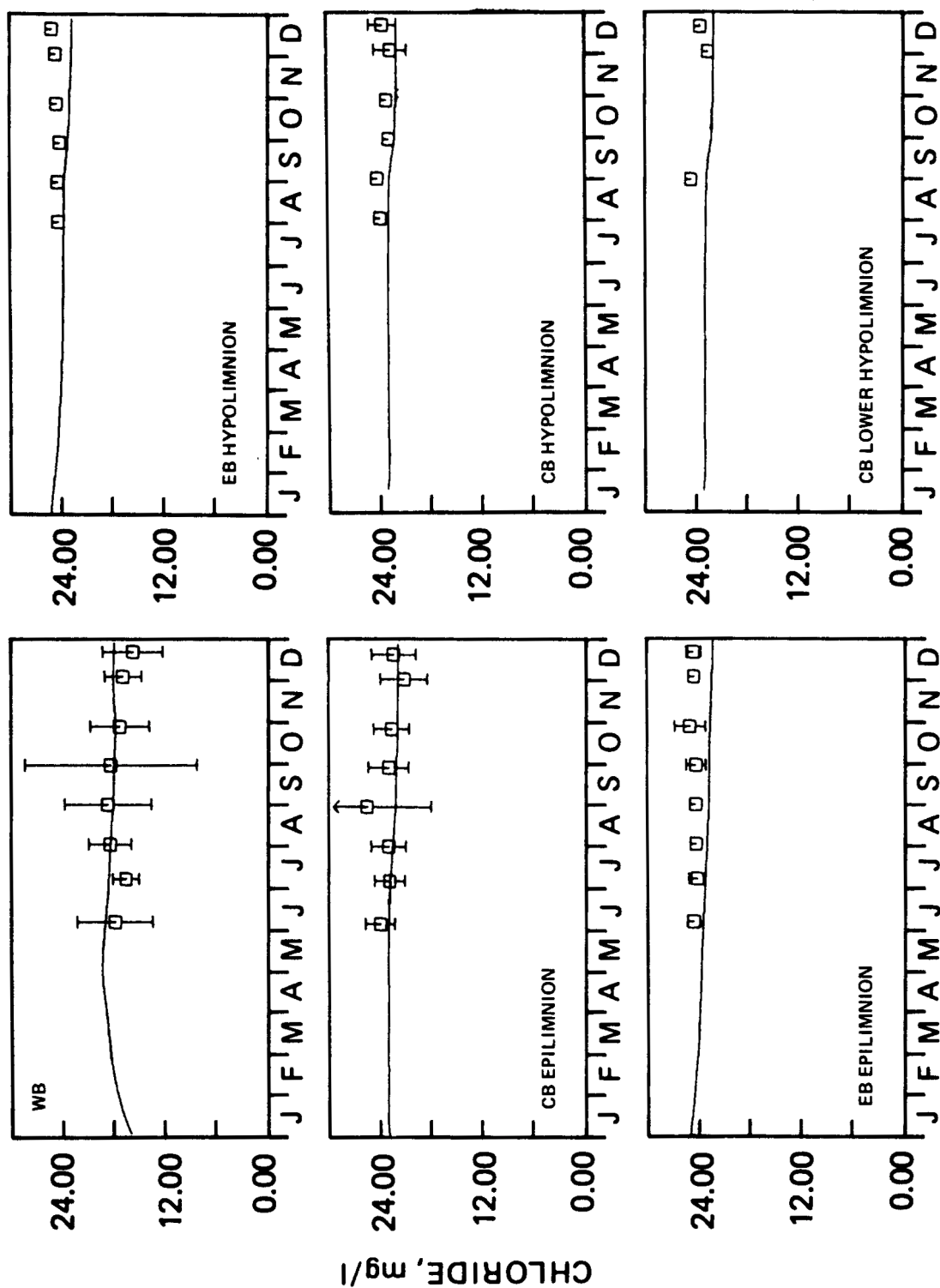


Figure 37. Lake Erie model transport calibration, 1970: Chlorides. Mass input rates of chlorides to the lake are included in the calculation.

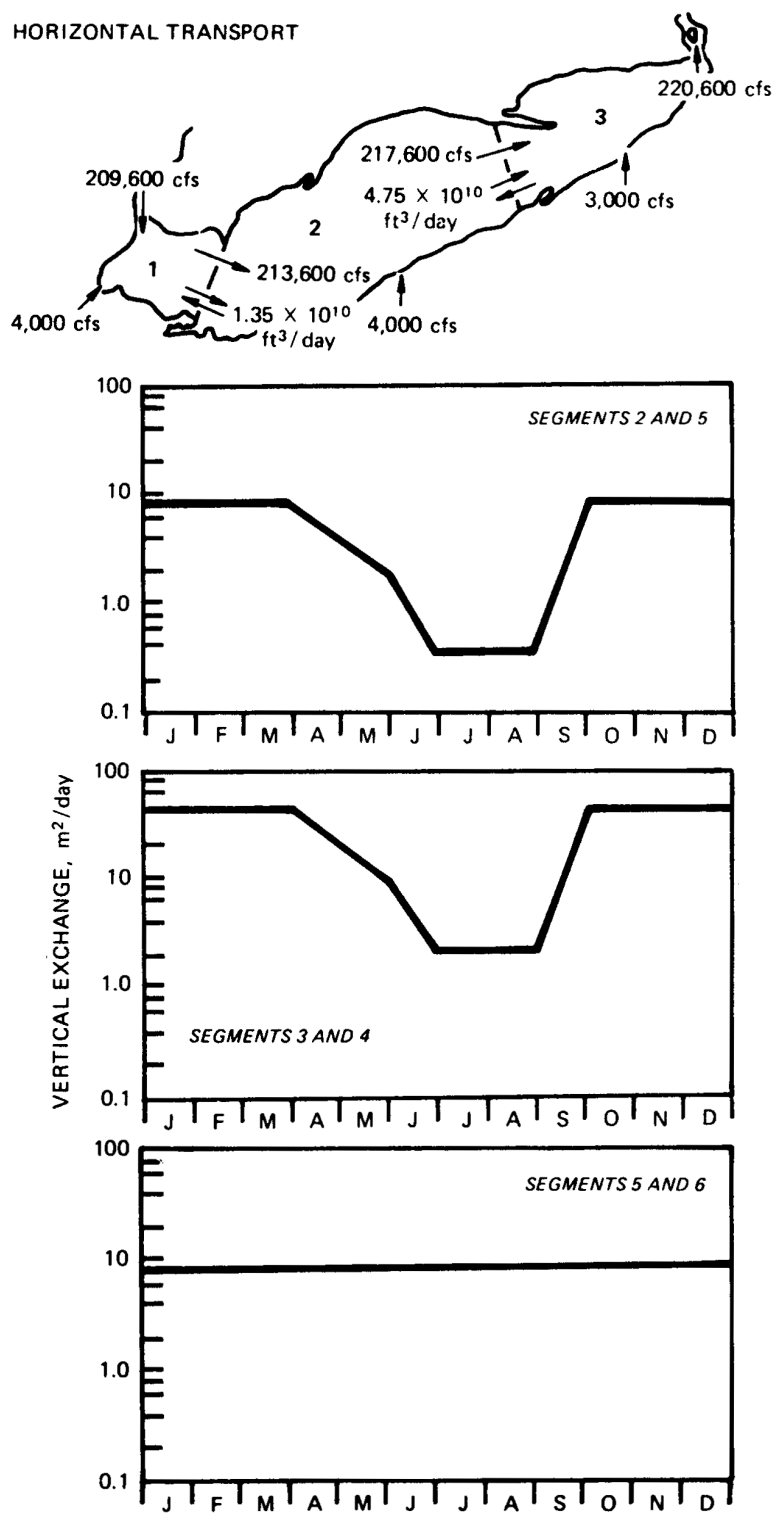


Figure 38. 1970 model transport regime. Horizontal transport and vertical exchanges (m²/day) resulting from the calibration.

from 1970, probably as a result of the differing wind speeds. Between the central basin epilimnion and hypolimnion, the unstratified dispersion is estimated to be $2 \text{ cm}^2/\text{sec}$ reducing to $0.1 \text{ cm}^2/\text{sec}$ during stratification. For the eastern basin, dispersion is lower than for 1970, $1.5 \text{ cm}^2/\text{sec}$ during unstratified period and $0.1 \text{ cm}^2/\text{sec}$ during stratification, during the entire year. In addition, the stratification started earlier in the year as evidenced by the significantly lower vertical dispersion coefficient during April and May. The results of the calculation are

shown in Figure 39 for the transport regime shown in Figure 40.

The transport regimes estimated using this methodology are applied to the calculations of dissolved constituents in the next chapter. The only modification is the addition of a sinking velocity for the particulates, which cannot be estimated from the dissolved tracers examined in this chapter.

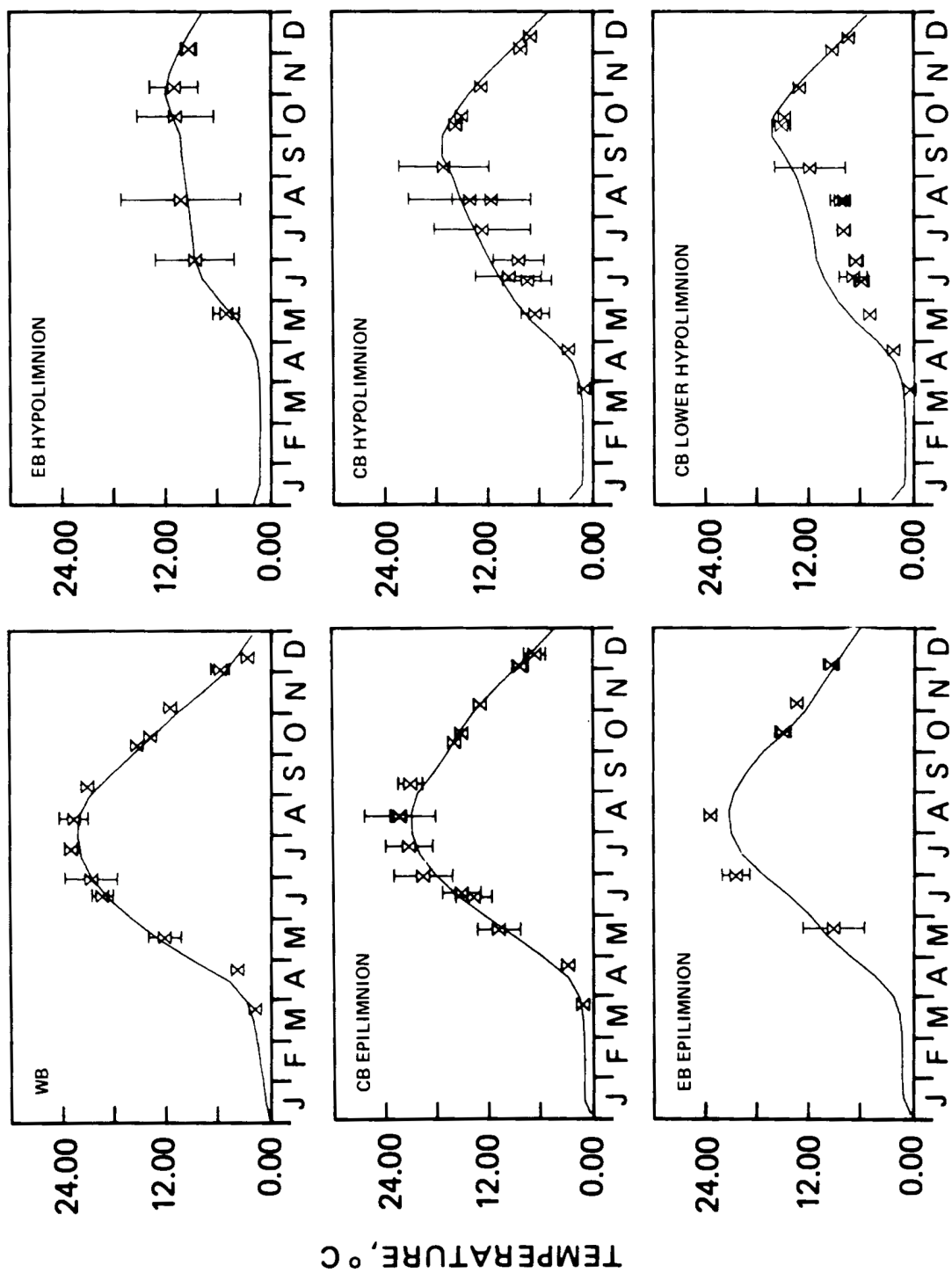


Figure 39. Lake Erie model transport calibration, 1975: Temperature. The calculated profiles use the transport coefficients given in Figure 40.

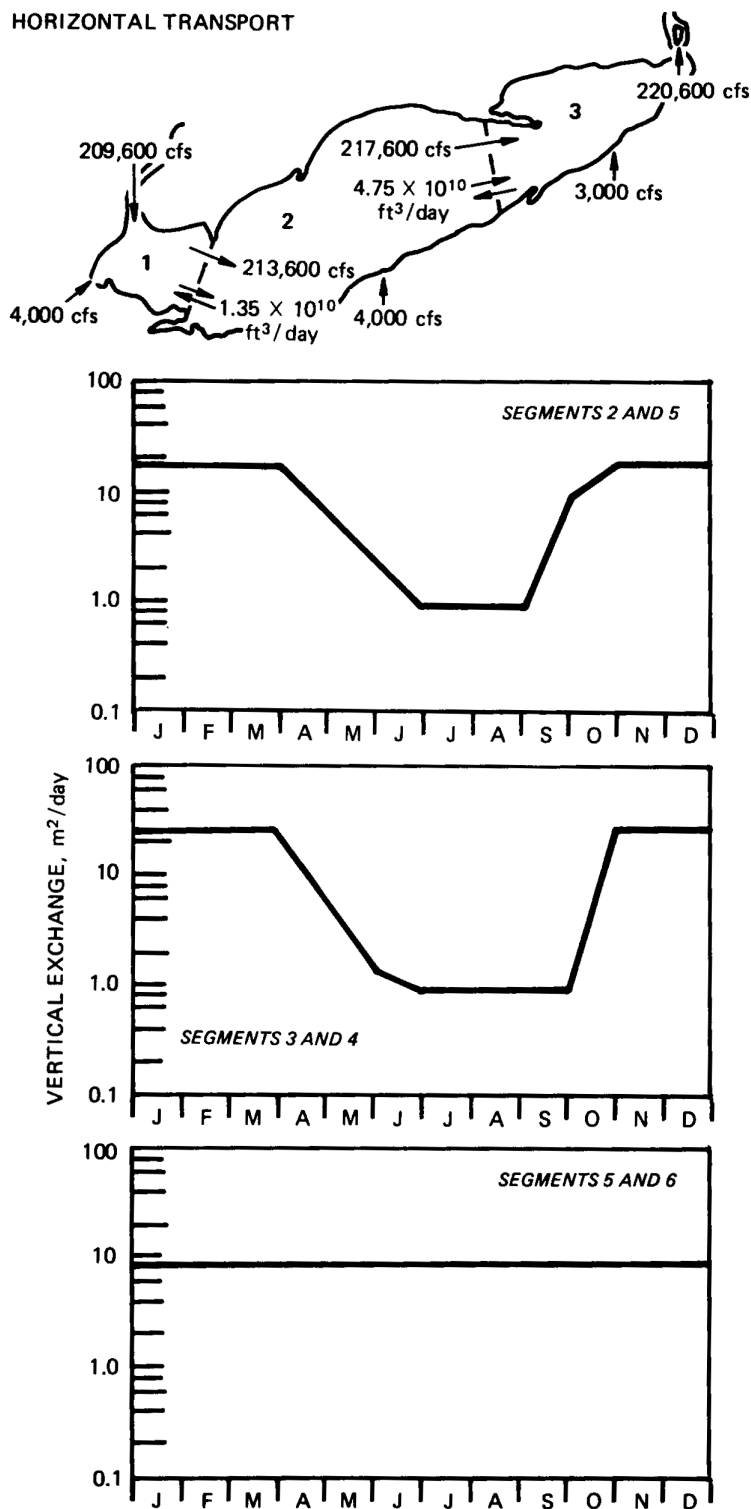


Figure 40. 1975 model transport regime. Horizontal transport are assumed to be the same as for 1970 while vertical exchanges differ as shown.

CHAPTER 9

STRUCTURE AND COMPUTATIONAL DETAILS

The detailed discussion of the previous chapters present the background and framework adopted for the kinetics and transport mechanisms being considered in this calculation. In this chapter, the overall structure is presented together with the details of the implementation. A discussion of the rationales which lead to the final choices are included in order to record the motivations involved and the assumptions and compromises that were necessary. The computational details are also discussed.

9.1 ONE-GROUP AND TWO-GROUP PHYTOPLANKTON KINETICS

The initial structure adopted for the Lake Erie kinetics followed the kinetic framework used for Lake Ontario (Thomann *et al.*, 1975) and Lake Huron/Saginaw Bay (Di Toro and Matystik, 1979). For these lakes, the phytoplankton are represented by a single chlorophyll concentration without regard to differing algal groups. However, this structure was not satisfactory for Lake Erie, especially in the central basin. The data display less evidence of the spring phytoplankton bloom characteristic of the other Great Lakes investigated. The Ontario-Huron kinetic structure consistently predicts a larger-than-observed spring chlorophyll bloom if the growth kinetic coefficients are kept within reported ranges. Hence, this kinetic structure was judged to be inadequate and it was necessary to re-evaluate the kinetics by examining the peculiar characteristics of Lake Erie in an effort to determine the cause of the failure.

The reactive silica distribution in the central and eastern basins of the lake reveal severe depletion in late spring. For 1970, the average epilimnion reactive silica concentrations in the central basin during the April and May CCIW cruises are 0.027 and 0.029 mg SiO₂/l, respectively. In the eastern basin, the values are 0.04 and 0.021, respectively. Typical half-saturation constants for SiO₂ range from 0.06 to 0.24 mg SiO₂/l (see Table 9). With Michaelis-Menten growth kinetics and the smallest reported half-saturation constant, the result is approximately a 75% growth rate reduction for silica dependent diatoms. Lake Erie phytoplankton biomass and species composition in 1970 (Munawar and Munawar, 1976) indicates that the diatoms predominate in the early spring comprising about 90% of the total crop by volume but by June have declined to 10% of the crop. During this same period, the total biomass decreases by greater than a factor of two. These facts indicate that the lack of a spring phytoplankton chlorophyll peak is due to a silica limitation of diatoms. Therefore, to properly account for the observed total chlorophyll distribution, it is necessary to separate the chlorophyll into that portion associated with diatoms and that associated with other phytoplankton. This is accomplished by including two chlorophyll concentrations in the calculation, one for the diatoms and one for the non-diatom algae. The relative concentrations of each chlorophyll type are calibrated by assigning chlorophyll-to-biomass ratios to the diatom and non-diatom chlorophyll and checking the percent diatom biomass against observed data (Munawar and Munawar, 1976). The chlorophyll

a-to-biomass ratios, obtained from linear regressions of chlorophyll versus diatom and non-diatom biomass using 1970 data are 1.24 and 2.32 $\mu\text{g Chl-a/mg dry wt}$ for diatoms and non-diatoms, respectively. The necessity of using different chlorophyll a-to-biomass ratios for diatoms and other groups has been demonstrated in Saginaw Bay as well (Dolan *et al.*, 1977).

The comparison of the one-group and two-group phytoplankton calculation, the latter including unavailable and available silica as well is given in Figure 41. For the western basin, the use of two phytoplankton groups does not materially improve the calibration. An examination of the reactive silica data, Figure 24, shows that this result is not unexpected. Silica limitation does not play an important role in this basin. An earlier investigation of the western basin confirmed this result (Di Toro *et al.*, 1975). In the central basin, the use of a two-group model has a dramatic effect on the results. Whereas, the one-group kinetics predicts a large spring bloom which does not appear in the data, the use of the two-group kinetics eliminates this bloom and, in fact, follows the spring chlorophyll data rather well. Silica limitation of the diatoms prevents the bloom from occurring. However, the fall bloom is simulated equally well by both calculations. The two-group kinetics provides no advantage here because silica does not have a significant effect in growth limitation during this period.

9.2 DETERMINATION OF ANOXIA

The determination of the areal extent of anoxia in the central basin is an important component of the calculation. The anoxic area controls the fraction of the sediment surface from which nutrients are regenerated into the water column. However, the horizontal and vertical spatial scale of the calculation is such that a direct computation of the anoxic area is not possible. A segment is either entirely oxic or anoxic. In Lake Erie, anoxia begins in a small area and increases until overturn. An empirical method

has been developed in order to simulate this effect.

Figure 42 is a plot of the cruise average dissolved oxygen for segment 5 and segment 6 of the central basin hypolimnion segments versus the minimum dissolved oxygen observed during that cruise. For segment 5, when the segment average dissolved oxygen is approximately 4 mg/l, the minimum observed dissolved oxygen in that segment reaches zero. For segment 6 at a segment average of 2 mg/l, the segment minimum reaches zero. The interpretation of these results is that as the average dissolved oxygen of segment 5 reaches 4 mg/l or as segment 6 reaches 2 mg/l, there will be an anoxic region somewhere within that segment volume.

In order to calculate the fraction of the segment which is anoxic, plots of cruise average dissolved oxygen versus the fraction of stations anoxic for that cruise for both segments 5 and 6 are constructed and shown in Figure 43. An anoxic station occurs if the observed dissolved oxygen at one meter from the bottom is less than 0.50 mg/l. From these plots, it is inferred that, to a reasonable approximation, the fractions of anoxic stations which is assumed to be equivalent to the fraction of the anoxic area increases linearly with decreasing mean dissolved oxygen. For segment 5 at a mean of 4 mg/l, anoxia is just beginning while at a segment average of 0 mg/l, 100% of the segment is anoxic. The regeneration of phosphorus and silica is calculated based on these plots as discussed subsequently.

9.3 EXOGENOUS VARIABLES

The water temperature, incident solar radiation, and photoperiod are specified externally. The extinction coefficient for each basin is computed using an observed correlation between the non-algal associated extinction coefficient and the wind velocity. The observed Secchi disk depth, SD, is converted to an extinction coefficient, K_e , using the relationship (Beeton, 1958):

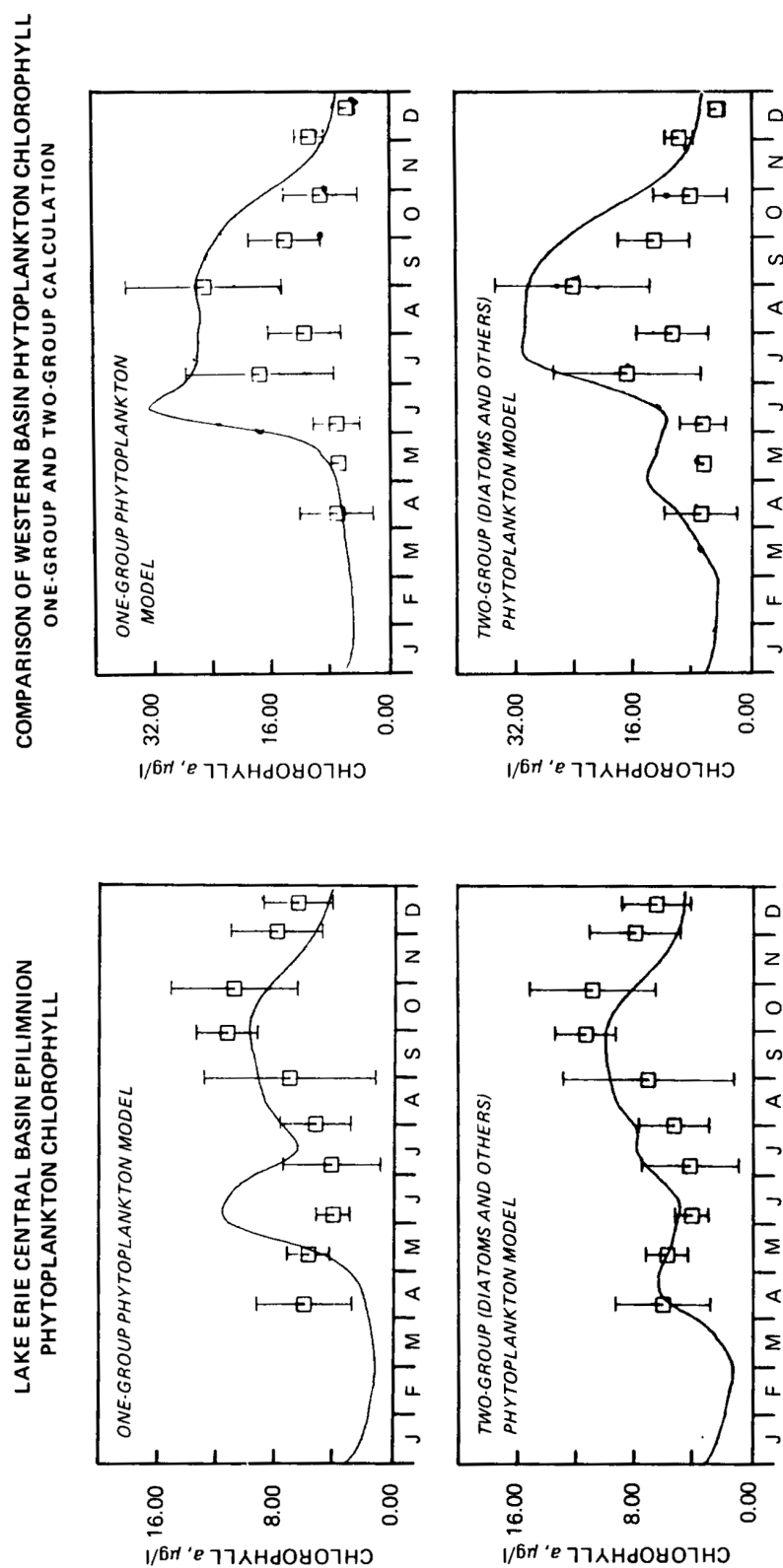


Figure 41. Comparison of one-group and two-group phytoplankton calculation (chlorophyll, µg/l) for Lake Erie central basin epilimnion (left) and western basin (right).

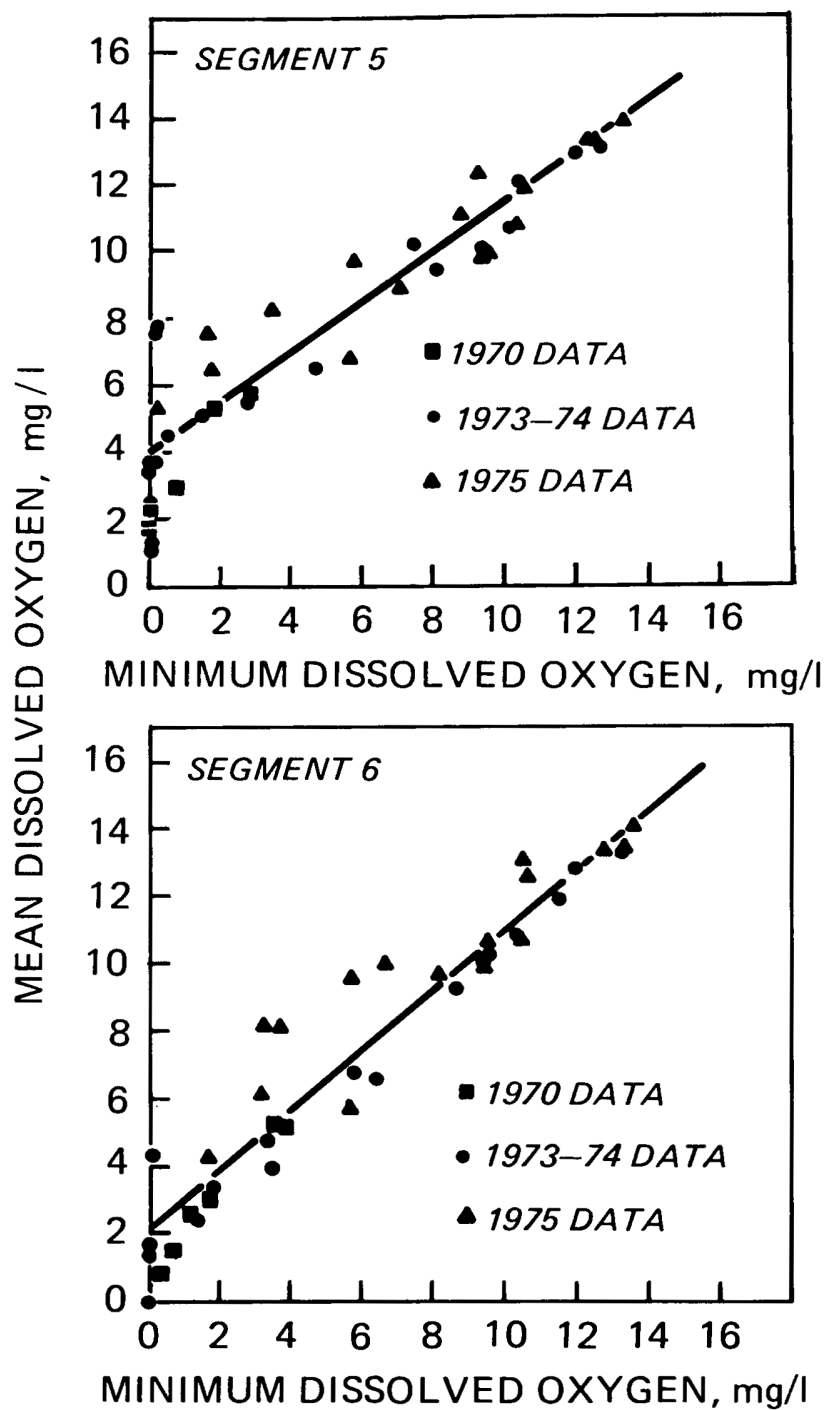


Figure 42. Mean dissolved oxygen ($\mu\text{g/l}$) for the central basin hypolimnion segments versus the minimum dissolved oxygen (mg/l) observed for each cruise.

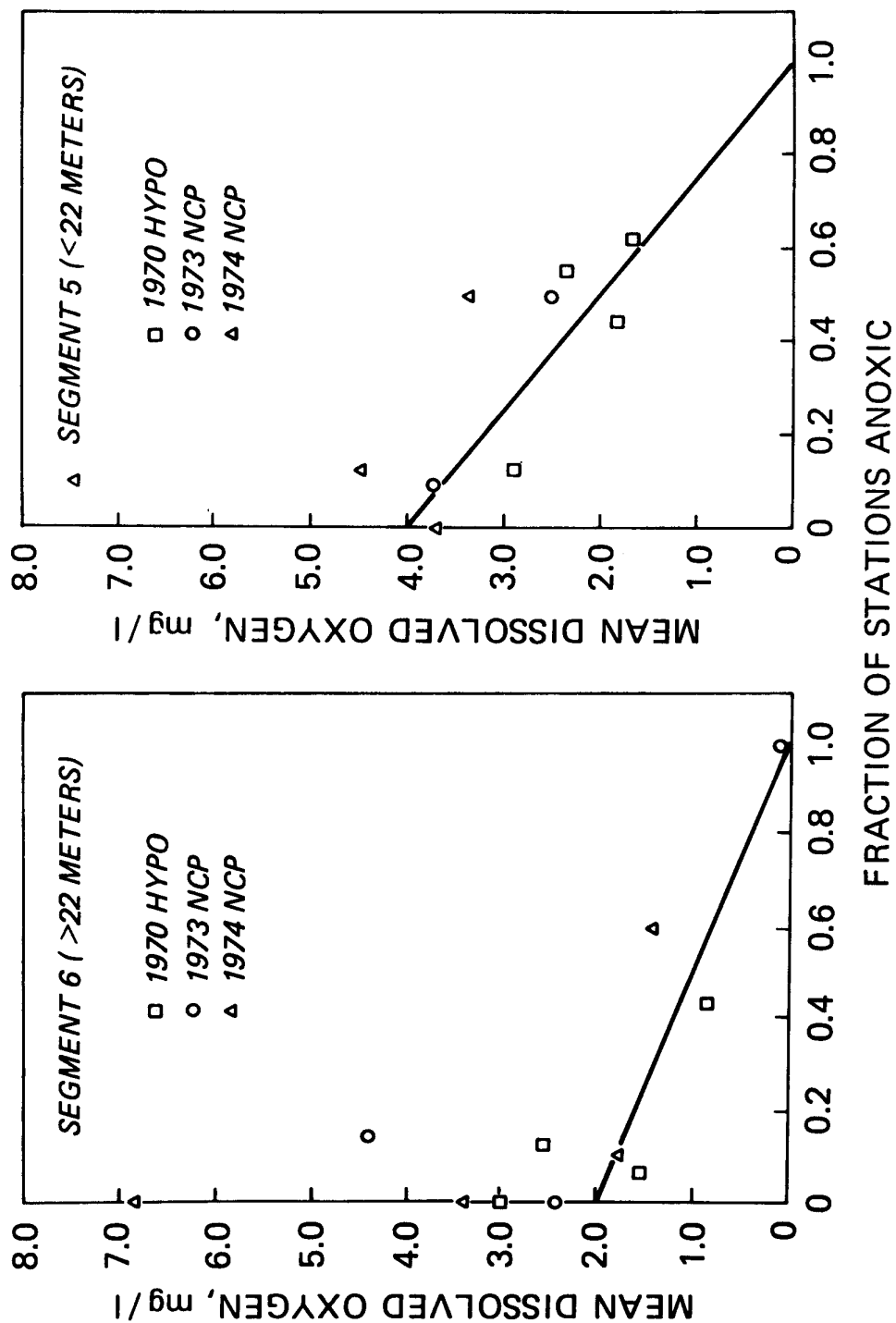


Figure 43. Cruise average dissolved oxygen (mg/l) for the central basin hypolimnion segments versus the fraction of stations anoxic for that cruise.

$$K_e = \frac{1.7}{SD} \quad (72)$$

The influence of the chlorophyll concentration is estimated using (Riley, 1956):

$$K_e = K'_e + 0.008[Chl-a] + 0.054[Chl-a]^{2/3} \quad (73)$$

which yields K'_e , the non-algal related extinction coefficient. A comparison of K'_e to wind velocity (IJC, 1969) is shown in Figure 44. The effect of wind suspension of particulate material is clearly seen. These correlations, together with the wind data for each basin, also shown in this figure, are used to calculate K'_e . The total extinction coefficient is then based on the calculated chlorophyll concentrations, in addition to the wind-related non-algal effect. The reason for this somewhat elaborate procedure is that under projected conditions of reduced chlorophyll concentration, the extinction coefficient would be reduced and this effect is important in increasing primary production and affecting the oxygen balance, as shown subsequently. The effect of ice cover over the lake is included by reducing the incident solar radiation by 70% (Wright, 1964) during the periods of reported ice cover (Webb, 1974), from the first of the year to day 60 for the western and central basins and day 90 for the eastern basin.

9.4 TIME SCALE

The intention of this calculation is to simulate the seasonal variation of the major water quality constituents involved in the eutrophication process. Short-term conditions such as storm events or diurnal variations of phytoplankton or dissolved oxygen are not considered. Rather, the seasonal changes of plankton, nutrients and dissolved oxygen distribution are characterized.

The differential equations which describe the kinetics and transport are solved using finite

difference techniques. The simple Euler-Cauchy method, with a provision for avoiding negative concentrations, is used for the integration. The time-step used is 0.5 days. Results are filed every 15 days except for the anoxic period evaluation which is based on the 0.5 day time-step. The fifteen state variables and the segments result in 150 simultaneous differential equations which are solved at each time-step. Approximately 122 equivalent central processor unit (CPU) seconds of execution time on a CDC 6600 are used for each one-year model run. This includes time for graphic display, overhead, and the chemical computation, as well as transport and kinetics.

9.5 CARBON DIOXIDE AND ALKALINITY

The relevance of computing a carbon dioxide mass balance is discussed in Chapter 6. As can be seen from the reaction kinetics stoichiometry, carbon dioxide and oxygen play opposite roles during primary production and aerobic oxidation. Therefore, the measurements of pH and alkalinity provide additional calibration information with virtually no additional degrees of freedom included in the formulation. The only complication is that the reactions involving the dissolved inorganic carbon species: $CO_2(aq)$, HCO_3^- , $CO_3^{=}$, and the hydrolysis products of water: H^+ and OH^- must be considered. Methods for including these reactions within the context of mass balance computations have been developed (Chen and Orlob, 1972) and generalized (Di Toro, 1976) so that any set of fast reversible reactions can be accommodated. The basic idea has been developed in Chapter 7: for species independent transport it suffices to compute mass balances for the components of the species. In the case of water column concentrations, the mixing is via large scale water motions and the transport is clearly species independent. The most convenient choice of components for the carbon dioxide-water species are total carbon dioxide, C_T , and alkalinity, A , where:

$$C_T = [CO_2(aq)] + [HCO_3^-] + [CO_3^{=}] \quad (74)$$

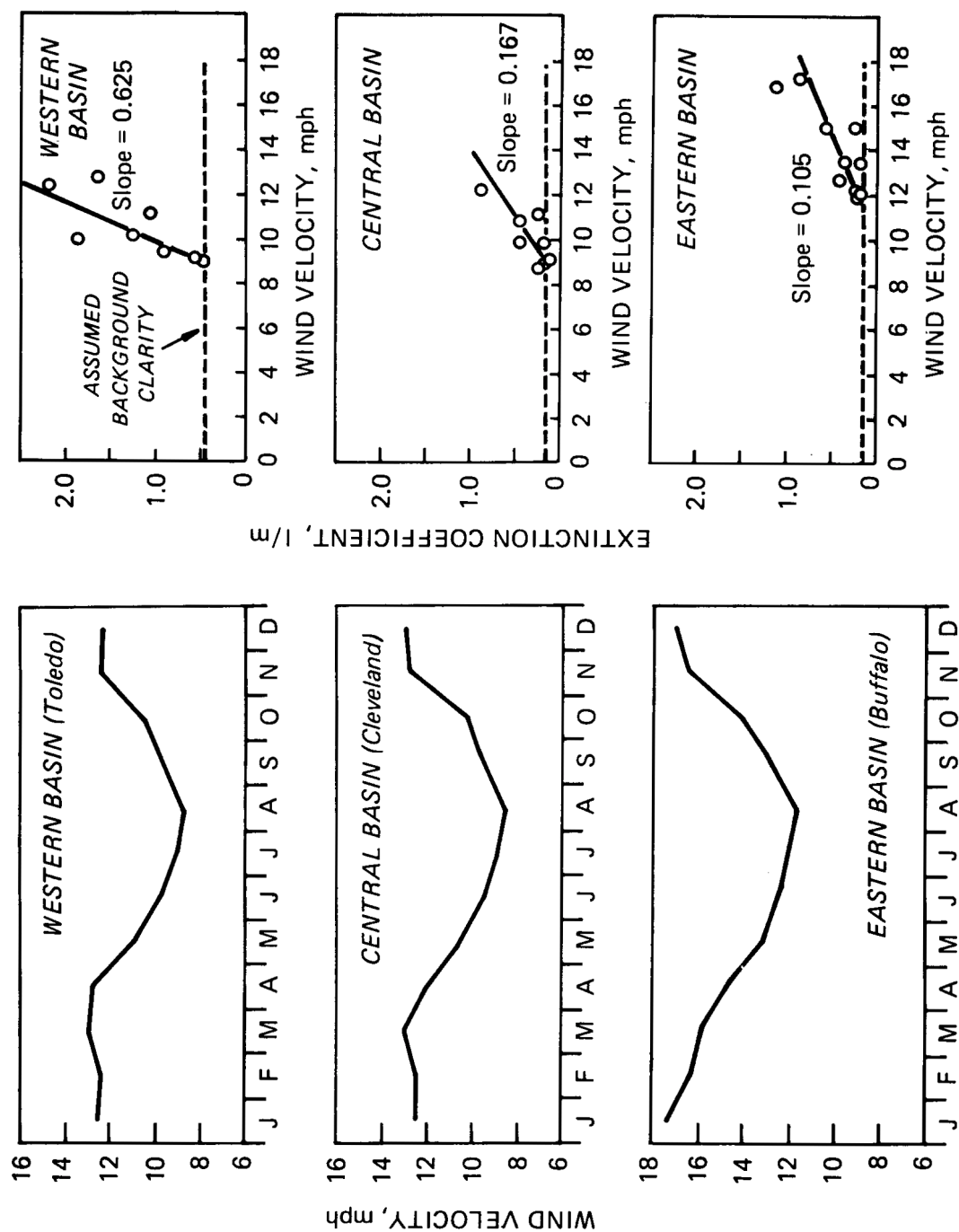
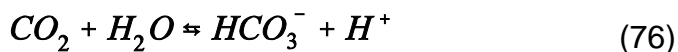


Figure 44. Average monthly wind velocities (mph) around Lake Erie (left) and variation of non-algal extinction coefficient (m^{-1}) with wind velocity (right).

$$A = [HCO_3^-] + 2[CO_3^{2-}] + [OH^-] - [H^+] \quad (75)$$

These components are conserved during any fast reversible reaction, for example:



It is clear that total carbon dioxide is conserved since any change in oxygen is compensated for by a change in HCO_3^- . The same is true for alkalinity since HCO_3^- and H^+ have opposite signs in the alkalinity definition. Therefore, the mass balance equations for these components are independent of the source-sink terms due to the fast reversible reactions. They include only the sources and sinks of total carbon dioxide and alkalinity due to the biological production and consumption reactions as specified in Tables 11-19.

It remains only to describe the method used to compute the species concentrations given the component concentrations as computed from mass balance equations. This is a straightforward chemical equilibrium calculation for which a number of methods are available (Van Zeggeren and Storey, 1970). The algorithm chosen for this application was developed by the Rand Corporation (Clasen, 1965) and it has been found to be quite reliable. The chemical thermodynamic constants required are listed in Table A-16 of the Appendix. The temperature dependence is calculated assuming the enthalpy and entropy changes for each reaction, ΔH_r° and ΔS_r° are independent of temperature. It has been verified (Thomann *et al.*, 1975) that the equilibrium constants, K_{eq} computed using the relationships:

$$\Delta G_r^\circ = \Delta H_r^\circ - T \Delta S_r^\circ \quad (77)$$

$$\Delta G_r^\circ = -RT \ln K_{eq} \quad (78)$$

where T is in $^\circ K$ and R is the universal gas constant within 5% of experimentally reported

over the temperature range of 0 to $30^\circ C$. The ionic strength correction is ignored since, for Lake Erie surface waters, it is small.

There is a significant additional computation burden associated with the chemical equilibrium computation and in order to lessen its impact on the overall computational requirement, the equilibrium calculation is done only every ten days. The computed species concentrations are assumed to be constant during the ten days and then they are updated. This has no effect on the accuracy of the rest of the computation since no reaction rates are functions of the species concentration. Only the air-water exchange of $CO_2(aq)$ is affected by this procedure and it to a negligible extent.

9.6 AIR-WATER INTERFACE EXCHANGE

For the segments with an air-water interface (segments 1, 2 and 3), the dissolved gases: $CO_2(aq)$ and $O_2(aq)$ are both subject to exchanges with their atmospheric counterparts: $CO_2(g)$ and $O_2(g)$. The exchanges can be thought of as slow reversible reactions of the form:



with first-order reaction rates K_L/H_i where K_L is the air-water surface exchange coefficient and H_i is the depth of segment i . The conventional formulation for the source term in the mass balance equation for total CO_2 in segment i , C_{ti} , is (O'Connor and Dobbins, 1958):

$$\frac{dC_{ti}}{dt} = \frac{K_L}{H_i} (CO_2(aq)_{si} - CO_2(aq)_i) \quad (81)$$

where $CO_2(aq)$ is the equilibrium (or saturated) concentration at the aqueous temperature in segment i corresponding to the atmospheric partial pressure of $CO_2(g)$. A similar equation applies for dissolved oxygen. The saturated

aqueous concentrations for CO_2 is computed from the chemical equilibrium requirements for Equations (79) and (80), that is that the change in Gibbs free energy, ΔG_r , for each reaction is zero:

$$\Delta G_r = \sum_{\text{products}} \Delta G - \sum_{\text{reactants}} \Delta G = 0 \quad (82)$$

so that, assuming the activity coefficients are unity:

$$\Delta G_{\text{CO}_2(\text{aq})}^{\circ} + RT \ln [\text{CO}_2(\text{g})] = \Delta G_{\text{CO}_2(\text{aq})}^{\circ} + RT \ln [\text{CO}_2(\text{aq})] \quad (83)$$

and, therefore:

$$\text{CO}_2(\text{aq})_{\text{si}} = \text{CO}_2(\text{g}) \exp \left\{ \Delta S_r^{\circ} / R + \Delta H_r^{\circ} / RT_i \right\} \quad (84)$$

where R is the universal gas constant and T_i is the aqueous temperature in degrees Kelvin. The appropriate thermodynamic constants are listed in Table A-17 in the Appendix.

The remaining parameter in Equation (81) that needs to be specified is the exchange coefficient, K_L for CO_2 and O_2 . For lakes, the predominant mechanism that influences the exchange coefficient is wind velocity and ice cover. During the period of ice cover, the exchange is set to zero (day 0 to day 60 for the western and central basins, and day 0 to day 90 for the eastern basin). Estimates have been made of the relationship between K_L and wind velocity (Weiller, 1975). For the sake of simplicity a constant exchange coefficient has been used for both CO_2 and O_2 : $K_L = 2$ m/day which is reasonable for the wind velocities over Lake Erie. As shown subsequently, this simplification is of no consequence in the dissolved oxygen calibration since the observations and calculations in the surface

segments are essentially saturated. For the carbon dioxide calculation including the wind velocity effect may improve the results of the pH calibration in the latter part of the year where, as shown subsequently, the computed pH is below that which is observed. The effect on the hypolimnion computations is negligible since only small differences in total CO_2 concentrations would result from this modification.

9.7 SETTLING VELOCITIES

The settling of particulates from the water column to the sediment is the principle mechanism by which nutrients are lost from the water column. The inclusion of this advective term in the mass balance equation is straightforward. Assume that segment 2 is below segment 1 and that for the variable c the settling velocity is w . The mass balance equations for these segments ignoring horizontal advection and reactions are:

$$V_1 \frac{dc_1}{dt} = E_{12} (c_2 - c_1) - w A_{12} c_1 \quad (85)$$

$$V_2 \frac{dc_2}{dt} = E_{12} (c_1 - c_2) + w A_{12} c_1 \quad (86)$$

where E_{12} is the exchanging flow and A_{12} is the interfacial cross sectional area. The term $w A_{12}$ is an equivalent unidirectional flow which is due not to water motions but rather to a settling of the particulates.

The settling velocity used in this computation represents both the settling through the thermocline and through the sediment water interface. It is possible that these two velocities are different due to the effects of resuspension which may be more pronounced at the interface. However, it is not possible to resolve this difference with the coarse vertical segmentation of the water column used in this calculation.

A more detailed parameterization of settling into the sediment would include not only a downward

settling velocity but an upward resuspension velocity as well. In this context, the single settling velocity used in these computations can be thought of as the settling velocity which represents the net flux due to the difference between the downward settling flux and the upward resuspension flux. Since the settling velocity is constant, it cannot account for increased resuspension flux during high wind periods. As shown subsequently, the computation underestimate the total phosphorus concentrations during this period.

9.8 MASS BALANCE EQUATIONS

The formulation of the mass balance equations for each variable in each segment is straightforward. For concentration C_{li} of variable l in segment i , the general mass balance equation is:

$$V_i \frac{dc_{li}}{dt} = \sum_k E_{ki} (c_{lk} - c_{li}) + \sum_k Q_{ki} c_{lk} + S_{li} V_i \quad (87)$$

where V_i is the segment volume, E_{ki} is the exchange flow between segments k and i , Q_{ki} is the advective or settling velocity flow from segment k to segment i , and S_{li} is the sum of the sources and sinks for variable l in segment i . The transport coefficients, which are determined from the temperature balance computations described in Chapter 8, are listed in Tables A-1 and A-2 for 1970 and 1975, respectively. The settling velocities which are determined from the calibration are listed in Table A-15.

The dynamic mass balance equations for both the water column and sediment segments are solved simultaneously to produce the

concentrations. Thus, although the sediment-water interactions were analyzed on a steady-state basis in Chapter 7, and a remarkably simple expression, Equation (63), describes the expected result, the dynamic mass balance equations are integrated for the results that follow. These take into account the time variable nature of the incoming fluxes of algal and detrital carbon and their subsequent conversion to sediment oxygen demand.

The sources and sinks due to the kinetics are easily constructed from Tables 11-19 corresponding to the reactions incorporated in the calculation. For example, consider variable 1, diatom chlorophyll a . It appears in the stoichiometry of reactions I, II, and III of the aqueous reactions and reaction XII of the sediment reactions. Thus, for the aqueous segments, the source term is:

$$S_{li} = R_{li} - R_{2i} - R_{3i} \quad (88)$$

where the R 's are the reaction rates in the tables evaluated with the diatom coefficients and concentrations in segment 1. The signs are determined by the location of the variable in the stoichiometric equation; it is positive if it occurs on the right-hand side of the equation since it is being produced by the reaction; otherwise, it is negative since it is being consumed by the reaction. The stoichiometric coefficients must multiply the reaction rates as they do in the stoichiometric equations. For diatom chlorophyll, they are unity but for other variables they are as indicated in the reaction stoichiometric equations in Tables 11-19. It should be clear that following the conventions, it is possible to construct the complete source terms for all variables in the computation.

CHAPTER 10

CALIBRATION

The final calibration is the result of approximately 150 model runs which were made in order to determine a consistent set of parameter values that are reasonable and reproduce the observed data for all the variables considered. The method employed is essentially trial-and-error. The starting point is a set of parameter values which have been used in the previous Lake Ontario (Thomann *et al.*, 1975) and Lake Huron/Saginaw Bay (Di Toro and Matystik, 1979) computations. As described in Chapter 9, it was necessary to consider diatom and non-diatom chlorophyll separately. The coefficients for their kinetics were then adjusted to reproduce the observed behavior. Zooplankton kinetic constants were also similarly adjusted. The remaining kinetic constants are essentially those used previously. In particular, the chlorophyll dependent recycle mechanism (Di Toro and Matystik, 1979) was found to apply to Lake Erie as well. The coefficient values used for the final calibration are listed in Tables 11-19. The data used for the calibration are from the 1970 and the 1973-1974 survey years. The comparison figures for the 1970 and 1973-1974 data are presented subsequently. The data plotting symbols are mean \pm standard deviations. The square symbol represents CCIW cruise data for 1970. The circle represents Project Hypo data for 1970. The triangle represents 1973 data. The diamond represents 1974 data. The computed lines are the same for both years since the conditions are similar for these years.

10.1 DISSOLVED OXYGEN

The dissolved oxygen comparisons for 1970 are shown in Figure 45 and for 1973-1974 data in Figure 46. The agreement is quite good with the computation duplicating all the major features of the temporal oxygen distribution within the various sections of the lake. As can be seen, the epilimnion dissolved oxygen follows the saturation oxygen concentration very closely during the entire year except for a small oxygen peak of supersaturation appearing in early July. This is due to photosynthetic production resulting from the increase in phytoplankton chlorophyll taking place at this time. In the central basin hypolimnion, the low oxygen values during the summer months are caused by a combination of phytoplankton decay within the hypolimnion and the oxygen demand exerted by the sediment. The increasing temperature which results in increasing reaction rates, the sinking of the phytoplankton which have grown in the epilimnion; and stratification which inhibits transfer of oxygen from the epilimnion to the hypolimnion, all contribute to the oxygen decline. The decline continues until overturn in early fall. At this time, there is a rapid increase in the hypolimnion dissolved oxygen which continues to the end of the year. The actual rate of vertical mixing during the latter stages of overturn appears to be more intense than the vertical mixing used in the calculation. These transport coefficients are estimated from the temperature distribution as described in Chapter 8. Since the temperature gradient is very small during the latter part of the year, the estimate of the vertical mixing coefficient is uncertain, and, based on the

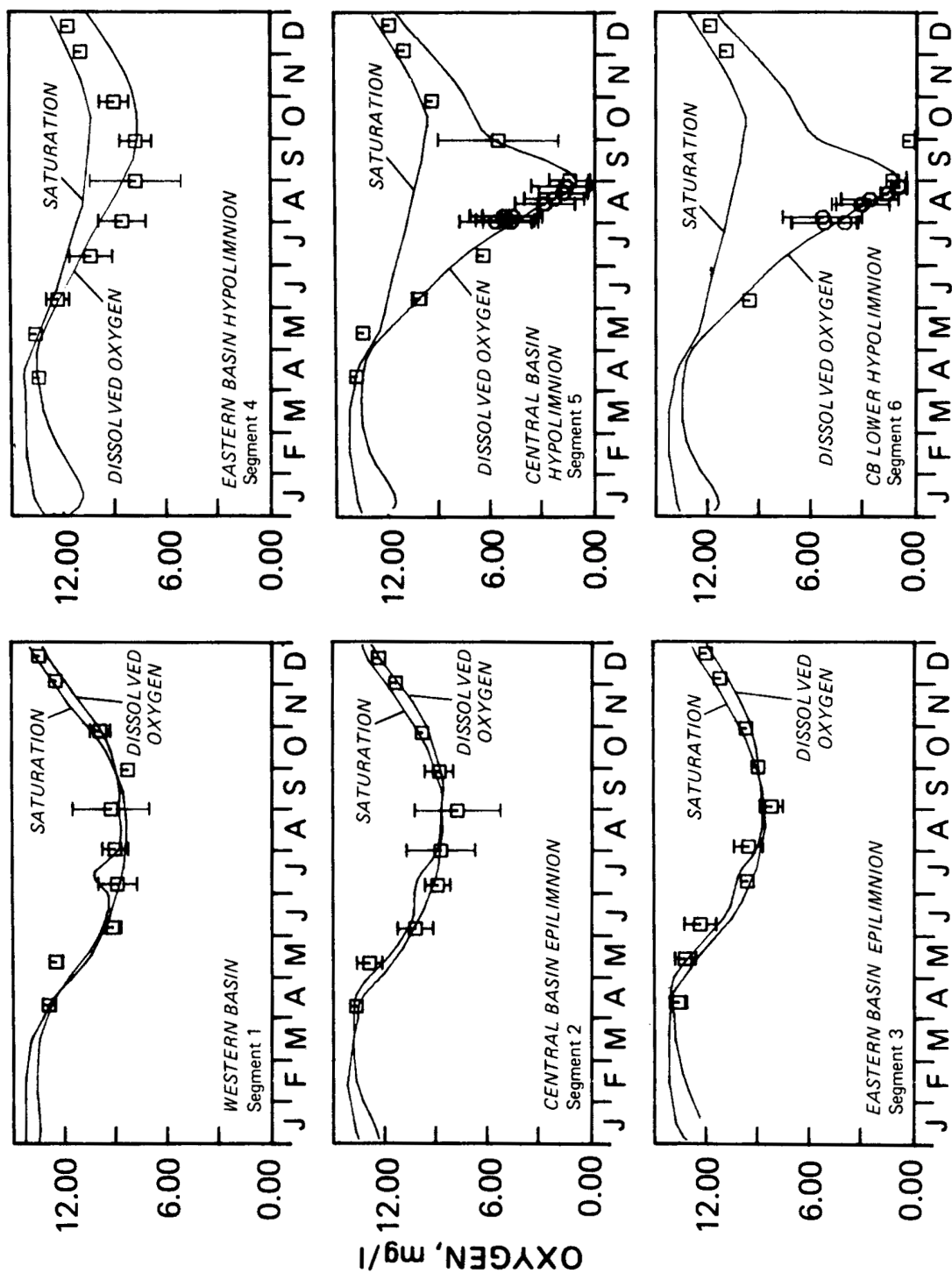


Figure 45. Lake Erie model calibration for dissolved oxygen (mg/l), 1970. Symbols: mean \pm standard deviation, lines are the computations.

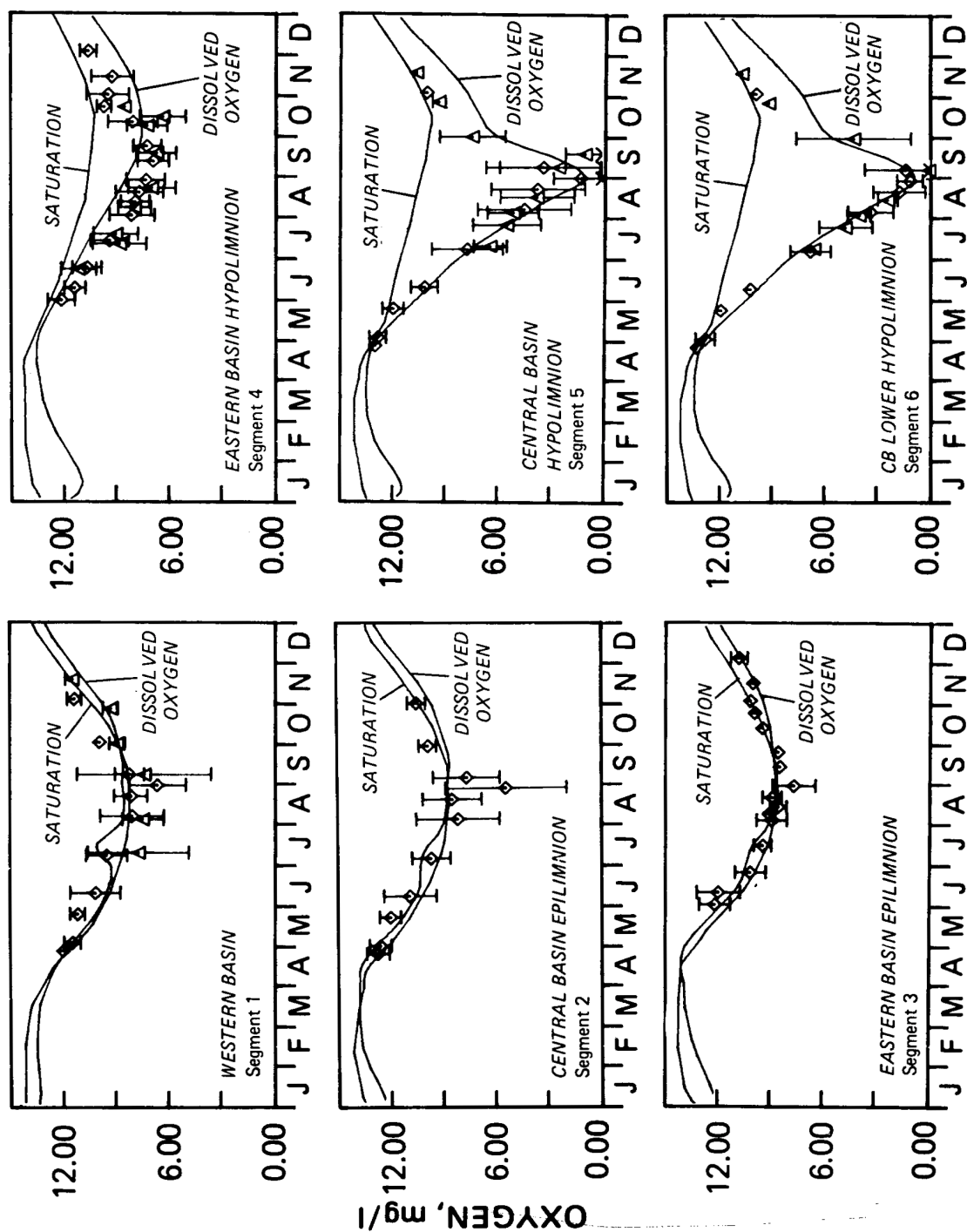


Figure 46. Lake Erie model calibration for dissolved oxygen (mg/l), 1973-1974.

results of the oxygen calculations, it should be larger.

Figure 47 illustrates the relative importance of the individual oxygen sinks. The bottom curve is the calibrated dissolved oxygen calculation for the central basin hypolimnion. Proceeding up from this curve are the results of sequentially removing the deep sediment oxygen demand, surface sediment oxygen demand, organic carbon oxidation (actually organic carbon oxidation + nitrification but the latter is insignificant) and finally, phytoplankton respiration. It is apparent that organic carbon oxidation represents the largest oxygen sink in the hypolimnion, making up about 43% of the total depletion at the time of minimum dissolved oxygen. The two components of the sediment oxygen demand (SOD) account for 40% of the total depletion at the time of minimum dissolved oxygen. Individually, the computed surface SOD accounts for 12% of the total depletion and the deep SOD accounts for 28%. The remaining 17% is due to phytoplankton respiration.

A summary of the computed sources and sinks of dissolved oxygen in the central basin

hypolimnion during the summer stratification is presented in Table 21.

The aqueous reactions: phytoplankton respiration and detrital organic carbon oxidation, consume a total of 5.08 mg O₂/l during the period of stratification. The oxygen decrease attributed to sediment oxidation is 3.58 mg O₂/l. These sinks are balanced by the only significant source considered in the computation: transport of dissolved oxygen through the thermocline which increases the concentration by 1.83 mg O₂/l. The net result is a decrease of 6.83 mg O₂/l during the 60 day period analyzed in this table.

An additional check on the validity of the oxygen calculation is available. As discussed earlier in this chapter, an empirical correlation has been developed which relates the average hypolimnetic dissolved oxygen to the anoxic area during a year. For the 1970 calibration year, the calculated maximum anoxic area is 6819 km². The anoxic area of the central basin for 1970 is reported to be 6600 km². Thus, calculated anoxic area is essentially the same as that determined from actual oxygen measurements.

Table 21. Sources and Sinks of Dissolved Oxygen, Central Basin Hypolimnion, 1970

Reaction Source (+) Sink (-)	Average Volumetric Depletion Rate (mg O ₂ /l-Day)	Dissolved Oxygen Change Day 180-240 (mg O ₂ /l)
Phytoplankton Respiration	-0.020	-1.20
Detrital Organic Carbon Oxidation	-0.0646	-3.88
Sediment Oxygen Demand	-0.0597	-3.58
Thermocline Transport	0.0305	1.83
Total Oxygen Change		-6.83

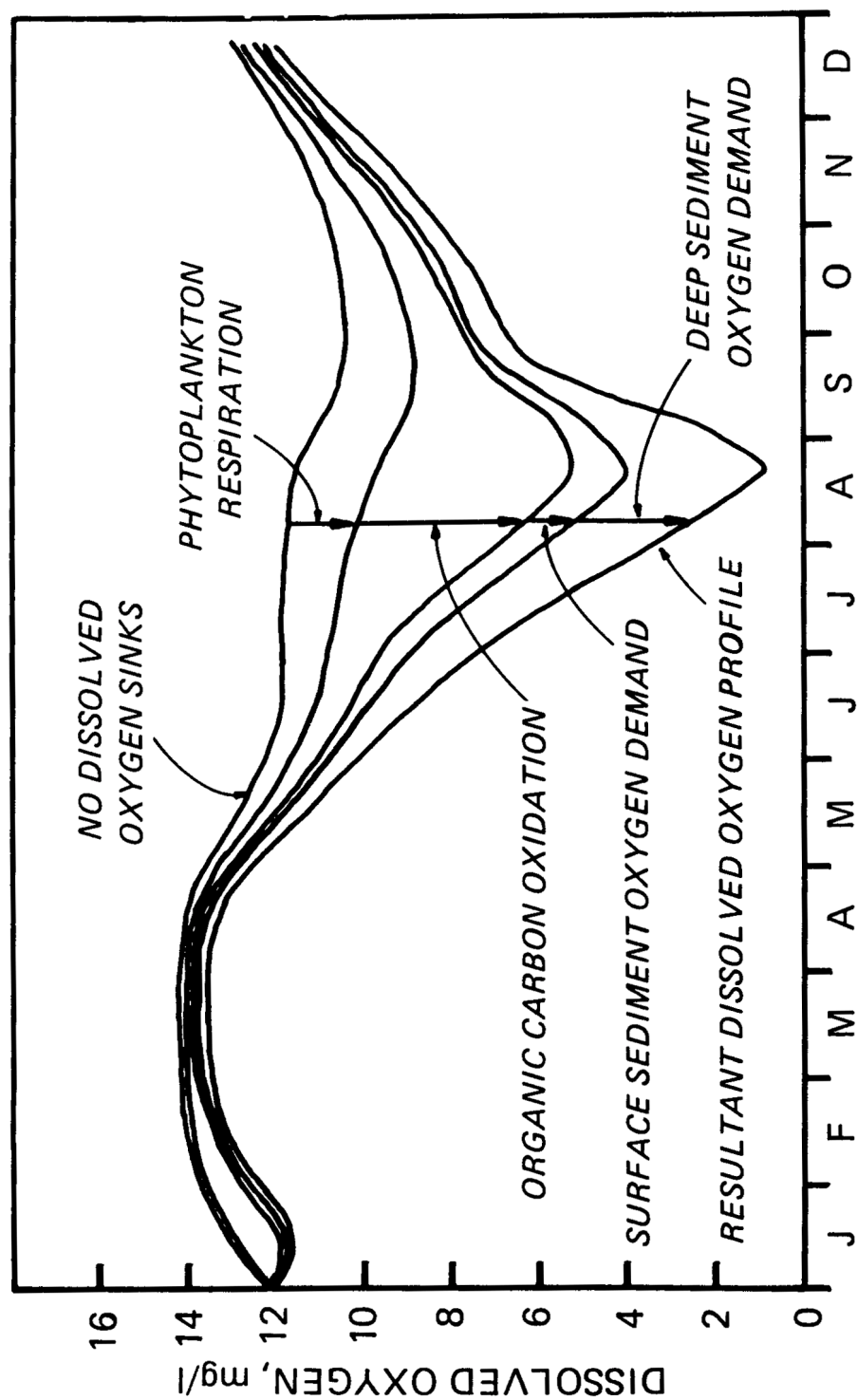


Figure 47. Dynamics of central basin hypolimnion dissolved oxygen calibration illustrating the relative importance of the individual oxygen sinks.

10.2 PHYTOPLANKTON

The results of the calibration for phytoplankton chlorophyll are shown in Figures 48 and 49. The calculated curve is the sum of the diatom chlorophyll and non-diatom chlorophyll. Calculated peak western and central basin chlorophyll is overestimated for the 1973-1974 calibration year but is in reasonable agreement with 1970 observations, as are the calculations for the other segments. The chlorophyll associated with each of these two groups together with the estimated fraction of diatom biomass (Munawar and Munawar, 1976) are shown in Figure 50 for 1970. Note that in all basins, the diatom begin to grow in early spring but are declining by the beginning of summer. The growth and death dynamic plots, Figures 51-53, reveal that this decline is due to a decrease in growth rate caused by nutrient limitation which allows respiration and grazing to exceed the growth rate. As shown subsequently, the nutrient limitation is caused by silica depletion.

Following the diatom decline, there is a bloom of non-diatoms in all three basins (segments 1, 2 and 3). The dynamic plots show that this bloom is delayed due to grazing pressure. The zooplankton population is high due to the early diatom bloom. The result is that the phytoplankton are suppressed until the herbivorous zooplankton decline due to predation by carnivorous zooplankton. At this time, there is a rapid increase in the non-diatom population. In the western basin, the population stabilizes at approximately 26 $\mu\text{g Chl-a/l}$. This is due to several factors. As would be expected, light and nutrient limitation are significant in controlling the size of the bloom. This can be seen in the nutrient limitation plots. Perhaps not as obvious is the contribution of phytoplankton settling to population limitation in the western basin. Examination of the dynamic plots for the western basin shows that settling constitutes an important loss rate throughout the year for both diatoms and non-diatoms. During the non-diatom summer bloom, settling is the largest non-diatom sink by approximately a factor of three. The shallow depth of the basin is the

reason for the importance of settling. The dynamic plots of the deeper central and eastern basin epilimnion show that settling never reaches the importance it does in the western basin. In these basins, nutrient limitation is the controlling factor for growth. The decline of the phytoplankton in late fall is due to decreasing light and temperature. The dynamic plots show that by this time there is very little nutrient limitation.

Figure 54 illustrates the growth rate reduction factors due to silica, nitrogen and phosphorus limitation effects. As discussed earlier, the spring bloom in all three basins is terminated by the depletion of silica. These plots show that for the western, central and eastern basins, the growth rates are reduced by a factor of 0.45, 0.15, and 0.15, respectively, due to silica limitation. The summer bloom in all three basins is phosphorus limited. As the plots show, the phosphorus factor is low while both the silica and nitrogen factors are high. For the western, central and eastern basins, phosphorus depletion results in growth rate reduction factors of 0.40, 0.21 and 0.21, respectively, while at the same time the nitrogen reduction factors are 0.83, 0.87 and 0.87. From these plots, it is clear that for all three basins, the spring bloom is silica limited and the summer-fall bloom is phosphorus limited. However, especially in the western basin, inorganic nitrogen is almost exhausted by the bloom so that if phosphorus limitation did not terminate the bloom, the nitrogen limitation would do so at essentially the same peak chlorophyll concentration, assuming that nitrogen fixation did not add significantly to the available fixed nitrogen sources.

These calculations of nutrient limitation effects also indicate that nutrient limitation is much more severe in the central and eastern basins than in the western basin. In the western basin, nutrient levels do not reach the low values seen in the other basins. This is due to the contribution of the other factors that limit growth in the western basin. As discussed previously, settling is important. In addition, the high turbidity level of the western basin and the resultant high light

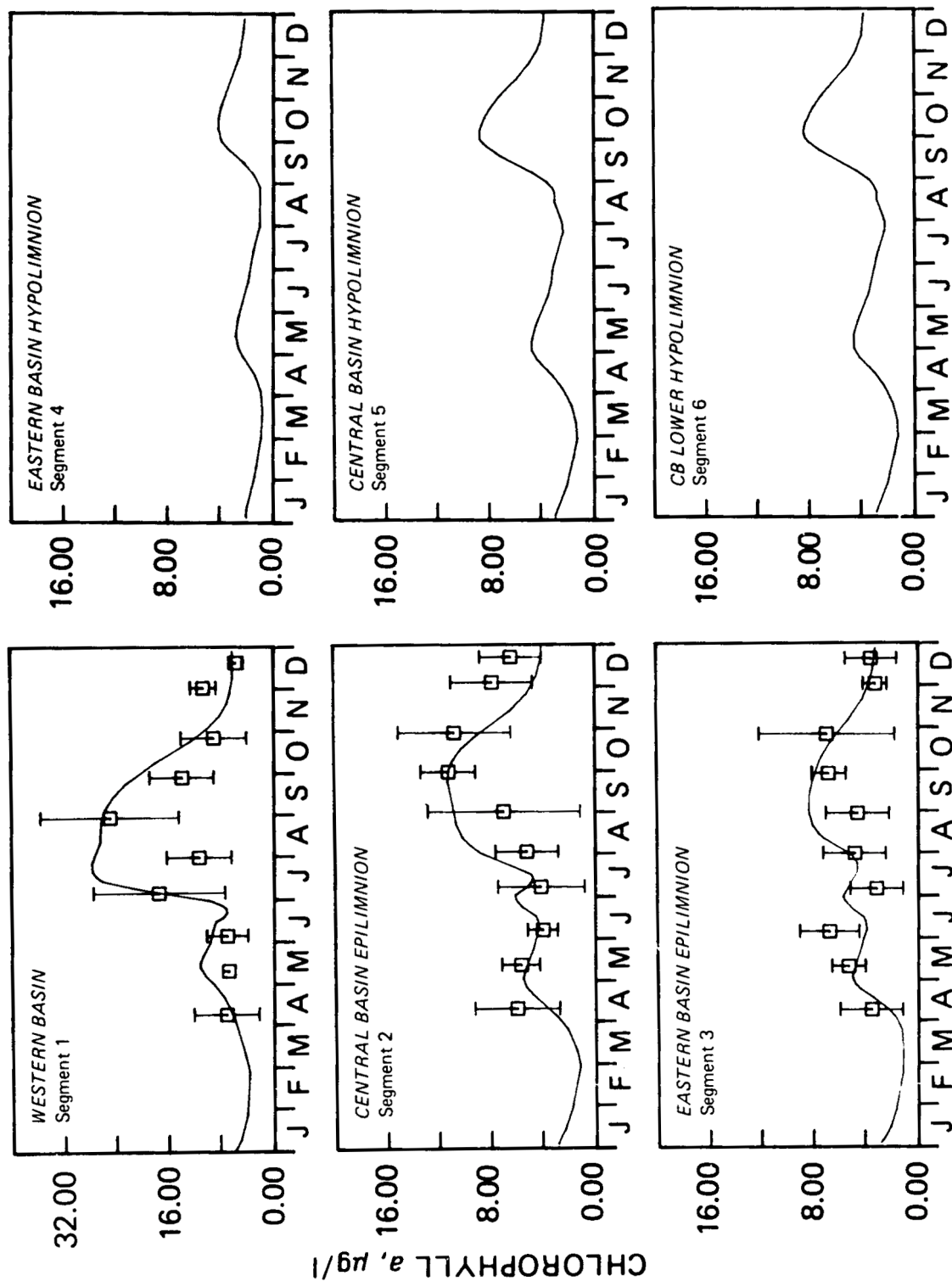


Figure 48. Lake Erie model calibration for phytoplankton chlorophyll ($\mu\text{g/l}$), 1970. The calculated curve is the sum of the diatom chlorophyll and non-diatom chlorophyll.

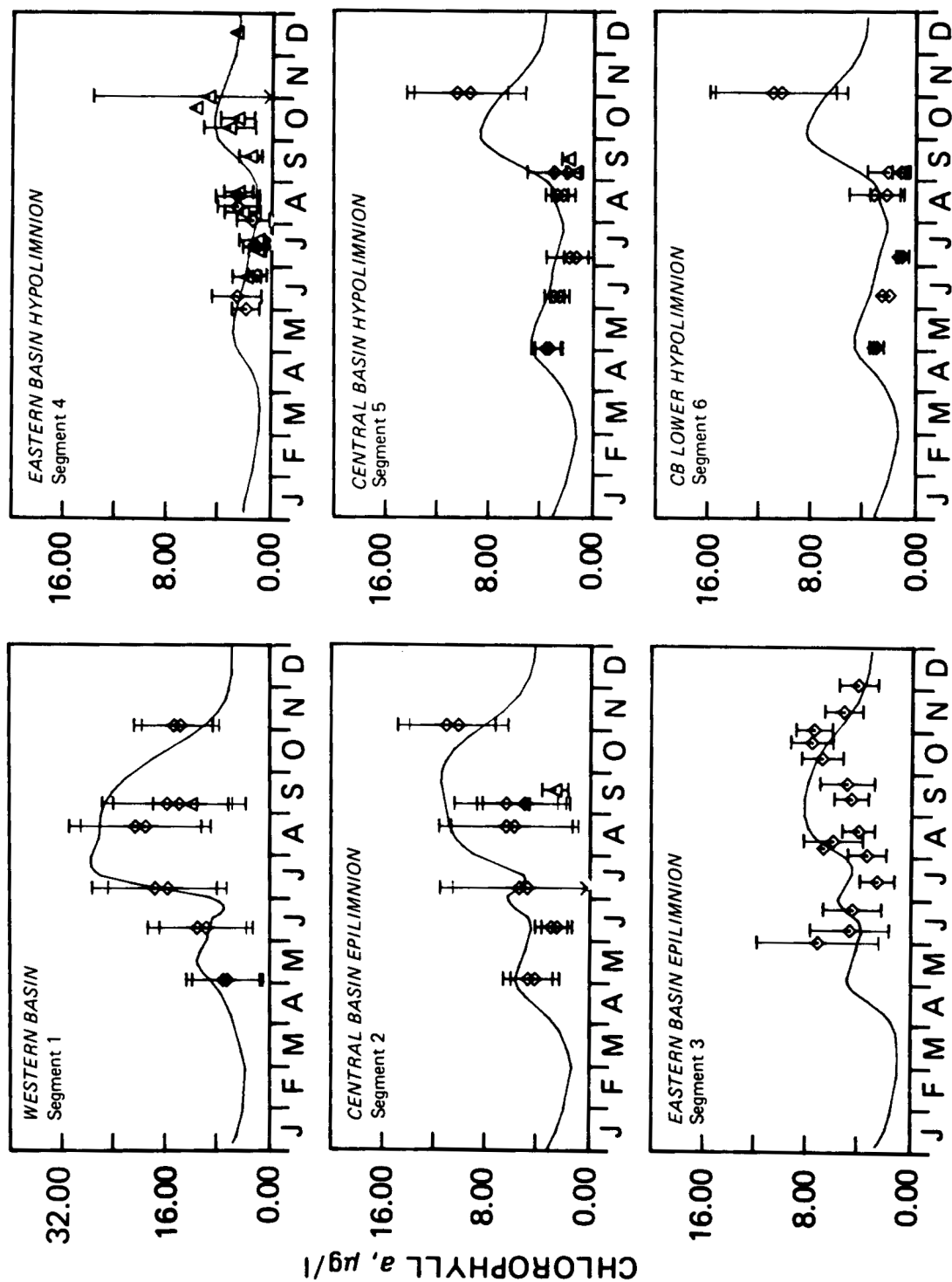


Figure 49. Lake Erie model calibration for phytoplankton chlorophyll ($\mu\text{g/l}$). 1973-1974. The calculated curve is the sum of the diatom chlorophyll and non-diatom chlorophyll.

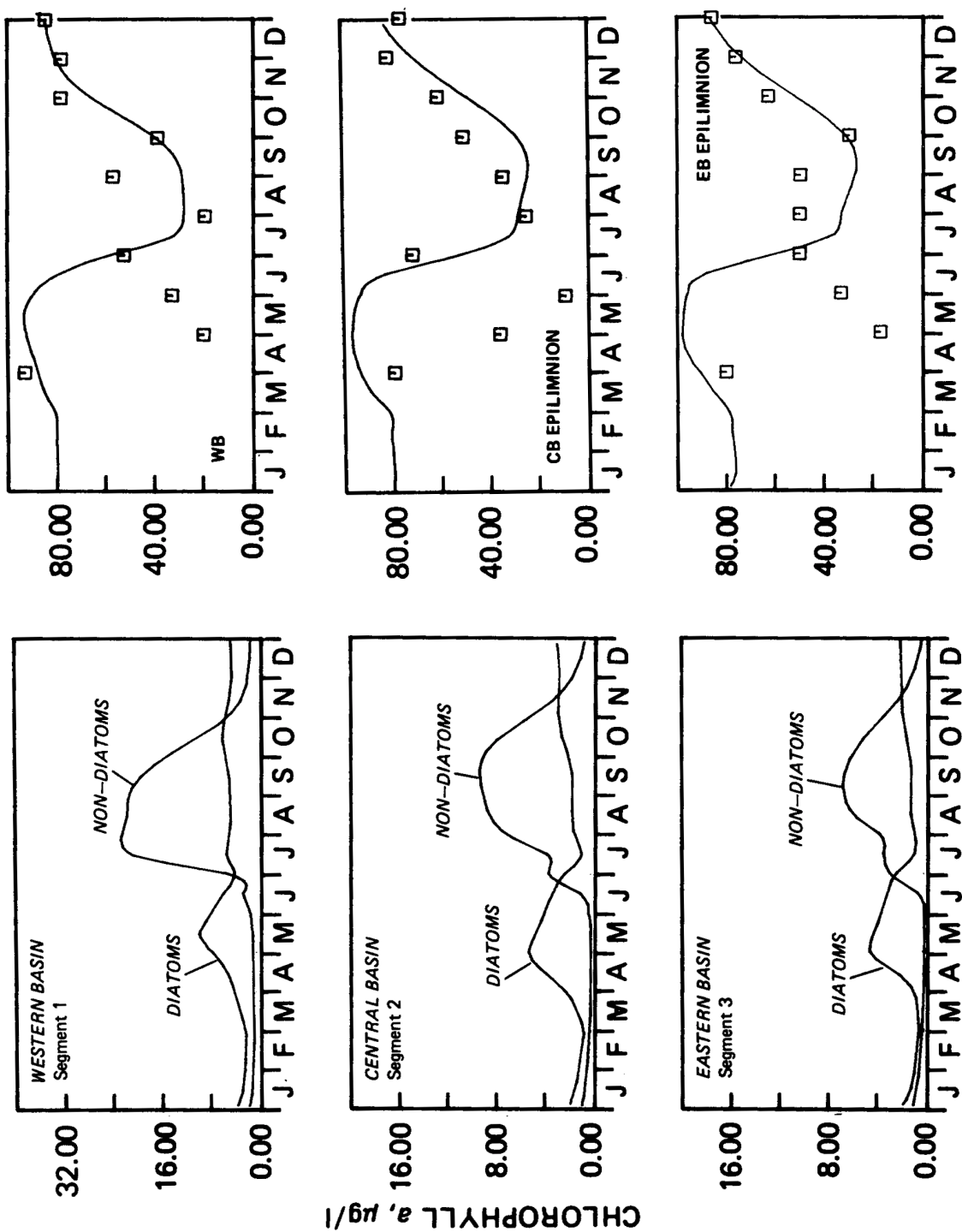


Figure 50. The distribution of chlorophyll ($\mu\text{g/l}$) between diatoms and non-diatoms (left) and model calibration for % diatom biomass (right).

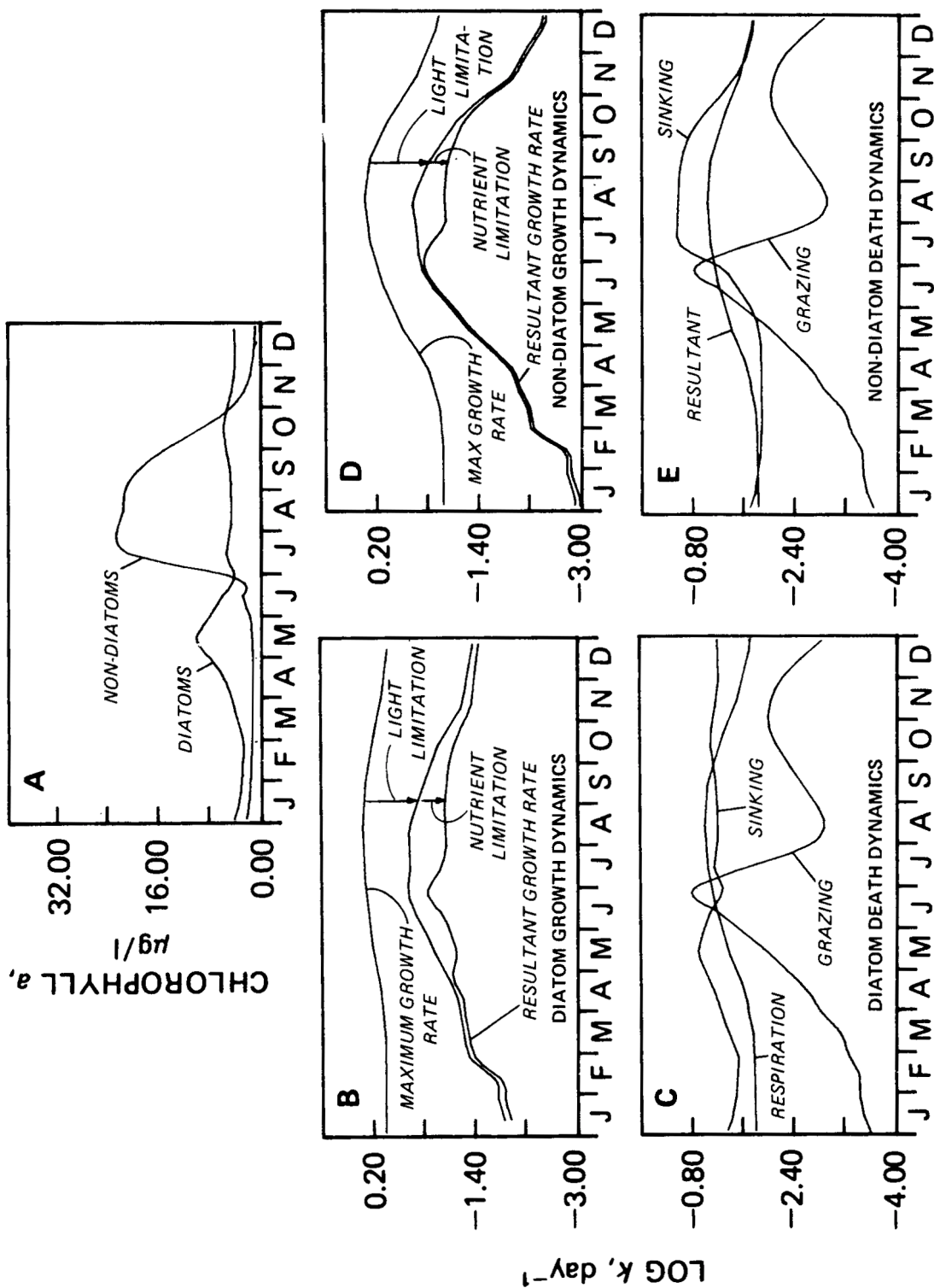


Figure 51. Western basin phytoplankton growth and death dynamics for diatoms (left) and non-diatoms (right). The curves are the calculated rates from the appropriate kinetic expressions.

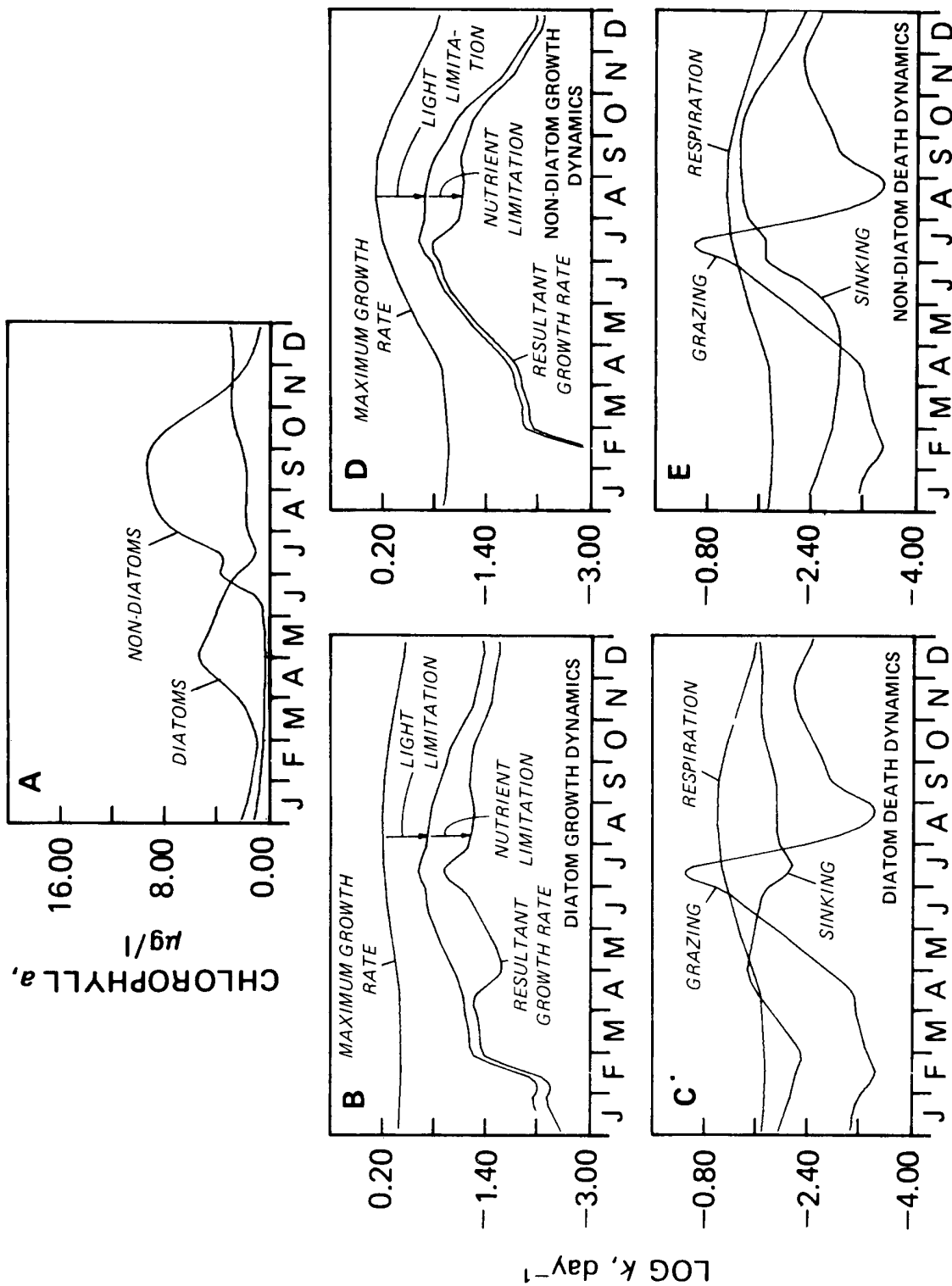


Figure 52. Central basin epilimnion phytoplankton growth and death dynamics for diatoms (left) and non-diatoms (right).

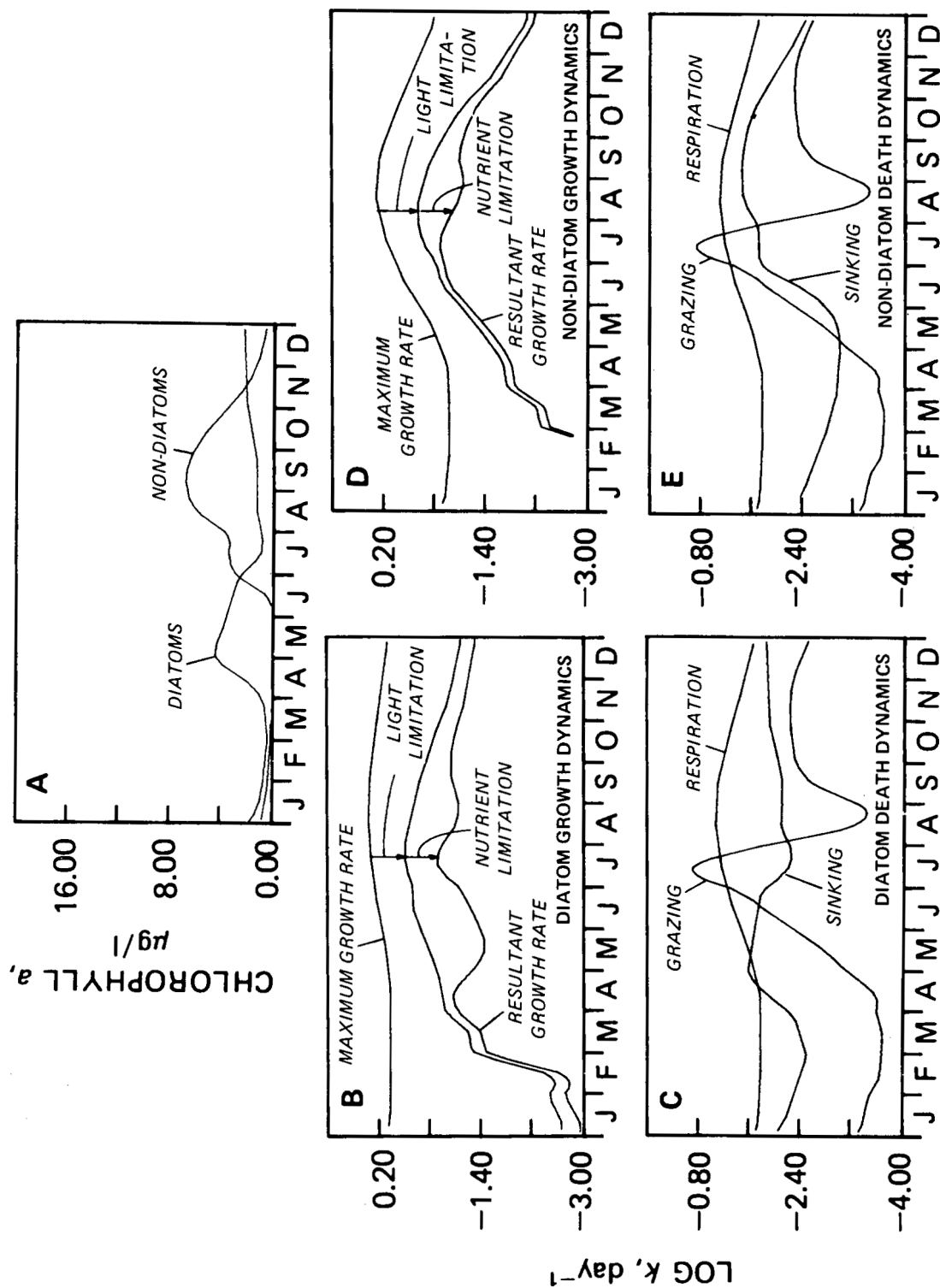


Figure 53. Eastern basin epilimnion phytoplankton growth and death dynamics for diatoms (left) and non-diatoms (right).

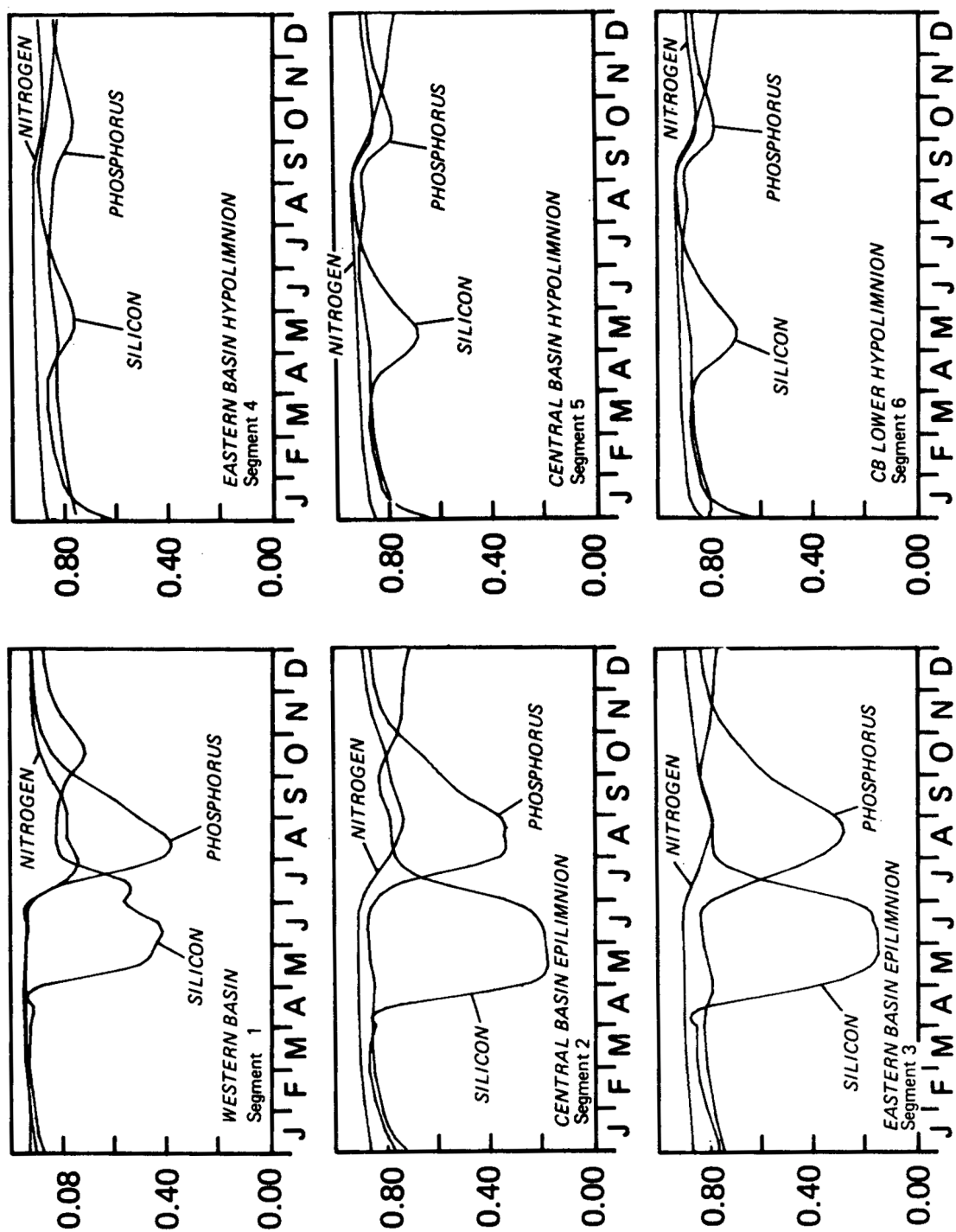


Figure 54. Lake Erie model calibration, nutrient limitation multipliers, 1970. The curves are the growth rate reduction factors due to silica, nitrogen and phosphorus limitation effects.

attenuation factor contribute to growth rate limitation.

10.3 NITROGEN

The distribution of the forms of nitrogen may be seen in Figure 55. The total nitrogen concentrations within the central and eastern basin epilimnia are fairly constant throughout the year. In the western basin, there is variation due to loading effects. All three of these segments exhibit similar patterns through the year. The non-living organic nitrogen concentration is stable until midsummer when there is an increase in concentration due to a combination of respiration of the phytoplankton and zooplankton populations which have increased just prior to this time and the excretion of organic nitrogen by predating zooplankton. There is a gradual decrease of the non-living organic nitrogen toward the end of the year as it is recycled to ammonia.

Ammonia concentrations are observed to be fairly constant in the epilimnia of the central and eastern basins throughout the year. This is due to two factors. First, the rate of nitrification is sufficiently rapid so that equilibrium is reached quickly. Second, because nitrate concentrations are much higher than ammonia, it is used as the algal nitrogen source in preference to the ammonia. In the western basin as the nitrate decreases it reaches the ammonia concentration level after which there is a depletion of ammonia as the phytoplankton preference structure switches from nitrate uptake to a more even nitrate-ammonia uptake. At this point, inorganic nitrogen is approaching limiting values. Note that in all three basins during the summer growth period, the nitrate concentration is lowered and the concentration of phytoplankton associated nitrogen increases. At this time, the total nitrogen remains approximately constant, but there is substantial variation within the individual nitrogen species; nitrate decreases, algal nitrogen increases and non-living organic nitrogen increases.

The increase in total nitrogen in the central basin hypolimnion is due to the recycling in the water column and the sediment. The calibration of the individual nitrogen species are shown in Figures 56-61. Organic nitrogen profiles, the sum of the computed phytoplankton and non-living organic nitrogen, are in reasonable agreement with observations in 1970. The 1973-1974 data is more variable especially in the eastern basin. The ammonia profiles, Figures 58 and 59, are in rough agreement with the observations. However, the computed phytoplankton uptake in the western basin is not observed in 1970, although it is suggested in the 1973-1974 data. The increase in recycled ammonia in the central basin hypolimnion is reproduced but the observed rapid mixing after overturn is not reproduced. This is consistent with the dissolved oxygen results and suggests a more rapid mixing at overturn.

The nitrate distributions in the surface sediments are in reasonable accord with observations for both years. The phytoplankton uptake is well reproduced in each segment. However, the hypolimnia are calculated to have considerably more nitrate than is observed in 1970. However, 1973-1974 data are in reasonable accord with the calculation. The cause of this discrepancy is uncertain at present.

10.4 PHOSPHORUS

The distribution of the phosphorus species, Figure 62, exhibit patterns very similar to those of the nitrogen species. Total phosphorus is approximately constant throughout the year. During the summer growth period, there is an increase in phytoplankton associated phosphorus and an equivalent decrease in available phosphorus. Unavailable phosphorus is increased due to respiration and excretion. In late fall and winter, phytoplankton phosphorus decreases gradually as it becomes unavailable phosphorus which is recycled to available phosphorus that increases in the absence of uptake.

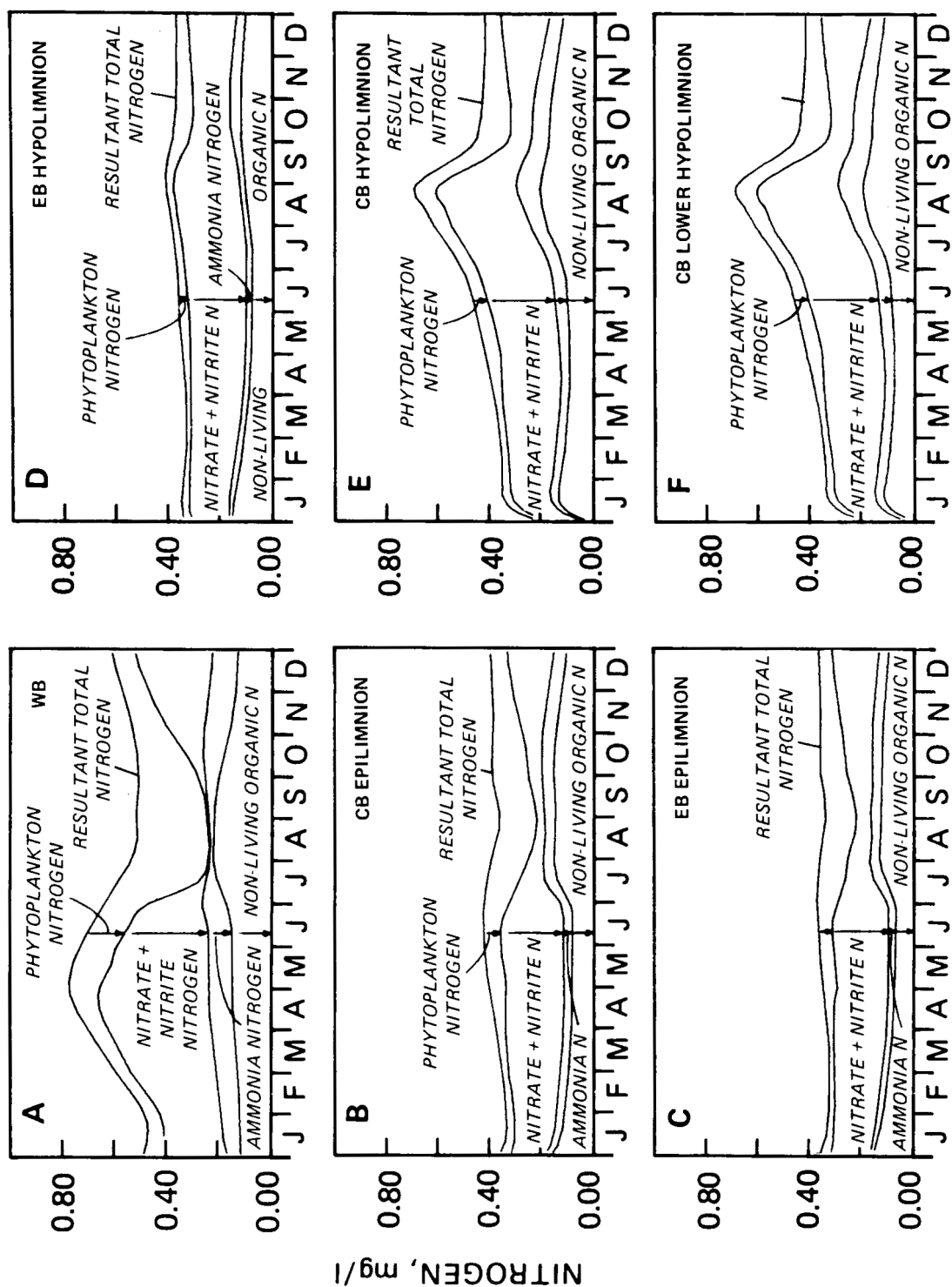


Figure 55. Calculated nitrogen species distribution. Non-living organic nitrogen, ammonia nitrogen, nitrate plus nitrite nitrogen, phytoplankton nitrogen and the resultant total nitrogen are shown.

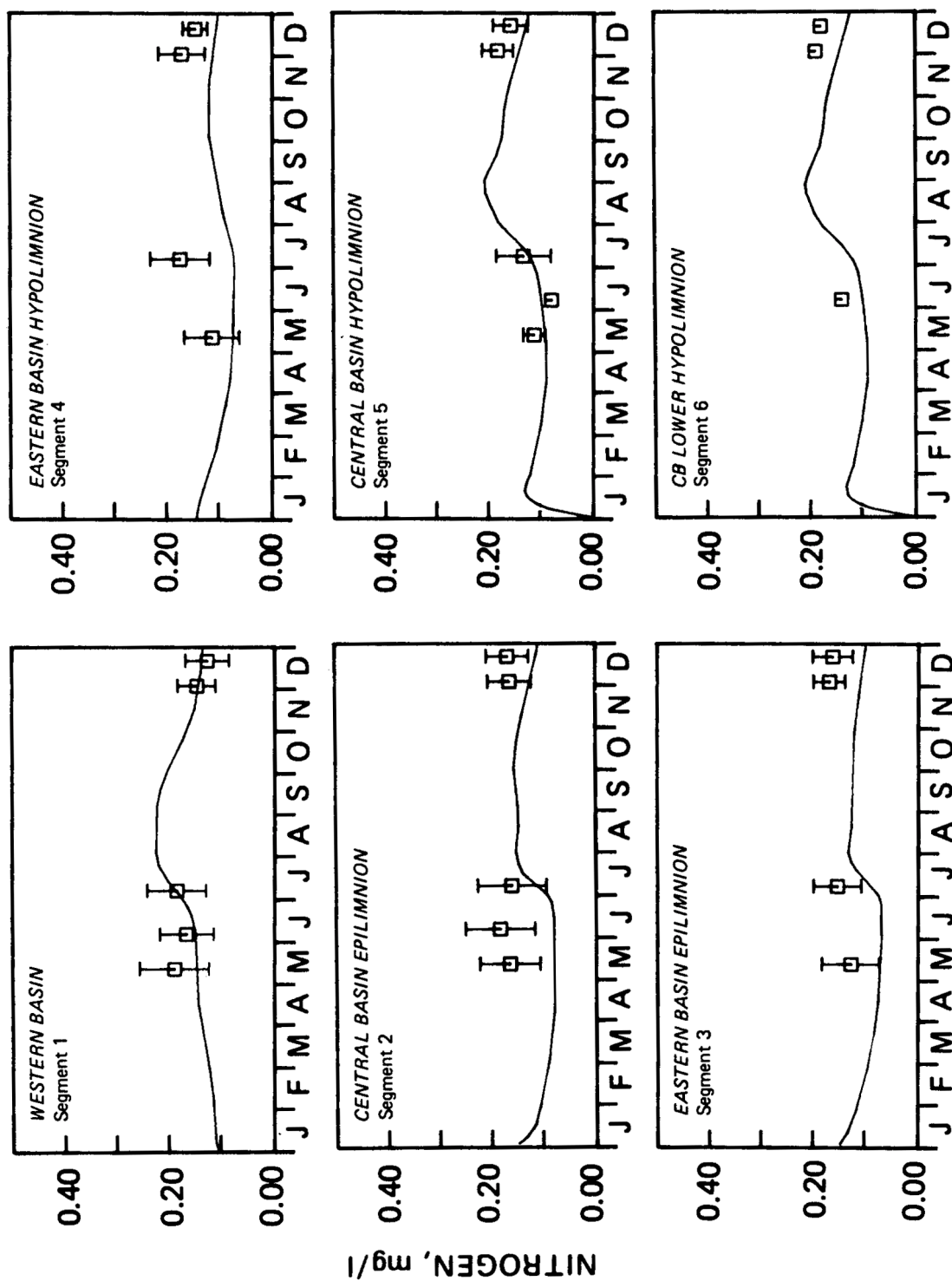


Figure 56. Lake Erie model calibration for organic nitrogen (mg N/l), 1970. Profiles are the sum of the computed phytoplankton and non-living organic nitrogen.

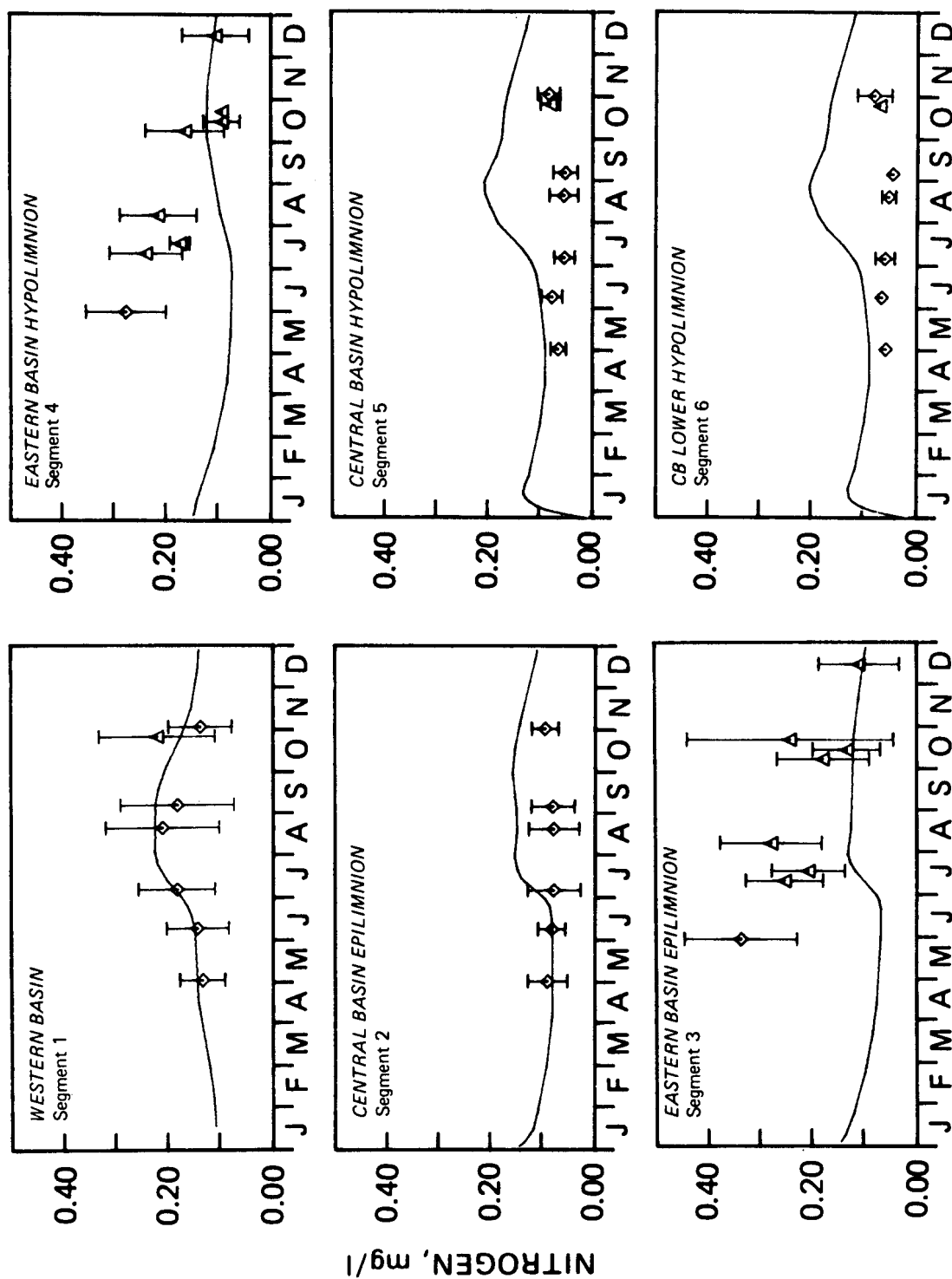


Figure 57. Lake Erie model calibration for organic nitrogen (mg N/l), 1973-1974. Profiles are the sum of the computed phytoplankton and non-living organic nitrogen.

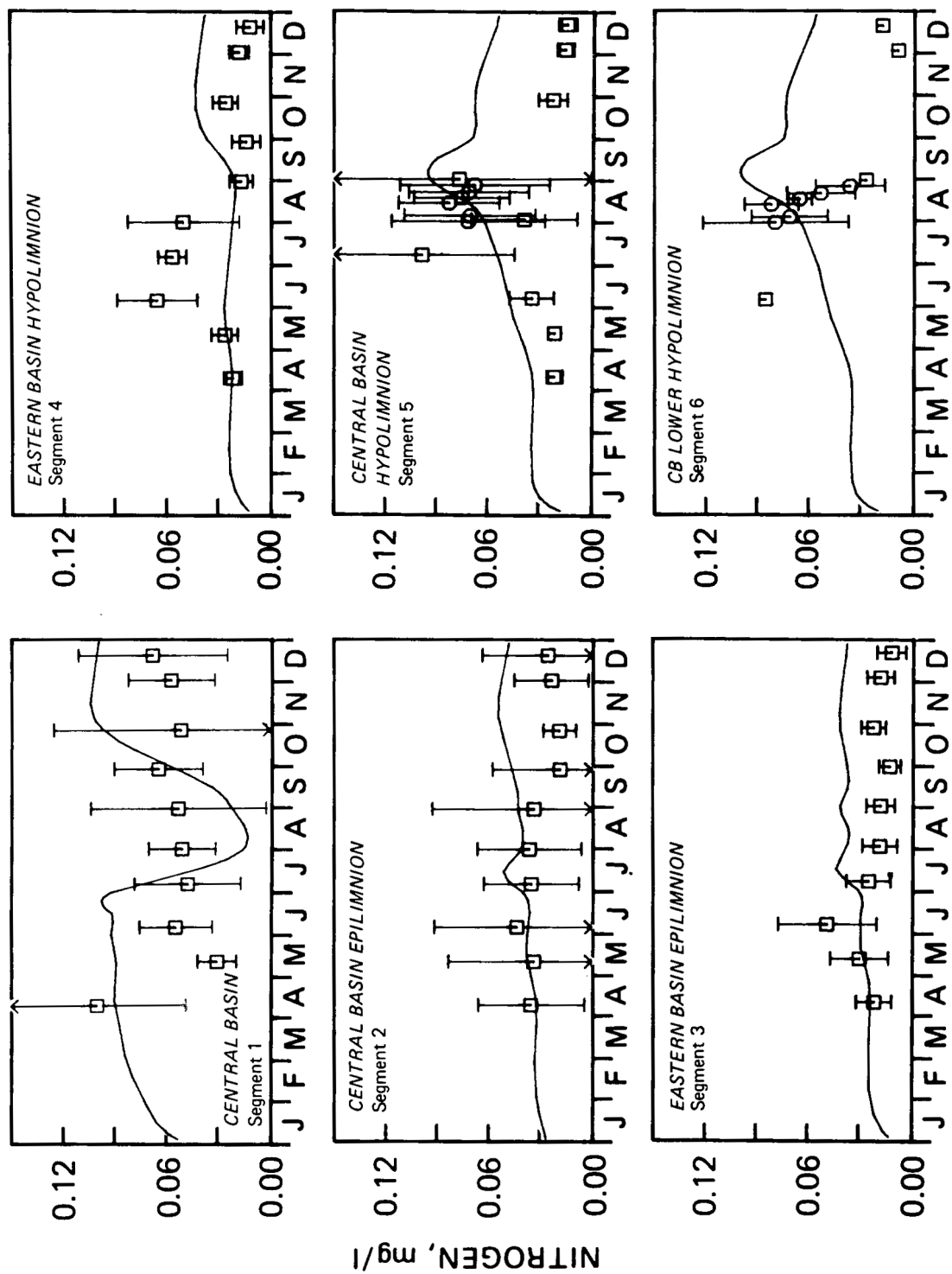


Figure 58. Lake Erie model calibration for ammonia nitrogen (mg N/l), 1970.

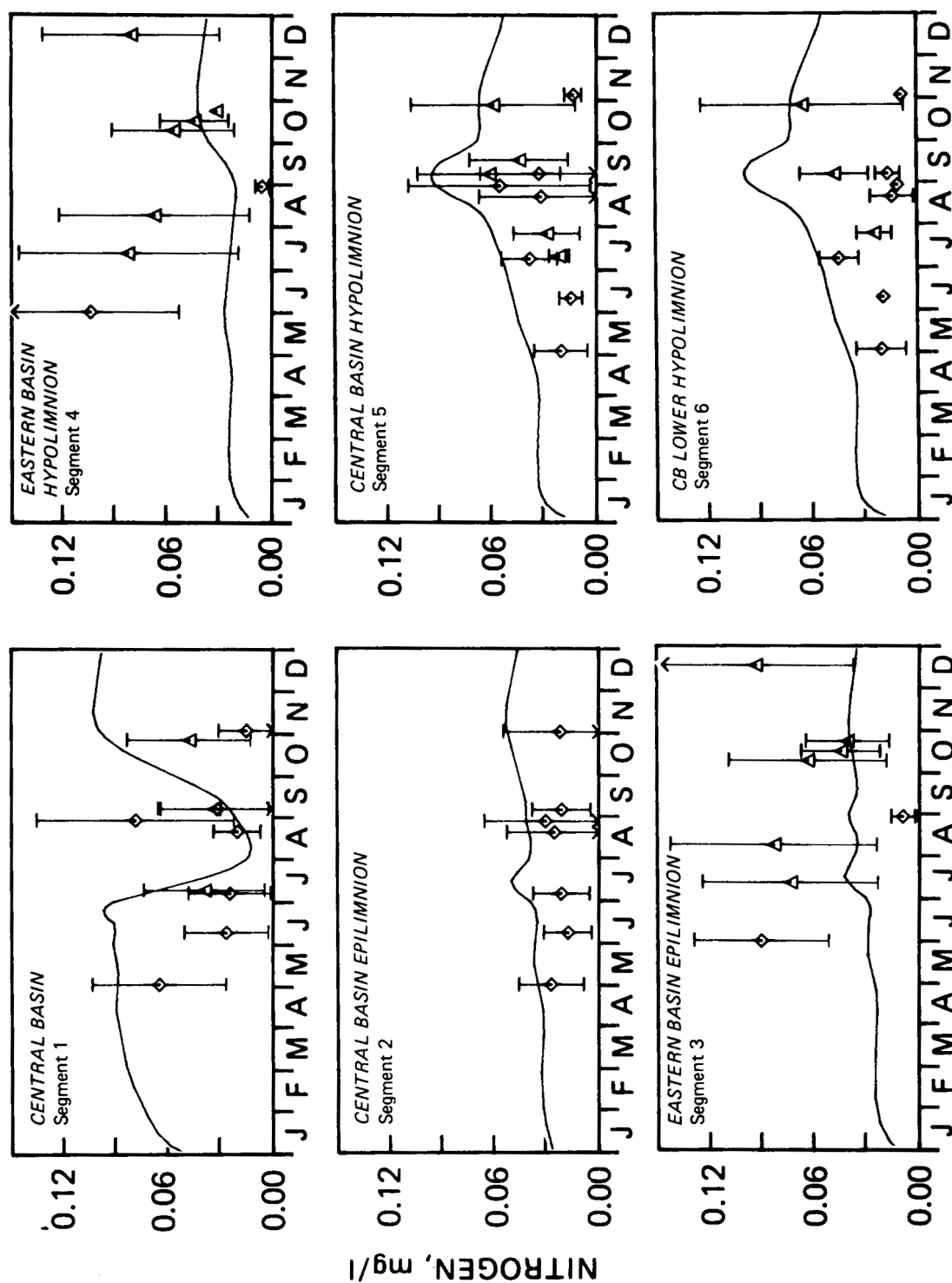


Figure 59. Lake Erie model calibration for ammonia nitrogen (mg N/l), 1973-1974.

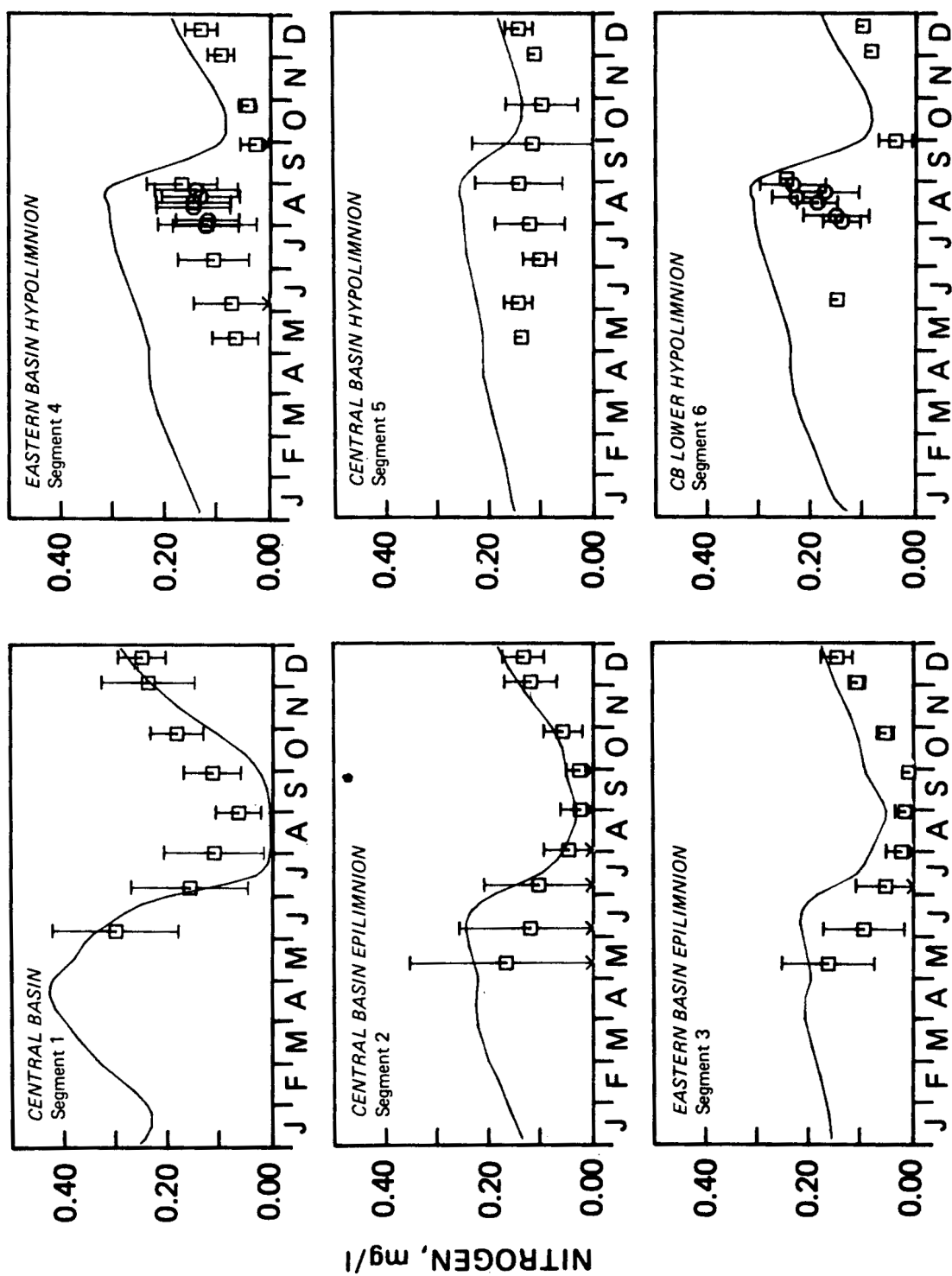


Figure 60. Lake Erie model calibration for nitrate nitrogen (mg N/l), 1970.

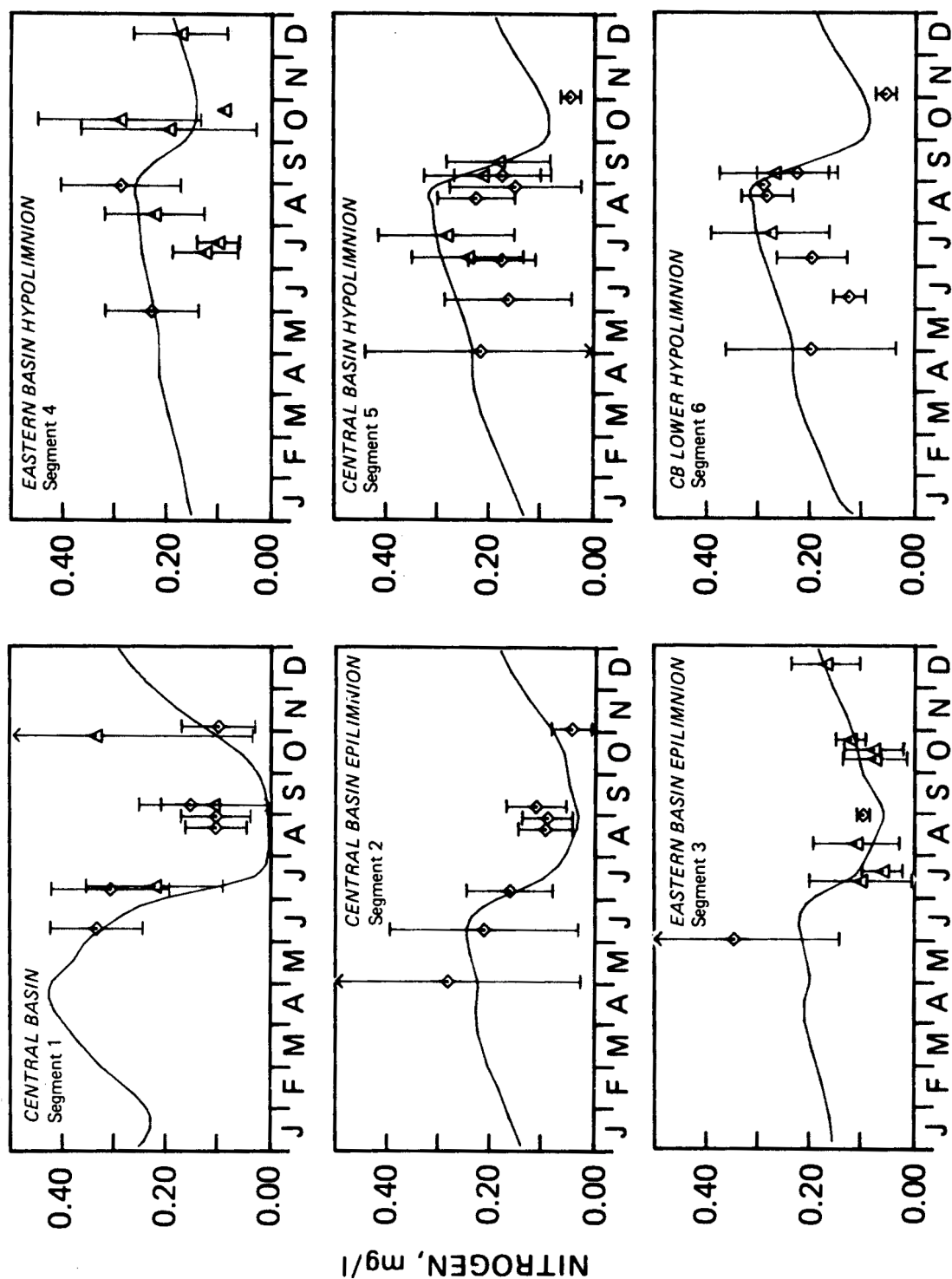


Figure 61. Lake Erie model calibration for nitrate nitrogen (mg N/l), 1973-1974.

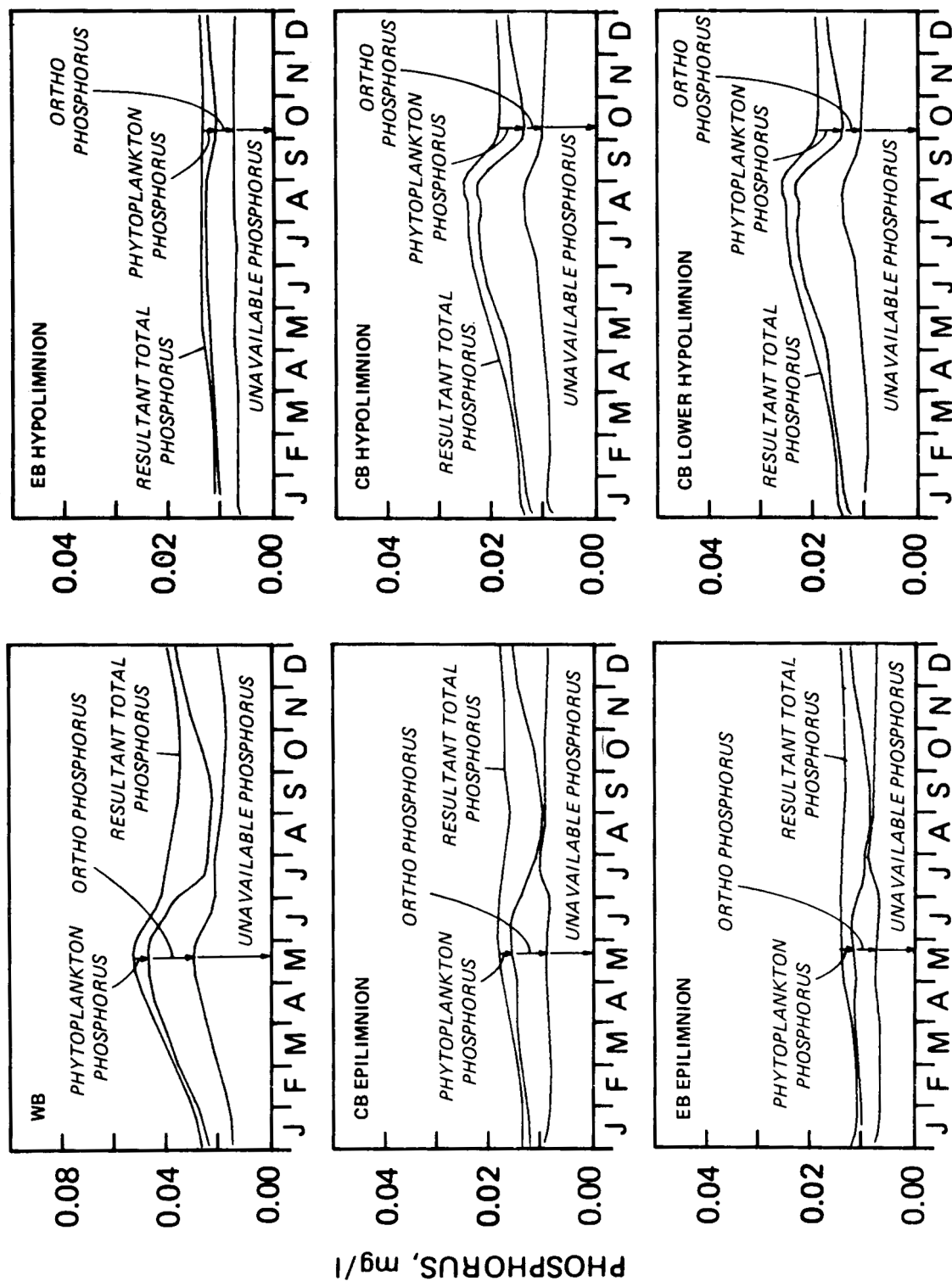


Figure 62. Calculated phosphorus species distribution. Unavailable phosphorus, orthophosphorus, phytoplankton phosphorus and the resultant total phosphorus are shown.

The results of the calibration for total phosphorus is shown in Figures 63 and 64. A discrepancy is apparent in the 1970 data. In the western basin, the data indicate high total phosphorus concentrations in the spring and fall. In all of the other segments, high total phosphorus concentrations appear consistently in late fall. This trend in the data is not calculated to occur, i.e., there is no mechanism incorporated in the model to account for this observation. A hypothesis for these high total phosphorus concentrations is that they are due to wind resuspension of bottom material. Figure 44 shows the monthly average wind velocity for the western, central and eastern basins over the year. Note that in all three basins the wind velocity is highest in the spring and fall. It is possible that these high winds stir the bottom sediments bringing particulate phosphorus into the water column. The fact that the total phosphorus distribution for the rest of the year is simulated properly indicates that the high phosphorus concentrations in late fall do not contribute to the following year's dynamics. If wind resuspension is the cause, then it is likely that the material will have settled again by the next spring. Since the total phosphorus mass balance is essentially correct from May to October, which is the critical time for phytoplankton growth and dissolved oxygen depletion, it appears that the wind induced resuspension is not significant mechanism for supplying phosphorus to the phytoplankton. The 1973-1974 data for total phosphorus are more variable and the trends are more difficult to discern. This is especially true for the eastern basin where the midsummer erratic data are suspect.

The calibration for orthophosphorus is shown in Figures 65 and 66. The observed summer uptake is reproduced by the calculation in the three surface segments but the spring concentrations are slightly higher than observed. A substantial discrepancy occurs in the central basin hypolimnion. The spring data indicate concentrations of about 1-2 $\mu\text{g PO}_4\text{-P/l}$ while the calculation yields concentrations in the range of 6-8 $\mu\text{g PO}_4\text{-P/l}$. For this same time period, the

central basin epilimnion calculations are close to the data. The data indicate that the orthophosphorus during the spring is higher in the epilimnion than in the hypolimnion. The calculation yields epilimnion and hypolimnion concentrations of close to the same magnitude due to the large exchange between the epilimnion and hypolimnion since stratification has not started and the lake is fairly isothermal. Examination of the temperature calibration plot, Figure 36, Chapter 8 shows that the fit to data is very good, especially at this time. Apparently, a vertical orthophosphorus gradient exists without an accompanying temperature gradient. The present structure is unable to simulate this feature and, therefore, the hypolimnion calculation of orthophosphorus is high. Fortunately, this discrepancy appears to be less significant for the phytoplankton dynamics in the epilimnion. During the summer growth period, the basin is stratified and the interaction between the hypolimnion and epilimnion is limited. At overturn, when the phosphorus in the hypolimnion is transported into the epilimnion, the calculated concentration agree with the observed concentration and the proper mass is transported.

However, the discrepancy is disturbing since it indicates that a significant mechanism is operating in the central basin hypolimnion that is not incorporated in the calculations. The results suggest that either the recycle in the hypolimnion is slower than that employed in the calculations, or that there exists a selective removal mechanism for orthophosphorus. Perhaps an adsorption mechanism is operating which binds the recycled orthophosphorus to particulates. Since regeneration of reduced iron and manganese occurs during anoxia, these metals would oxidize to form amorphous oxides and hydroxides which have a high adsorption capacity. This might prove a sufficient quantity of particles for this mechanism to be significant.

10.5 SILICA

The calibration results for reactive silica are shown in Figure 67. The data for the western

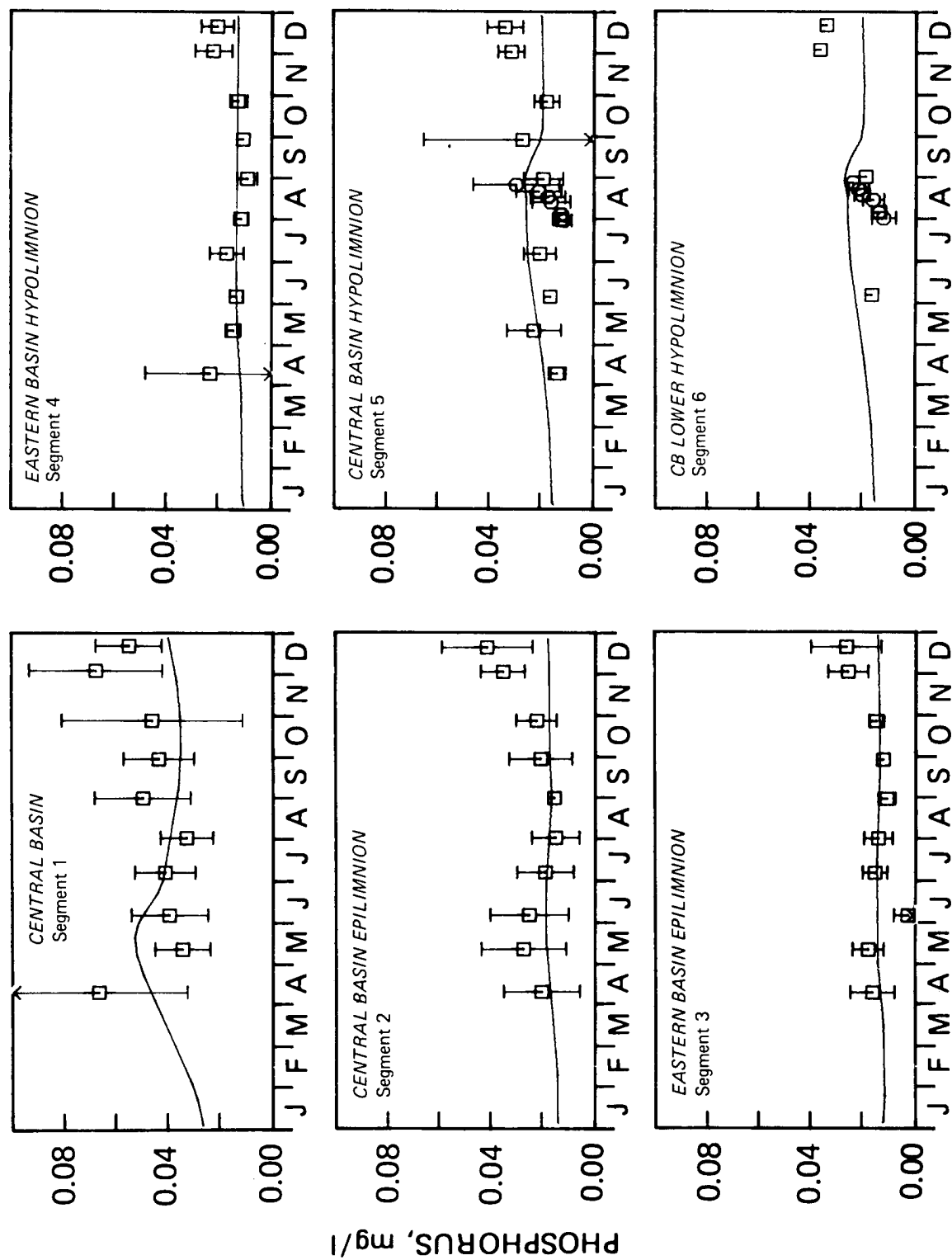


Figure 63. Lake Erie model calibration for total phosphorus (mg $\text{PO}_4\text{-P/l}$), 1970.

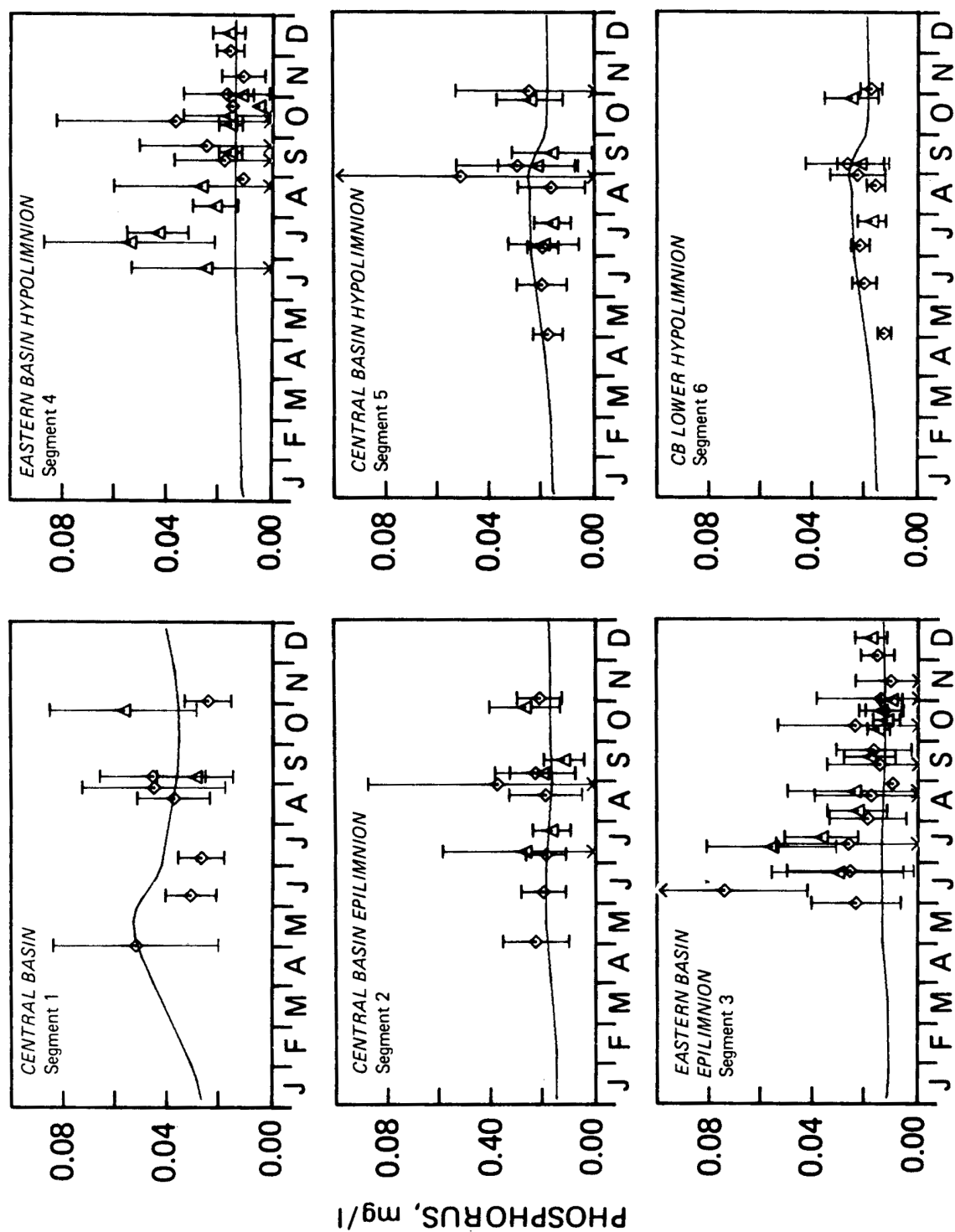


Figure 64. Lake Erie model calibration for total phosphorus (mg $\text{PO}_4\text{-P/l}$), 1973-1974.

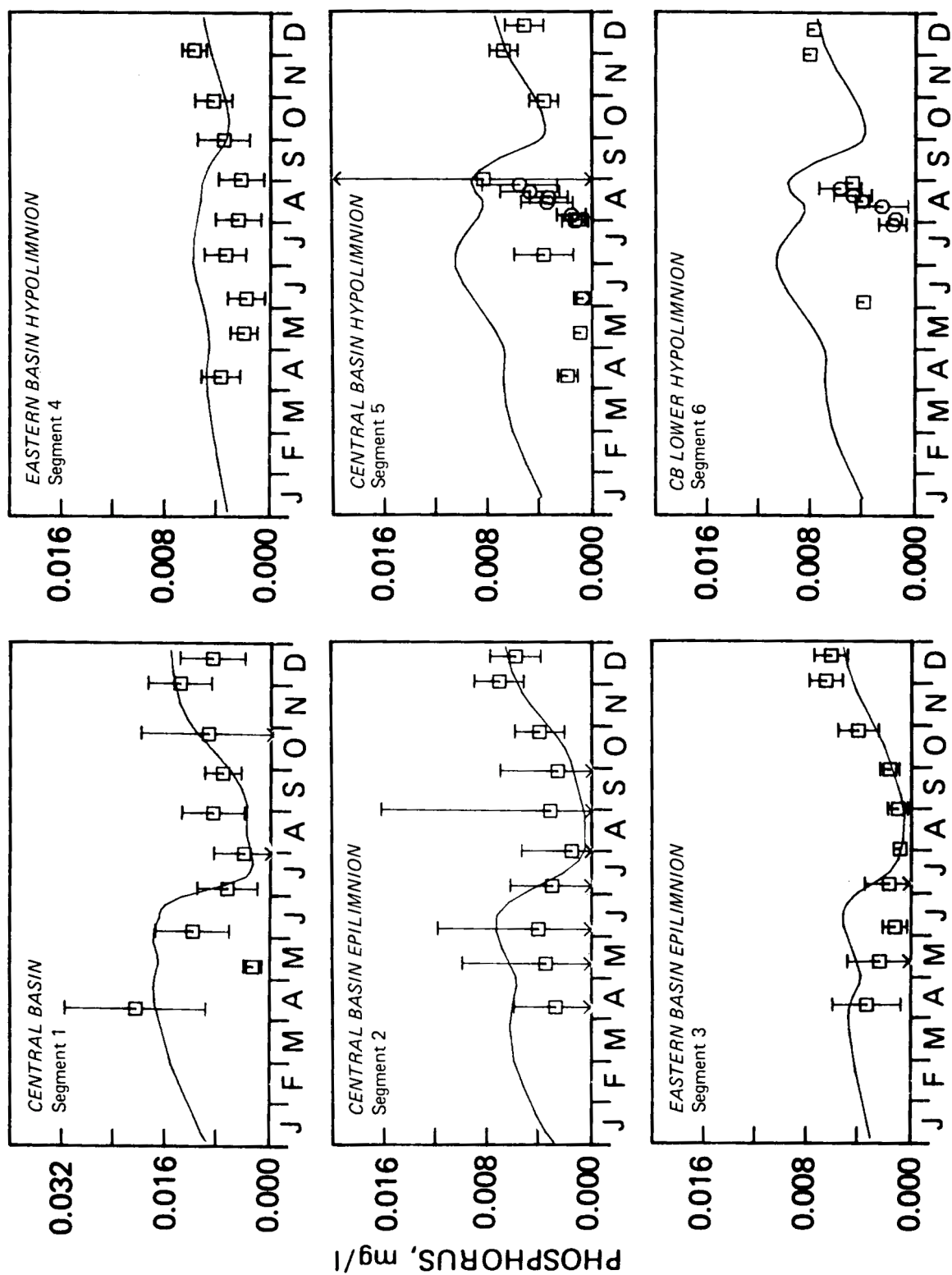


Figure 65. Lake Erie model calibration for orthophosphorus (mg $\text{PO}_4\text{-P/l}$), 1970.

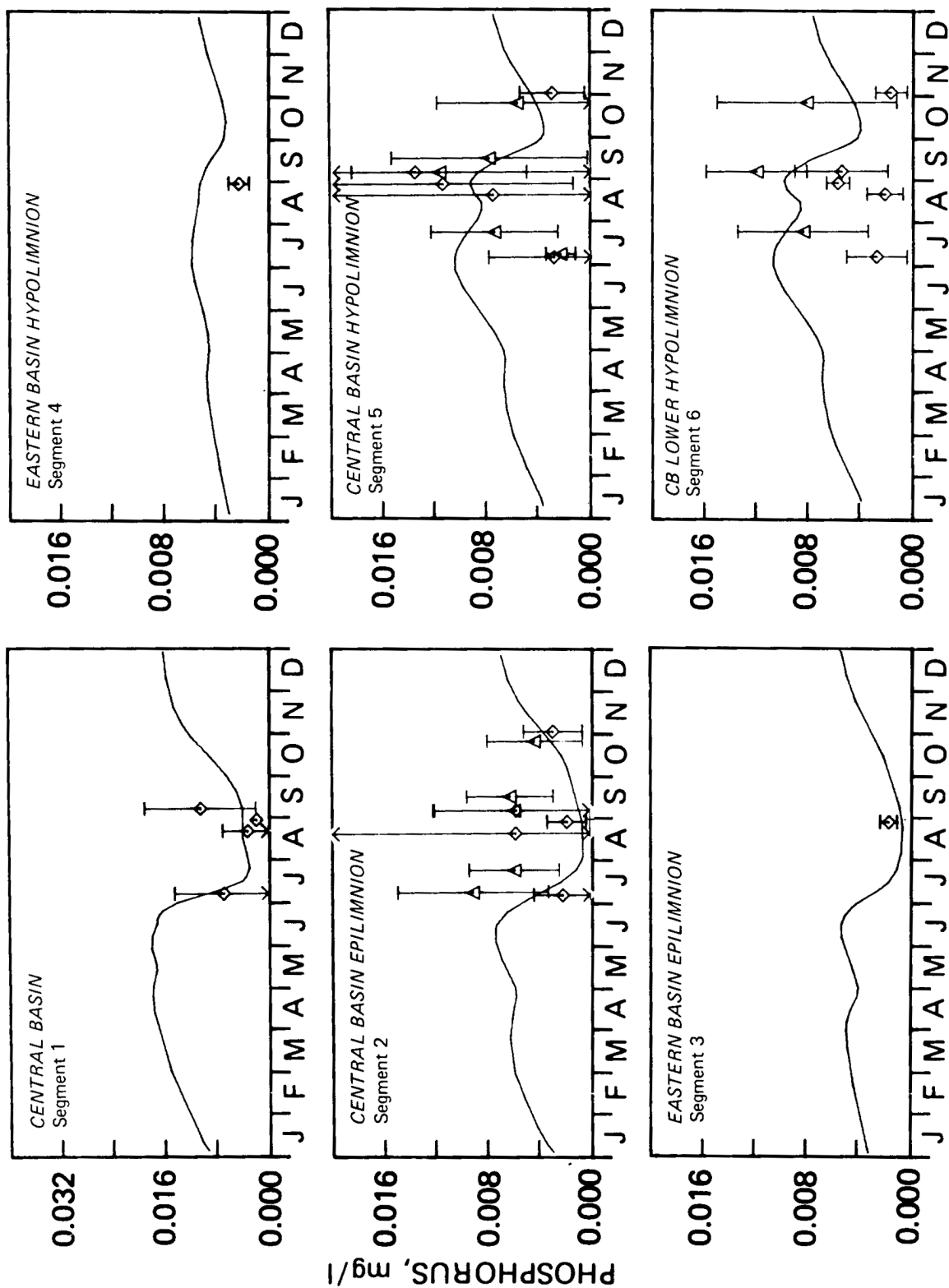


Figure 66. Lake Erie model calibration for orthophosphorus (mg $\text{PO}_4\text{-P/l}$), 1973-1974.

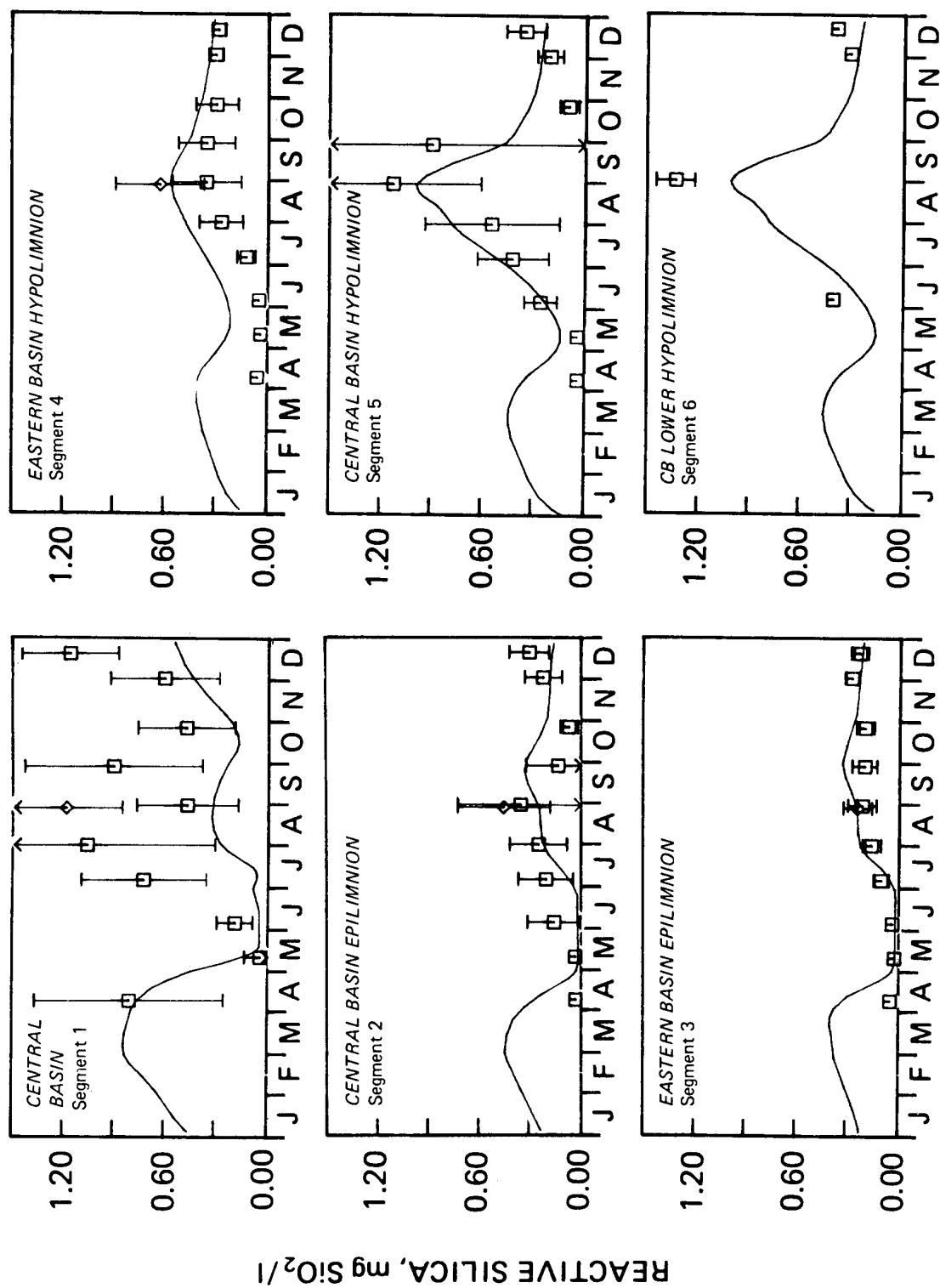


Figure 67. Lake Erie model calibration for reactive silica (mg SiO₂/l), 1970.

basin appears to confirm the early spring uptake by the diatoms. The summer and fall data are quite variable and scattered. This may reflect a highly variable loading. Since total silica data is lacking, there is no confirmation from a total mass balance calculation. The results for the central and eastern basin epilimnion are remarkably consistent and reproduce the observed patterns: the spring uptake and the subsequent regeneration during the summer and fall. The eastern basin hypolimnion concentrations are larger than observed for an as yet uncertain reason. The central basin hypolimnion results reproduce the regeneration of silica during anoxia and the reduction during overturn as the silica rich bottom waters mix with the silica poor surface waters.

10.6 SECCHI DISK DEPTH

Figure 68 gives the western, central and eastern basin calibration results for Secchi disk depth. In all three basins, the calculation follows the data very well. Note that the Secchi depth is low in spring and fall and high in summer. This indicates much higher turbidity in the spring and fall. As discussed previously with regard to phosphorus resuspension, winds are highest in spring and fall. The effect of the winds is incorporated into the Secchi disk depth calculation as discussed previously.

10.7 ZOOPLANKTON CARBON

The results of the calibration for zooplankton carbon are shown in Figure 69. The data used, reported by Watson (1974, 1976), is part of the 1970 CCIW dataset. It represents hauls from 50 meters to the surface or from two meters above the bottom to the surface at stations with a depth less than 40 meters. The calculation has been adjusted accordingly by weighting the surface and bottom segment calculations. In all three basins, the timing of the model is consistent with the data. The zooplankton peak is earliest in the western basin and latest in the eastern basin. This is due to the temperature differences and resultant phytoplankton growth timing between the basins. The zooplankton begin to grow after

the diatom bloom. The growth of the non-diatoms is initially inhibited due to the presence of the zooplankton. The total zooplankton population is decreasing by midsummer in all three basins even though the carnivorous zooplankton increase until August.

The dynamics of the zooplankton populations are shown in Figure 70. Respiration exceeds the growth rate until phytoplankton populations develop. This occurs first in the western basin and later in the eastern basin. As the herbivorous populations develop, the carnivorous commence growth and exert grazing pressure which exceeds the growth rate and decreases the herbivorous population. The assimilation and grazing rate reduction factors are smallest in the western basin where chlorophyll concentrations are largest. This reduces the absolute grazing and assimilation rates in the western basin relative to the eastern basin. A similar effect is postulated for Saginaw Bay and Lake Huron (Di Toro and Matystik, 1979). As pointed out in that study, the zooplankton calculations are very sensitive to the parameter values used in the kinetics. Thus, the zooplankton results must be regarded as preliminary, particularly in view of the sparcity of zooplankton data.

10.8 CARBON

Because of the importance of organic carbon oxidation in the dissolved oxygen balance in the central basin, both total inorganic carbon and non-living organic carbon are included as state variables in the calculation. Data for both these variables are not available. However, data for alkalinity, pH and BOD are available. These variables are used, together with observed primary production, in order to calibrate the inorganic and organic carbon kinetics.

The results for pH and alkalinity are shown in Figures 71 and 72. The alkalinity calibration is not wholly satisfactory, although the discrepancies are emphasized due to the plotting scales employed. Uncertainties in loading information contribute to the difficulties.

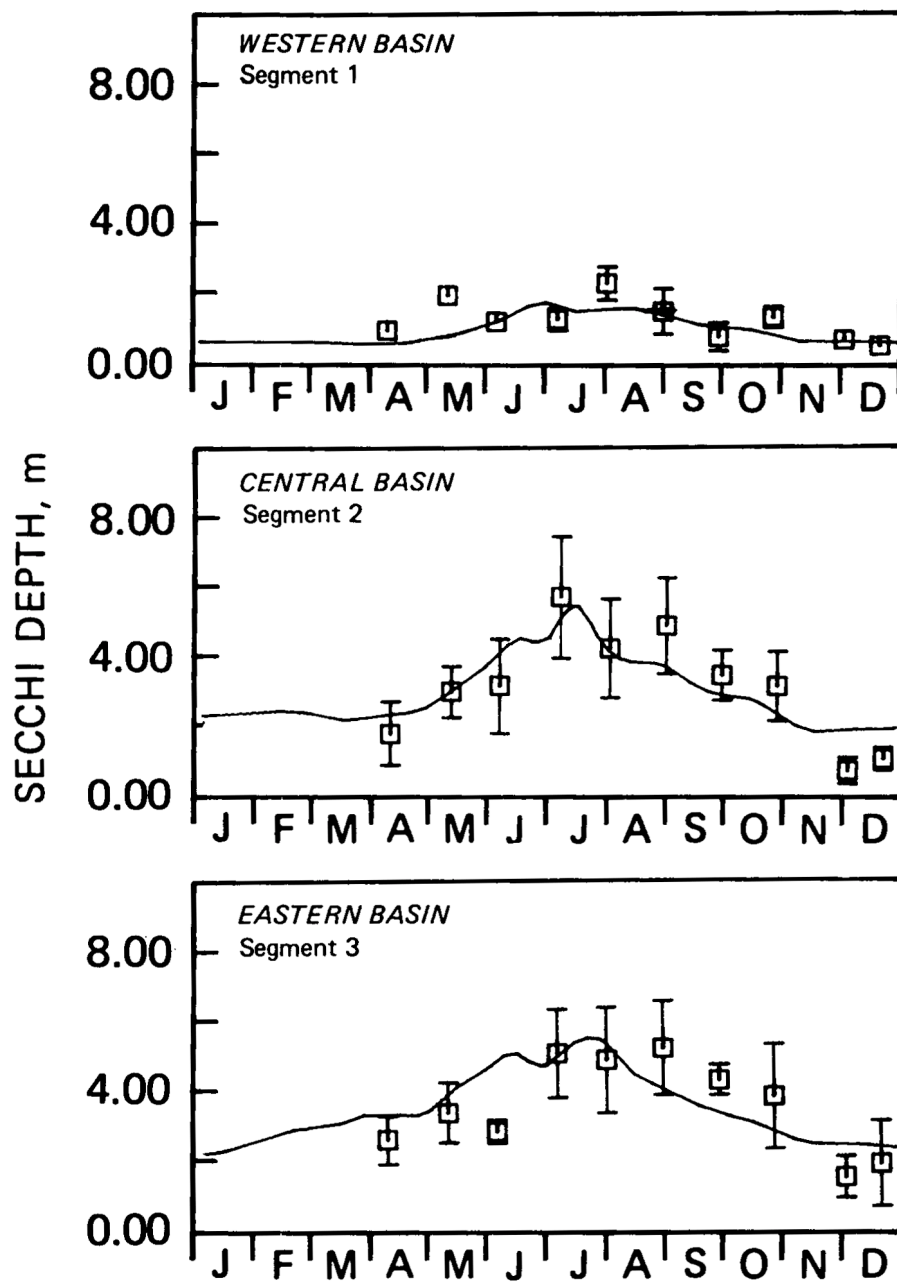


Figure 68. Lake Erie model calibration for Secchi depth (m), 1970.

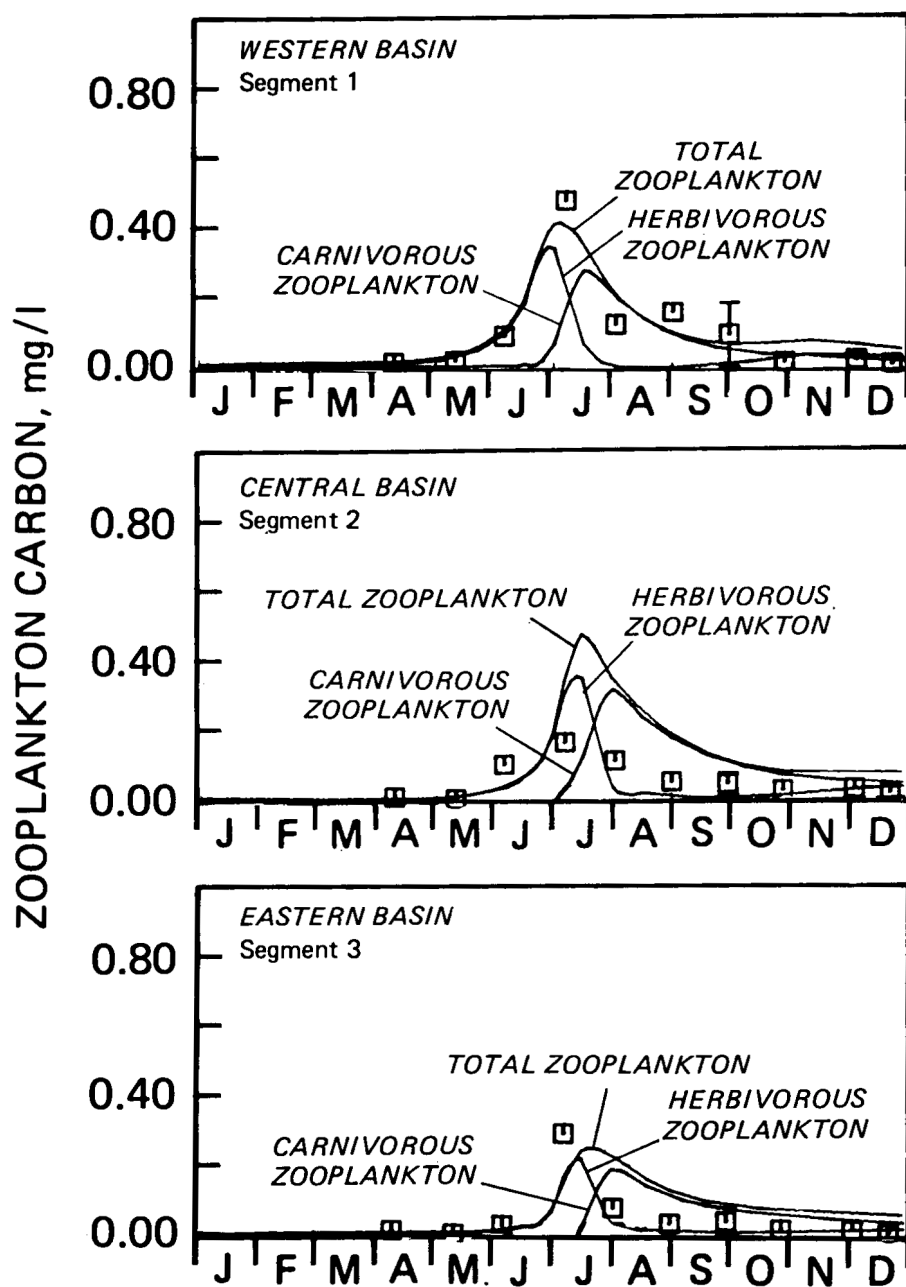


Figure 69. Lake Erie model calibration for zooplankton carbon (mg/l), 1970.

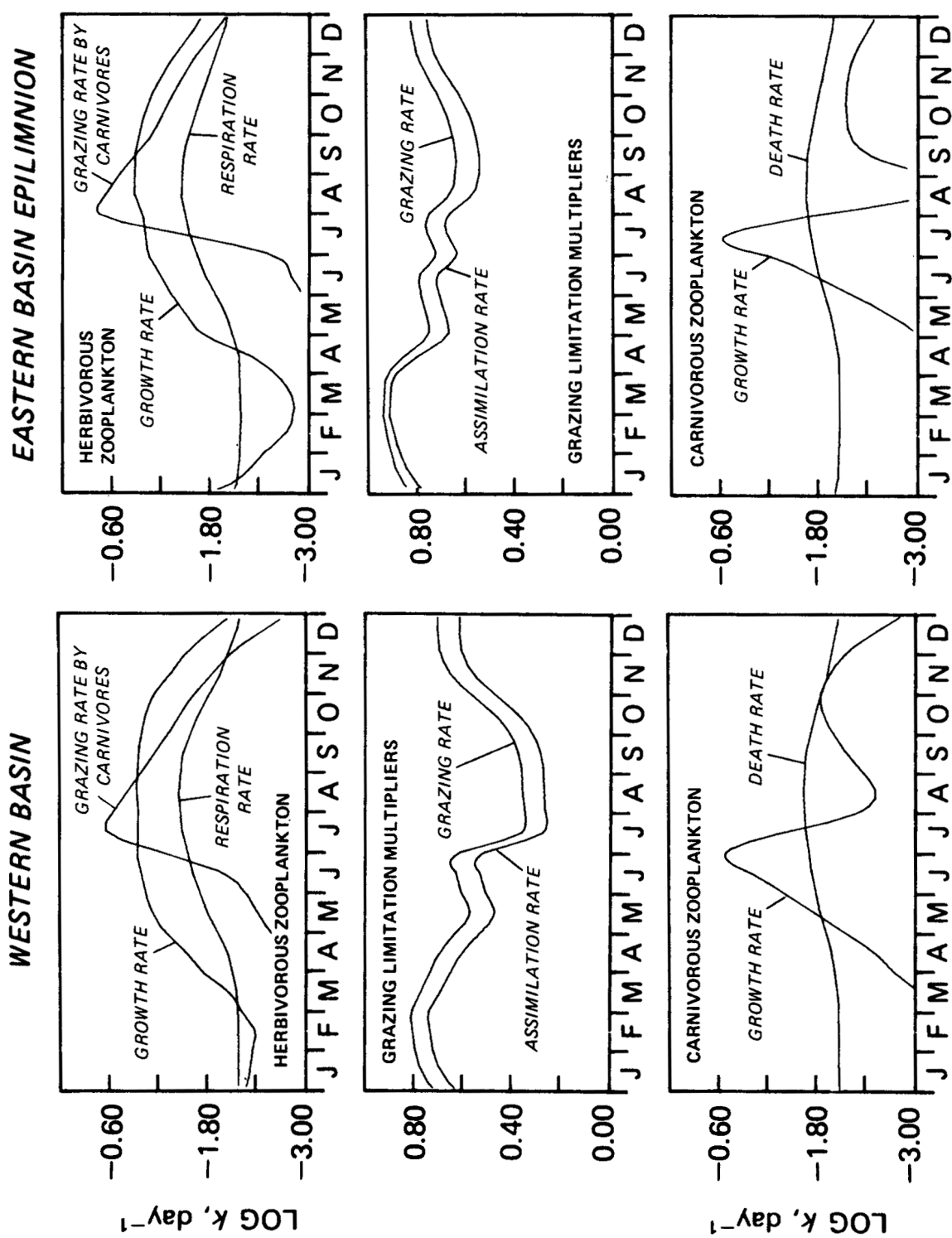


Figure 70. Dynamics of zooplankton population for western basin (left) and eastern basin epilimnion (right). The curves are the calculated rates from the appropriate kinetic expressions.

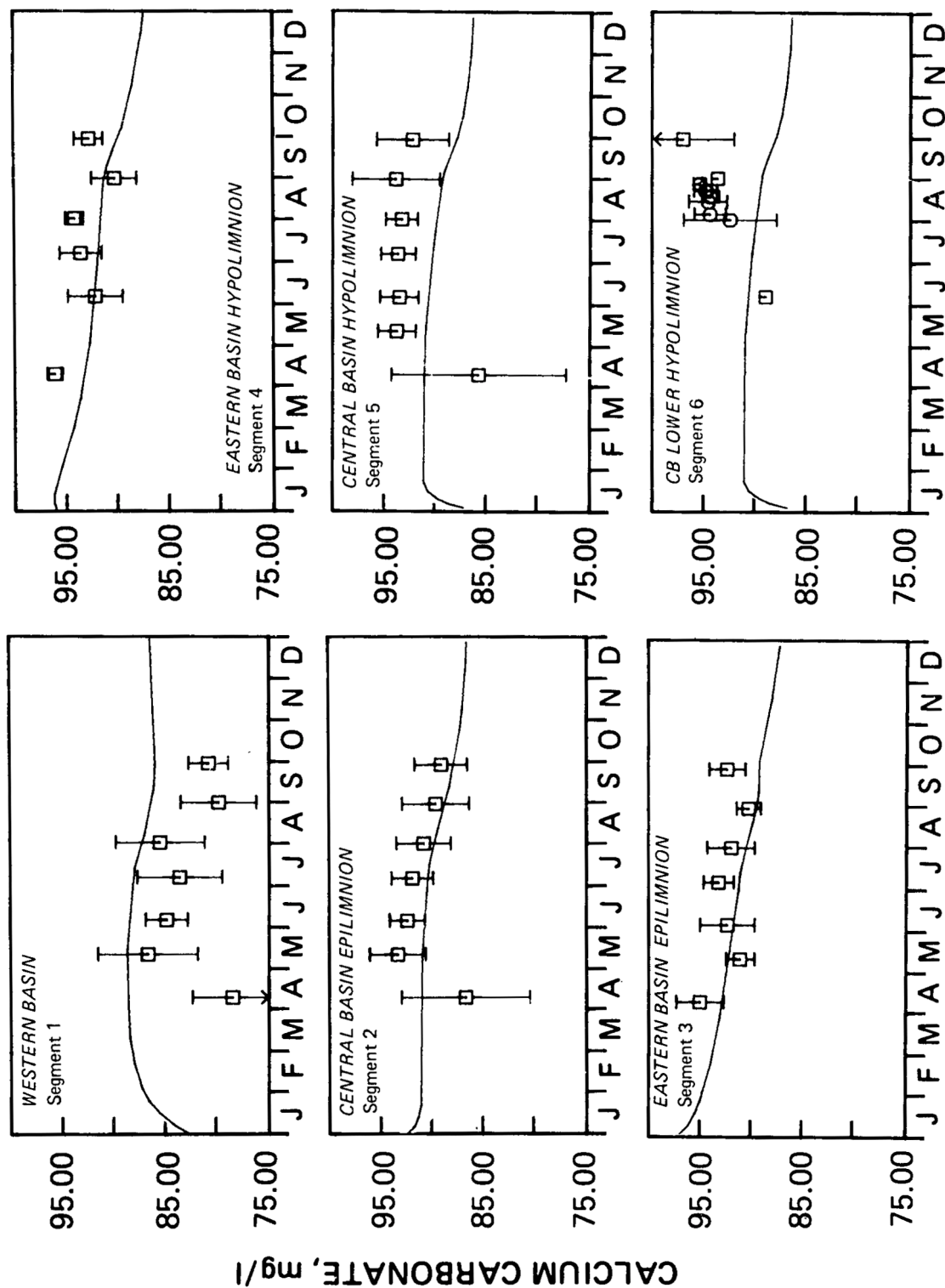


Figure 71. Lake Erie model calibration for alkalinity, expressed as mg/l, of calcium carbonate equivalents, 1970.

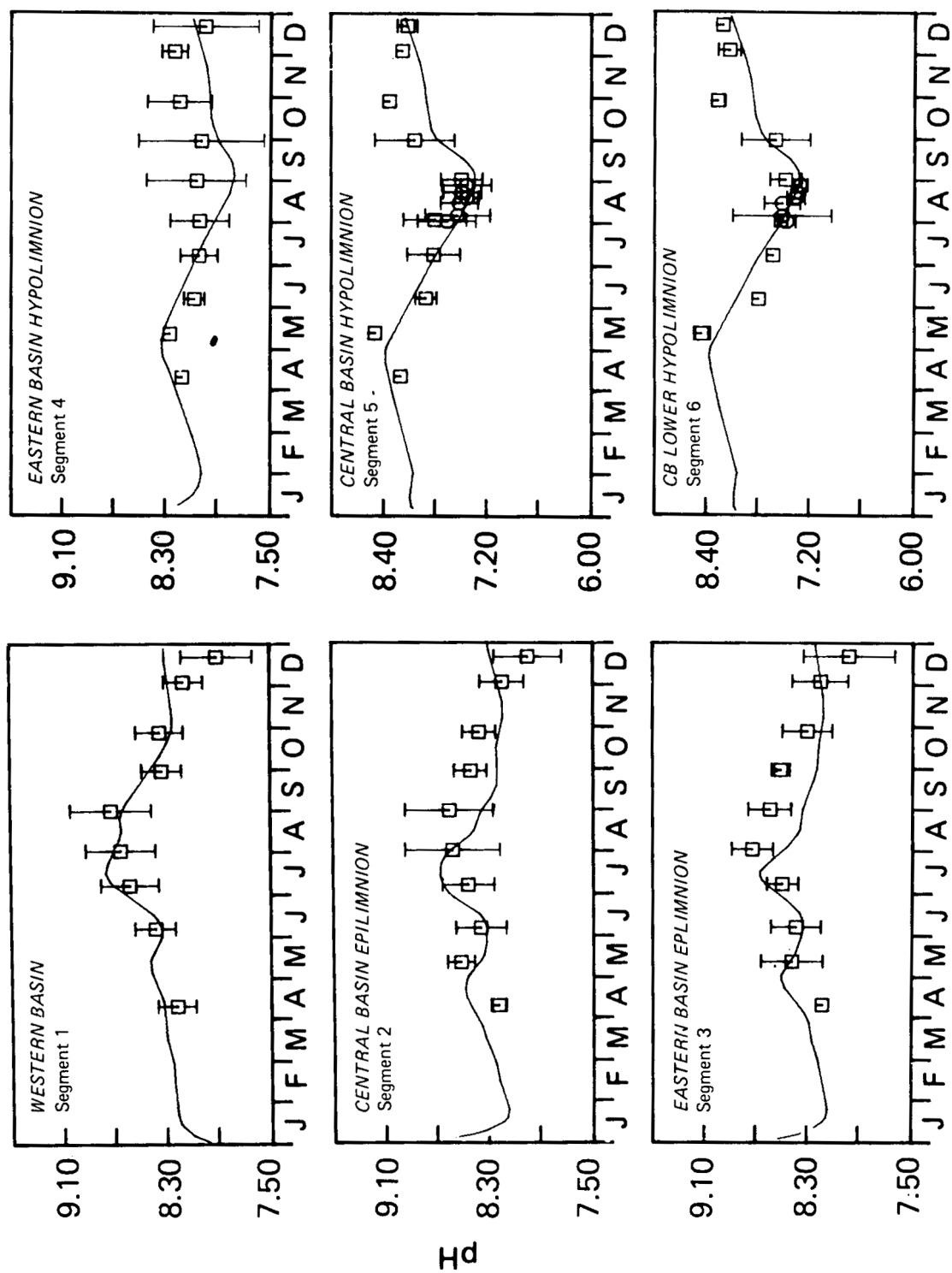


Figure 72. Lake Erie model calibration for pH, 1970.

However, alkalinity is not of direct concern; it is only useful for the computation of pH. The alkalinity inaccuracies are not significant since they amount to only a few percent error and do not severely impact the pH calculation. The pH results are quite good for the western basin and are reasonable for the central and eastern basin epilimnia. The central basin hypolimnion results are quite dramatically reproduced.

In the epilimnion, there is an increase in pH during the summer due to the uptake of inorganic carbon by the phytoplankton. In the hypolimnion, there is a decrease in pH during the summer due to an increase in inorganic carbon resulting from a combination of the respiratory oxidation of non-refractory organic carbon, phytoplankton respiration, and the sediment release of inorganic carbon. The rapid increase of pH in the hypolimnion in late summer-early fall is due to overturn. Again, the calculated mixing is not quite rapid enough.

10.9 PRODUCTION AND RESPIRATION RATES

The calibration calculations are a method of inferring the kinetic constants of the relevant rate expression from measurements of the state variables. This indirect procedure is necessary because direct measurements of all the relevant rates of production, respiration, and recycle are not available and, in some cases, impractical. However, two conventional measurements of rates are: primary production and BOD. As pointed out in the kinetics section, gross primary production corresponds to the rate of algal synthesis while net primary production subtracts the endogenous respiration rate. Since both these reaction rates are being evaluated in the calculation, it is a simple matter to compare these to the observed rates. Figure 73 presents the results. The observations are shipboard ^{14}C measurements. The four-fold decrease in primary production from the western to the eastern basin is mainly due to the chlorophyll differences. The calculated results are in agreement with observations with the exception of the late fall measurements which indicate

more production is occurring than is being calculated.

The two major classes of sinks of dissolved oxygen in the hypolimnia of lakes are the respiratory processes in the water column and the sediment. For Lake Erie, the former are dominated by algal respiration and organic carbon oxidation and a direct calibration of these rates is of major importance. Fortunately, a series of BOD measurements were made in 1967 which form the basis of this calibration. A BOD measurement can be regarded as a direct experimental determination of the total water column respiration exerted in five days in oxygen units. Since the relevant reaction rates are being evaluated in the calculation, a direct comparison is possible. The algal respiration, and detrital organic carbon oxidation rates are adjusted to 20°C , the incubation temperature of the BOD measurement, and are multiplied by five days and compared to observation. The result is shown in Figure 74. Both epilimnia and hypolimnia observations are in accord with the calculation. This is significant in the central basin hypolimnion since the water column components of the oxygen sinks are of major importance in the oxygen balance.

10.10 SEDIMENT CALIBRATION

The other major oxygen sink in the central basin is that generated by the oxidation of the oxygen equivalents which result from the decomposition of sedimentary organic carbon. The magnitude of the flux of oxygen demand is determined by the incoming flux of detrital and algal carbon; the sedimentation velocity and interstitial water dispersion coefficient; and the rate constants for the algal and detrital organic carbon decomposition reactions. For the steady-state case, the relationships between these parameters and flux of oxygen equivalents is given by Equation (63). The interstitial ammonia concentration and flux is similarly determined, Equations (45) and (46), by the incoming fluxes of algal and detrital nitrogen. Hence, it is important that these fluxes be reproduced by the computation.

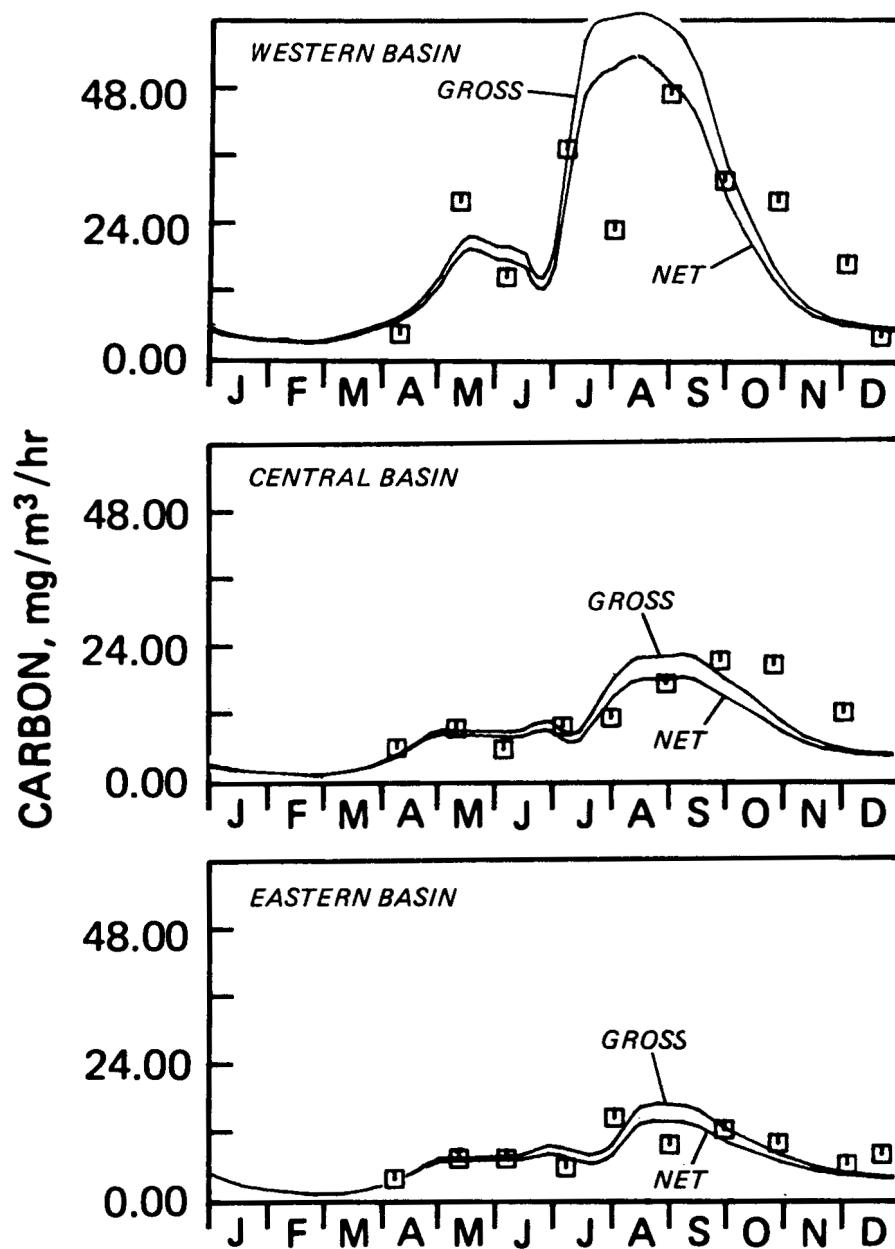


Figure 73. Lake Erie model calibration for the rate of primary production expressed as mg/m³/hr of carbon, 1970. Observations are shipboard ¹⁴C measurements.

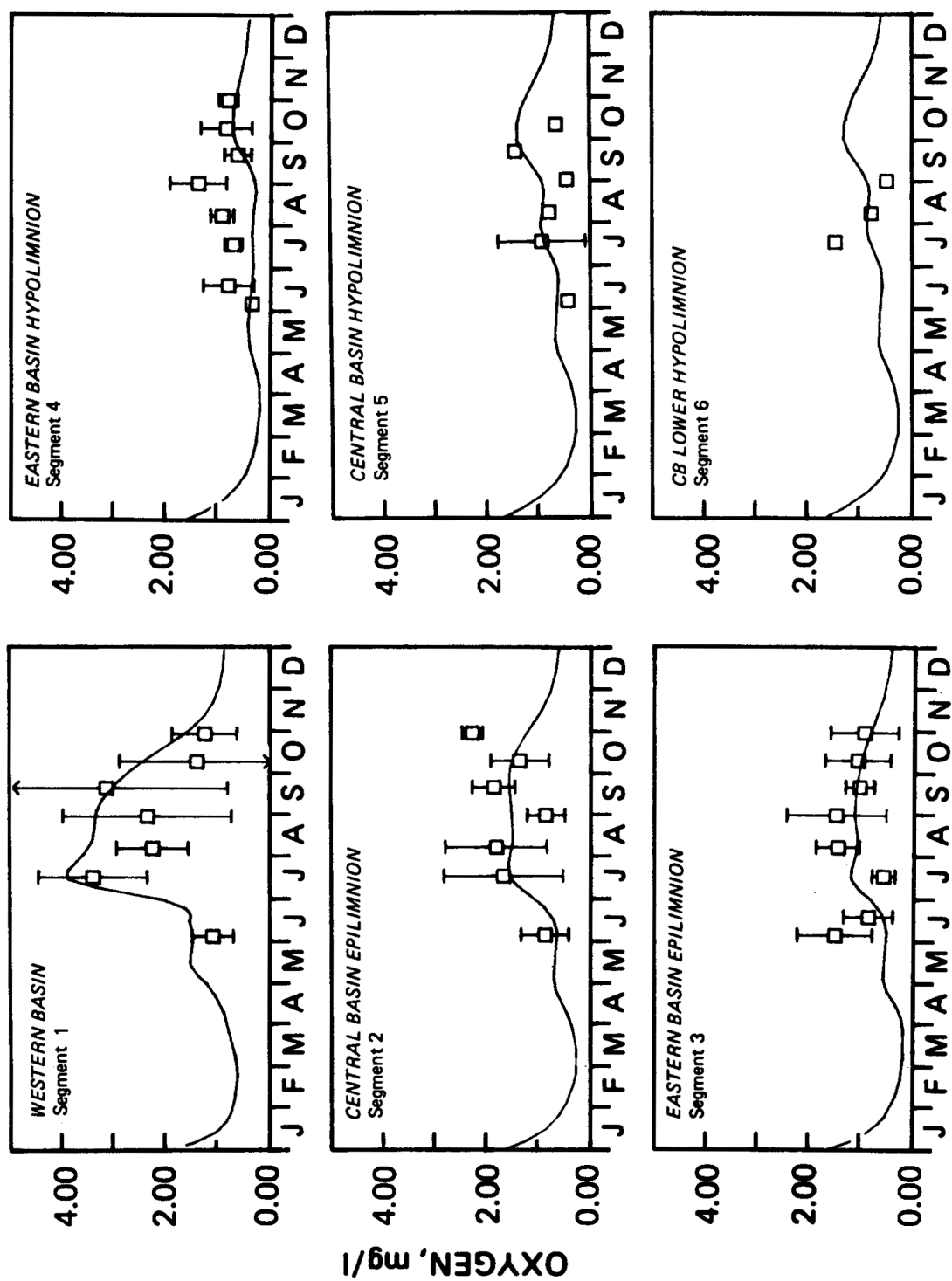


Figure 74. Lake Erie model calibration for biochemical oxygen demand ($\text{mg O}_2/\text{l}$), 1967.

The fluxes to the sediment are determined by the aqueous concentration of total chlorophyll, organic nitrogen and organic carbon and their settling velocities (0.1 m/day and 0.2 m/day, respectively). A comparison of computed and estimated sedimentation fluxes are shown in Table 22. The computed fluxes are simply the product of the yearly average concentrations and the appropriate settling velocity; the estimates are from dated cores (Kemp *et al.*, 1976), three in the western basin, two in the central basin, and one in the eastern basin. The computed western and central basins flux are slightly lower for organic carbon and higher for nitrogen and phosphorus than the mean of the estimates from the cores. The eastern basin estimate appears to be unrealistically high for the three constituents. The transport parameters of

importance are the sedimentation velocity and the dispersion coefficient. Table 23 lists the estimates. The sedimentation velocity used is the mean of that determined from dated cores (Kemp *et al.*, 1976, 1974). The dispersion coefficient is in the high range of the estimates from interstitial radionuclides profiles (Lerman and Lietzke, 1975). As can be seen from Equation (63), the critical dimensionless parameter group is wH/E' which is much smaller than one for even the smaller estimates of the dispersion coefficient. This implies that, for the five cm layer at least, dispersion is not the rate limiting step in the generation of the flux.

The reaction rate constants for the decomposition of algal and detrital particulates determine the fluxes from these species. The

Table 22. Annual Sedimentation Fluxes

	Computed	Estimated (Kemp <i>et al.</i> , 1976)
Variable	mg/m ² /day	
Organic Carbon		
Western Basin	173.	279.0, 227.0, 53.4
Central Basin	73.7	167.0, 87.8
Eastern Basin	37.8	457.0
Nitrogen		
Western Basin	44.3	31.4, 23.7, 5.75
Central Basin	30.0	11.6, 23.2
Eastern Basin	21.8	62.5
Phosphorus		
Western Basin	6.18	9.73, 9.59, 2.05
Central Basin	3.03	3.15, 6.58
Eastern Basin	1.94	19.5

Table 23. Transport Parameters

	This Work	Estimates	Reference
Sedimentation Velocity (cm/yr)	0.61	0.61 ± 0.43	Kemp <i>et al.</i> , 1974
Dispersion Coefficient (cm ² /day)	1.9	0.17 - 1.73	Lerman and Lietzke, 1975

former is chosen using the results of anaerobic algal decay experiments. The rate used, 0.02 day^{-1} at 20° , corresponds to $w/KH \sim 10^{-2}$ which is small relative to one, so that essentially all the labile sedimented algal carbon and nitrogen are returned to the overlying water. Even an order of magnitude smaller rate would cause a recycle of $\sim 90\%$ so it is reasonably certain that the labile fraction, 70%, of the algal nutrients are returned.

The reaction rate constant for the detrital nitrogen and carbon are assumed to be the same. The value is chosen so that the observed interstitial concentration of ammonia nitrogen is reproduced by the calculation. A reaction rate constant of 0.091 yr^{-1} at 20°C reproduces the annual average observed interstitial ammonia concentration (1.66 mg N/l) in the top six cm for five core samples at each of the three stations in the central basin taken from the late spring through the fall (Weiller). For that rate, the dimensionless number $w/KH = 1.34$ and 43% of the detrital nitrogen is returned to the overlying water. However, at the average sediment temperature (which is assumed to be equal to the overlying hypolimnion temperature) of $\sim 8^\circ\text{C}$, the outgoing flux is $\sim 25\%$ of the incoming flux.

If it is assumed that detrital carbon reacts at this rate as well, the flux of oxygen equivalents for the central basin is calculated by Equation (63) to be: $J_{O_2} = 125 \text{ mg O}_2/\text{m}^2/\text{day}$ at 20°C or $49.6 \text{ mg O}_2/\text{m}^2/\text{day}$ at 8°C , the temperature of the

sediment. Observed sediment oxygen demands are appreciably higher. Measured rates, corrected for benthic algal photosynthetic activity yielded estimates of 400 to $700 \text{ mg/m}^2/\text{day}$ during Project Hypo (Lucas and Thomas, 1971). In addition, the central basin dissolved oxygen calibration indicated that an additional sink was required. If $550 \text{ mg O}_2/\text{m}^2/\text{day}$ at 20°C (or $218.4 \text{ mg O}_2/\text{m}^2/\text{day}$ at 8°C) is introduced into the sediment segment representing the flux of oxygen equivalents from the deeper sediment layers, then the central basin oxygen balance results are in agreement with observation. It is interesting to note that with this additional source of oxygen equivalents to the surface sediment layer, the observed BOD and chemical oxygen demand (COD) of the interstitial waters bracket the calculated results as shown in Table 24. These measurements can be taken to approximate the total oxygen equivalents of the reduced species in the interstitial waters. They, therefore, provide another check for the calculation.

However, the total sediment oxygen demand used in the computation which is the sum of the surface and deep sediment contribution amounts to $268 \text{ mg O}_2/\text{m}^2/\text{day}$ (at 8°C). This is still significantly less than the observed range of 400 - $700 \text{ mg O}_2/\text{m}^2/\text{day}$ (Lucas and Thomas, 1971). The cause of this discrepancy is uncertain at present.

Table 24. Computed and Observed Sediment Interstitial Water Concentrations, Central Basin

Variable	Computed	Observed	Reference
	Average \pm Standard Deviation	Average \pm Standard Deviation	
NH ₃ (mg N/l)	1.74 \pm 0.44	1.66 \pm 0.68	Weiller
O ₂ Equivalents (mg O ₂ /l)	-48.5 \pm 25.8	-24.5 (0-92)* -71.6 (-36, -125)**	USACOE (1974)

* Average (range) of interstitial water - biochemical oxygen demand

**Average (range) of interstitial water - chemical oxygen demand

CHAPTER 11

VERIFICATION

As discussed in the data section of the this report, 1975 is used for verification of the Lake Erie model because of the abnormal oxygen conditions which occurred in that year. As is seen in the data comparison plots, phytoplankton and nutrient concentrations in 1975 were approximately the same as in the years 1970-1974. However, oxygen conditions in 1975 were radically different. The central basin of the lake did not become anaerobic as it had for the preceding years. This difference in behavior provides a good test of the ability of the model to predict lake oxygen concentrations, a parameter of prime concern in Lake Erie.

The verification calculations are made using 1975 conditions (loadings, etc.) but with no changes in the kinetics. The major changes reflect the altered physical conditions; the depth of the thermocline is altered and the transport is recalibrated to reflect the unusual thermal condition of the lake in 1975. Figure 35 shows the two meter vertical average temperature profiles used to determine the thermocline depth for both the calibration and verification years. For the calibration year, the depth is 17 meters and for the verification year, the depth is 13 meters. It should be noted that the 17 meter thermocline is the normal depth for the lake. The 13 meter thermocline is due to a combination of unusually low wind speeds and low net heat input to the lake in 1975.

The results of the verification for chlorophyll and the nutrients are shown in Figures 75-81. The results are comparable to the calibration. Western basin chlorophyll concentrations are

underestimated in the spring and overestimated in the summer. An early central basin bloom is not reproduced but the remainder of the year is reasonable, although the hypolimnion concentration is underestimated. Ammonia concentrations are slightly overestimated but the nitrate concentrations are well reproduced in the epilimnion. With the exception of the March-April conditions, which are attributed to wind induced resuspension, the calculated total phosphorus concentrations are in reasonable agreement with observation as are the orthophosphorus and silica calculations.

The most striking feature of the verification is the dissolved oxygen comparison, shown in Figure 82. The agreement in the central basin hypolimnion is remarkable especially when compared to the lower oxygen concentrations in the 1970 and 1973-1974 calibrations. The higher oxygen concentrations in 1975 are basically due to the larger volume of the hypolimnion in that year. It is easy to see that the sediment oxygen demand, which is a constant on an areal basis, would result in a smaller volumetric depletion rate in 1975. However, as is apparent in Table 25, the sinks due to phytoplankton respiration and organic carbon oxidation are reduced as well. The estimated total phosphorus loading in 1975, 20,400 metric tons/yr is 11.7% lower than that for 1970, 23,100 metric tons/yr. This is reflected in the 12.9% reduction in average central basin epilimnion chlorophyll during stratification and the 8.75% reduction in organic carbon concentration. The reduction in the hypolimnion are more dramatic, however. This is due to two

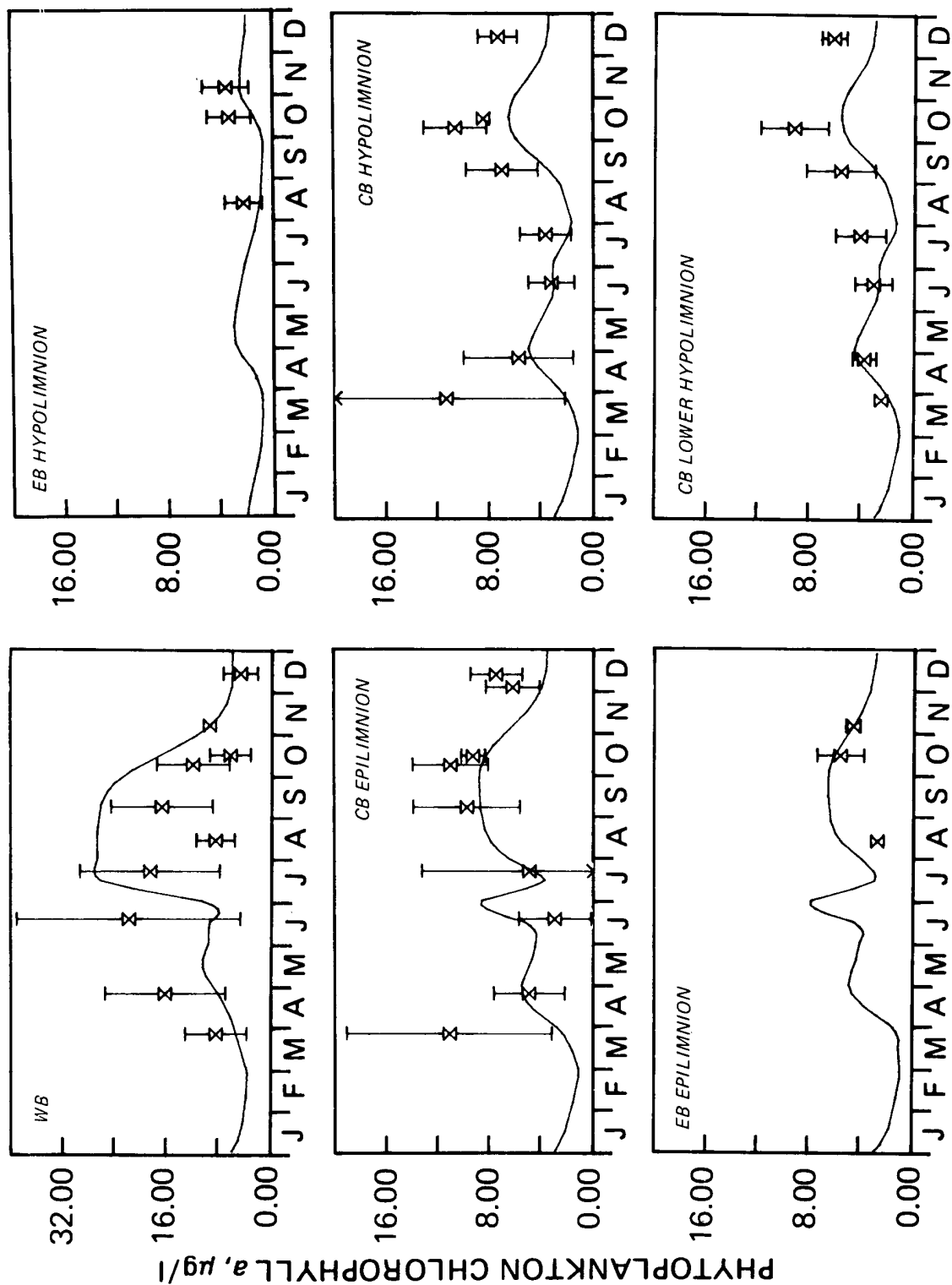


Figure 75. Lake Erie model verification for phytoplankton chlorophyll ($\mu\text{g/l}$), 1975. Symbols: means \pm standard deviations, lines are the computations.

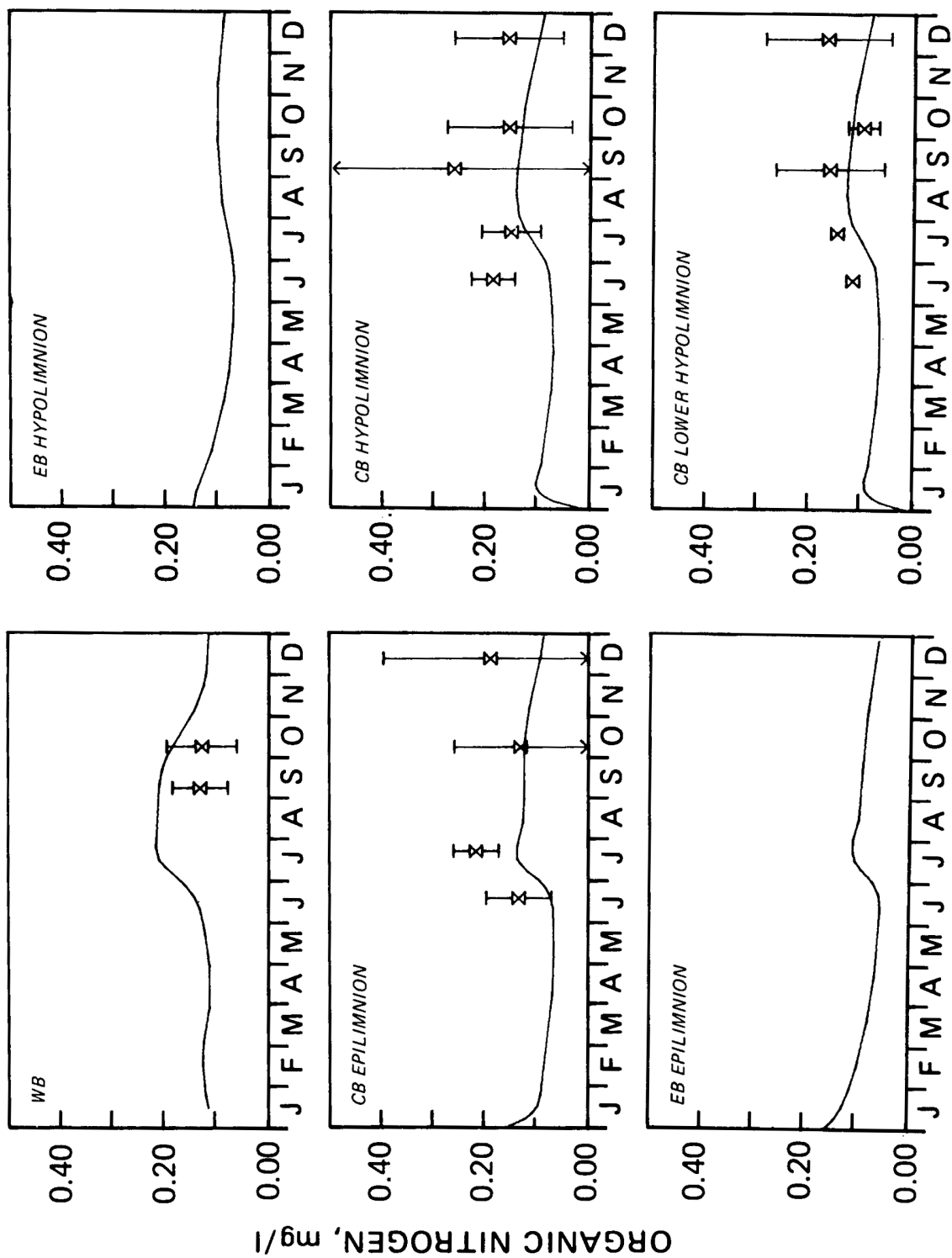


Figure 76. Lake Erie model verification for organic nitrogen (mg N/l), 1975.

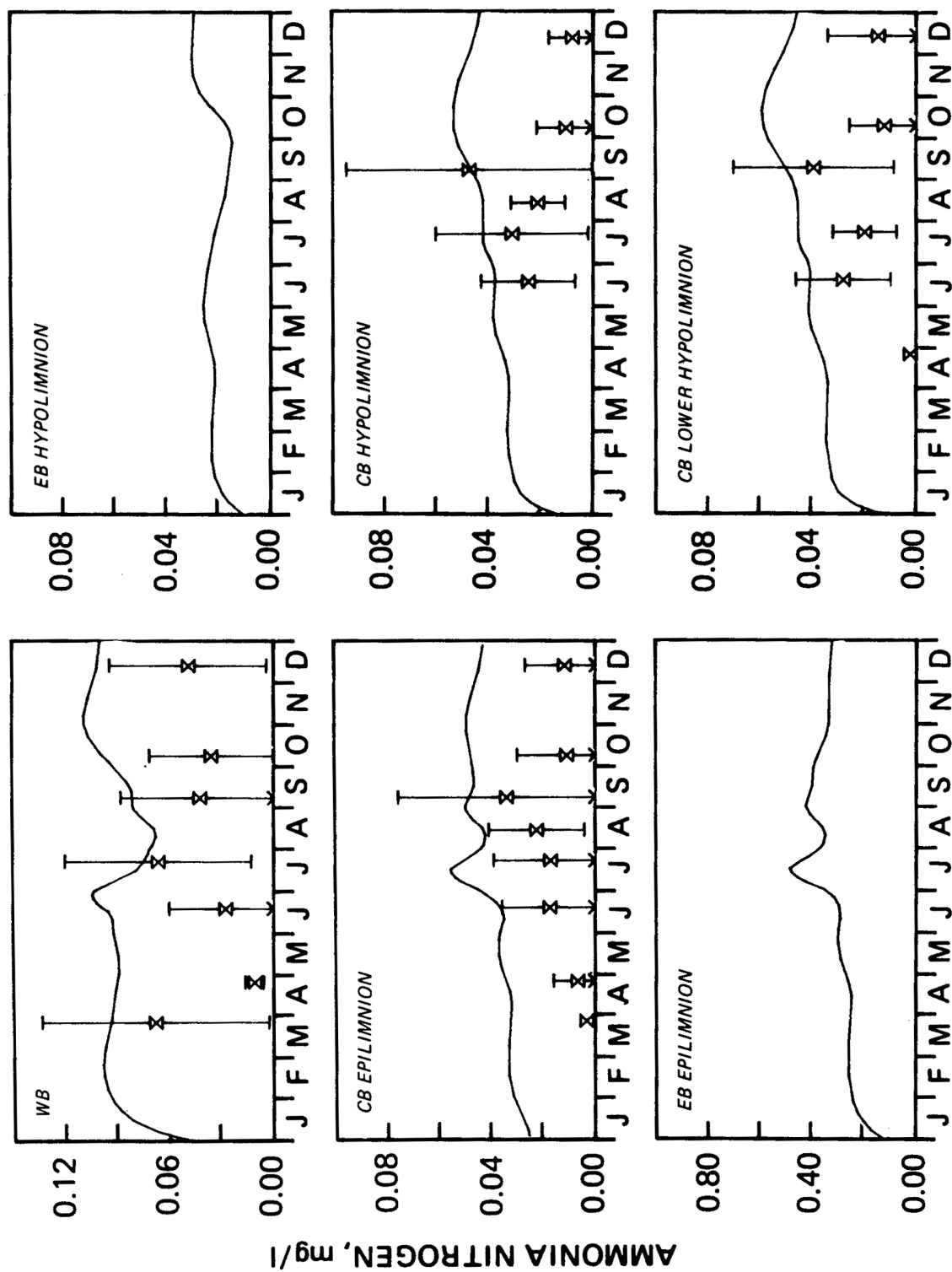


Figure 77. Lake Erie model verification for ammonia nitrogen (mg N/l), 1975.

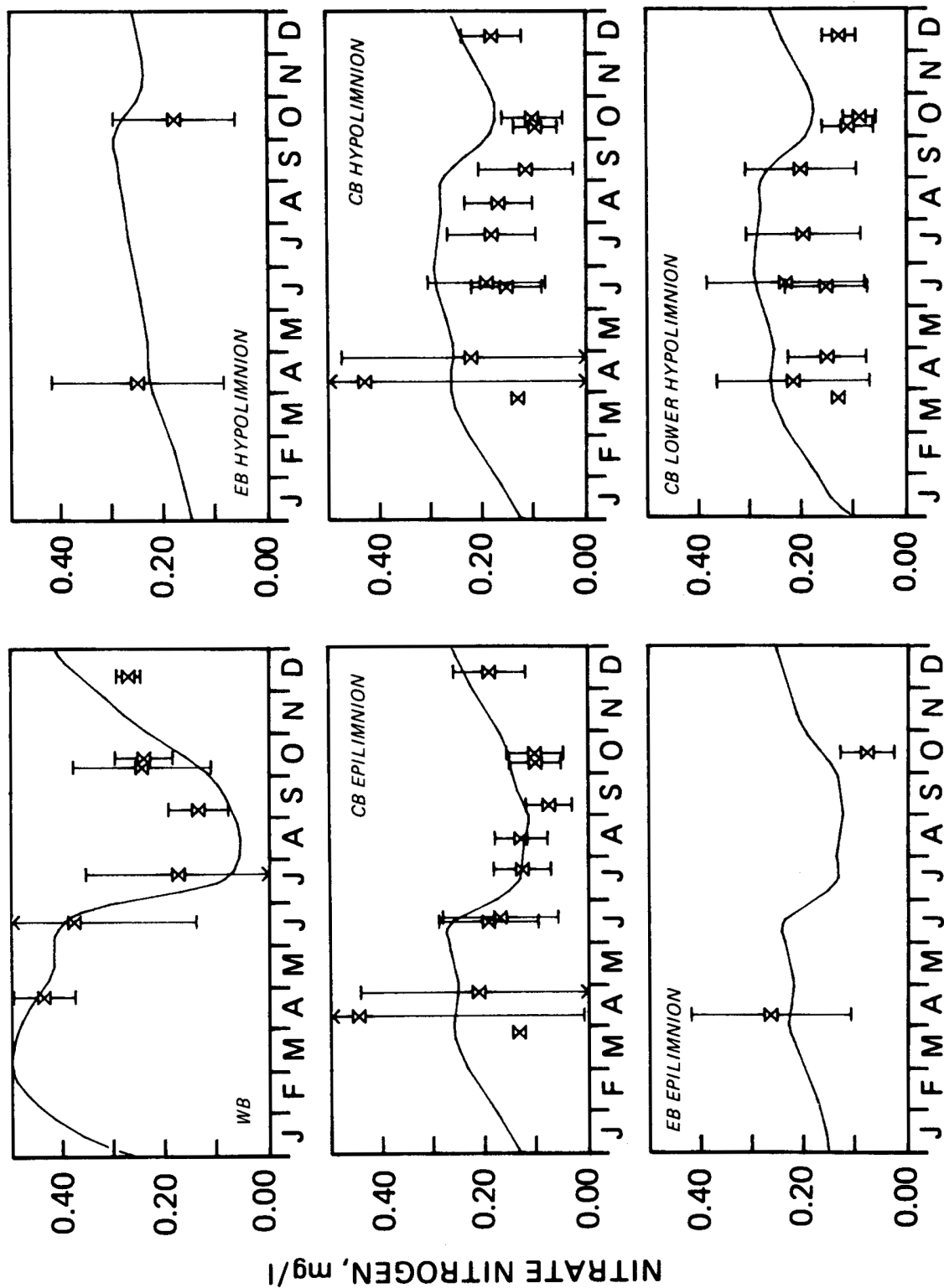


Figure 78. Lake Erie model verification for nitrate nitrogen (mg N/l), 1975.

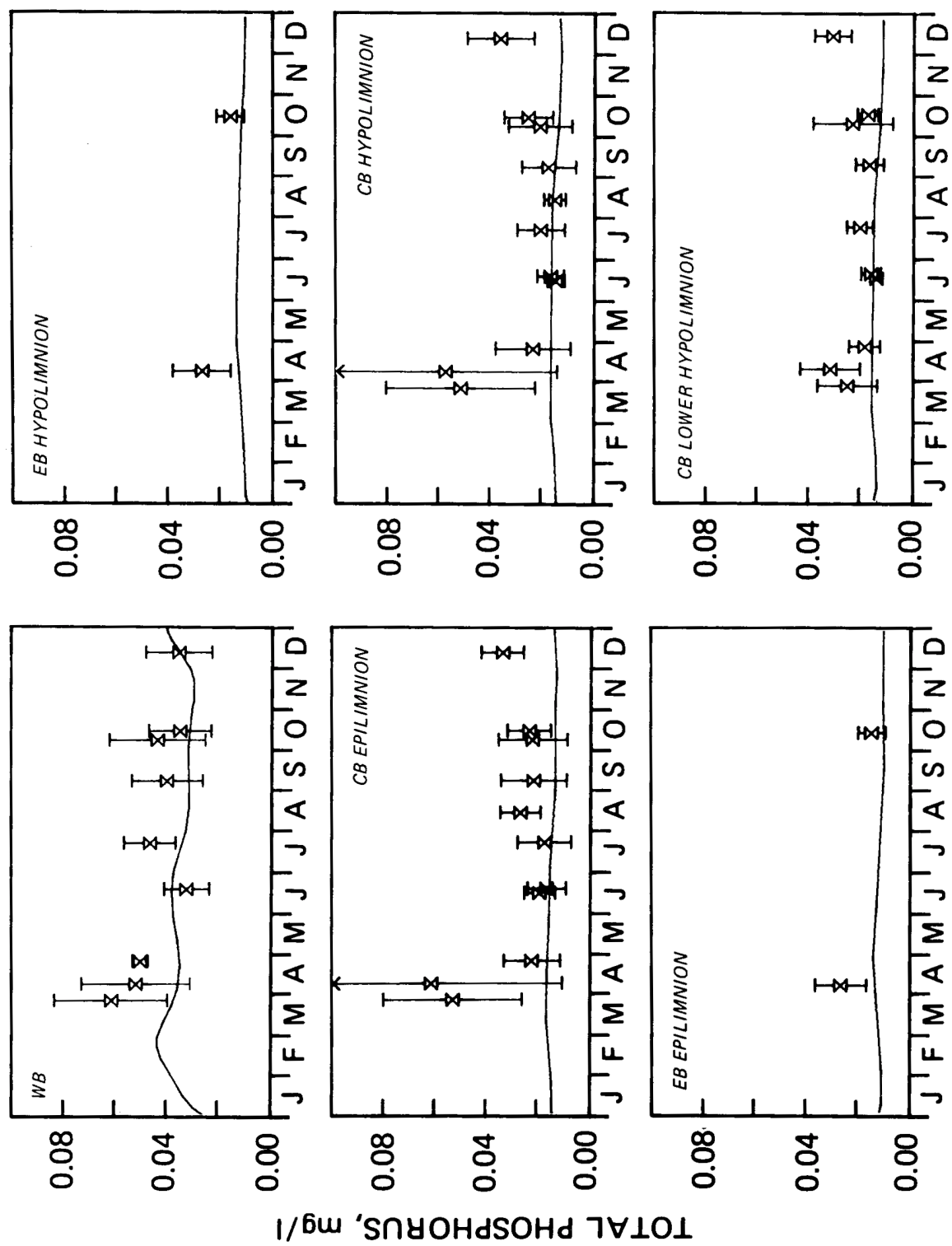


Figure 79. Lake Erie model verification for total phosphorus (mg $\text{PO}_4\text{-P/l}$), 1975.

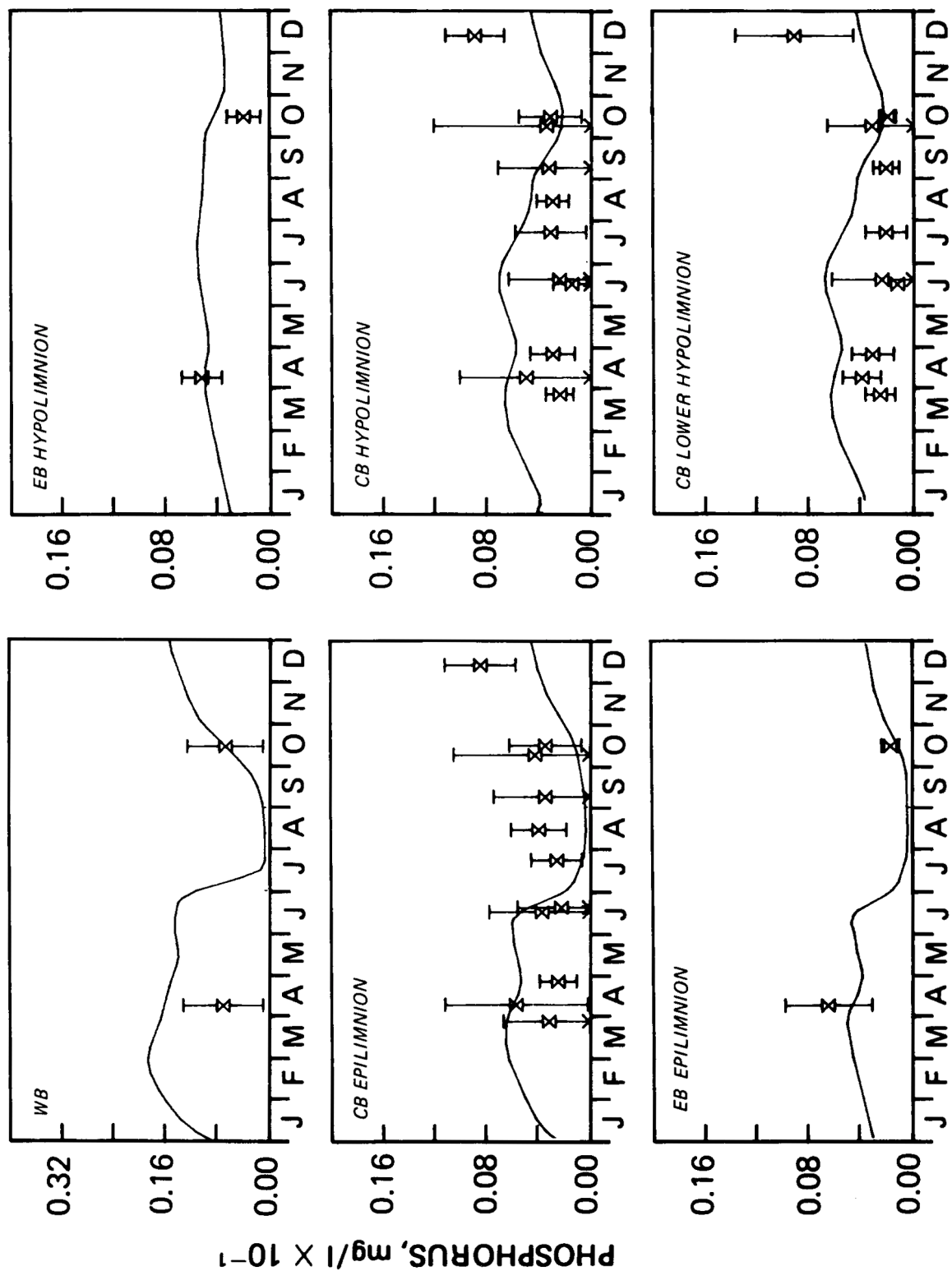


Figure 80. Lake Erie model verification for orthophosphorus (mg PO₄-P/l), 1975.

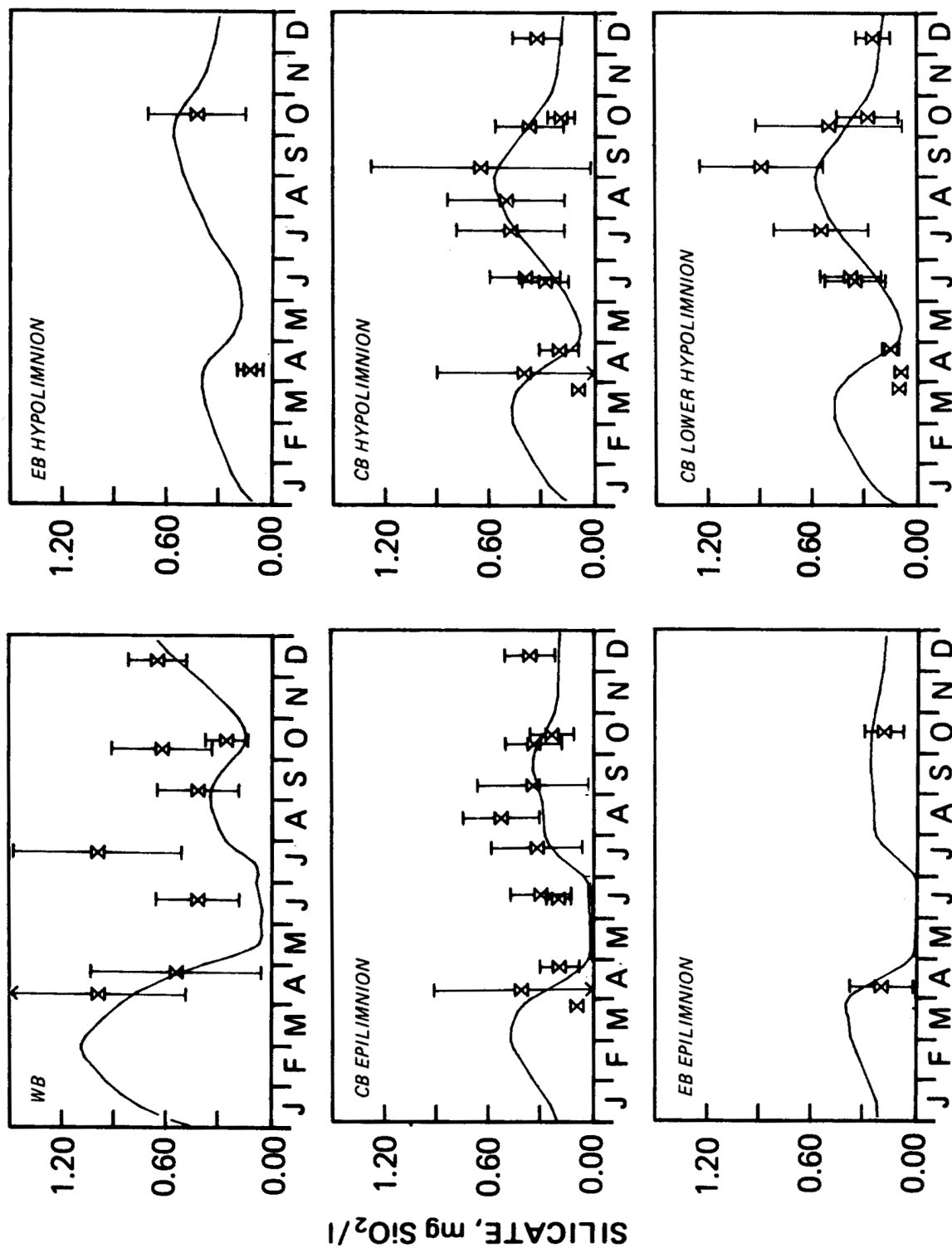


Figure 81. Lake Erie model verification for reactive silica (mg SiO₂/l), 1975.

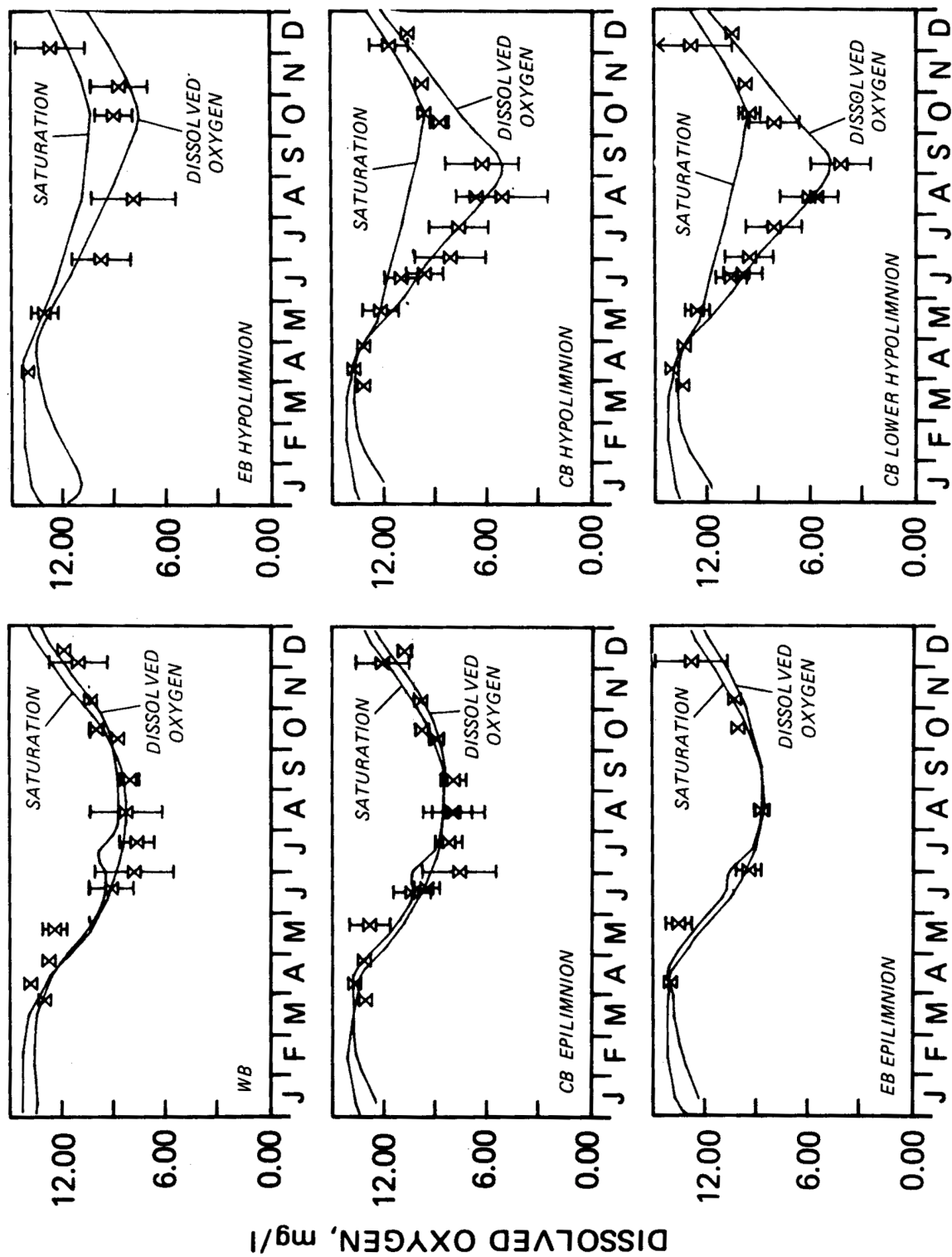


Figure 82. Lake Erie model verification for dissolved oxygen (mg/l), 1975. Note that 1975 oxygen conditions are radically different than 1970 in central basin hypolimnion.

Table 25. Calculated Average* Central Basin Concentrations and Oxygen Consumption Rates for 1970 and 1975

Variable	Year	Epilimnion	Hypolimnion
Phytoplankton Chlorophyll ($\mu\text{g Chl } a/\text{l}$) (% Change)	1970 1975	8.32 7.25 (-12.9)	2.89 2.35 (-18.7)
Organic Carbon ($\text{mg C}/\text{l}$) (% Change)	1970 1975	0.400 0.365 (-8.8)	0.310 0.212 (-31.6)
Phytoplankton Respiration ($\text{mg O}_2/\text{l}/\text{day}$) (% Change)	1970 1975	0.125 0.107 (-14.4)	0.0200 0.0165 (-17.5)
Organic Carbon Oxidation ($\text{mg O}_2/\text{l}/\text{day}$) (% Change)	1970 1975	0.108 0.098 (-9.31)	0.0568 0.0394 (-30.6)

*Average from day 180 to day 240.

factors. The vertical exchange in the central basin is less in 1975 than 1970, compare Figures 38 and 40, and the flux of chlorophyll and organic carbon due to the settling velocity across the thermocline is diluted into a large hypolimnion volume, thus reducing the resulting concentrations. The combined effects produce a reduction in hypolimnion concentrations of 19% and 31.5% for chlorophyll and organic carbon concentrations and, since the rates of oxygen consumption are proportional to these concentrations, a reduction in the utilization rates as well. The interactions of these factors produces the 1975 dissolved oxygen distribution and it is clear that an analysis of the mass balance and changing sources and sinks requires a rather complex and complete calculation.

The successful oxygen verification indicates that the determination of the contribution of the various components which interact to produce the oxygen profile is reasonable. The difference between the verification and the calibration oxygen profile is due to a combination of water column and sediment sink interactions. The balance between these sinks is important since the percentage reduction is not uniform for each sink. If the magnitudes were not correctly estimated by the calibration, then the reductions would not have resulted in the proper oxygen profile for the verification.

The contributions of each of the oxygen sinks to the central basin hypolimnion 1975 oxygen profile are shown in Figure 83 and Table 26. At the time of minimum dissolved oxygen, organic carbon oxidation accounts for almost 47% of the depletion, sediment oxygen 31%, and

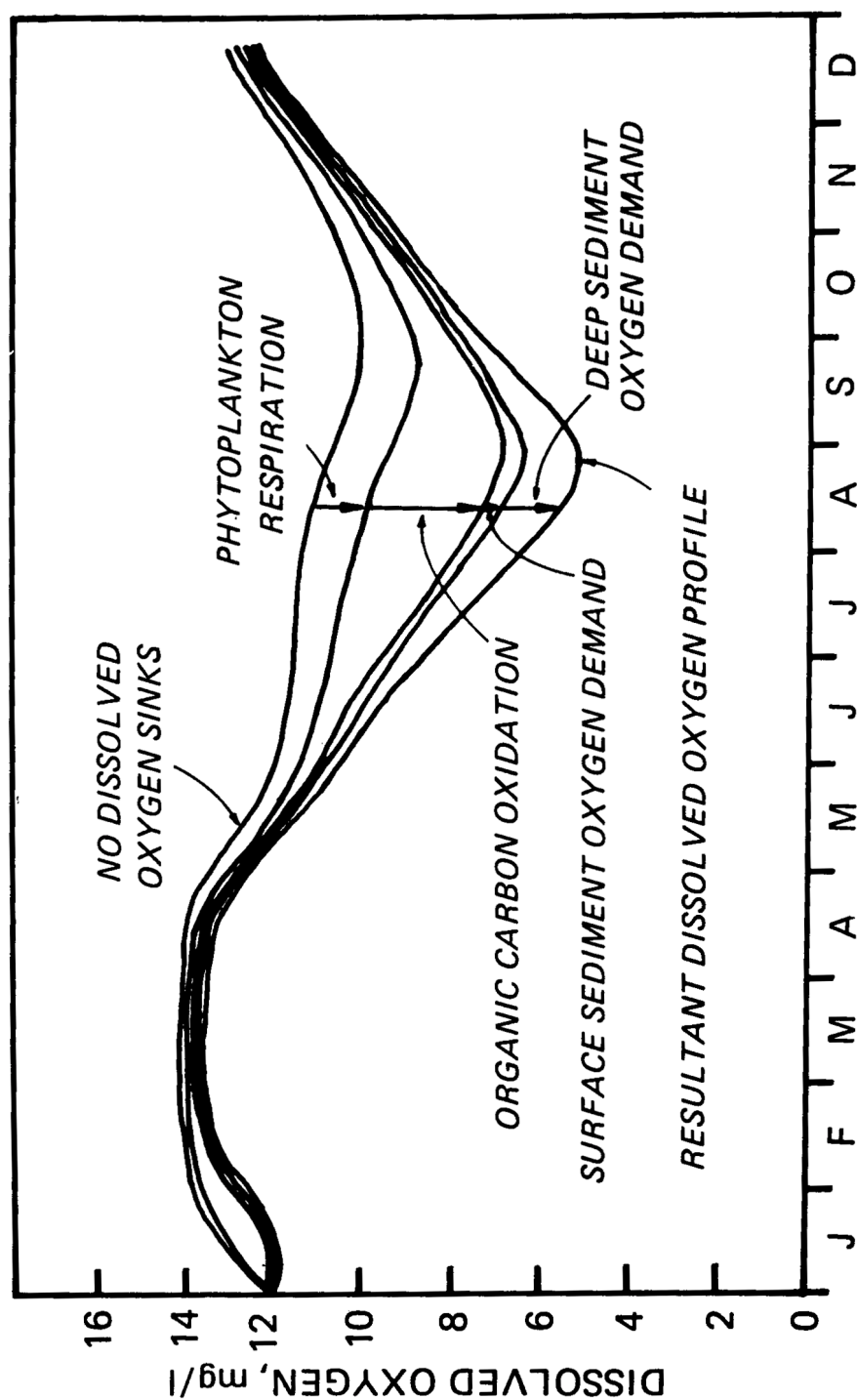


Figure 83. Dynamics of central basin hypolimnion dissolved oxygen. The contributions of each of the oxygen sinks for the 1975 oxygen profile are shown.

Table 26. Percentage Contribution of Oxygen Sinks to Dissolved Oxygen Deficit at the Time of Minimum Dissolved Oxygen in the Central Basin Hypolimnion

Oxygen Sink	Percent Contribution	
	1970	1975
Deep Sediment Oxygen Demand	28.7	22.8
Surface Sediment Oxygen Demand	11.5	8.2
Organic Carbon Oxidation	42.5	46.9
Phytoplankton Respiration	17.3	22.1

phytoplankton respiration 22%. The comparable 1970 contributions are: 43%, 40%, and 17% so that in 1970 the water column contributed 60% and the sediment contributed 40%. In 1975, the water column contributed 69% and the sediment contributed 31%.

11.1 ANALYSIS OF CALIBRATION AND VERIFICATION ERROR

The comparisons of computed and observed concentrations for the calibration (1970, 1973-1974) and verification (1975) years have been made using graphical presentations. These are easy to interpret and give a direct visual impression of the quality of the comparisons. However, they lack a quantitative dimension with which to assess statistically the extent of the agreement achieved. Although a complete analysis has not been performed for all variables, results are available for three principal variables in the central basin: dissolved oxygen, chlorophyll *a*, and total phosphorus. For each year of calibration and verification, the residuals, that is the epilimnion and hypolimnion of the central basin, have been analyzed. The results are given in Table 27. The mean residual, and its standard error are tabulated, as well as the standard deviations of the residuals. The median relative error, where the relative error is $|\text{calculated} - \text{observed}|/\text{observed}$, is also

included. This latter variable has been analyzed in detail for a Lake Ontario computation (Thomann, 1979).

The means of the residuals for dissolved oxygen and chlorophyll are, for the most part, not statistically difference from zero (t-test at the 95% level of significance). Those that fail this test are indicated on the table. This indicates that the model is not biased relative to the data. The total phosphorus results, however, indicate a statistically significant bias.

The standard deviation of the residuals for dissolved oxygen are between 0.6 and 1.3 $\mu\text{g O}_2/\text{l}$, for chlorophyll *a* between 2.2 and 3.4 $\mu\text{g/l}$, and for total phosphorus between 6.9 and 15 $\mu\text{g/l}$. The values for dissolved oxygen will be used subsequently to establish a lower bound for the prediction error.

A comparison of the calibration and prediction error is instructive. In nearly all cases, the mean residual is larger for the verification (1975) than for the 1970 calibration. The same is true for the residuals standard deviation and the median relative error. This is not unexpected since the verification calculation was not adjusted to fit the data. The average ratio of verification (1975) to calibration (1970) residual standard deviation is

Table 27. Calibration and Verification Residual Analysis

		Residual			Median Relative Error (%)
		Mean	Standard Error	Standard Deviation	
Dissolved Oxygen (mg/l)					
Epilimnion	1970	-0.1308	0.188	0.595	3.6
	73-74	-0.1649	0.381	1.263	7
	1975	-0.2439	0.238	0.953	6
Hypolimnion	1970	0.5645*	0.245	0.775	12.2
	73-74	0.6286	0.249	1.084	15
	1975	0.2943	0.233	0.932	8.3
Chlorophyll a (µg/l)					
Epilimnion	1970	0.0964	0.798	2.524	31.6
	73-74	-2.6924*	0.974	3.376	63
	1975	1.8616	1.316	3.316	20.6
Hypolimnion	1970	NODA***	NODA***	NODA***	NODA***
	73-74	0.9646	0.576	2.154	52
	1975	3.2651**	0.734	2.934	40
Total Phosphorus (µg/l)					
Epilimnion	1970	10.68**	2.3	7.21	41
	73-74	9.90**	2.0	6.88	41
	1975	18.42**	4.0	13.46	53.3
Hypolimnion	1970	1.56	2.2	8.92	35
	73-74	3.40	2.9	10.16	21.2
	1975	14.02**	4.4	14.5	40.5

* Failed t-test at 95% level of significance.

** Failed t-test at 99% level of significance.

***No observed data available.

1.52 which suggests that the scatter is ~ 50% larger for the verification than the calibration.

During the calibration procedure the major emphasis was placed on the 1970 rather than the 1973-1974 data. This is apparent in the residual standard deviation and median relative error results in Table 27. For dissolved oxygen, the 1975 verification residual standard deviations are actually smaller than the 1973-1974 result.

For chlorophyll, they are comparable and for total phosphorus, the 1975 residual standard deviation is larger than the 1973-1974 result. Again, this is not unexpected. The transport calibration was made using 1970 data. The 1973-1974 data served as confirmatory rather than primary data for calibration. As a consequence, it is not as closely reproduced by the calculation.

CHAPTER 12

ESTIMATED EFFECTS OF PHOSPHORUS LOADING REDUCTIONS

In this chapter, a series of calculations are presented which are an attempt to estimate the consequences of phosphorus loading reductions to Lake Erie. Nitrogen loading reductions are not considered because the possibility of increased nitrogen fixation by blue-green algae during periods of excess phosphorus concentrations is not addressed in the calculation.

A number of uncertainties exist in the present model which limit the accuracies of these estimates. Perhaps the most severe is in the dynamics of the generation of the sediment oxygen demand. Only the surface layer is considered, the deeper layers are included by externally specifying their effect on sediment oxygen demand. Thus, the calculation is not a complete mass balance involving both sediments and water column. The vertical segmentation of the central basin is not fine enough to resolve the vertical gradients in a comprehensive way which limits the resolution that can be achieved in the calibration. The horizontal exchanges of the central basin hypolimnion are uncertain and may be significant. The water column oxygen consumption data (BOD) are meager and not available for either the calibration or verification year, nor are adequate sediment oxygen demand measurements available. In light of these and other uncertainties, the estimates to be presented in this chapter must be viewed with caution. Although they represent the most comprehensive attempt to date that directly addresses the dissolved oxygen mass balance together with the nutrients and phytoplankton interrelationships, they are, as yet, only estimates whose accuracy is difficult to assess.

Further efforts are required to refine the quantitative formulations and to verify the kinetics from independent experiments. This is an ongoing process and it is expected that as more data are collected and analyzed within the general framework of these calculations the confidence in their descriptive and predictive ability will increase.

In order to make at least some quantitative assessment of the error associated with the predictions a crude analysis based on the error of calibration is included. It should be stressed that this analysis is very preliminary and is intended more as a guideline than as a rigorous evaluation.

12.1 TIME TO STEADY-STATE

Lake Erie appears to be in equilibrium with the current phosphorus loading. This is not unexpected since the loading have been essentially constant for the last five years, see Figures 9-13, and hydraulic residence time which sets the upper bound on the time to reach steady-state in the water column is approximately 2.5 years so that in five years the lake would be at 87% of equilibrium if only hydraulics control. Phosphorus sedimentation decreases the time to approximately four years as shown in Table 28, a yearly summary of a projection calculation to be discussed subsequently. Water column concentrations of phosphorus and chlorophyll have reached their equilibrium by the fourth year. However, dissolved oxygen concentrations and the estimated area of anoxia are still changing in the

Table 28. Results of Simulation of Phosphorus Point Source Reduction to 0.1 mg/l

		Year 1	Year 2	Year 3	Year 4	Year 5
Yearly Average Phosphorus (Central Basin Epilimnion)	$\mu\text{g PO}_4\text{-P/l}$	10.96	9.33	9.17	9.14	9.14
Summer Average Chlorophyll (Central Basin Epilimnion)	$\mu\text{g Chl-a/l}$	3.84	3.56	3.49	3.476	3.474
Summer Average Dissolved Oxygen (Central Basin Hypolimnion-Segment 5)	$\text{mg O}_2\text{/l}$	5.90	6.0	6.03	6.05	6.06
Anoxic Area	km^2	1342	952	800	744	700

fifth year. This is due to the considerably longer time to steady-state for the sediment segments. This is discussed in more detail subsequently.

The loading to the lake is a combination of point sources (industries and municipalities) and diffuse sources (runoff). The point sources are fairly constant while the diffuse source are a function of tributary flow. To determine the loadings for projections, the average water year based on U.S. Geological Survey (USGS) flow data is used to calculate diffuse loadings. These diffuse loadings are combined with 1975 point source loadings to yield the current load. This load is termed the base year load. It has been calculated, as have all the loadings used in these calculations, by the USACOE, Buffalo District. Tables A-10 to A-12 summarize these loadings.

The reductions of phosphorus loading follow guidelines provided by the USEPA. Initially, point sources are reduced to a 1 mg/l effluent level for all treatment plants. At this loading level, two separate scenarios are followed. In the first scenario, point sources are reduced from 1 mg/l to 0.5 mg/l and then 0.1 mg/l. In the second scenario, point sources are held at 1

mg/l and reductions are made in diffuse source loadings exclusive of Detroit River diffuse sources.

Depending on which of the two scenarios is followed, there is a difference in the computed effect on lake conditions for the same total loading. Removal of diffuse sources is computed to have less of an effect on the important water quality parameters than does removal of point sources. This is caused by the differences in the ratio of available or orthophosphorus to total phosphorus for diffuse and point sources. Point sources have a higher ortho to total phosphorus ratio than do diffuse sources. If point sources are removed more orthophosphorus is removed per unit mass of total phosphorus than if diffuse sources are removed. The result is less phosphorus entering the lake which is immediately available for growth. Since a higher percentage of the phosphorus load is now in the unavailable fraction, the percentage of the phosphorus which is particulate is also increased. This results in a greater phosphorus loss due to settling. Consequently, the concentration of phosphorus in the water column is decreased. In other

words, the removal of point sources has a greater impact in improving water quality than diffuse source removal because more orthophosphorus is removed and, in addition, a greater fraction of the total phosphorus is in the unavailable form. Thus, the proportion of phosphorus that can be removed by sinking is also increased resulting in lower lake phosphorus concentrations and lower phytoplankton chlorophyll concentrations. These points are illustrated in Figure 84. This figure shows the unavailable and orthophosphorus loads to the western basin under two reduction schemes. The solid line is the phosphorus load with point sources reduced to 0.5 mg/l. The dashed line is the phosphorus load with the diffuse sources reduced by 25% after point sources are reduced to 1 mg/l. The total phosphorus load is approximately the same for both cases. With the point source reduction, the lake total phosphorus load is 12,652 metric tons/yr and with the diffuse source reduction it is 12,547 metric tons/yr. The plot of unavailable phosphorus shows that this fraction of the load

is higher with point source reduction, and the orthophosphorus plot shows that this fraction of the load is lower with point source reduction.

12.2 SIMULATION RESULTS

The results are a summary of the last year calculation for a five-year simulation for which the loadings are reduced to the indicated level at the beginning of the first year. All loading reductions are uniform across the lake. Except for a comparison to the USACOE's Plan IX, there are no basin specific removals.

The annual whole lake, phosphorus loading at a number of reductions are shown in Table 29.

The results for phytoplankton chlorophyll are shown in Figure 85. They represent the epilimnion concentration averaged for June 15 to September 5. For the reasons explained above, there are separate responses for point and

Table 29. Loading Condition Versus Annual Total Phosphorus Load

Loading Condition	Total Phosphorus Load (Metric Tons/Yr)*
Base Year	19182
1 mg/l Point Sources	14195
0.5 mg/l Point Sources	12652
0.1 mg/l Point Sources	11419
1 mg/l Point Sources + 10% Diffuse Reduction**	13535
1 mg/l Point Sources + 20% Diffuse Reduction	12876
1 mg/l Point Sources + 40% Diffuse Reduction	11558
1 mg/l Point Sources + 60% Diffuse Reduction	10240
1 mg/l Point Sources + No Diffuse Sources	7600

* Excluding atmospheric loading.

**Excluding the diffuse source contribution to the Detroit River.

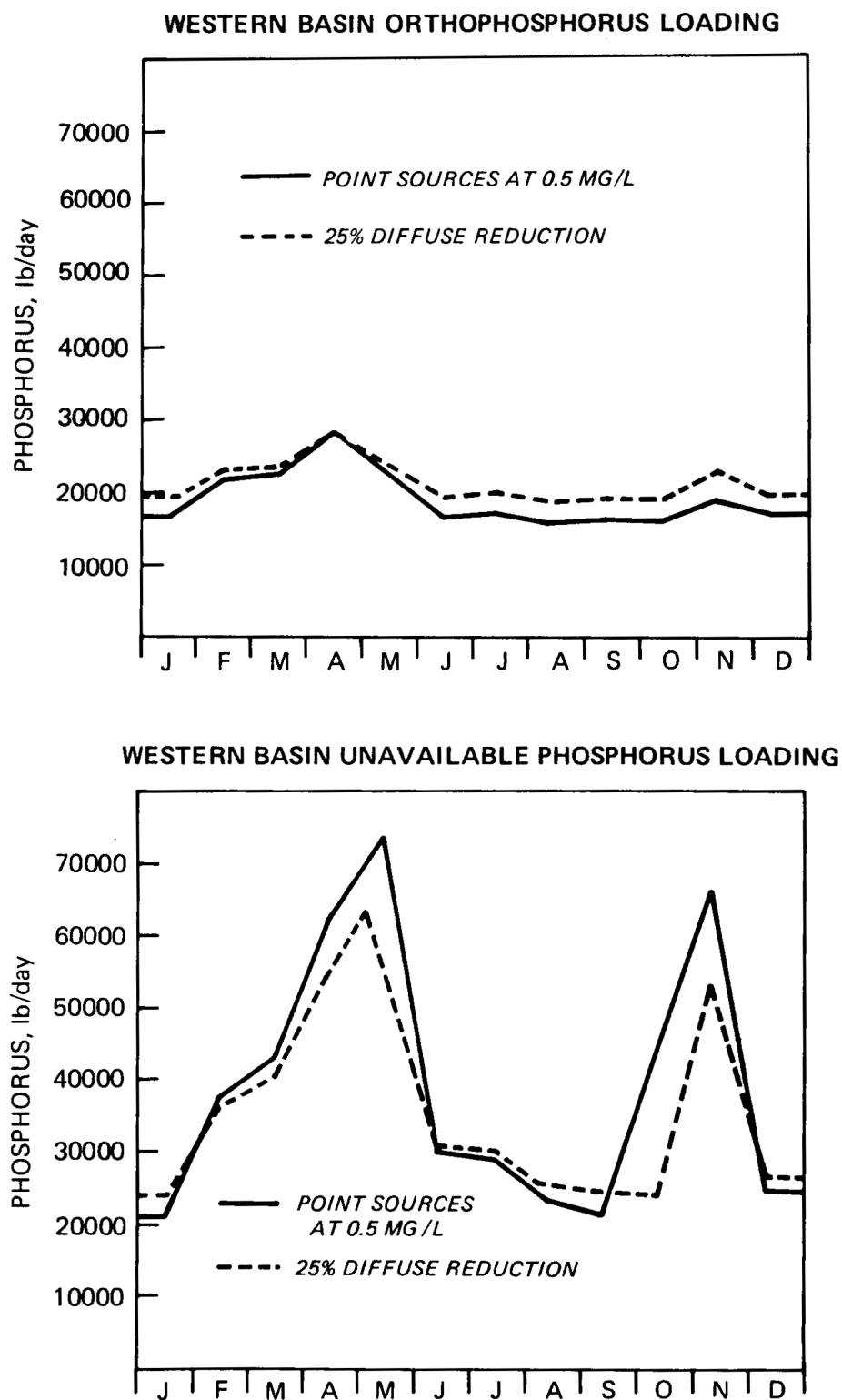


Figure 84. Western basin loads (lbs/day) for orthophosphorus (top) and unavailable phosphorus (bottom) under two reduction schemes: (a) with point sources reduced to 0.5 mg/l and (b) diffuse sources reduced by 25% after point sources are reduced to 1 mg/l.

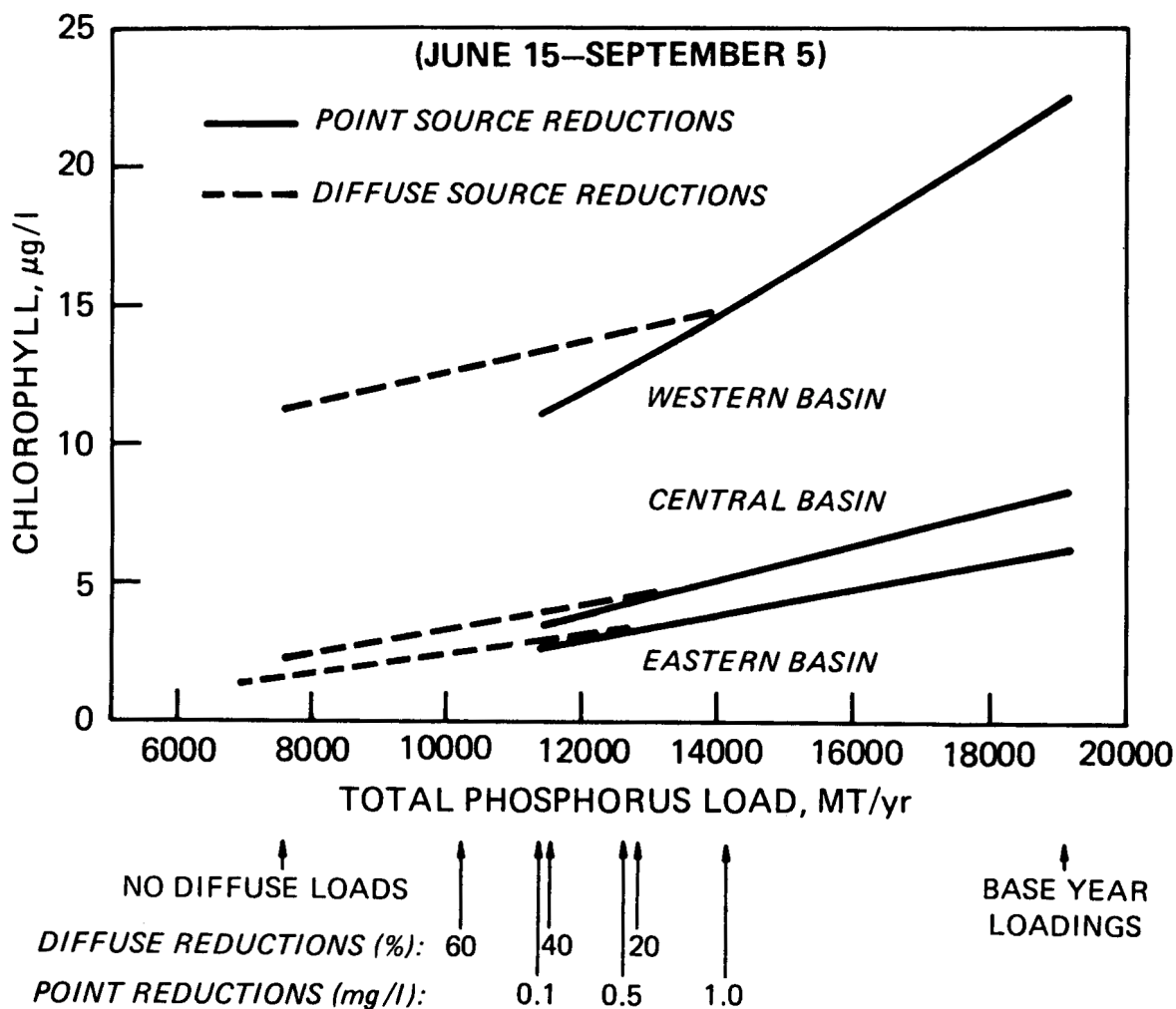


Figure 85. Summer average epilimnion chlorophyll ($\mu\text{g/l}$) versus lake total phosphorus loading (metric tons/yr). There are separate responses for point and diffuse source reductions and for each basin.

diffuse source reductions. There is a greater effect in the western basin than in the central and eastern basins. This is due to the large percentage of the load that enters in the western basin and its short detention time. Conditions in the basin are dominated by the incoming load. Changes in that load cause significant changes in the basin. An important calculation is that even with substantial load reductions, the western basin average summer chlorophyll will still be above what is generally considered the mesotrophic-eutrophic level.

The effect of phosphorus load reductions on the average epilimnion summer total phosphorus is shown in Figure 86. As is expected, the pattern is similar to the chlorophyll results. However, there is one major difference. There is a large difference in phytoplankton chlorophyll between point and diffuse reductions than in total phosphorus. If point sources are reduced so that the total phosphorus load is reduced to 1200 metric tons/yr, the resultant calculated chlorophyll and phosphorus concentrations in the western basin are about 12 and 20 $\mu\text{g/l}$, respectively. To achieve these same levels with diffuse source reductions a load of about 8,700 metric tons/yr is needed for chlorophyll and a load of about 10,300 metric tons/yr is needed for phosphorus. In other words, an extra 3,300 metric tons/yr of phosphorus must be removed under diffuse reduction to achieve the 12 $\mu\text{g/l}$ chlorophyll level. An extra 1,700 metric tons/yr of phosphorus must be removed under diffuse reduction to achieve the 20 $\mu\text{g/l}$ phosphorus level. Both these levels are met with the same total load reduction in point reduction.

Figure 87 shows the effects of the phosphorus load reductions on light penetration expressed as average summer Secchi disk depth. Load reductions will result in a significant increase in water clarity in the central and eastern basin. In the western basin, there is only a small increase in clarity as the load decreased. Also, as the load decreases the rate of increase of western basin clarity declines since most of the light attenuation in the western basin is caused by high turbidity levels rather than phytoplankton.

Even with substantial decreases in phytoplankton, light extinction rates remain high. The converse is true in the other basins.

The phosphorus discharge to Lake Ontario as a function of phosphorus load is shown in Figure 88. This loading is calculated based on the eastern basin epilimnion concentration and the existing flow to the Niagara River. A factor accounting for the difference in concentration between the whole eastern basin and the area near the outlet is included in the calibration. This factor is the ratio of the average concentration at the four stations closest to the Niagara and the eastern basin epilimnion average. A value of 1.18 has been calculated using 1970 CCIW cruise data.

Perhaps the variable of most interest with regard to load reductions is dissolved oxygen, particularly, the effect on anoxia in the central basin. The methods used to stimulate the central basin oxygen concentrations as well as the area of anoxia has been discussed in Chapter 9. However, the structure of the sediment calculation raises a question as to its applicability to oxygen predictions under loading reductions. The sediment oxygen demand is composed to two parts: a surface layer (5 cm) demand which is dynamically calculated, and a demand for the rest of the sediment which is externally specified. Under loading reductions, the surface segment responds to the input changes and the oxygen demand dynamically adjusts. However, the deep sediment demand, since it is externally specified, remains constant. This is likely to be a good assumption during the short time period used for the simulations (five years). However, the deep sediment will ultimately also be affected by the reduced load.

In order to estimate the change in water column oxygen conditions due to the eventual effect of the loading reductions on the deep sediment, a coupling of the deep sediment oxygen demand to the surface sediment demand has been incorporated into the calculations. The deep sediment demand is reduced each year of the simulation by the same percentage as the

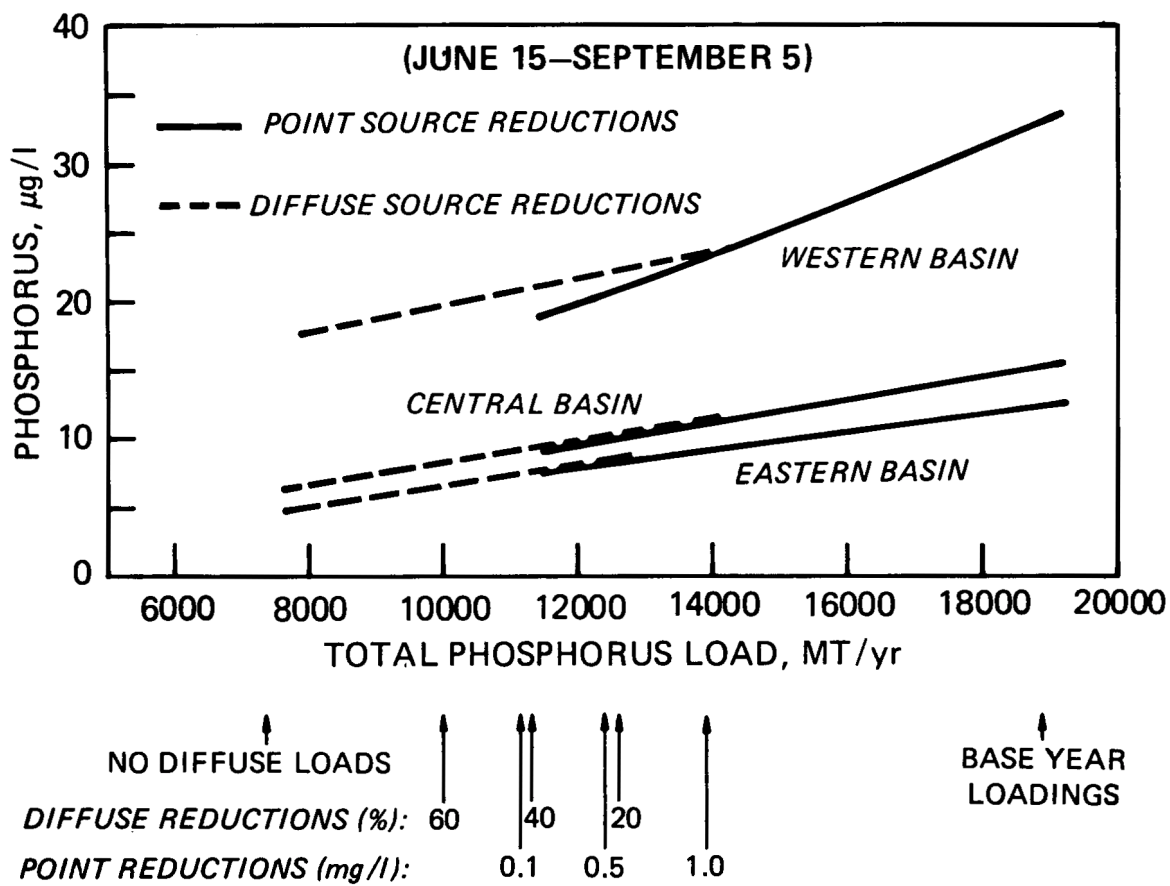


Figure 86. Summer average epilimnion total phosphorus ($\mu\text{g PO}_4\text{-P/l}$) versus lake total phosphorus loading (metric tons/yr). The pattern is similar to the chlorophyll results.

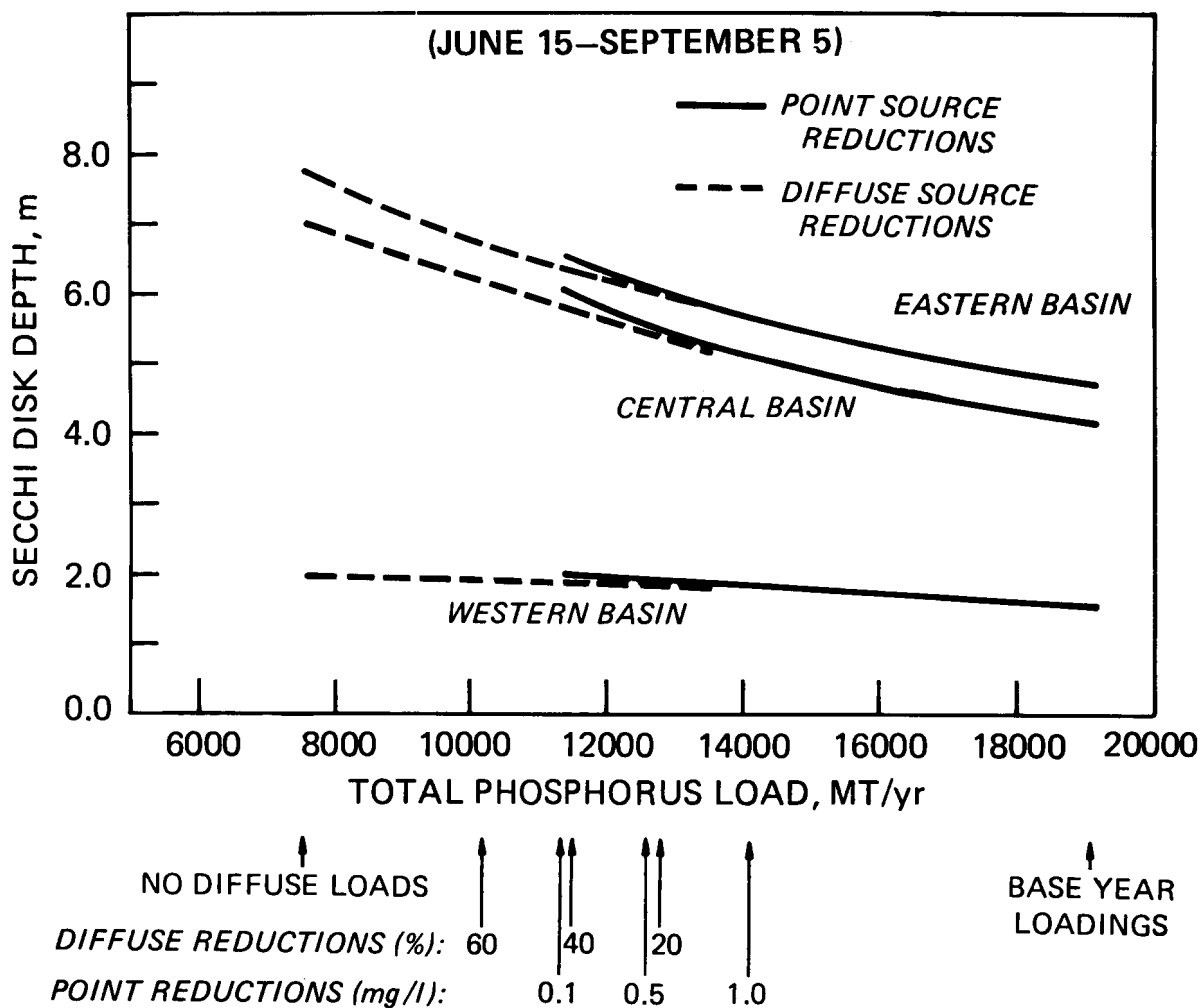


Figure 87. Summer average Secchi disk depth (m) versus lake total phosphorus loading (metric tons/yr). Load reductions will result in a significant increase in water clarity in the central and eastern basins.

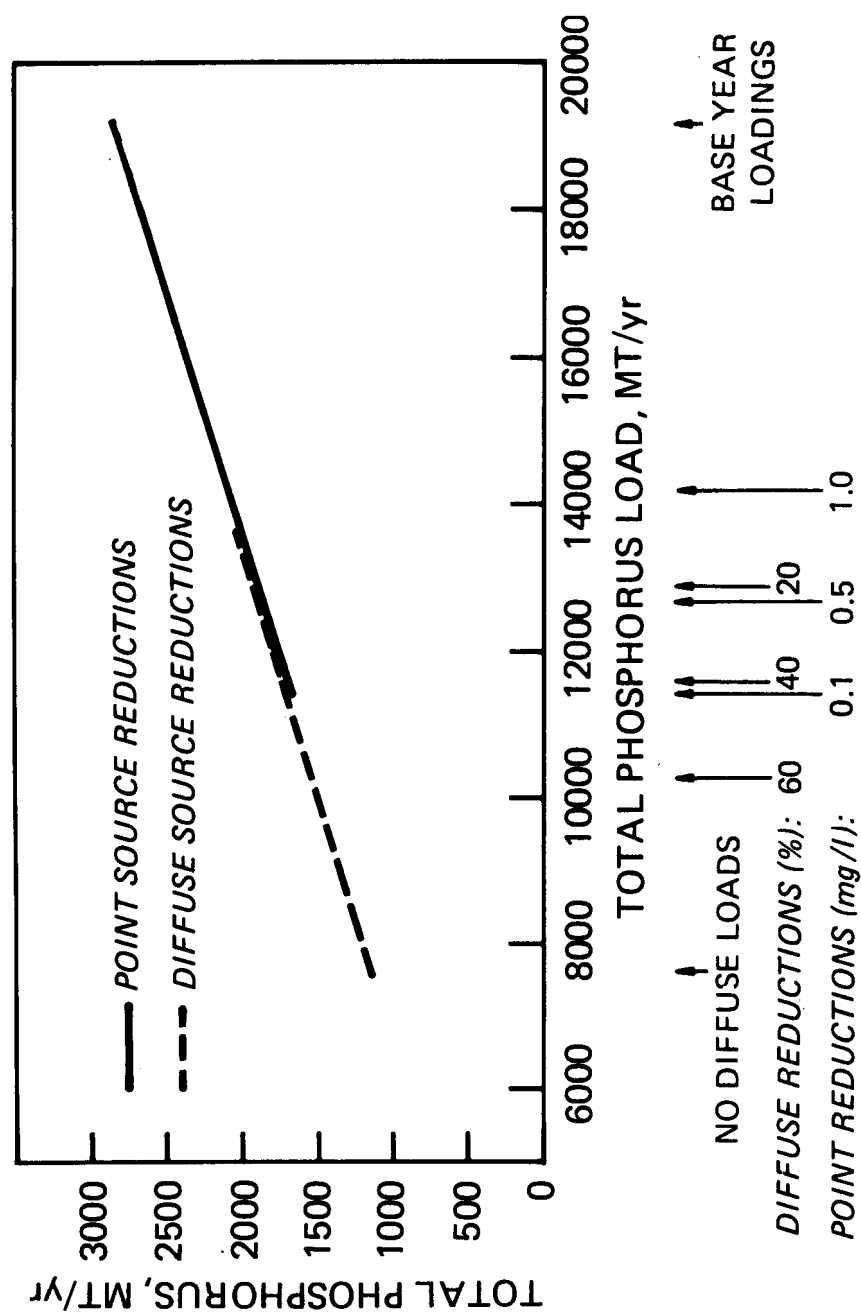


Figure 88. Total phosphorus discharge to Lake Ontario versus lake total phosphorus loading (metric tons/yr). This loading is calculated based on the eastern basin epilimnion concentration and the existing flow to the Niagara River.

oxygen demand reduction that is calculated for the surface sediment. This adjustment is meant only to simulate the magnitude of the reduction in deep sediment oxygen demand and not its progression in time. A fully dynamic calculation of this effect is beyond the scope of this initial effort. However, it is a key component in any calculation with attempts to estimate the time required to reach an equilibrium with a changed loading. The projections relating to dissolved oxygen have two sets of results: one to represent the short-term effect where only the surface sediment oxygen demand responds to loading changes and the other to represent the long-term or ultimate effect when the entire sediment oxygen demand has responded to loading changes.

Figure 89 shows the effect of reducing phosphorus on the maximum anoxic area to be expected in any year. Using the short-term and ultimate effect to bracket the estimate, the estimate is that anoxia will be eliminated when the phosphorus load is reduced to between 10,500 and 12,600 metric tons/yr under point source reduction and between 9,500 and 12,200 metric tons/yr under diffuse source reduction. These loadings correspond to a point source effluent concentration range from about 0 to 0.5 mg/l phosphorus and a reduction in diffuse sources of between 30 and 70 percent with a 1.0 mg/l point source effluent. Higher chlorophyll concentrations under diffuse reductions is the reason for the greater anoxic area at the same total phosphorus loading. The extra chlorophyll and detrital organic carbon settles into the hypolimnion where it increases the oxygen demand through respiration and oxidation.

The oxygen consumption rate necessary to maintain oxic conditions may be found in the phosphorus loading versus oxygen depletion rate plot, Figure 90. The consumption rate is the sum of all water column and sediment oxygen sinks in the hypolimnion. It does not include the dissolved oxygen being transported across the thermocline from the epilimnion. It is, therefore, larger than the actual observed depletion rate. Using the loadings given above, the

consumption at the point of zero anoxic area is found to be 0.089 mg/l/day. The current depletion rate (base year) is 0.13 mg/l/day. Thus, a reduction of 0.041 mg/l/day, or 32%, is necessary to prevent anoxia.

The dissolved oxygen concentrations calculated in these simulations are volume averages for each segment. For the two segments comprising the central basin hypolimnion, it is straightforward to calculate the volume average concentration for the entire hypolimnion at any point in time. Two sets of calculations are presented: the volume average hypolimnion concentration just prior to overturn, Figure 91; and the temporal average during the period of stratification of the volume average hypolimnion concentration, Figure 92. The oxygen concentration just prior to overturn are used to establish the area of anoxia. This figure may be used in conjunction with the minimum versus volume average dissolved oxygen plot, Figure 42, to determine an estimate of the absolute minimum dissolved oxygen to occur in the basin at any loading rate.

Certain specific phosphorus reductions are of special interest. These include the reductions necessary to achieve zero anoxic area, to achieve a minimum dissolved oxygen of 1 mg/l, or to maintain phosphorus concentrations at or below 20, 15, and 15 $\mu\text{g/l}$ in the western, central and eastern basins, respectively. The effect of these reductions on conditions in the lake as well as the effect of specific point source reductions is shown in Table 30. The ranges given in the table represent the span from the short-term effect to the ultimate effect. The results shown in this table may be obtained directly from the loading reduction plots.

Simulations of the effects of reducing phosphorus loadings on the in-lake phosphorus concentration has also been performed by the USACOE, Buffalo District. The model used is a phosphorus mass balance model considering each basin as a completely mixed unit with no dispersive exchange between basins. Phosphorus exchange with the sediment is

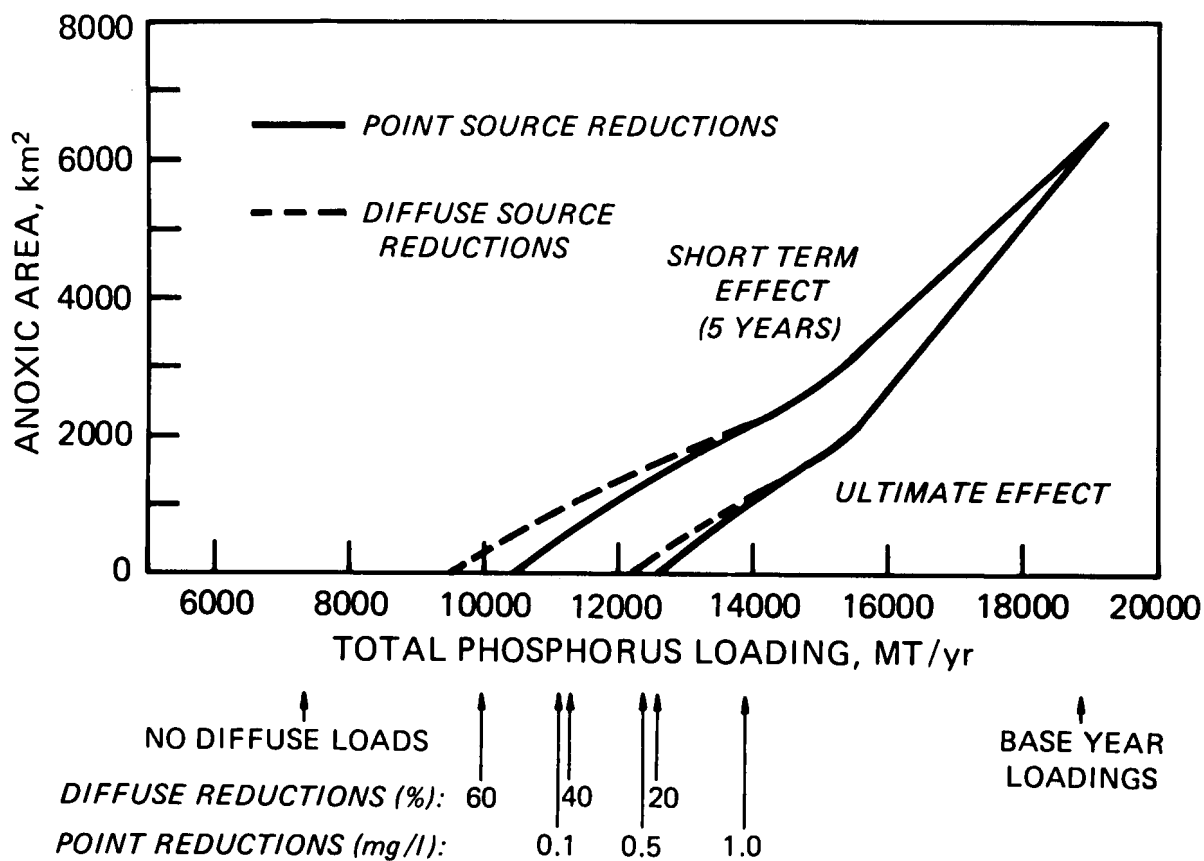


Figure 89. Area of anoxia (km²) versus lake total phosphorus loading (metric tons/yr) showing both the short-term and ultimate effects.

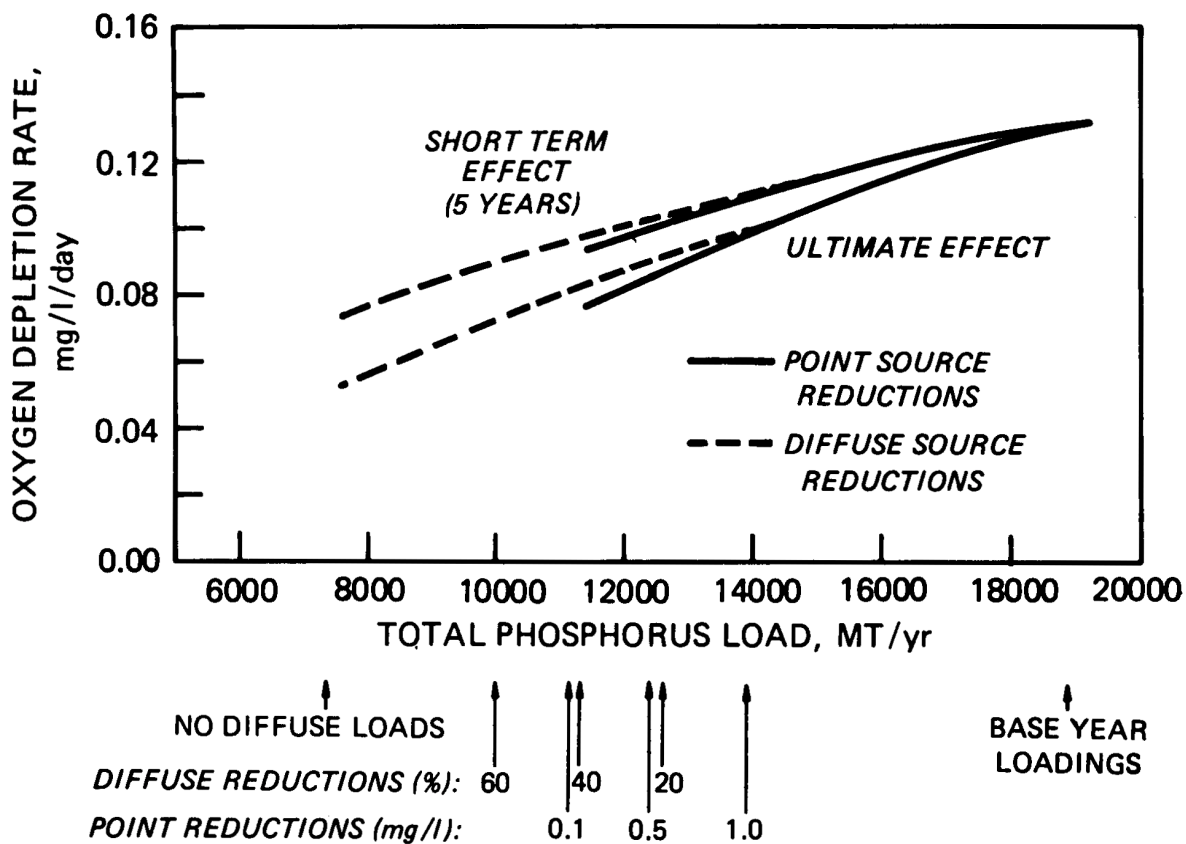


Figure 90. Central basin hypolimnion oxygen consumption rate (mg/l/day) versus lake total phosphorus loading (metric tons/yr). The consumption rate is the sum of all water column and sediment oxygen sinks in the hypolimnion.

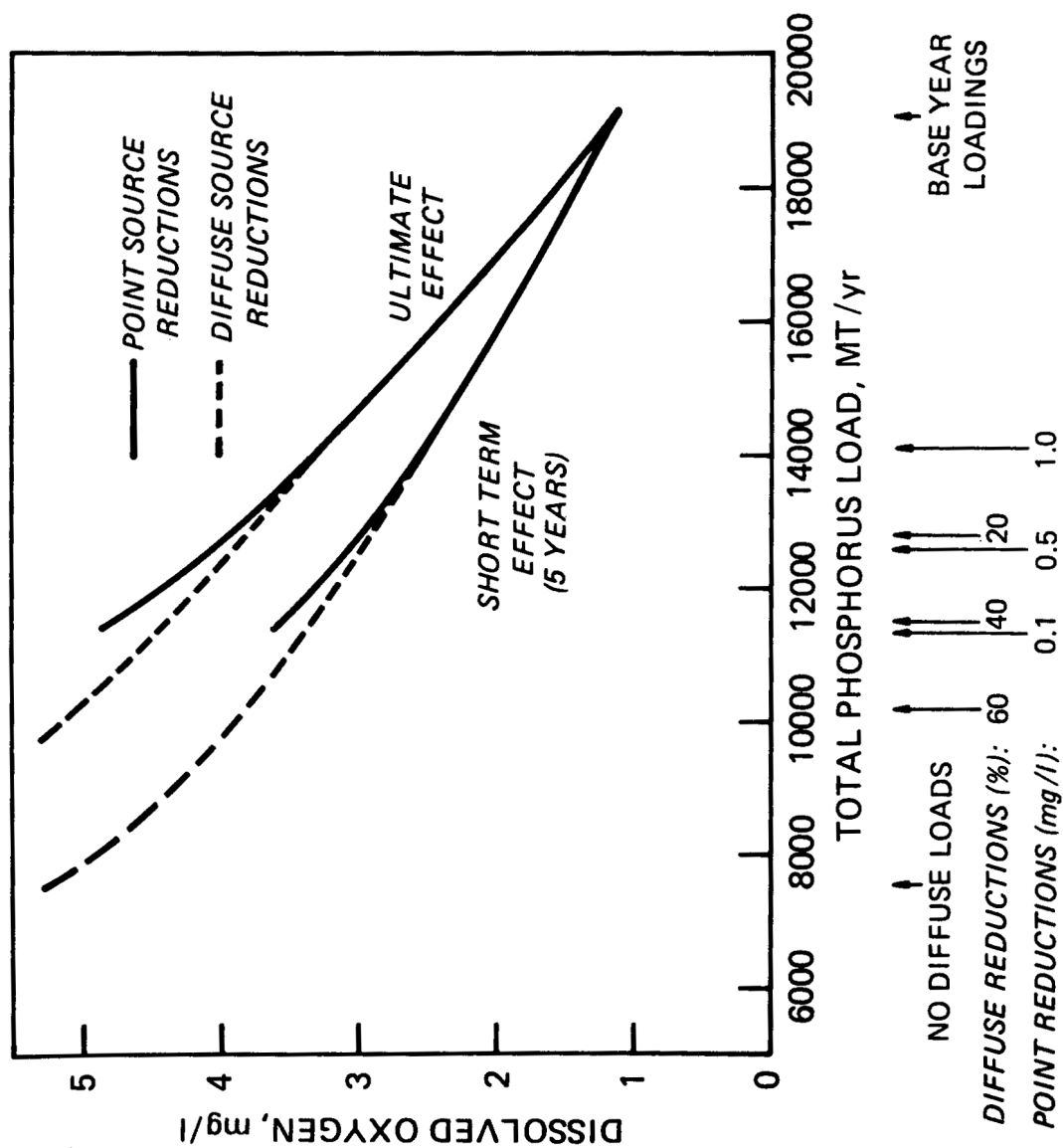


Figure 91. Minimum central basin hypolimnion dissolved oxygen (volume averaged concentration just prior to overturn in mg/l) versus lake total phosphorus loading (metric tons/yr).

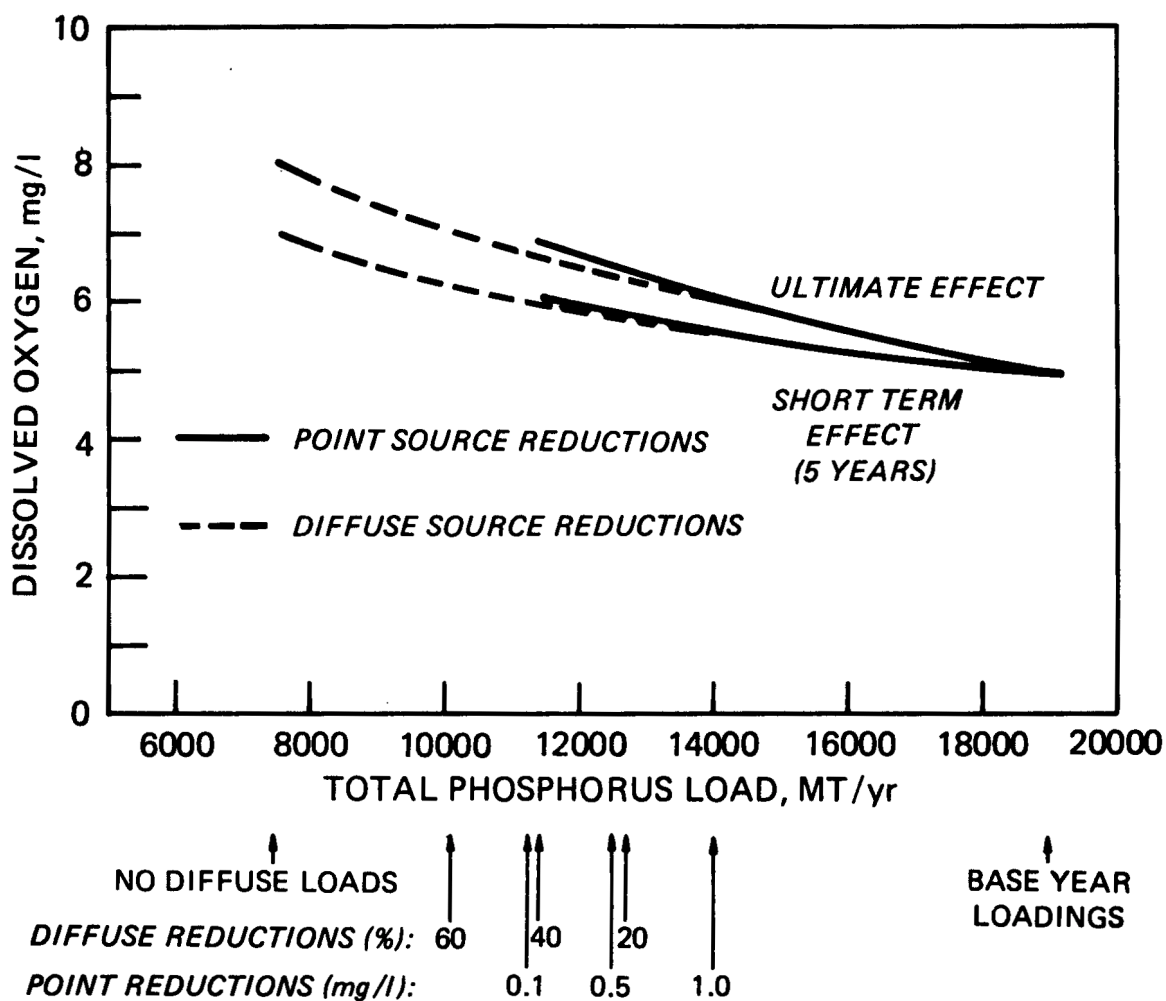


Figure 92. Summer average central basin hypolimnion dissolved oxygen (mg/l) versus lake total phosphorus loading (metric tons/yr).

Table 30. Simulation Results* - Summer Averages

Criteria	Reduction Type	Lake Loading	Western Basin		
			Chlorophyll a (µg/l)	Total Phosphorus (µg/l)	Secchi (Meters)
No Anoxia	D	9500-12200	12.3-14.0	19.0-21.7	1.92-1.85
	P	10500-12600	10.0-12.7	17.5-21.0	2.10-1.91
Minimum Dissolved Oxygen of 1.0 mg/l	D	8200-10600	11.7-12.9	18.0-20.2	1.97-1.90
	P	9100-11500	8.0-11.2	14.8-19.0	2.2-2.0
Total Phosphorus of 20, 15, and 15 µg/l or Less in Western, Central and Eastern Basins, Respectively	D	10500	12.9	20	1.90
	P	12100	11.8	20	1.96
Point Sources at 1 µg/l Total Phosphorus	P	14195	14.9	23.5	1.8
Point Sources at 0.5 µg/l Total Phosphorus	P	12652	12.8	20.9	1.9
Point Sources at 0.1 µg/l Total Phosphorus	P	11419	11.1	18.8	2.0
Criteria	Reduction Type		Central Basin		
			Chlorophyll a (µg/l)	Total Phosphorus (µg/l)	Secchi (Meters)
No Anoxia	D		3.1-4.2	7.8-9.9	6.35-5.56
	P		2.8-4.2	8.3-10.0	6.5-5.56
Minimum Dissolved Oxygen of 1.0 mg/l	D		2.5-3.5	6.7-8.7	6.80-6.00
	P		1.9-3.5	7.2-9.2	7.3-6.0
Total Phosphorus of 20, 15, and 15 µg/l or Less in Western, Central and Eastern Basins, Respectively	D		3.5	8.5	6.04
	P		3.8	9.5	5.74
Point Sources at 1 µg/l Total Phosphorus	P		5.2	11.5	5.1
Point Sources at 0.5 µg/l Total Phosphorus	P		4.2	10.2	5.6
Point Sources at 0.1 µg/l Total Phosphorus	P		3.5	9.2	6.0

*Ranges given are short-term - ultimate range.

Table 30. Simulation Results* - Summer Average (Continued)

Criteria	Reduction Type	Eastern Basin		
		Chlorophyll a (µg/l)	Total Phosphorus (µg/l)	Secchi (Meters)
No Anoxia	D	2.2-3.2	6.2-8.2	6.98-6.16
	P	2.3-3.2	6.9-8.3	7.0-6.10
Minimum Dissolved Oxygen of 1.0 mg/l	D	1.7-2.6	5.2-7.0	7.45-6.62
	P	1.6-2.7	5.9-7.5	7.7-6.5
Total Phosphorus of 20, 15, and 15 µg/l or Less in Western, Central and Eastern Basins, Respectively	D	2.6	7.0	6.65
	P	3.0	8.0	6.29
Point Sources at 1 µg/l Total Phosphorus	P	4.0	9.5	5.7
Point Sources at 0.5 µg/l Total Phosphorus	P	3.3	8.4	6.1
Point Sources at 0.1 µg/l Total Phosphorus	P	2.7	7.6	6.5
Criteria	Reduction Type	Central Basin Hypolimnion		
		Oxygen Consumption Rate (mg/l/day)	Summer Average Dissolved Oxygen (mg/l)	Anoxic Area (km ²)
No Anoxia	D	0.088	6.4	-
	P	0.088	6.4	-
Minimum Dissolved Oxygen of 1.0 mg/l	D	0.078	6.8	-
	P	0.078	6.8	-
Total Phosphorus of 20, 15, and 15 µg/l or Less in Western, Central and Eastern Basins, Respectively	D	0.92-0.76	6.1-6.9	700-0
	P	0.98-0.83	5.9-6.6	1400-0
Point Sources at 1 µg/l Total Phosphorus	P	0.11-0.10	5.5-6.0	2268-1236
Point Sources at 0.5 µg/l Total Phosphorus	P	0.10-0.088	5.8-6.5	1473-34.8
Point Sources at 0.1 µg/l Total Phosphorus	P	0.093-0.077	6.0-6.9	698-0

*Ranges given are short-term - ultimate range.

incorporated. A full description of the model as well as its results is presented in the USACOE Lake Erie Waste Management Study (USACOE, 1975). Phosphorus concentrations of 80, 15 and 15 $\mu\text{g P/l}$ in the western, central and eastern basins, respectively, are proposed as objectives in order to provide significant rehabilitation of Lake Erie. A series of alternatives have been developed in order to meet these criteria and Plan IX succeeded in meeting the objective. This plan calls for the reduction of treatment plant effluents to 1 mg $\text{PO}_4\text{-P/l}$ for all treatment plants with capacities equal to or greater than one-million gallons per day. In addition, there is to be a 37% diffuse source reduction in the western basin and a 24% diffuse source reduction in the eastern basin.

This phosphorus reduction scheme has been simulated using the Lake Erie model employed for the above calculations. A comparison with the USACOE results is shown in Table 31. Except for dissolved oxygen, the results are fairly consistent. However, the results for dissolved oxygen indicate that these phosphorus levels are not sufficient to provide the significant rehabilitation the USACOE is striving for. The short-term analysis indicates that the anoxic area will be about 1733 km^2 , reducing ultimately to 500 km^2 of anoxic area. The calculated oxygen

consumption rate ranges from 0.106 to 0.093 mg/l/day between the short-term and ultimate conditions. There will be substantial reduction in chlorophyll levels with the average summer chlorophyll being reduced from about 37% in the western basin, 45% in the central basin and 45% in the eastern basin. Secchi depth is calculated to improve by 18, 29 and 27% in the western, central and eastern basins, respectively.

12.3 ON THE UNCERTAINTY OF THE PREDICTIONS

An important and, unfortunately, difficult problem is to evaluate the level of uncertainty associated with the predictions. Broadly speaking, there are two classes of uncertainty which can be associated with the predictions. These might be called structural uncertainty due to physical, chemical, and biological processes which have been misrepresented or entirely ignored, and parameter uncertainty due to miscalibration and data uncertainty. There appears to be no general way of evaluating the level of structural uncertainty since if one knew that processes were incorrectly specified, one would presumably correct that specification. The same is true for important processes that have been

Table 31. Comparison of Results - This Work and the USACOE Phosphorus Model

Loading Condition	Basin	Total Phosphorus Concentration, $\mu\text{g PO}_4\text{-P/l}$	
		This Work	USCOE
Present* (Base Year)	Western	36.	37.
	Central	16.3	18.
	Eastern	12.4	22.
USACOE Plan IX	Western	23.5	20.
	Central	11.	12.
	Eastern	8.4	15.

*USACOE model uses the 1973 loadings = 19607 metric tons/yr. This work uses the base year = 19182 metric tons/yr.

entirely ignored. An attempt has been made to evaluate the range of prediction uncertainty due to the long-term versus short-term behavior of the sediment under reduced phosphorus loadings but no general method is available to cope with other sources of structural uncertainty.

The effect of parameter uncertainty can be evaluated using sensitivity analysis. However, it is now known *a priori* how uncertain the parameters are and, therefore, what are reasonable ranges for the sensitivity analysis.

Consider another approach. If it is assumed that there are no data errors, then the calibration uncertainty is due entirely to parameter uncertainty. Under projected conditions, it is likely that projection uncertainty is at least as large as calibration uncertainty since if a "projection" were made using the calibration conditions the correct "projection" uncertainty would be the known calibration uncertainty. Hence, it seems reasonable to assume that calibration uncertainty is the lower bound of prediction uncertainty.

An application of this line of reasoning can be made to the uncertainty of prediction associated with Figure 91, the minimum central basin hypolimnion dissolved oxygen versus lake total phosphorus loading. This figure, together with Figures 42 and 92, are combined to evaluate the area of anoxia to be expected for various total phosphorus loadings. As can be seen in Figure 91, the relationship between minimum dissolved oxygen, C_{\min} , and phosphorus loading, W , is roughly linear so that a Taylor series expansion about W_o yields:

$$C_{\min}(W) = C_{\min}(W_o) + \left(\frac{\partial C_{\min}}{\partial W}\right)_o (W - W_o) \quad (89)$$

where $C_{\min}(W)$ is the minimum dissolved oxygen projected to occur at loading rate W . If $C_{\min}(W)$ and W are thought of as random variables then the variance of these quantities are related by the equation:

$$V\{C_{\min}(W)\} = \left(\frac{\partial C_{\min}}{\partial W}\right)_o^2 V\{W\} \quad (90)$$

For the calibration and verification conditions, the statistical analysis of the dissolved oxygen residuals gave a residual standard deviation of 0.5 - 1.0 mg/l (variance of 0.25 - 1.0 mg²/l²). If it is assumed that this calibration variance is a reasonable estimate of $V\{C_{\min}(W)\}$, which is the projection variance, then from Figure 91 $\partial W / \partial C_{\min} = 2000$ (metric tons/yr) (mg/l) (at $W = 10,000$ metric tons/yr) and taking the square root of Equation 90 yields:

$$\sigma_W = \left| \frac{\partial W}{\partial C_{\min}} \right| \sigma_{C_{\min}} \quad (91)$$

where σ_W is the standard deviation of the projected loading and $\sigma_{C_{\min}}$ is the standard deviation of the projected minimum dissolved oxygen. For $\sigma_{C_{\min}} = 0.5$ mg/l, $\sigma_W = 1000$ metric tons/yr and for $\sigma_{C_{\min}} = 1.0$ mg/l, $\sigma_W = 2000$ metric tons/yr. Hence, if the calibration standard deviation is taken as a measure of the projection uncertainty of minimum dissolved oxygen, the corresponding projected loading to achieve a specified minimum dissolved oxygen is uncertain to between 1000 and 2000 metric tons/yr depending on the choice of $\sigma_{C_{\min}}$. At $W = 10,000$ metric tons/yr, this amounts to between a 10 and 20% uncertainty of predictions.

APPENDIX

LAKE ERIE MODEL INPUT INFORMATION

The purpose of this Appendix is to summarize the input information necessary to make the calculations discussed in this report. The kinetics are described in the body of this report (Tables 11-19). Where this is not the case, references are presented here.

MORPHOMETRY AND HYDRODYNAMIC REGIME

The morphometry and hydrodynamic regime for 1970 is presented in Table A-1. The modified segmentation and transport regime for 1975 is presented in Table A-2.

PHYSICAL EXOGENOUS VARIABLES

Water Temperature

The temperature distribution is constructed from cruise averages for each segment using 1970 CCIW data. These data are the same as that used for the calibration of the transport regime. Winter values have been estimated due to the absence of cruise data for this period. These temperatures are given in Table A-3.

Solar Radiation

Solar radiation data for Lake Erie are available from Mateer (IJC, 1969) and Richards and Loewen (FWPCA, 1968). The Mateer data are over the lake data while the Richards and Loewen data are recorded at Cleveland and adjusted by a lake-to-land ratio. The Richards and Loewen data are used and these are listed in Table A-4 as well as the data from Mateer.

Photoperiod

The photoperiod data used in the Lake Erie model are taken from the photoperiod information given by Thomann *et al.* (1975) and listed in Table A-5. This data is calculated from sunrise and sunset information reported in the World Almanac.

Background Water Clarity

The non-chlorophyll related extinction coefficient is a function of wind velocity. This function is shown in Figure 44. The wind velocity is also given in that figure.

Oxygen Transfer Coefficient

The oxygen transfer coefficient used is temporally and spatially constant. It is set at two meters/day which is within the observed range for the lakes at the prevailing wind velocities.

BIOLOGICAL AND CHEMICAL EXOGENOUS VARIABLES

Nutrient Loadings

Phosphorus, nitrogen and silica loadings monthly or by basin have been provided by the USACOE, Buffalo District. These inputs are discussed in Chapter 4. The tabulation for both the calibration and verification years is given for the western basin in Table A-6, the central basin in Table A-7 and for the eastern basin in Table A-8. These nutrients are inputted as mass loadings. The loading information for the chloride

Table A-1. Morphometry and Hydrodynamic Regime for 1970

Segment	Representation	Volume (10 ⁶ ft ³)	Depth (Meters)	Inflow (cfs)	Outflow (cfs)
1	Western Basin	7.972 x 10 ⁵	7.5	213,600	213,600
2	Central Basin Epilimnion	8.284 x 10 ⁶	17	213,600	217,600
3	Eastern Basin Epilimnion	3.247 x 10 ⁶	17	217,600	220,600
4	Eastern Basin Hypolimnion	2.921 x 10 ⁶	23	0	0
5	Central Basin Hypolimnion	1.535 x 10 ⁶	5	0	0
6	Central Basin Lower Hypolimnion	2.648 x 10 ⁵	2	0	0
7	Western Basin Sediment	5.313 x 10 ³	0.05	0	0
8	Central Basin Sediment	9.975 x 10 ³	0.05	0	0
9	Central Basin Sediment	6.350 x 10 ³	0.05	0	0
10	Eastern Basin Sediment	0.546 x 10 ³	0.05	0	0

Table A-1. Morphometry and Hydrodynamic Regime for 1970 (Continued)

Exchange Segments	Interfacial Area (10 ⁶ ft ²)	Characteristic Length (Meters)	Exchange (10 ⁶ ft ³ /day)
1-2	3.49	1.2 x 10 ⁵	1.35 x 10 ⁴
2-3	9.69	1.6 x 10 ⁵	4.75 x 10 ⁴
2-5	1.01 x 10 ⁵	11.2	*
3-4	4.49 x 10 ⁴	32.0	*
5-6	4.04 x 10 ⁴	3.8	2.99 x 10 ⁵
7-1	3.24 x 10 ⁴	3.275	3.25 x 10 ²
8-5	6.08 x 10 ⁴	2.6	7.68 x 10 ²
9-6	4.04 x 10 ⁴	1.025	1.28 x 10 ³
10-4	4.49 x 10 ⁴	10.0	1.91 x 10 ²

Table A-1. Morphometry and Hydrodynamic Regime for 1970 (Continued)

Time Variable Exchange (10 ⁶ ft ³ /day)								
Exchange Segments	Exchange	Time	Exchange	Time	Exchange	Time	Exchange	Time
2-5	250000.	0.	250000.	90.	50000.	150.	10000.	180.
	10000.	220.	10000.	240.	200000.	260.	250000.	270.
	250000.	365.						
3-4	200000.	0.	200000.	90.	40000.	150.	10000.	180.
	10000.	220.	10000.	240.	137000.	260.	200000.	270.
	200000.	365.						

Table A-2. 1975 Resegmentation

Segment	Representation	Volume (10 ⁶ ft ³)	Depth (Meters)	Inflow (cfs)	Outflow (cfs)	Exchange Segments	Interfacial Area (10 ⁶ ft ²)
2	Central Basin Epilimnion	6.589 x 10 ⁶	13	213,600	217,600	2-5	1.51 x 10 ⁵
3	Eastern Basin Epilimnion	2.599 x 10 ⁶	13	217,600	220,600	3-4	5.38 x 10 ⁴
4	Eastern Basin Hypolimnion	3.568 x 10 ⁶	27	0	0		
5	Central Basin Hypolimnion	3.230 x 10 ⁶	9	0	0		

1975 Vertical Exchanges (10⁶ ft³/day)

Exchange Segment	Exchange	Time	Exchange	Time	Exchange	Time	Exchange	Time
2-5	776800.	0.	776800.	90.	97100.	150.	38840.	180.
	38840.	220.	38840.	240.	275000.	260.	388400.	270.
	776800.	300.	776800.	365.				
3-4	191380.	0.	191380.	90.	95190.	150.	6346.	180.
	6346.	220.	6346.	240.	6346.	260.	6346.	270.
	191380.	300.	191380.	365.				

Table A-3. Water Temperature °C

Segment	0	15	45	75	105	135	165	195	225	255	285	315	345	365
1	1.0	1.0	1.0	2.0	5.7	13.38	18.73	22.4	23.83	22.11	16.19	8.29	3.09	1.0
2	3.0	2.0	1.0	2.0	3.25	9.94	15.69	20.33	22.11	21.53	17.27	10.85	5.0	3.0
3	4.0	2.0	1.0	1.0	1.61	6.63	14.19	19.55	22.34	21.22	16.85	11.42	6.15	4.0
4	4.0	2.0	1.0	1.0	0.80	3.46	6.41	8.71	11.48	12.46	13.18	10.49	6.51	4.0
5-6	3.0	2.0	1.0	1.0	2.27	6.18	7.85	10.19	12.25	14.74	16.0	11.40	6.06	3.0

Table A-4. Solar Radiation Data

Month	Solar Radiation at Cleveland Langleys/Day	Lake-to-Land Ratio*	Solar Radiation on Lake* Langleys/Day	Solar Radiation From Mateer Langleys/Day
January	123	0.8	98	110
February	177	0.8	142	190
March	300	0.8	240	290
April	365	0.89	325	390
May	509	1.09	555	450
June	546	1.19	650	550
July	523	1.15	602	550
August	458	1.28	586	470
September	360	1.33	479	370
October	246	1.37	337	240
November	129	1.08	140	130
December	100	0.9	90	90

*Values used in the calculation.

Table A-5. Photoperiod Data

Julian Date	Photoperiod in Days
0	0.375
15	0.385
45	0.435
75	0.50
105	0.57
135	0.626
165	0.658
195	0.646
225	0.599
255	0.532
285	0.466
315	0.405
345	0.370
365	0.375

Table A-6. Loadings to Lake Erie Western Basin (kg/day), Calibration Year - 1970, Verification Year - 1975

Month	Total Phosphorus		Orthophosphorus		Organic Nitrogen		NH ₃ -N		NO ₂ -NO ₃ -N		Dissolved Silica	
	1970	1975	1970	1975	1970	1975	1970	1975	1970	1975	1970	1975
Jan	31500	46594	12300	17800	122500	151900	55200	85900	107800	367500	432000	831700
Feb	44500	57365	15700	20500	149900	169600	65600	87700	239100	377200	678800	907600
Mar	53000	38128	18000	16400	176800	139900	75800	81600	297900	342200	803100	798000
Apr	63500	37693	20200	16600	197700	143700	82100	83300	355300	309000	918700	773500
May	66000	43967	17700	16700	170100	139800	71400	80100	288900	344900	853900	846000
Jun	44200	44026	15400	16800	160200	141100	70300	81600	157400	340900	598300	844800
Jul	44800	35299	15800	14800	122800	132200	71700	80100	163200	224000	609400	631600
Aug	41600	34776	15200	15100	160100	134200	70600	80500	131900	249500	546900	656800
Sep	39800	37286	15000	16000	158600	139200	70000	82400	125300	269400	528000	720600
Oct	40200	34059	15200	14500	158800	128300	70100	77700	133900	210700	542200	600400
Nov	42700	31173	15500	14400	161800	127100	71300	77200	166400	208800	584300	519900
Dec	48400	51751	16400	17100	166000	139700	72500	79500	219000	305500	692300	895200

Table A-7. Loadings to Lake Erie Central Basin (kg/day), Calibration Year - 1970, Verification Year - 1975

Month	Total Phosphorus		Orthophosphorus		Organic Nitrogen		NH ₃ -N		NO ₂ -NO ₃ -N		Dissolved Silica	
	1970	1975	1970	1975	1970	1975	1970	1975	1970	1975	1970	1975
Jan	13500	18500	4400	4600	17600	35200	16100	24300	44100	109000	103400	256900
Feb	16800	25000	5200	5200	25700	42800	21400	28500	82100	123100	189100	308200
Mar	18500	16900	5400	4700	29200	36800	21600	25000	93400	107700	203500	260200
Apr	17800	6800	5400	2500	26700	12200	19200	13100	103100	35500	206700	75600
May	11100	7600	4100	2700	13500	12400	13900	12500	60100	21600	109900	96700
Jun	10100	9400	4100	2900	12600	16800	13300	16500	48200	43400	89500	112400
Jul	8300	4500	3500	1800	7900	5000	12000	9700	27200	13900	45900	26600
Aug	7600	6200	3400	2300	6200	9400	11300	11600	17100	29500	27300	55700
Sep	8100	9800	3400	3200	7700	18100	12600	16600	17600	56100	35700	122600
Oct	9600	5500	3700	2200	11300	8000	14900	11500	24400	25200	60500	54200
Nov	13300	5300	4400	2100	20500	7600	20300	11400	49400	21500	114700	47300
Dec	13700	11700	4900	3300	21900	22700	19200	19300	70400	68300	147800	15600

Table A-8. Loadings to Lake Erie Eastern Basin (kg/day), Calibration Year - 1970, Verification Year - 1975

Month	Total Phosphorus		Orthophosphorus		Organic Nitrogen		NH ₃ -N		NO ₂ -NO ₃ -N		Dissolved Silica	
	1970	1975	1970	1975	1970	1975	1970	1975	1970	1975	1970	1975
Jan	2400	4200	900	800	6400	12700	2700	4000	6200	20500	28800	69500
Feb	3300	5600	1000	900	10800	16500	3500	4700	11300	25700	51900	84600
Mar	4700	9100	1200	1600	11900	18900	4400	6100	24700	50000	72000	132800
Apr	11500	15000	2100	2000	29100	22700	7700	6800	56900	58700	154100	149700
May	3800	2600	1200	800	9400	9800	3600	3800	20000	17200	52800	45100
Jun	2200	3800	900	700	5800	11400	2500	3800	5400	17700	21700	64700
Jul	2400	1400	1000	600	5900	5000	2700	2400	8700	5000	27100	19300
Aug	2800	2400	1000	800	5700	6800	2700	2900	6200	12100	25000	32000
Sep	3000	2100	1000	700	8000	6900	3300	2800	11300	11700	38300	29100
Oct	3100	1700	1000	600	8200	7900	3100	2500	12900	6900	43800	24900
Nov	5400	2200	1300	700	19200	7100	5400	2900	27700	13800	79800	32600
Dec	5800	4700	1500	1100	15000	15200	5600	4900	37100	32800	92100	81700

calculations is given in Table A-9. The phosphorus loading used for the projections are given in Tables A-10, A-11, and A-12. The loading input of the other state variables as well as atmospheric nutrient loads are in the form of boundary concentration conditions (mass/unit volume). Boundary conditions, since they are always associated with a flow regime (volume/unit time), can also be viewed as mass loadings in the water body. The boundary conditions used are given in Table A-13.

Initial Conditions

The initial conditions are shown in Table A-14. The integration starts the first of January and these values reflect the measured values for this part of the year.

Table A-9. Mass Loading of Chlorides to Lake Erie (Metric Tons/Day), Calibration Year - 1970, Verification Year - 1975

Month	Western Basin		Central Basin		Eastern Basin	
	1970	1975	1970	1975	1970	1975
January	5990	8590	3450	4180	174	312
February	7500	8850	3730	4320	237	379
March	8690	8170	3980	4540	350	616
April	9190	8300	3860	3330	817	744
May	8480	8180	3190	3970	307	273
June	7950	8270	2640	3790	175	293
July	8090	7740	1350	1430	193	159
August	7870	7860	1020	1770	167	247
September	7790	8140	1770	3650	213	219
October	7820	7480	2570	3280	235	193
November	8010	7430	3690	3220	376	240
December	8350	8190	3930	5360	483	409

Table A-10. Phosphorus Loads Used for Projections - Western Basin (kg/day)

Month	Base Year							
	Total Phosphorus				Orthophosphorus			
	Detroit River	Point	Non-Point	Total	Detroit River	Point	Non-Point	Total
Jan	27450	2960	1020	31430	12590	1470	680	14740
Feb	27210	2940	10800	40950	12480	1450	2940	16870
Mar	26250	2960	14410	43620	12040	1480	3540	17060
Apr	27690	2960	24730	55380	12700	1480	5700	19880
May	27690	2960	27380	58030	12700	1480	3200	17380
Jun	28290	2960	4390	35640	12970	1480	430	14880
Jul	28530	2870	4280	35690	13080	1470	560	15110
Aug	28530	2830	1200	32550	13080	1210	240	14530
Sep	28770	2380	800	31960	13190	1110	460	14760
Oct	27570	2890	810	31270	12640	1330	480	14450
Nov	27330	2960	23890	54180	12530	1480	2790	16800
Dec	27090	2960	3060	33110	12420	1480	960	14860

Month	Point Source Reduced to 1 mg/l							
	Total Phosphorus				Orthophosphorus			
	Detroit River	Point	Non-Point	Total	Detroit River	Point	Non-Point	Total
Jan	17070	1140	1990	20190	7390	570	1150	9130
Feb	16960	1140	11750	29860	7360	570	3380	11320
Mar	16320	1140	15380	32840	7070	570	4030	11680
Apr	17200	1140	25700	44030	7470	570	6190	14230
May	17190	1140	28350	46680	7450	570	3690	11710
Jun	17600	1140	5360	24100	7533	570	920	9030
Jul	17740	1140	5140	24000	7680	570	1040	9290
Aug	17740	1130	1970	20840	7677	570	410	8680
Sep	17900	1130	1110	20130	7733	500	590	8830
Oct	17160	1130	1670	19970	7420	560	790	8740
Nov	17000	1140	24860	43000	7330	570	3270	11170
Dec	16870	1140	4030	22030	7290	570	1440	9320

Table A-11. Phosphorus Loads Used for Projections - Central Basin (kg/day)

Month	Base Year					
	Total Phosphorus			Orthophosphorus		
	Non-Point	Point	Total	Non-Point	Point	Total
Jan	3820	5210	9040	620	2060	2680
Feb	16460	5490	21950	2390	2380	4770
Mar	8550	5480	14030	1390	2380	3770
Apr	4040	5370	9410	910	2260	3170
May	3570	4850	8230	620	2060	2680
Jun	960	5290	6250	190	2200	2390
Jul	250	4740	4990	130	1790	1920
Aug	100	4190	4290	90	1710	1800
Sep	550	4470	5010	100	1800	1890
Oct	1060	4930	5990	180	1980	2160
Nov	4300	5360	9660	720	2170	2890
Dec	4730	5480	10220	820	2410	3230

Month	Point Sources Reduced to 1 mg/l					
	Total Phosphorus			Orthophosphorus		
	Non-Point	Point	Total	Non-Point	Point	Total
Jan	5210	1960	7170	1000	1090	2090
Feb	18180	1960	20140	2820	1370	4190
Mar	10260	1960	12220	1820	1370	3190
Apr	5620	1960	7580	1330	1260	2590
May	4520	1960	6480	970	1120	2090
Jun	2440	1960	4390	550	1240	1790
Jul	1070	1940	3010	190	1060	1250
Aug	230	1910	2140	100	1010	1110
Sep	1010	1930	2940	170	1050	1220
Oct	2080	1950	4030	410	1110	1520
Nov	5850	1950	7800	1060	1220	2290
Dec	6450	1960	8410	1230	1410	2650

Table A-12. Phosphorus Loads Used for Projections - Eastern Basin (kg/day)

Month	Base Year					
	Total Phosphorus			Orthophosphorus		
	Non-Point	Point	Total	Non-Point	Point	Total
Jan	1030	1010	2040	50	490	540
Feb	1290	1010	2300	170	480	650
Mar	4290	1010	5300	360	500	870
Apr	8520	1010	9530	1220	500	1710
May	2070	1010	3080	320	480	800
Jun	620	1010	1630	100	470	570
Jul	710	970	1680	150	470	610
Aug	530	940	1470	140	460	600
Sep	850	940	1790	140	460	610
Oct	850	960	1810	130	470	590
Nov	2440	1010	3450	450	490	940
Dec	4190	1010	5200	690	490	1180

Month	Point Sources Reduced to 1 mg/l					
	Total Phosphorus			Orthophosphorus		
	Non-Point	Point	Total	Non-Point	Point	Total
Jan	1090	510	1600	80	240	320
Feb	1350	510	1870	200	230	430
Mar	4350	510	4860	390	260	650
Apr	8580	510	9090	1250	250	1490
May	2130	510	2640	350	230	580
Jun	680	510	1190	130	220	350
Jul	770	470	1240	180	220	390
Aug	590	440	1030	170	210	390
Sep	910	440	1350	170	210	390
Oct	910	470	1380	160	220	380
Nov	2500	510	3020	480	240	720
Dec	4252	510	4770	720	240	960

Table A-13. Boundary Conditions

System	Western Basin Segment 1	Central Basin Segment 2	Eastern Basin Segment 3	Units
Non-Diatom Chlorophyll	3.0	3.0	3.0	µg Chl <i>a</i> /l
Herbivorous Zooplankton	0.02	0.02	0.02	mg C/l
Organic Nitrogen	0	0	0	
Ammonia Nitrogen*	0.023	6.549	3.45	mg N/l
Nitrate Nitrogen	0	0	0	
Unavailable Phosphorus	0	0	0	
Orthophosphorus*	.000348	.099	.0522	mg P/l
Carnivorous Zooplankton	0.01	0.01	0.01	mg C/l
Total Inorganic Carbon	1.80	1.76	1.82	meq/l
Alkalinity	1.75	1.9	1.9	meq/l
Non-Living Organic Carbon	0.206	4.24	5.06	mg C/l
Dissolved Oxygen	8.0	8.0	8.0	mg O ₂ /l
Diatom Chlorophyll	5.0	5.0	5.0	µg Chl <i>a</i> /l
Unavailable Silica	0.2	2.0	0.2	mg Si/l
Available Silica	0	0	0	

*Atmospheric loads.

Table A-14. Lake Erie Model Initial Conditions

System	Segment										Units
	1	2	3	4	5	6	7	8	9	10	
Non-Diatom Chlorophyll	2.0	1.0	1.0	1.0	1.0	1.0	220.	110.	110.	70.	µg Chl a/l
Herbivorous Zooplankton	0.01	0.01	0.005	0.005	0.03	0.03	0.0001	0.004	0.004	0.007	mg C/l
Organic Nitrogen	0.1065	0.154	0.151	0.146	0.01	0.01	40.	30.	30.	25	mg N/l
Ammonia Nitrogen	0.05	0.0254	0.0188	0.0105	0.0139	0.036	4.5	3.2	1.2	1.0	mg N/l
Nitrate Nitrogen	0.2564	0.1343	0.1543	0.1470	0.1304	0.105	0.27	0.28	0.37	0.3	mg N/l
Unavailable Phosphorus	0.014	0.01	0.0515	0.0055	0.0083	0.0083	10.0	5.0	5.0	4.0	mg P/l
Orthophosphorus	0.009	0.0026	0.003	0.003	0.0041	0.0041	40.	15.	15.	8.5	mg P/l
Carnivorous Zooplankton	0.005	0.005	0.005	0.005	0.03	0.03	.0001	.0001	.0001	.0001	mg C/l
Total Inorganic Carbon	1.70	1.80	1.92	1.92	1.75	1.75	4.58	2.7	2.0	2.0	meq/l
Alkalinity	1.65	1.85	1.95	1.92	1.71	1.71	1.71	1.71	1.71	1.71	meq/l
Non-Living Organic Carbon	1.0	1.0	1.0	1.0	1.0	1.0	230.	112.	112.	100.	mg C/l
Dissolved Oxygen	13.45	12.35	12.02	11.81	12.06	11.90	-73.	-23.	-35.	-30.	mg O ₂ /l
Diatom Chlorophyll	4.0	2.0	2.0	1.0	2.0	2.0	520.	100.	100.	55.	µg Chl a/l
Unavailable Silica	0.2	0.1	0.1	0.05	0.05	0.05	60.	20.	20.	10.	mg Si/l
Available Silica	0.2	0.1	0.1	0.05	0.05	0.05	400.	150.	150.	100.	mg Si/l

Table A-15. Settling Velocities (m/day)

Diatom Chlorophyll	0.1
Non-Diatom Chlorophyll	0.1
Herbivorous Zooplankton	0.0
Carnivorous Zooplankton	0.0
Detrital Organic Nitrogen	0.2
Ammonia Nitrogen	0.0
Nitrate Nitrogen	0.0
Unavailable Phosphorus	0.2
Soluble Reactive Phosphorus	0.1
Unavailable Silica	0.2
Soluble Reactive Silica	0.0
Detrital Organic Carbon	0.2
Dissolved Inorganic Carbon	0.0
Alkalinity	0.0
Dissolved Oxygen	0.0

Table A-16. Chemical Thermodynamic Parameters for Aqueous Phase Computation

Components*	ΔH_f° (kcal/mole)	S_f° (cal/mole °K)
H ₂ O	-68.315	16.71
H ⁺	0.0	0.0
CO ₂ (g)	-94.051	51.06
Species (Aqueous Phase)		
H ₂ CO ₃ **	-167.22	44.8
HCO ₃ ⁻	-165.39	21.8
CO ₃ ⁼	-161.84	-13.6
H ₂ O	-68.315	16.71
H ⁺	0	0
OH ⁻	-54.970	-2.57

*With this choice of components, CO₂ corresponds to C_T and H⁺ corresponds to negative alkalinity.

**H₂CO₃(aq) = H₂CO₃(aq) + CO₂(aq) \approx CO₂(aq).

Table A-17. Equations for Oxygen and Carbon Dioxide Aqueous Saturation

$$O_{2S} = 14.652 + T(-0.41022 + T * (0.00791 - 0.000077774 * T))$$

for O_{2S} in mg/l and T in °C

$$CO_{2S} = 3.16 \cdot 10^{-4} \exp(4.854/RT - 0.02297/R)$$

for CO_{2S} in mole/liter

$$R = 0.0019872 \text{ kcal/deg mole}$$

$$T = \text{°Kelvin}$$

REFERENCES

- Beeton, A.M. 1958. Relationship Between Secchi Disc Readings and Light Penetrations in Lake Huron. *Trans. Am. Fish. Soc.*, 87:73-79.
- Berner, R.A. 1974. Kinetic Models for the Early Diagenesis of Nitrogen, Sulfur, Phosphorus and Silicon in Anoxic Marine Sediments. In: E.D. Goldberg (Ed.), *The Sea, Volume 5*. John Wiley and Sons, Incorporated, New York, New York.
- Bierman, V.J., JR. 1976. Mathematical Model of the Selective Enhancement of Blue-Green Algae by Nutrient Enrichment. In: R. Canale (Ed.), *Modeling Biochemical Processes in Aquatic Ecosystems*, pp. 1-32. Ann Arbor Science Publishers, Ann Arbor, Michigan.
- Bierman, V.J., Jr., F.H. Verhoff, and T.L. Poulson. 1973. Multi-Nutrient Dynamic Models of Algal Growth and Species Competition in Eutrophic Lakes. Presented at the Symposium Modeling of the Eutrophication Process, Utah State University, Logan Utah, September 5-7, 1973. 65 pp.
- Brewer, P.G. and J.C. Goldman. 1976. Alkalinity Changes Generated by Phytoplankton Growth. *Limnol. Oceanogr.*, 21(1):108-117.
- Brunk, I.W. 1964. Hydrology of Lakes Erie and Ontario. Great Lakes Research Division, The University of Michigan, Ann Arbor, Michigan. Publication Number 11, pp. 205-1216.
- Burns, N.M. 1976. Nutrient Budgets for Lake Erie, 1970. *J. Fish. Res. Board Canada*, 33(3):520-536.
- Burns, N.M. and C.P. Ross. 1972. Project Hypo - An Intensive Study of the Lake Erie Central Basin Hypolimnion and Related Surface Phenomena. U.S. Environmental Protection Agency, Region V, Fairview Park, Ohio. Technical Report TS-05-71-208-24, 182 pp.
- Canada Centre for Inland Waters. 1967. Limnological Data Report, Lake Erie. Canadian Oceanographic Data Centre, Canada Centre for Inland Waters, Burlington, Ontario, Canada.
- Canada Centre for Inland Waters. 1970. Limnological Data Report, Lake Erie. Canadian Oceanographic Data Centre, Canada Centre for Inland Waters, Burlington, Ontario, Canada.
- Canadian Hydrographic Service. 1971. Lake Erie. Chart Number 882.
- Chen, C. 1970. Concepts and Utilities of Ecological Model. *J. San. Engin. Div. ASCE*, 96(SA5):1085-1097.
- Chen, C.W. and G.T. Orlob. 1972. Ecological Simulation for Aquatic Environments. Report to the Office of Water Resources Research, Water Resources Engineers, Incorporated, Walnut Creek, California. Publication OWRR C-2044.
- Clasen, R.J. 1965. The Numerical Solution of the Chemical Equilibrium Problem. Rand Corporation, Santa Monica, California. Publication Number RM-4345-PR.

Conway, H.L., R.J. Harrison, and C.O. Davis. 1976. Marine Diatoms Grown in Chemostats Under Silicate or Ammonium Limitation. II. Transient Response of *Skeletonema costatum* to a Single Addition of the Limiting Nutrient. *Marine Biol.*, 35:187-199.

Csanady, G.T. 1964. Turbulence and Diffusion in the Great Lakes. Great Lakes Research Division, The University of Michigan, Ann Arbor, Michigan. Publication Number 11, pp. 326-339.

Davis, C.O. 1976. Continuous Culture of Marine Diatoms Under Silicate Limitation. II. Effects of Light Intensity on Growth and Nutrient Uptake of *Skeletonema costatum*. *J. Phycol.*, 12:291-300.

Derecki, J.A. 1964. Variation of Lake Erie Evaporation and Its Causes. Great Lakes Research Division, The University of Michigan, Ann Arbor, Michigan. Publication Number 11, pp. 217-227.

Di Toro, D.M. 1976. Combining Chemical Equilibrium and Phytoplankton Models - A General Methodology. In: R. Canale (Ed.), *Modeling Biochemical Processes in Aquatic Ecosystems*, pp. 233-256. Ann Arbor Science Publishers, Ann Arbor, Michigan.

Di Toro, D.M., D.J. O'Connor, and R.V. Thomann, Jr. 1971. A Dynamic Model of the Phytoplankton Population in the Sacramento San Joaquin Delta. *Advances in Chemistry Series* 106, pp. 131-180. American Chemical Society, Washington, D.C.

Di Toro, D.M., D.J. O'Connor, R.V. Thomann, and J.L. Machini. 1975. Phytoplankton-Zooplankton-Nutrient Interaction Model for Western Lake Erie. In: B. Patten (Ed.), *Systems Analysis and Simulation in Ecology*, Volume III, pp. 423-474. Academic Press, New York, New York.

Di Toro, D.M., R.V. Thomann, D.J. O'Connor, and J.L. Machini. 1977. Estuarine Phytoplankton Biomass Models - Verification Analyses and Preliminary Applications. In: E.D. Goldberg (Ed.), *The Sea*, Volume 6, pp. 969-1018. John Wiley and Sons, Incorporated, New York, New York.

Di Toro, D.M. and W.F. Matystik. 1979. Mathematical Models of Water Quality in Large Lakes, I. Lake Huron and Saginaw Bay. U.S. Environmental Protection Agency, Office of Research and Development, Environmental Research Laboratory, Duluth, Minnesota. EPA-600/3-80-056.

Dolan, D.M., V.J. Bierman, Jr., M.H. Dipert, and R.D. Giest. 1977. Statistical Analysis of the Spatial and Temporal Variability of the Ratio Chlorophyll *a*-to-Phytoplankton Cell Volume in Saginaw Bay, Lake Huron. Presented at the 20th Conference on Great Lakes Research, International Association for Great Lakes Research, The University of Michigan, Ann Arbor, Michigan. May 10-12, 1977.

Droop, M.R. 1973a. Some Thoughts on Nutrient Limitation in Algae. *J. Phycol.*, 9:264-272.

Droop, M.R. 1973b. Nutrient Limitation in Osmotrophic Protista. *Am. Zoologist*, 13:209-214.

Droop, M.R. 1974. The Nutrient Status of Algal Cells in Continuous Culture. *J. Marine Biol. Assoc. United Kingdom*, 54:825-855.

Edinger, J.E. and J.C. Geyer. 1968. Analyzing Steam Electric Power Plant Discharges. *J. Sanit. Engin. Div., ASCE*, 94(SA4):611-623.

Eppley, R.W. and E.H. Renger. 1974. Nitrogen Assimilation of an Oceanic Diatom in Nitrogen-Limited Continuous Culture. *J. Phycol.*, 10:15-23.

Federal Water Pollution Control Administration (FWPCA). 1968. Lake Erie Report, A Plan for Water Pollution Control. Great Lakes Region, Federal Water Pollution Control Administration, U.S. Department of the Interior, Chicago, Illinois. 107 pp.

Foree, E.C. and P.L. McCarty. 1970. Anaerobic Decomposition of Algae. *Environ. Sci. Technol.*, 4(10):842-849.

Gedney, R.T. 1971. Numerical Calculations of the Wind Driven Currents in Lake Erie. Ph.D. Thesis, Case Western Reserve University, Cleveland, Ohio. 258 pp.

Glooschenko, W.A., J.E. Moore, M. Munawar, and R.A. Vollenweider. 1974. Primary Production in Lakes Ontario and Erie: A Comparative Study. *J. Fish. Res. Board Canada*, 31(3):253-263.

Goldberg, E.D. and M. Koide. 1963. Rates of Sediment Accumulation in the Indian Ocean. In: H. Geiss and E.D. Goldberg (Eds.), *Earth Science and Meteorites*, pp. 90-102. North-Holland Company, Amsterdam, Germany.

Great Lakes Basin Commission. 1976. Great Lakes Basin Framework Study, Appendix I: Alternate Frameworks. Great Lakes Basin Commission, Ann Arbor, Michigan. 476 pp.

Hamblin, P.F. 1971. Circulation and Water Movement in Lake Erie. Department of Energy, Mines and Resources, Ottawa, Ontario, Canada. Scientific Series Number 7, 48 pp.

Harrison, P.J.; H.L. Conway, and R.C. Dugdale. 1976. Marine Diatoms Grown in Chemostats Under Silicate or Ammonium Limitation. 1. Cellular Chemical Composition and Steady-State Growth Kinetics of *Skeletonema costatum*. *Marine Biol.*, 35:177-186.

Howard, D.L., *et al.* 1970. Biological Nitrogen Fixation to Lake Erie. *Science*, 169:61-62.

Hydroscience, Incorporated. 1973. Limnological Systems Analysis of the Great Lakes - Phase I. Hydroscience, Incorporated, Westwood, New Jersey. 474 pp.

Imboden, D.M. 1975. Interstitial Transport of Solutes in Non-Steady-State Accumulating and Compacting Sediments. *Earth Planet. Sci. Letters*, 27:221-228

International Joint Commission. 1969. Report to the International Joint Commission on the Pollution of Lake Erie, Lake Ontario and the International Section of the St. Lawrence River, Volume 2. International Lake Erie Water Pollution Board and the International Ontario-St. Lawrence River Water Pollution Board, International Joint Commission, Windsor, Ontario, Canada. 316 pp.

International Joint Commission. 1973. Great Lakes Water Quality Annual Report to the International Joint Commission. Great Lakes Water Quality Board, International Joint Commission, Windsor, Ontario, Canada. 315 pp.

International Joint Commission. 1974a. 1973 Annual Report to the International Joint Commission. Great Lakes Water Quality Board, International Joint Commission, Windsor, Ontario, Canada. 115 pp.

International Joint Commission. 1974b. Flow Calculation Methods, Detroit River Range 3.9. International Joint Commission, Windsor, Ontario, Canada.

International Joint Commission. 1975. Great Lakes Water Quality Third Annual Report, Appendix B: Annual Report of the Surveillance Subcommittee. Great Lakes Water Quality Board, International Joint Commission, Windsor, Ontario, Canada. 212 pp.

International Joint Commission. 1976. Great Lakes Water Quality, Fourth Annual Report, Appendix B: Annual Report of the Surveillance Subcommittee. Great Lakes Water Quality Board, International Joint Commission, Windsor, Ontario, Canada. 162 pp.

Kemp, A.L.W., T.W. Anderson, R.L. Thomas, and A. Mudrochova. 1974. Sedimentation Rates and Recent Sediment History of Lakes Ontario, Erie, and Huron. *J. Sedim. Petrol.*, 44(1):207-218.

Kemp, A.L.W., R.L. Thomas, C.I. Dell, and J.M. Jaquet. 1976. Cultural Impact on the Geochemistry of Sediments in Lake Erie. *J. Fish. Res. Board Canada*, 33(3):440-462.

Ketchum, B.H. 1939. The Absorption of Phosphate and Nitrate by Illuminated Cultures of *Nitzschia closterium*. *Am J. Botany*, 26.

Lerman, A. and H. Taniguchi. 1972. Strontium-90 - Diffusional Transport in Sediments of the Great Lakes. *J. Geophys. Res.*, 77(3):474.

Lerman, A. and T.A. Lietzke. 1975. Upgrade and Migration of Tracers in Lake Sediments. *Limnol. Oceanogr.*, 20(4):497-510.

Lucas, A.M. and N.A. Thomas. 1971. Sediment Oxygen Demand in Lake Erie's Central Basin, 1970. In: D.V. Anderson and J.S. Seddon (Eds.), *Proceedings of the 14th Conference on Great Lakes Research*, pp. 781-787. Braun-Brumfield Publishers, Ann Arbor, Michigan.

McCarty, P.L. 1971. Energetics and Kinetics of Anaerobic Treatment. In: *Anaerobic Biological Treatment Processes*, Advance Chemical Series Number 105, pp. 91-107. American Chemical Society, Washington, D.C.

Munawar, M. and I.F. Munawar. 1976. A Lakewide Study of Phytoplankton Biomass and Its Species Composition in Lake Erie, April-December 1970. *J. Fish. Res. Board Canada*, 33(3):581-600.

National Oceanic and Atmospheric Administration. 1974. Lake Erie, Chart Number 5. Lake Survey Center, National Oceanic and Atmospheric Administration, Detroit, Michigan.

National Oceanic and Atmospheric Administration. 1975. Mean Monthly Discharge of Detroit River, Detroit, Michigan. Lake Survey Center, National Oceanic and Atmospheric Administration, Detroit, Michigan.

Nriagu, J.O. 1972. Stability of Vivianite and Ion-Pair Formation in the System $\text{Fe}_3(\text{PO}_4)_2 - \text{H}_2\text{PO}_4 - \text{H}_2\text{O}$. *Geochim. Cosmochim. Acta*, 36:459.

Nriagu, J.O. 1976. Dissolved Silica in Pore Waters of Lakes Ontario, Erie and Superior Sediments. Canada Centre for Inland Waters, Burlington, Ontario, Canada.

O'Connor, D.J. and W.E. Dobbins. 1958. Mechanisms of Reaeration in Natural Streams. *Trans. Am. Soc. Civil Engin.*, 123:655.

O'Connor, D.J. and R.V. Thomann. 1972. Water Quality Models: Chemical, Physical, and Biological Constituents. In: G.H. Ward and W.H. Espey (Eds.), *Estuarine Modeling: An Assessment*, pp. 102-169. U.S. Environmental Protection Agency, Water Quality Office, Washington, D.C. EPA 16070 DZV 02/71.

Okubo, A. 1971. Oceanic Diffusion Diagrams. *Deep Sea Res.*, 18:789-802.

Ontario Ministry of the Environment. 1972. Great Lakes Water Quality Data 1972; St. Clair River, Detroit River, Lake Erie. Ontario Ministry of the Environment, Toronto, Ontario, Canada. 155 pp.

Paasche, E. 1973. Silicon and the Ecology of Marine Plankton Diatoms. I. *Thalassiosira pseudonana* (*Cyclotella nana*) Grown in a Chemostat With Silicate as Limiting Nutrient. *Marine Biol.*, 19:117-126.

- Rhee, G.-Y. 1973. A Continuous Culture Study of Phosphate Uptake, Growth Rate and Polyphosphates in *Scenedesmus* sp. J. Phycol., 9:495-506.
- Rhee, G.-Y. 1974. Phosphate Uptake Under Nitrate Limitation by *Scenedesmus* sp. and Its Ecological Implications. J. Phycol., 10:470-475.
- Rhee, G.-Y. 1978a. Continuous Culture in Phytoplankton Ecology. In: W.R. Droop and H.W. Jannasch (Eds.), Advances in Aquatic Microbiology, Volume 2, pp. 151-203. Academic Press, New York, New York.
- Rhee, G.-Y. 1978b. Effects of NP Atomic Ratios and Nitrate Limitation on Algal Growth, Cell Composition, and Nitrate Uptake. Limnol. Ocean., 23(1):10-25.
- Riley, G.A. 1956. Oceanography of Long Island Sound, 1952-1954. II. Physical Oceanography. Bull. Bingham Oceanogr. Coll., 15:15-46
- Robbins, J.A. 1977. Personal Communication. Great Lakes Research Division, The University of Michigan, Ann Arbor, Michigan.
- Rodgers, G.K. 1965. The Thermal Bar in the Laurentian Great Lakes. Great Lakes Research Division, The University of Michigan, Ann Arbor, Michigan. Publication Number 13, pp. 358-363.
- Scavia, D. and R.A. Park. 1976. Documentation of Selected Constructs and Parameter Values in the Aquatic Model CLEANER. Ecol. Modelling, 2(1):33-58.
- Sly, P.G. 1976. Lake Erie and Its Basin. J. Fish. Res. Board Canada, 33(3):355-370.
- Thomann, R.V., D.M. Di Toro, R. Winfield, and D.J. O'Connor. 1975. Mathematical Modeling of Phytoplankton in Lake Ontario, I. Model Development and Verification. U.S. Environmental Protection Agency, Office of Research and Development, National Environmental Research Center, Corvallis, Oregon. EPA-660/3-75-005, 177 pp.
- Thomann, R.V. 1979. Measures of Verification. Presented at the National Workshop on Verification of Water Quality Models. U.S. Environmental Protection Agency, Environmental Research Laboratory, Athens, Georgia and Hydrosience, Inc., Westwood, New Jersey.
- Tilman, D. and S.S. Kilham. 1976. Phosphate and Silicate Growth and Uptake Kinetics of the Diatom *Asterionella formosa* and *Cyclotella meneghiniana* in Batch and Semi-Continuous Cultures. J. Phycol., 12:375-383.
- U.S. Army Corps of Engineers. 1974. Sediment Investigation in the Anoxic Region of Lake Erie With an Emphasis on Phosphorus. Lake Erie Wastewater Management Study. U.S. Department of the Army, U.S. Army Corps of Engineers, Great Lakes Laboratory, Buffalo District, Buffalo, New York.
- U.S. Army Corps of Engineers. 1975. Lake Erie Wastewater Management Study, Preliminary Feasibility Study, Volumes 1 and 2. U.S. Department of the Army, U.S. Army Corps of Engineers, Great Lakes Laboratory, Buffalo District, Buffalo, New York. 383 pp.
- Van Zeggeren, F. and S.H. Storey. 1970. The Computation of Chemical Equilibria. Cambridge University Press, Cambridge, England.
- Watson, N.H.F. 1974. Zooplankton of the St. Lawrence Great Lakes - Species Composition, Distribution and Abundance. J. Fish. Res. Board Canada, 31(5):783-794.
- Watson, N.H.F. 1976. Seasonal Distribution and Abundance of Crustacean Zooplankton in Lake Erie. J. Fish. Res. Board Canada, 33(3):612-621.
- Webb, M.S. 1974. Surface Temperatures of Lake Erie. Water Res. Res., 10(2):199-210.
- Weiller, R.R. The Composition of the Interstitial Water of Sediments in the Central Basin of Lake Erie. Unpublished Report. Canada Centre for Inland Waters, Burlington, Ontario, Canada.

Weiller, R.R. 1975. Carbon Dioxide Exchange and Productivity. *Verh. Internat. Verein. Limnol.*, 19:694-703.

Wright, R.T. 1964. Dynamics of a Phytoplankton Community in an Ice-Covered Lake. *Limnol. Oceanogr.*, 9(2):163-178.

Yaksich, S.M. 1978. Nutrient Loadings to Lake Erie, Lake Erie Wastewater Management Study. U.S. Department of the Army, U.S. Army Corps of Engineers, Buffalo District, Buffalo, New York.

TECHNICAL REPORT DATA (Please read Instructions on the reverse before completing)		
1. REPORT NO. EPA-600/3-80-065	2.	3. RECIPIENT'S ACCESSION NO.
4. TITLE AND SUBTITLE Mathematical Models of Water Quality in Large Lakes; Part 2: Lake Erie		5. REPORT DATE JULY 1980 ISSUING DATE
		6. PERFORMING ORGANIZATION CODE
7. AUTHOR(S) Dominic M. Di Toro John P. Connolly		8. PERFORMING ORGANIZATION REPORT NO.
9. PERFORMING ORGANIZATION NAME AND ADDRESS Manhattan College Environmental Engineering and Science Division Bronx, New York 10471		10. PROGRAM ELEMENT NO.
		11. CONTRACT/GRANT NO. R803030
12. SPONSORING AGENCY NAME AND ADDRESS Environmental Research Laboratory Office of Research and Development U.S. Environmental Protection Agency Duluth, Minnesota 55804		13. TYPE OF REPORT AND PERIOD COVERED Final
		14. SPONSORING AGENCY CODE EPA/600/03
15. SUPPLEMENTARY NOTES Large Lakes Research Station, 9311 Groh Road, Grosse Ile, Michigan 48138		
16. ABSTRACT <p>This research was undertaken to develop and apply a mathematical model of the water quality in large lakes, particularly Lake Huron and Saginaw Bay (Part 1) and Lake Erie (Part 2).</p> <p>A mathematical model was developed for analysis of the interactions between nutrient discharges to Lake Erie, the response of phytoplankton to these discharges, and the dissolved oxygen depletion that occurs as a consequence. Dissolved oxygen, phytoplankton chlorophyll for diatoms and non-diatoms, zooplankton biomass, nutrient concentrations in available and unavailable forms, and inorganic carbon are considered in the model. Extensive water quality data for Lake Erie was analyzed and statistically reduced. Comparison of data from 1970 and 1973-1974 to model calculations served for calibration of the model. A verification computation was also performed for 1975, a year when no anoxia was observed.</p> <p>Recent developments in phytoplankton growth and uptake kinetics are included in this analysis. The methods of sedimentary geochemistry are expanded to include an analysis of sediment oxygen demand within the framework of mass balances. Projected effects of varying degrees of phosphorus removal on dissolved oxygen, anoxic area, chlorophyll, transparency and phosphorus concentration are presented.</p>		
17. KEY WORDS AND DOCUMENT ANALYSIS		
a. DESCRIPTORS Mathematical Models Water Quality	b. IDENTIFIERS/OPEN ENDED TERMS Great Lakes Lake Erie Ecological Modeling	c. COSATI FIELD/GROUP 08/H
18. DISTRIBUTION STATEMENT Release Unlimited	19. SECURITY CLASS (<i>This Report</i>)	21. NO. OF PAGES 249
	20. SECURITY CLASS (<i>This Page</i>)	22. PRICE